

**Synthesis and Evaluation of Novel Small
Molecules as Potential Anti-Cancer Agents for
The Treatment of Solid Tumors**

A THESIS

SUBMITTED TO THE FACULTY OF

UNIVERSITY OF MINNESOTA

BY

LUCAS SOLANO

IN PARTIAL FULFILLMENT OF THE REQUIREMENTS

FOR THE DEGREE OF

DOCTOR OF PHILOSOPHY

Venkatram R. Mereddy

MAY 2019

© Lucas Solano 2019

ACKNOWLEDGEMENTS

My research would have been impossible without the aid and support of Dr. Venkatram R. Mereddy, my thesis advisor. He has provided and continues to provide valuable advice, support, and expert guidance towards my personal and professional development.

I would like to express gratitude to Dr. Jon Holy for his mentorship and guidance during my Ph.D. work. He has taught me many things including molecular biology and fluorescence microscopy.

I am highly thankful to Dr. Teresa Rose-Hellekant for her help in training me in establishing tumor models, surgical procedures and other *in vivo* techniques.

I am grateful to Dr. Jon Rumbley for his constant support and expertise in biochemistry.

I would also like to thank all faculty and staff in College of Pharmacy, Department of Chemistry and Biochemistry, School of Medicine, and Integrated Biosciences for the knowledge and help they have provided me during my Ph.D.

I would especially like to thank Dr. Subash Jonnalagadda for helping me realize what I am capable of accomplishing, his continued mentorship and friendship.

I would like to acknowledge Departments of Chemistry and Biochemistry, College of Pharmacy, Integrated Biosciences, DOD-BCRP, Whiteside Clinical Research Institute, University of Minnesota, Randy Shaver Cancer Research Community for the financial support of my thesis work.

I would like to thank Shirisha and Sravan Jonnalagadda, Grady Nelson, Conor Ronayne, Melissa Hill, Erica Lueth, Kaija Kottke, and all of the present and past lab members for their support for the past several years. I would also like to thank my family for being there to support me every step of the way.

ABSTRACT

Lucas Solano, *Synthesis and Evaluation of Novel Small Molecules as Potential Anti-Cancer Agents for The Treatment of Solid Tumors*, Doctor of Philosophy (Integrated Biosciences), University of Minnesota.

The primary focus of this thesis is to design, synthesize, characterize and evaluate novel small molecules as potential anti-cancer agents for the treatment of solid tumors. In this regard, we carried out three projects and synthesized numerous molecules with distinct mechanisms of actions. In project one, we synthesized indazole appended diphenyl urea molecules as multi-tyrosine kinase targeted anti-cancer agents. The lead candidate compounds exhibited excellent cell proliferation inhibition against various solid tumor cell lines including, murine metastatic breast cancer 4T1, murine glioblastoma Gl261-Luc2, human triple negative breast cancer MDA-MB-231, human pancreatic MIAPaCa-2, and human colorectal adenocarcinoma WiDr. The lead candidate compounds were found to be well tolerated in healthy mice and exhibited significant tumor growth reduction in WiDr xenograft and 4T1 syngraft flank models in mice. In the second project, we have introduced a novel cytotoxicity enhancing pharmacophore with SN_2/SN_2' isomerization with nucleophilic cellular components. As an application of this pharmacophore, we appended to piperazinyl curcuminoids and synthesized several highly soluble quaternary ammonium derivatives. All of the synthesized compounds were evaluated for their cell proliferation inhibition

against three cancer cell lines, MIAPaCa-2, WiDr, and MDA-MB-231. The lead candidate compound was tested in a MIAPaCa-2 xenograft in mice and it exhibited significant tumor growth inhibition.

In project three, we designed and synthesized chalcone appended cyanocinnamic acids as potential glycolysis and mitochondrial oxidative phosphorylation inhibitors for the treatment of cancers. Chalcone acts as an irreversible covalent linker and the doubly activated cyanoacrylic acid unit as a potential reversible inhibitor of monocarboxylate transports and mitochondrial pyruvate carriers. The synthesized compounds have been evaluated for cell proliferation, glycolysis, and mitochondrial inhibition properties.

TABLE OF CONTENTS

Acknowledgements.....	i
Abstract.....	ii
Table of contents.....	iii
List of schemes.....	vii
List of tables.....	x
List of figures.....	x
List of abbreviations.....	xxiv

Chapter 1: Design of Novel Angiogenesis Inhibitors as Potential Anticancer Agents

1.1 Introduction

1.1a Cancer Heterogeneity and Hallmarks

1.1b Tyrosine Kinases and their role in cancer

1.1c Epidermal growth factor receptor (EGFR) family

1.1d EGFR Inhibitors

1.1e Fibroblast growth factor receptor (FGFR) family

1.1f Vascular endothelial growth factor receptor (VEGFR) family

1.2: Results and discussion

1.2a Synthesis of carboxy indazole diphenyl ureas as anticancer agents

1.2b Cell proliferation study of compounds 1.5a-1.5k using MTT assay

1.2e Endothelial Cell Tube Formation Assay of compounds 1.5i and 1.8i

1.2f Systemic toxicity evaluation of N,N-dialkyl/diaryl o-methoxy CHC derivatives 3h-3k in CD-1 mice: Results and discussion

1.2g In vivo anticancer efficacy studies using lead candidate compounds:

Anticancer efficacy of compounds 1.5i, 1.7i, and 1.8i in colorectal adenocarcinoma WiDr flank model

1.2h Anticancer efficacy of lead candidate compound 1.8i in syngeneic 4T1-luc2 flank model:

1.3 Conclusions

1.4 Experimental

1.4a Chemicals and methods of compound characterization

1.4b Synthesis of compounds 1-1.8i

1.4c Cell lines and culture conditions

1.4d MTT assay

1.4e Endothelial Cell Tube Formation Assay

1.4f Ethical Considerations for animal studies

1.4g General procedure for systemic toxicity evaluation

1.4h Anticancer efficacy of compound 1.5i, 1.7i, and 1.8i in WiDr flank model

1.4i Anticancer efficacy of compound 1.8i in 4T1 flank model:

1.5 NMR Spectra

Chapter 2: Synthesis and Evaluation of Piperazinyl Curcuminoids Salts

2.1 Introduction

2.1a Natural products as Medicinal Agents

- 2.1b Turmeric and its anticancer agent Curcumin
- 2.1c Chemical properties of Curcumin
- 2.1d Curcumin as a therapeutic agent
- 2.1e Curcumin formulations
- 2.1f Baylis-Hillman reaction
- 2.1g Quaternary ammonium salts
- 2.1h Mitochondrial targeting agents with Quaternary salts

2.2 Results and Discussion:

- 2.2a Synthesis of piperazine substituted curcumin analogs
- 2.2b Cell proliferation/cytotoxicity study of compounds 2d-2f:
- 2.2c Design of novel water soluble curcuminoids as potential anticancer agents
- 2.2d Cell proliferation/cytotoxicity study of compounds 2g-2m:
- 2.2e Fluorescence microscopy study of compound 2i in MIAPaCa-2 cells
- 2.2f Systemic toxicity evaluation of compound 2i in CD-1 mice
- 2.2g Anticancer efficacy of compound 2i in pancreatic cancer MIAPaCa-2 xenograft model in athymic nude mice

2.3 Conclusions

2.4 Experimental

- 2.4a Synthesis of compounds
- 2.4b Cell lines and culture conditions
- 2.4c MTT assay

- 2.4d Florescence microscopy study
- 2.4e Ethical Considerations for animal studies
- 2.4f General procedure for systemic toxicity evaluation
- 2.4g Anticancer efficacy of compound 2i in MIAPaCa-2 flank model

2.5 NMR Spectra

CHAPTER 3: Synthesis and Biological Evaluation of Chalcone Appended

Cyanoacrylic acids

3.1 Introduction

- 3.1a Evolution of hallmarks of cancer: A focus on tumor metabolism
- 3.1b Glycolysis and its relation to Warburg effect
- 3.1c Monocarboxylic acid transporters (MCTs) and their importance in metabolism
- 3.1d Mitochondrial pyruvate carriers
- 3.1e CHC as MCT1 inhibitor
- 3.1f SAR studies on CHC
- 3.1g Other MCT1 inhibitors
- 3.1j Pyrazole methylpropanoic acid derivatives as MCT4 inhibitors
- 3.1k UK-5099
- 3.1l Chalcones as a therapeutic agent
- 3.1m Synthesis of Chalcones
- 3.1n Chalcones as natural product and drug candidates:

3.1o Chalcones as anticancer agents TUB091 and TUB099

3.2 Results and Discussion:

3.2a Synthesis of chalcone appended cyanoacrylic acid

3.2b In vitro MTT based cell proliferation inhibition

3.2c Seahorse XFe96® analyzer

3.3 Conclusion

3.4 Experimental

3.4b Cell lines and culture conditions

3.4c MTT assay

3.4d Seahorse XFe96® assessment of glycolysis and mitochondrial respiration

3.5 NMR Spectra

References

LIST OF SCHEMES

Scheme 1.1: Synthesis of aminoindazole carboxylate **1.3**.

Scheme 1.2. Synthesis of ureido benzoic acids **1.4a-1.4k**

Scheme 1.3: Synthesis of carboxy indazole based diphenyl ureas **1.5a-1.5k**.

Scheme 1.4: Synthesis of aminoamide appended indazole ureas

Scheme 2.1: Synthesis of piperidone curcuminoids as anticancer agents

Scheme 2.2: Synthesis of azole based curcuminoids

Scheme 2.3: Baylis-Hillman reaction

Scheme 2.4: Conversion of Baylis-Hillman alcohols to acetates and bromides

Scheme 2.5: S_N2' capability of BH acetates.

Scheme 2.6: Synthesis of BH bromide derived peptidomimetics

Scheme 2.7: Synthesis of 3-benzylidene-pyrrolidine-2,5-dione using BH bromide

Scheme 2.8: Synthesis of Baylis-Hilman substituted imidazoles and triazoles

Scheme 2.9: Synthetic schemes for biologically active Baylis Hillman derived symmetrical curcumin-like template

Scheme 2.10. Structures of synthesized piperiziny curcumin analogs

Scheme 2.11: Synthesis of Baylis Hillman bromides

Scheme 2.12. Synthesis of quaternary ammonium curcuminoids

Scheme 2.13. Synthesis of morpholino quaternary ammonium salts

Scheme 3.1: Knoevenagel condensation of substituted benzaldehydes with cyanoacetic acid to form CHC based derivatives

Scheme 3.2: A representative scheme for the synthesis of the library of *N,N*-dialkyl amino CHC derivatives

Scheme 3.3: The Claisen-Schmidt condensation to synthesize chalcones

Scheme 3.4: Carbonylative Heck coupling reaction to synthesize chalcones

Scheme 3.5: Sonogashira isomerization coupling to synthesize chalcones

Scheme 3.6: Suzuki-Miyaura coupling reaction to synthesize chalcones

Scheme 3.7: Synthesis of chalcone substituted cyanocinnamic acids **3d-3f**

LIST OF TABLES

Table 1.1: MTT IC₅₀ (μM) values of compounds **1.5a-k** in, 4T1, GL261-luc2, MDA-MB-231 MIAPaCa-2, and WiDr cell lines

Table 1.2: Cell proliferation inhibition of water soluble metabolically stable ureas

Table 2.1: Cell proliferation inhibition activity of **2g-2m** in MDA-MB-231, MIAPaCa-2 and 4T1 cell lines

LIST OF FIGURES

Figure 1.1: Hallmarks of cancer

Figure 1.2: Structure of anilino-pyrimidine template pharmacophore of EGFR inhibitors

Figure 1.3: Structure of EGFR inhibitor Erlotinib

Figure 1.4: Structure of EGFR inhibitor gefitinib

Figure 1.5: Structure of EGFR inhibitor afatinib

Figure 1.6: Structure of FGFR inhibitor AZD4547

Figure 1.7: Structure of FGFR inhibitor infigratinib

Figure 1.8: Structure of FGFR inhibitor ponatinib

Figure 1.9: Clinically used VEGFR inhibitors for cancer therapy

Figure 1.10: Structure of VEGFR inhibitor sunitinib

Figure 1.11: structure of lenvatinib

Figure 1.12: Structure of VEGFR inhibitor nintedanib

Figure 1.13: Structure of pharmacologically important indazole template observed in new-generation VEGFR inhibitors

Figure 1.14: Structure of VEGFR inhibitor axitinib

Figure 1.15: Structure of VEGFR inhibitor pazopanib

Figure 1.16. Structure of the diphenyl urea pharmacophore found in new-generation multityrosine kinase inhibitors sorafenib and regorafenib

Figure 1.17: Structure of sorafenib

Figure 1.18: Structure of VEGFR inhibitor regorafenib

Figure 1.19: Fused indazole-diphenyl urea-based structural template

Figure 1.20. Structures of synthesized ureido benzoic acids **1.4a-1.4k**.

Figure 1.21. Structures of carboxy indazole diphenyl urea candidate compounds **1.5a-1.5k**

Figure 1.22: A CYP450 mediated metabolism and B lead compound **1.5i** sites of metabolic stability and low water solubility.

Figure 1.23: Graphical representation of Cell proliferation inhibition in different cell line

Figure 1.24: Tube formation assay of compounds **1.5i** and **1.8i** in HUVEC cells

Figure 1.25: Lead candidate compounds **1.5i**, **1.7i** and **1.8i** for further *in vivo* studies

Figure 1.26: Systemic toxicity study of compounds in CD-1 mice

Figure 1.27: Anticancer efficacy study in colorectal adeno carcinoma WiDr flank model. (A) Tumor volumes (B) tumor weights

Figure 1.28: Anticancer efficacy study in 4T1 tumor model

Figure 2.1: Curcumin in its keto and enol form

Figure 2.2 Therapeutic properties of curcumin

Figure 2.3: Multiple modes of biological activity of curcumin

Figure 2.4: Metabolites of curcumin

Figure 2.5 Modification sites of curcumin, red circle highlights aromatic substitution, blue α , β unsaturation, green diketo and yellow denotes carbonyl

Figure 2.6: Synthesis of carboxylic and ester based curcuminoids

Figure 2.7: Structure of hydrazinocurcuminoid

Figure 2.8: Structure of lead candidate compound with substitution on central carbon

Figure 2.9: structure of modified mono ketones and alcohols of curcuminoid origin

Figure 2.10: S_N2 , S_N2' , and 1,4 addition capabilities of Baylis-Hillman bromides

Figure 2.11: structure of 1-134-83

Figure 2.12: Structural template for various alky chain containing benzalkonium chlorides

Figure 2.13: Structure of cetylpyridinium chloride

Figure 2.14: Structure of ESC8

Figure 2.15: Examples of mitochondrial targeting agents.

Figure 2.16. Structures of synthesized quaternary ammonium curcuminoids

Figure 2.17. Cell proliferation inhibition of compounds **2i-2m** on 4T1, MDA-MB-231, and MIAPaCa-2

Figure 2.18. Fluorescence microscopy of MIAPaCa-2 cells treated with parent curcumin (10uM) and lead candidate **2i** salt (10uM) for 24 hours. Note candidate **2i** exhibited fluorescent characteristics when excited using a GFP filter set

Figure 2.19: Systemic toxicity study of compound **2i**

Figure 2.20: Tumor growth inhibition study of **2i** in MIAPaCa-2 flank xenograft study

Figure 3.1: Metabolic symbiosis and Warburg effect in cancer cells

Figure 3.2: Inhibition of MCT1 and/or MCT4 leads to a decrease in tumor growth

Figure 3.3: Chemical structure of MCT1 inhibitor CHC

Figure 3.4: The SAR study of the *N,N*-dialkyl/diaryl substituted CHC derivatives

Figure 3.5: Structure of AZD3965

Figure 3.6: Lead MCT4 inhibitor 2-((1-(2-chlorobenzyl)-5-(3-substituted phenyl)-1H-pyrazol-3-yl)methoxy)-2-methylpropanoic acids

Figure 3.7: Structure of UK-5099

Figure 3.8: Structural template of chalcones

Figure 3.9 Biological activities of Chalcones

Figure 3.10: Examples of clinically explored chalcones

Figure 3.11: Structure of xanthoangelol

Figure 3.12: Structure of TUB091 and TUB099

Figure 3.13: Reversible and irreversible units in chalcone cyanocinnamic acid structure

Figure 3.14: Mitochondrial stress test in (A) 4T1, (B) MDA-MB-231 and (C) WiDr cell lines using compounds **3d-3e**. The OCR values were calculated using

wave software. The average+SEM values of at least three independent experimental values were calculated.

Figure 3.15: Maximal respiration in (A) 4T1, (B) MDA-MB-231 and (C) WiDr cell lines using compounds **3d-3f**. The OCR values were calculated using wave software. The average+SEM values of at least three independent experimental values were calculated.

Figure 3.16: ATP production in (A) 4T1, (B) MDA-MB-231 and (C) WiDr cell lines using compounds **3d-3f**. The OCR values were calculated using wave software. The average+SEM values of at least three independent experimental values were calculated.

Figure 3.17: Proton leak in (A) 4T1, (B) MDA-MB-231 and (C) WiDr cell lines using compounds **3d-3f**. The OCR values were calculated using wave software. The average+SEM values of at least three independent experimental values were calculated.

Figure 3.18: Spare respiratory capacity in (A) 4T1, (B) MDA-MB-231 and (C) WiDr cell lines using compounds **3d-3f**. The OCR values were calculated using wave software. The average+SEM values of at least three independent experimental values were calculated.

Figure 3.19: Glycolytic stress test in (A) 4T1, (B) MDA-MB-231 and (C) WiDr cell lines using compounds **3d-3f**. The ECAR values were calculated using wave

software. The average+SEM values of at least three independent experimental values were calculated.

Figure 3.20: Glycolysis in (A) 4T1, (B) MDA-MB-231 and (C) WiDr cell lines using compounds **3d-3f**. The ECAR values were calculated using wave software. The average+SEM values of at least three independent experimental values were calculated.

Figure 3.21: Glycolytic capacity in (A) 4T1, (B) MDA-MB-231 and (C) WiDr cell lines using compounds **3d-3f**. The ECAR values were calculated using wave software. The average+SEM values of at least three independent experimental values were calculated.

Figure 3.22: Glycolytic reserve in (A) 4T1, (B) MDA-MB-231 and (C) WiDr cell lines using compounds **3d-3f**. The ECAR values were calculated using wave software. The average+SEM values of at least three independent experimental values were calculated.

LIST OF ABBREVIATIONS

MTR	multityrosine kinase
TKR	tyrosine kinase receptors
EGFR	epidermal growth factor receptor
VEGFR	vascular endothelial growth factor receptor

FGFR	fibroblast growth factor receptor
PDGFR	platelet derived growth factor receptor
NSCLC	non-small cell lung cancer
ATP	adenosine triphosphate
MCT	monocarboxylic acid transporter
SLC16	solute carrier 16
kDa	kilo Dalton
OxPhos	oxidative phosphorylation
ER	estrogen receptor
HER-2	human epidermal growth factor-2
TNBC	triple negative breast cancer
HIF-1 α	hypoxia inducing factor
NF- κ B	nuclear factor kappa-light-chain-enhancer
PR	progesterone receptor
ROS	reactive oxygen species
DNA	deoxyribonucleic acid
CHC	α -Cyano-4-hydroxy cinnamic acid
μ mol	micromoles
mM	millimolar
IC ₅₀	inhibition of 50% of the activity or cell growth
MPC	mitochondrial pyruvate carrier
FDA	food and drug administration

3-BPA	3-bromopyruvic acid
mg/Kg	dosage in milligram per kilogram of mouse
F	fluoro
Br	bromo
CN	cyano functional group
NO ₂	nitro functional group
CH ₃ CN	acetonitrile
NH ₄ Ac	ammonium acetate
OH	hydroxy functional group
DMF	<i>N,N</i> -dimethylformamide
POCl ₃	phosphorus (V) oxychloride
R-Br	alkyl/allyl bromide
H ₂ O	water
CNCH ₂ COOH	cyanoacetic acid
HBr	hydrobromic acid
H ₂ SO ₄	sulfuric acid
PBr ₃	phosphorous tribromide
nM	nanomolar
SEM	standard error of the mean
SAR	structure-activity relationship
K ₂ CO ₃	potassium carbonate
SRB	sulforhodamine-B

MTT	3-(4,5-dimethylthiazol-2-yl)-2,5-diphenyltetrazolium
bromide	
MEM	minimum essential medium
DMEM	Dulbecco's minimum essential medium
PI	propidium iodide
FCM	flow cytometry
acetyl CoA	acetyl coenzyme A
DMSO	dimethyl sulfoxide
ip	intraperitoneal
bid	twice a day
qd	once a day
CYP	cytochrome P450 enzyme
PBS	phosphate buffered saline
EtOH	ethanol
NaOH	sodium hydroxide
GST	glycolysis stress test
MST	mitochondrial stress test
ECAR	extracellular acidification rate
OCR	oxygen consumption rate
mpH	milli pH
pmol	pico moles
FCCP	carbonyl cyanide-4-(trifluoromethoxy)phenylhydrazone

ETC	electron transport chain
Dox	doxorubicin
^1H NMR	Proton (^1H) nuclear magnetic resonance spectrum
^{13}C NMR	Carbon (^{13}C) nuclear magnetic resonance spectrum
HRMS	high resolution mass spectrometer
FBS	fetal bovine serum
ATCC	American type cell culture
TLC	thin layer chromatography
HCl	hydrochloric acid
Hz	Hertz
MHz	Mega Hertz
J	Coupling constant
CDCl_3	deuterated chloroform
mA	milli amperes
PBST	phosphate buffered saline with Tween 20

Chapter 1: Design of Novel Angiogenesis Inhibitors as Potential Anticancer Agents

1.1 Introduction

1.1a Cancer Heterogeneity and Hallmarks

Cancer research and treatment options have advanced tremendously over the past several decades and the development of novel and improved cancer therapies largely depends on a thorough understanding of the cellular, molecular and biochemical underpinnings of cancer progression. In this regard, cancer is a result of the accumulation of genetic and epigenetic mutations that drive normal cells to grow and divide uncontrollably.¹ Frequently, these mutations arise in genes that control the cell cycle, DNA repair machinery, apoptosis, metabolism, proliferative signaling pathways, and many others where such mutations give rise to aggressive and malignant cell proliferation. Although cancer can vary widely by type, six major processes are conserved among all cancers which result in cancer sustenance and progression. Specifically, Hanahan and Weinberg have identified distinct hallmark characteristics which include the malignant cell's ability to sustain proliferative signaling, evade growth suppressors, activate invasion and metastasis, enable replicative immortality, induce angiogenesis, and resist cell death (**Figure 1.1**).¹ Recent literature reports have indicated that pharmacological disruption of pathways in cancer associated with angiogenesis and sustaining proliferative signaling may offer effective approaches to develop anticancer therapies.²⁻⁵ Based on the clinical success of such inhibitors, the

development of novel and improved inhibitors of angiogenesis and signaling pathways continue to be attractive targets for future cancer therapies.



Figure 1.1: Hallmarks of cancer

1.1b Tyrosine Kinases and Their Role in Cancer

Tyrosine kinases, a subclass of protein kinase, are an important class of enzymes responsible for the transfer of a phosphate group from ATP to tyrosine residues of target proteins. As a result of phosphorylation, tyrosine kinases act as an "on" or "off" switch for many cellular functions including enzyme activity, sub cellular localization, signal transduction, cell division, and cell recruitment.⁶⁻⁹ Tyrosine kinases are susceptible to mutations that result in hyperactivity and can lead to the development and progression of cancer.⁶⁻⁹

Receptor tyrosine kinases are a subclass of kinases that have a primary role in transmembrane signaling. Currently, 58 receptor tyrosine kinases are known which have been categorized into 20 sub-families. Examples of receptor kinases are epidermal and fibroblast growth factor receptors (EGFR and FGFR) which play important roles in signaling cellular proliferation, differentiation, and apoptosis, and vascular endothelial growth factor receptors (VEGFR) responsible for stimulating angiogenesis.^{2,5,6,10-12} Receptor kinases consist of an extracellular domain, a transmembrane domain and an intracellular catalytic domain. The extracellular domain binds to specific ligands from outside the cell and allows the cells to send and receive signals from other cells. The transmembrane domain operates by anchoring the kinase to the membrane whereas the intracellular catalytic domain binds and phosphorylates the substrates.⁶ Binding of the extracellular domain results in structural rearrangements that turn on the intracellular domain. This activation can act in different ways such as, allowing for the binding of ATP or substrates. Functions of receptor tyrosine kinases are similar to other kinases but have an emphasis in cellular differentiation,

metabolism, adhesion, motility, and death.⁶ In oncogenesis, receptor kinases are altered by gene mutation or chromosome translocation often resulting in the overexpression or hyper activation of the receptor function - conferring non-regulated ligand-dependent cancer cell growth.^{6,7,9,13}

As mentioned, there are numerous sub-types of receptor tyrosine kinases that play specific roles in both normal cell function and malignant transformation. In this regard, the following sections will introduce the function of these different receptor sub-types and outline receptor tyrosine kinase inhibitors used for anticancer applications.

1.1c Epidermal growth factor receptor (EGFR) family

EGFR is a member of the ErbB subfamily of receptor tyrosine kinases and was the first member to be identified. The ErbB family is comprised of four receptor tyrosine kinases, Her1 (EGFR, ErbB1), Her2 (Neu, ErbB2), Her3 (ErbB3), and Her4 (ErbB4).^{2,14} Changes in expression and function of ErbB kinases result in a variety of disease states where its deactivation can lead to neurodegenerative diseases, such as multiple sclerosis, Alzheimers, and Parkinson's, while its hyper activation correlates with formation and progression of solid tumors.^{2,10,14-16} Specifically, ErbB1 and ErbB2 have been found to be overexpressed in many cancers including gliomas, breast, ovarian, bladder, and non-small-cell lung carcinoma (NSCLC).^{10,14,16} Due to their important role in cancer progression, numerous drug candidates have undergone pre-clinical investigation. It has been found that inhibition of EGFR often results in cytostatic effects as opposed to apoptosis *in vitro*. However, literature reports indicate that

in vivo inhibition of EGFR results in tumor regression and can be explained by several factors including both cytostatic and apoptotic effects. Interestingly, EGFR inhibitors have been shown to act on other factors such as angiogenesis and are typically supplemented with anti-VEGFR therapies for cancer treatment.^{11,17} In this regard, numerous EGFR inhibitors have been developed which will be outlined in the following sections.

1.1d EGFR Inhibitors

Two important classes of EGFR inhibitors include synthetic small molecules and antibody-based therapies. Throughout the development of small molecule inhibitors, pre-clinical investigation has led to the optimization of the important anilino-pyrimidine pharmacophore for EGFR binding and inhibition (**Figure 1.2**). In this regard, the following potent synthetic EGFR inhibitors contain a conserved anilino-pyrimidine template. These inhibitors include reversible inhibitors erlotinib gefitinib, and irreversible inhibitor afatinib (**Figure 1.3, 4, and 5**).

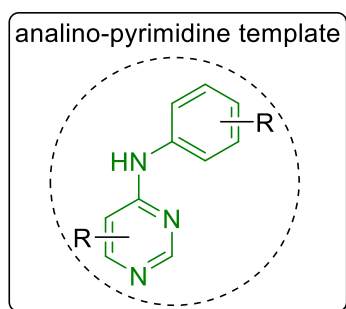


Figure 1.2: Structure of anilino-pyrimidine template pharmacophore of EGFR inhibitors.

Erlotinib is a receptor tyrosine kinase inhibitor marketed by Genentech, which acts on the epidermal growth factor receptor (EGFR). The IC₅₀ of erlotinib

for EGFR is 2nM in cell free assays.¹⁸ Erlotinib inhibits growth of a panel of NSCLC cell lines including A549, H322, H3255, H358 H661, H1650, H1975, H1299, H596 with IC₅₀ values in the low nanomolar range.¹⁹ Currently, it is used to treat NSCLC, pancreatic cancer and several other types of cancer.^{2,17,20} Recent studies demonstrate that erlotinib is also a potent inhibitor of JAK2V617F, which is a mutant form of tyrosine kinase JAK2 found in most patients with polycythemia vera.²¹ Further investigations are underway to study the potential use of erlotinib in the treatment of JAK2V617F-positive PV and other myeloproliferative disorders

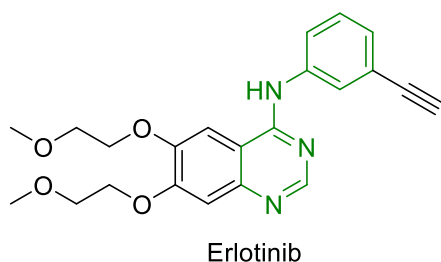


Figure 1.3: Structure of EGFR inhibitor Erlotinib

Gefitinib is a receptor tyrosine kinase inhibitor marketed by AstraZeneca, which acts on the EGFR by binding the ATP binding site (**Figure 1.4**). Gefitinib was the first selective inhibitor of EGFR. Similar to erlotinib, gefitinib also shows inhibition properties on multiple cancer types including NSCLC.^{22,23} In 2003, gefitinib was approved as monotherapy for the treatment of patients with locally advanced or metastatic NSCLC after failure of both platinum-based and docetaxel chemotherapies. However, in 2005 this approval was rescinded due to

the lack of ability to extend the life of patients. In the meantime gefitinib received approval in numerous other countries and in 2015 was reapproved for clinical use on NSCLC, this time as a first-line of treatment.²⁴

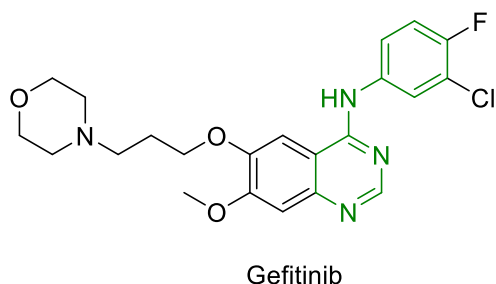


Figure 1.4: Structure of EGFR inhibitor gefitinib

Afatinib is an irreversible receptor tyrosine kinase inhibitor marketed by Boehringer Ingelheim, which acts on EGFR (**Figure 1.5**). It is a direct competitor of erlotinib for the treatment of NSCLC. One limitation of EGFR targeted therapies includes acquired resistance due to genetic mutations. T790M is a gatekeeper mutation of EGFR and results in over 50% of acquired resistance of tyrosine kinase inhibitors through a substitution of threonine with methionine at position 790 of exon 20. In addition to being an irreversible inhibitor, afatinib is one of the therapies that can treat patients with T790M mutations that do not respond to erlotinib and gefitinib therapies.

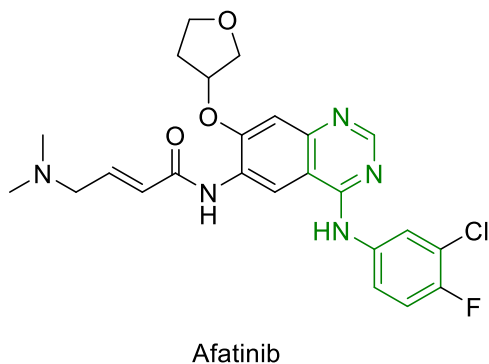


Figure 1.5: Structure of EGFR inhibitor afatinib

1.1e Fibroblast growth factor receptor (FGFR) family

FGFRs are a class of receptor tyrosine kinases that have function similar to VEGFR. FGFRs bind over 20 different growth factor ligands making it one of the largest among the receptor tyrosine kinase families.^{12,25} They play an important role during embryonic development, angiogenesis, wound healing, cell proliferation and differentiation.^{12,25} It has also been reported that upregulation of FGFR occurs as a resistance mechanism to anti-VEGF therapies.^{17,18,23} In addition to their role in angiogenesis, they are also speculated to have a major role in another hallmark of cancer, sustaining proliferative signaling.^{1,26} This signaling occurs through downstream activation of PI3K/AKT/mTOR and RAS/RAF/ERK pathways.²⁶ Targeting of FGFRs complement EGFR and VEGFR therapy resulting in reduction of angiogenesis as well as inhibition of proliferative signaling.^{17,18,23}

AZD4547 is a potent inhibitor of FGFR-1,2 and 3 with an $IC_{50} < 5nM$. AZD4547 was shown to inhibit proliferation in a dose-dependent manner in several cancer cell-lines that are known to overexpress fibroblast growth

factor (FGF) receptors (**Figure 1.6**).²⁷⁻²⁹ In KMS11, KG1a and SUM52PE cell-lines, AZD4547 inhibited FGFR tyrosyl phosphorylation and the phosphorylation of the downstream signaling molecules p42/p44MAP kinases.²⁷ AZD4547 has undergone clinical trials in previously treated patients with FGFR altered stage IV squamous cell lung cancer and showed acceptable safety but minimal activity.²⁸

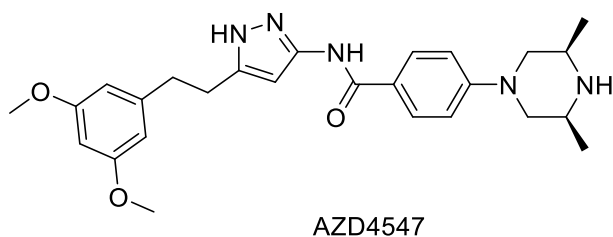
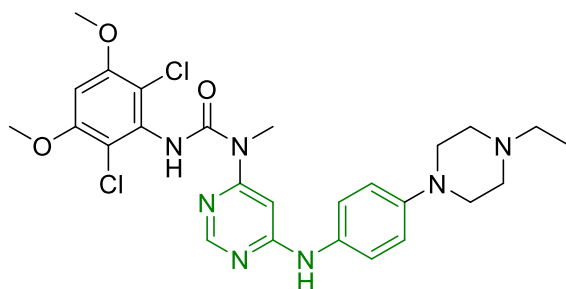


Figure 1.6: Structure of FGFR inhibitor AZD4547.

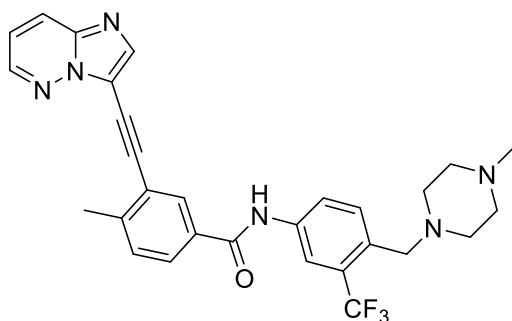
Infigratinib is potent and selective inhibitor of FGFR1/2/3 with IC₅₀ of ~1.0 nM of each FGFR.³⁰ Infigratinib also has good potency against VEGFR2 and low levels of activity against other tyrosine kinases (**Figure 1.7**). Infigratinib induces apoptosis and vessel normalization and improves the overall survival of mice bearing FGFR-driven HCCs and has shown synergy with microtubule-depolymerizing agent vinorelbine.^{30–32} Currently, infigratinib is undergoing phase III clinical trials as a first line of treatment for cholangiocarcinoma.



Infigratinib

Figure 1.7: Structure of FGFR inhibitor infigratinib.

Ponatinib is a novel, potent multi-target inhibitor of VEGFR2, FGFR1, and PDGFR α with activities ranging in 0.5 to 5 nM (**Figure 1.8**).³³ Additionally, ponatinib is a potent inhibitor of Bcr-Abl tyrosine kinase with T315I mutations. The T315I mutation confers resistance in cells as it prevents other Bcr-Abl inhibitors from binding to the Abl kinase.^{34,35} It is clinically indicated for treating accelerated phase chronic myelogenous leukemia, acute lymphoblastic leukemia, chronic myeloid leukemia, and chronic myelocytic leukemia.



Ponatinib

Figure 1.8: Structure of FGFR inhibitor ponatinib.

1.1f Vascular endothelial growth factor receptor (VEGFR) family

VEGFRs are typical tyrosine kinase receptors (TKRs) comprised of three domains, an extracellular domain, a transmembrane domain, and a cytoplasmic domain. VEGFRs are a sub family of platelet-derived growth factor receptors (PDGFRs). VEGFRs differ from PDGFRs in the number of Ig-like domains on the extracellular portion and the intracellular domain contains the same motifs resulting in different downstream signaling.^{26,36} VEGFR exists in three forms: VEGFR-1, VEGFR-2, and VEGFR-3. The function of VEGFR-1 is to act as a “dummy” receptor and modulate activators of VEGFR-2. VEGFR-2’s major role is proangiogenic signaling. The function of VEGFR-3 is not clearly understood; however, literature reports indicate it may have a role in lymphangiogenesis.^{3,37} VEGF and VEGFRs play a major role in the recruitment of endothelial cells to form a network of capillaries. Overexpression of VEGF and VEGFRs have been linked to recurrence, metastasis, and poor prognosis in breast, colon, renal, bladder, and head and neck cancers.^{10,11,38,39}

Owing to the importance of VEGFR in cancer progression, numerous synthetic small molecules have been developed as VEGFR inhibitors targeting a wide variety of cellular processes in numerous cancer types (**Figure 1.9**).

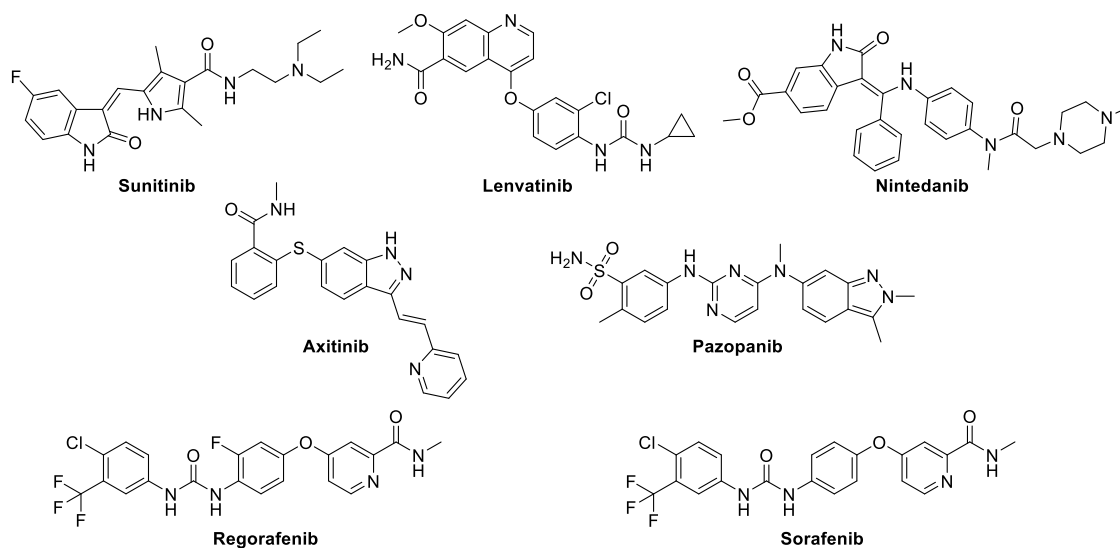


Figure 1.9: Clinically used VEGFR inhibitors for cancer therapy.

VEGFR inhibitors

Sunitinib is a potent ATP-competitive inhibitor of VEGFR2 and PDGFR β with IC₅₀ values of 9 nM and 8 nM in cell free assays (**Figure 1.10**).⁴⁰ It also exhibits good activity against FGFR-1 and EGFR amongst other kinases.⁴¹ Sunitinib has been approved for the treatment of renal cell carcinoma and imatinib resistant gastrointestinal stromal tumors.^{42,43}

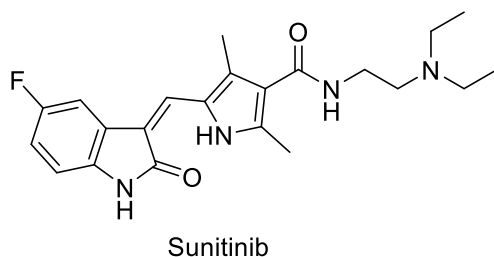


Figure 1.10: Structure of VEGFR inhibitor sunitinib.

Lenvatinib is a potent multi receptor tyrosine kinase inhibitor with inhibition of VEGFR1/2/3, FGFR1/2/3/4, PDGFR α , KIT, and RET (**Figure 1.11**).⁴⁰ Lenvatinib is indicated for the treatment of patients with locally recurrent or metastatic, progressive, radioactive iodine refractory differentiated thyroid cancer.^{44,45} Typically, patients with thyroid cancer have very high rates of survival except in patients with radioactive iodine refractory differentiated thyroid cancer making lenvatinib especially useful in this sub set of patients. Lenvatinib has recently received approval as a second-line of defense for advanced renal cell carcinomas.

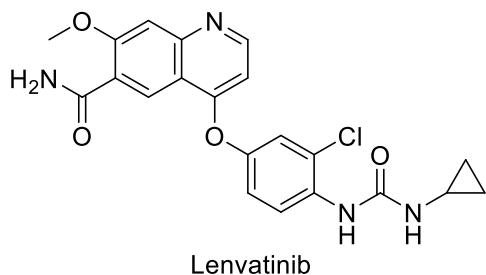


Figure 1.11: structure of Lenvatinib

Nintedanib is a potent receptor tyrosine kinase inhibitor for VEGFR1/2/3, FGFR1/2/3 and PDGFR α/β with IC₅₀ values ranging from ~10-100 nM.⁴⁰ Inhibition occurs through binding of ATP binding site resulting in decreased intracellular signaling (**Figure 1.12**). Nintedanib also inhibits the following non receptor tyrosine kinases, Lck, Lyn, and Src.⁴⁶ It has received

approval for use as a combination agent with docetaxel as a second line treatment for advanced, metastatic, or recurring NSCLC. In addition to cancer, nintedanib has been approved for use in idiopathic pulmonary fibrosis.⁴⁷ FGFR, PDGFR, and VEGFR have been implicated in the pathogenesis of idiopathic pulmonary fibrosis making multityrosine kinase inhibitors attractive candidates for treatment.

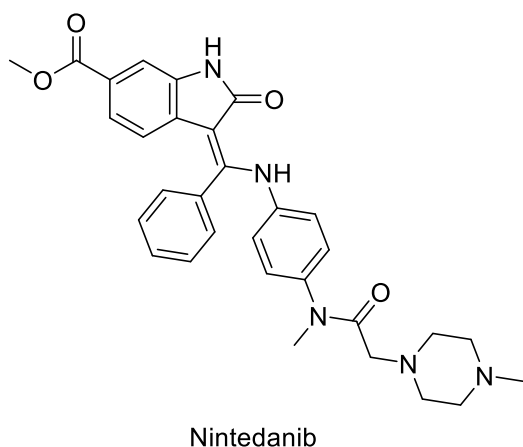


Figure 1.12: Structure of VEGFR inhibitor nintedanib.

Design of novel indazole based VEGFR inhibitors: New-generation VEGFR inhibitors.

Nitrogen-containing heterocycles are pharmacologically important scaffolds, and they are present in numerous FDA-approved and commercially available drugs.⁴⁸⁻⁵⁰ Indazoles are a class of heterocycles comprised of a benzene fused to a pyrazole and can exist as 1*H*-indazole, 2*H*-indazole, and 3*H*-indazole (**Figure 1.12**).⁴⁸⁻⁵⁰ Indazoles exhibit a wide range of biological

properties such as anti-inflammatory, antimicrobial, anti-HIV, antihypertensive, and anticancer activities.⁴⁸⁻⁵⁰ Specifically, pazopanib and axitinib are tyrosine kinase inhibitors that are in clinical use for the treatment of various cancers that include indazole and diphenyl urea based structural template (**Figure 1.12-17**).⁵¹⁻

56

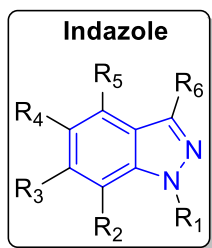


Figure 1.13: Structure of pharmacologically important indazole template observed in new-generation VEGFR inhibitors.

Axitinib is a multi-target inhibitor developed by Pfizer as an inhibitor of VEGFR1/2/3 and PDGFR β with IC₅₀ values ranging from 0.1-2.0 nM (**Figure 1.14**).⁵⁷ Axitinib has been approved by FDA for renal cell carcinoma after showing an increase of progression free survival.⁵⁵⁻⁵⁷ Investigations of axitinib are ongoing for the treatment of second-line defense of kidney, thyroid, and pancreatic cancers. Axitinib has also been evaluated in chronic myeloid leukemias with a mutated BCR-ABL1 gene that are resistant to other tyrosine kinase inhibitors such as imatinib.⁵⁸

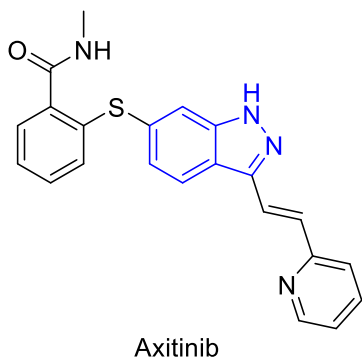


Figure 1.14: Structure of VEGFR inhibitor axitinib.

Pazopanib is a novel indazole based multi-target inhibitor of VEGFR1/2/3, PDGFR, and FGFR, exhibiting IC₅₀ values between 10 and 150 nM (**Figure 1.15**).⁵⁹ Pazopanib is developed by GlaxoSmithKline and received approval for the treatment of renal cell carcinoma and previously treated soft tissue sarcoma.^{51–54}

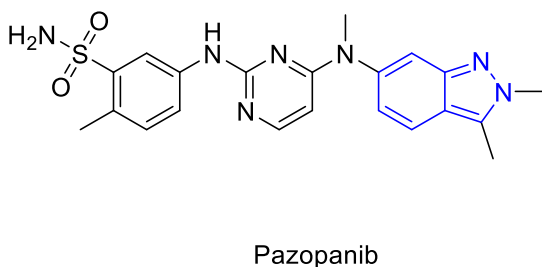


Figure 1.15: Structure of VEGFR inhibitor pazopanib.

Development of diphenyl urea-based VEGFR inhibitors (Figure 1.16)

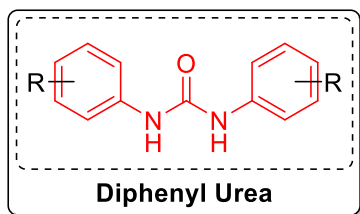


Figure 1.16. Structure of the diphenyl urea pharmacophore found in new-generation multityrosine kinase inhibitors sorafenib and regorafenib.

Sorafenib is a diphenyl urea based multi tyrosine kinase inhibitor with potent activity in the 5-100nM range against Raf, VEGFR, PDGFR, and cKit marketed by Bayer (**Figure 1.17**).^{60,61} Sorafenib's novelty is its ability to simultaneously target the Raf/Mek/Erk pathway. Sorafenib has been indicated for the treatment of advanced renal cell carcinoma, gastrointestinal stromal tumors, hemangiosarcoma, unresectable hepatocellular carcinoma, locally recurrent refractory to radioactive iodine treatment thyroid carcinoma, and metastatic refractory to radioactive iodine treatment thyroid carcinoma.^{55,62–66}

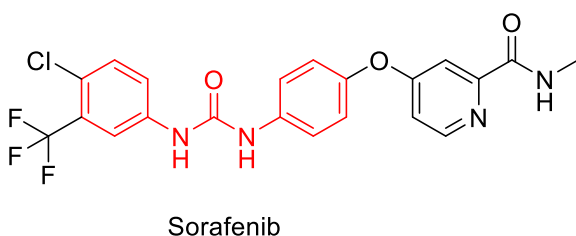


Figure 1.17: Structure of sorafenib.

Regorafenib is an orally bioavailable diphenyl urea based multi tyrosine kinase inhibitor marketed by Bayer. Regorafenib is structurally very similar to sorafenib with increased potency and pharmacokinetic/dynamic properties. Inhibition of Raf, VEGFR, PDGFR, and cKit range from 1-25nM (**Figure 1.18**).^{67,68}

Regorafenib is up to 83% bioavailable with a half-life of 20-30 hours compared to sorafenib with only 49% bioavailability.⁶⁹ Regorafenib is indicated for the treatment of patients with metastatic colorectal cancer who have been previously treated with fluoropyrimidine-, oxaliplatin- and irinotecan-based anti-VEGF chemotherapy, and, if KRAS wild type, an anti-EGFR therapy. In addition to metastatic colorectal cancer, regorafenib has also received approval for metastatic gastrointestinal stromal tumor, locally advanced gastrointestinal stromal tumor, refractory, unresectable gastrointestinal stromal tumors, locally recurrent or metastatic, progressive differentiated thyroid carcinoma refractory to radioactive iodine treatment, and advanced hepatocellular carcinoma.^{5,63,67-74}

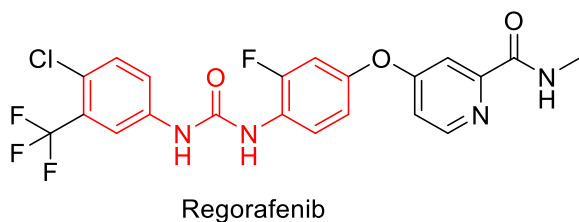


Figure 1.18: Structure of VEGFR inhibitor regorafenib.

1.2: Results and discussion

1.2a Synthesis of carboxy indazole diphenyl ureas as anticancer agents

Owing to the previous pharmacological track-record of both indazole and diphenyl urea structural templates toward VEGFR inhibition, we sought to synthesize novel fused indazole-diphenyl urea-based drug candidates (**Figure 1.19**).

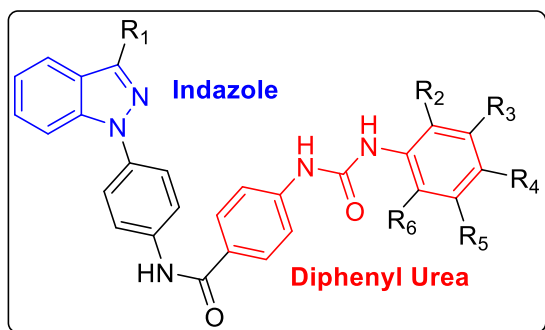
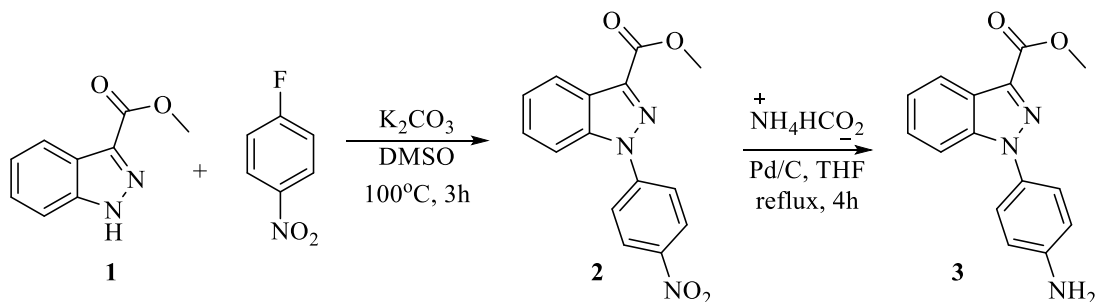


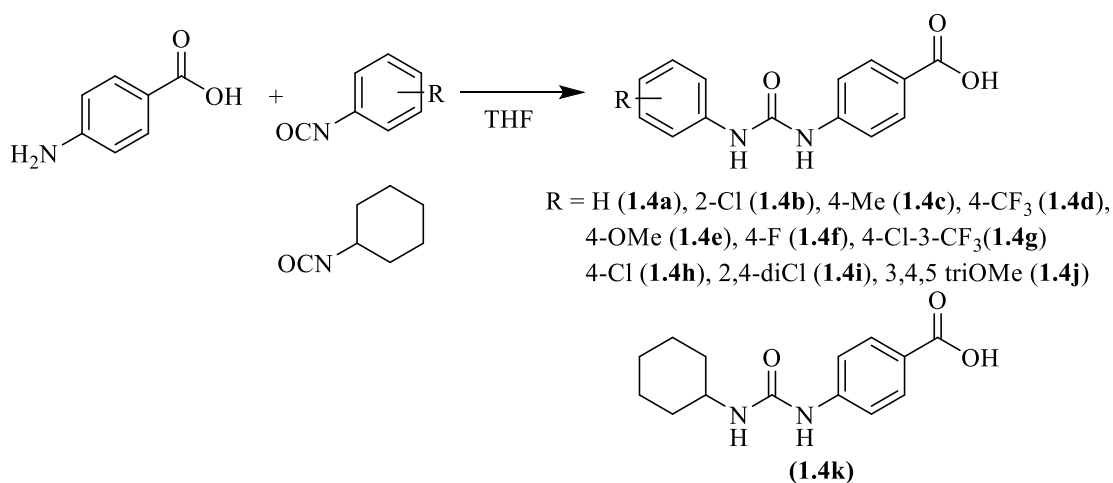
Figure 1.19: Fused indazole-diphenyl urea-based structural template

We started the synthesis of indazole derivatives by using commercially available indazole 3-carboxylic acid. The acid was treated with thionyl chloride in ice-cold methanol to obtain 1H-indazole-3-carboxylate **1**. This product was further reacted with 1-fluoro-4-nitrobenzene in the presence of potassium carbonate in DMSO to get the nitro-phenyl indazole carboxylate **2**. The nitro group in **2** was then reduced with palladium carbon and ammonium formate to obtain aminoindazole carboxylate **3** in good yield (**Scheme 1.1**).



Scheme 1.1: Synthesis of aminoindazole carboxylate **1.3**.

We then synthesized ureido benzoic acids **1.4a-1.4k**, 4-(3-phenylureido)benzoic acid, 4-(3-(2-chlorophenyl)ureido)benzoic acid, 4-(3-(4-tolyl)ureido)benzoic acid, 4-(3-(4-(trifluoromethyl)phenyl)ureido)benzoic acid, 4-(3-(4-methoxyphenyl)ureido) benzoic acid, 4-(3-(4-fluorophenyl)ureido)benzoic acid, 4-(3-(4-chlorophenyl) ureido)benzoic acid, 4-(3-(2,4-dichlorophenyl)ureido)benzoic acid, 4-(3-(4-chloro-3-(trifluoromethyl)phenyl)ureido)benzoic acid, 4-(3-(3,4,5-trimethoxyphenyl)ureido)benzoic acid, 4-(3-cyclohexylureido)benzoic acid by reacting 4-aminobenzoic acid with corresponding isocyanates in THF in excellent yields (**Scheme 1.2, Figure 1.20**).



Scheme 1.2. Synthesis of ureido benzoic acids **1.4a-1.4k**

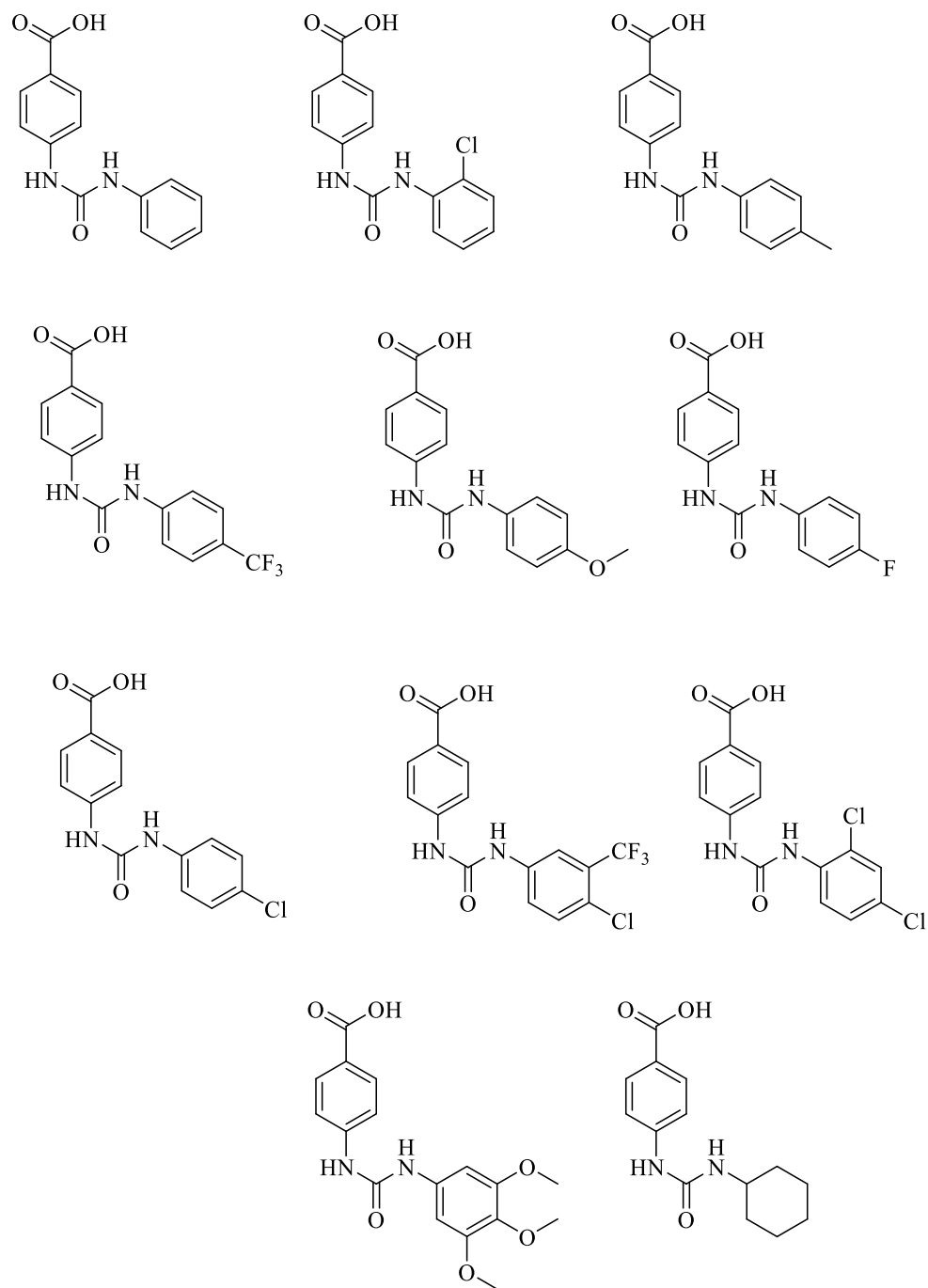
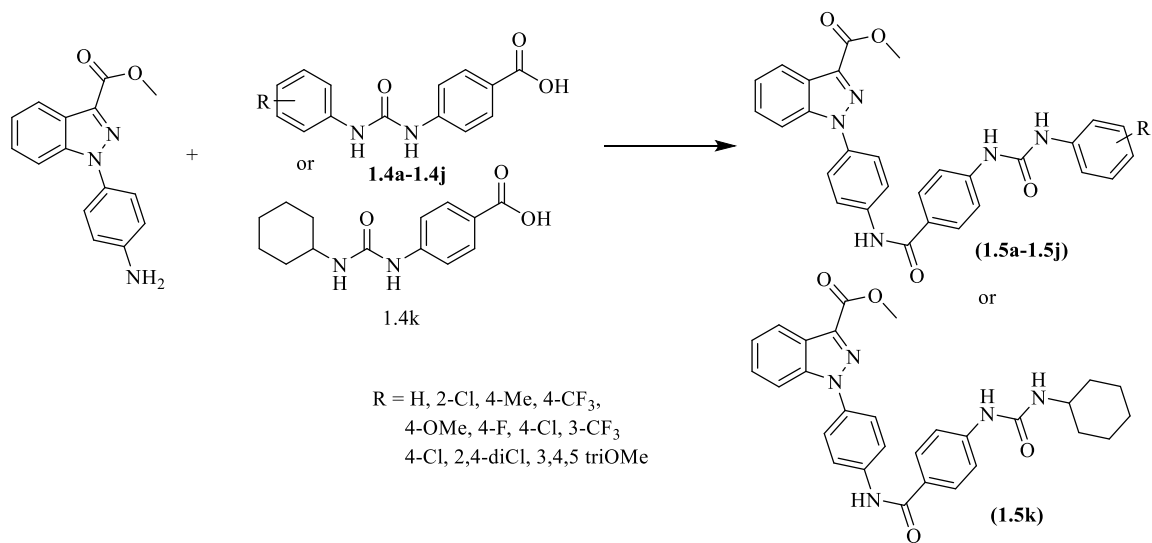


Figure 1.20. Structures of synthesized ureido benzoic acids **1.4a-1.4k**.

Next, we coupled the amine group in indazole unit and the corresponding ureido benzoic acid in DMF with EDC and HOBT overnight to form carboxy

indazole based diphenyl ureas (**1.5a-1.5k**) in good to moderate yields (**Scheme 1.3, Figure 1.21**).



Scheme 1.3: Synthesis of carboxy indazole based diphenyl ureas **1.5a-1.5k**.

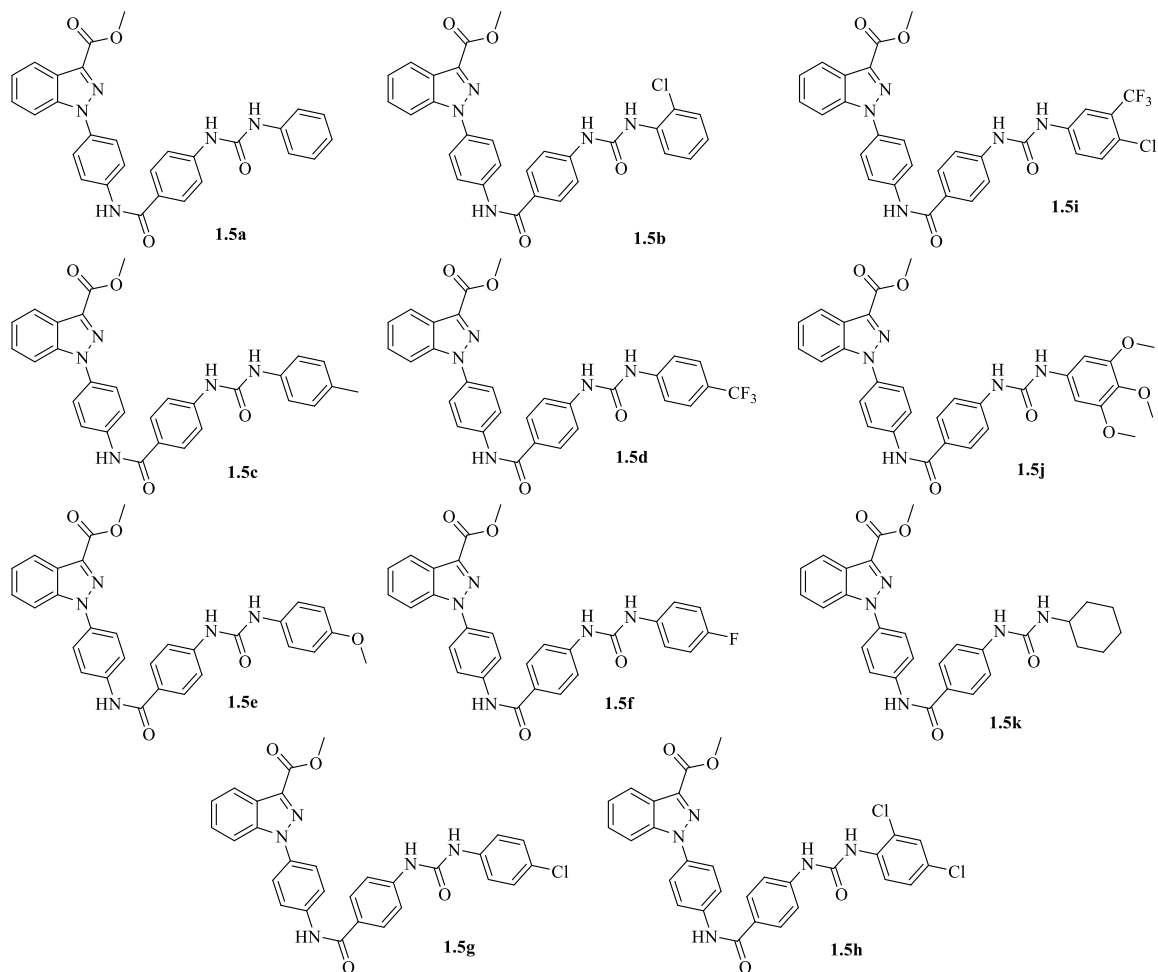


Figure 1.21. Structures of carboxy indazole diphenyl urea candidate compounds **1.5a-1.5k**

1.2b Cell proliferation study of compounds 1.5a-1.5k using MTT assay

After synthesizing compounds **1.5a-1.5k** we evaluated these compounds for cell proliferation inhibition properties to explore their potential as anticancer agents. Initial *in vitro* cell proliferation studies of the synthesized compounds **1.5a-1.5k** were carried out using 3-(4,5-dimethylthiazol-2-yl)-2,5-diphenyltetrazolium bromide (MTT) assay. This colorimetric assay measures the reduction of MTT to formazan by cellular mitochondrial reductase as a measure of cell viability.

For this assay, we utilized five cell lines including murine metastatic breast cancer cell line 4T1, murine glioma cell line GL261-luc2, human triple negative breast cancer cell line MDA-MB-231, human pancreatic cancer cell line MIAPaCa-2, and human colorectal adenocarcinoma cell line WiDr (**Table 1.1**).

In 4T1 cell line, compounds **1.5a-1.5k** showed IC₅₀ values between 0.9 and 5.0 μM, whereas 4-methoxy and 3, 4, 5-trimethoxy derivatives **1.5e** and **1.5j** did not exhibit IC₅₀ values up to the maximum concentration tested of 50 μM.

In GL261-luc2 cell line, compounds **1.5a-1.5k** showed IC₅₀ values between 0.8 and 3.7 μM, whereas 4-methoxy and 3, 4, 5-trimethoxy derivatives **1.5e** and **1.4j** exhibited IC₅₀ values up to 24.8 and 32.2 μM, respectively.

In MDA-MB-231 cell line, compounds **1.5a-1.5k** exhibited IC₅₀ values between 0.5 and 3.7 μM, whereas 3, 4, 5-trimethoxy derivative **1.5j** exhibited IC₅₀ values up to 26.4 μM.

In MIAPaCa-2 cell line, compounds **1.5a-1.5k** showed IC₅₀ values between 3.1 and 11.0 μM, whereas 2-chloro derivative **1.5b** exhibited IC₅₀ value up to 30.2 μM and 4-methoxy and 3, 4, 5-trimethoxy derivatives **1.5e** and **1.5j** did not exhibit IC₅₀ values up to 50 μM.

In WiDr cell line, compounds **1.5a-1.5k** showed IC₅₀ values between 0.6 and 8.1 μM, whereas 4-methoxy **1.5e** did not exhibit toxicity up to 50 μM concentration and 3, 4, 5-trimethoxy derivatives **1.5j** exhibited IC₅₀ value of 26.6 μM.

Based on the results obtained from cell proliferation inhibition studies, we selected compound **1.5i** as a lead derivative. **1.5i** showed consistently exhibited good potency amongst the lowest IC₅₀ values against all the tested cell lines (**Table 1.1**).

Table 1.1: MTT IC₅₀ (μM) values of compounds **1.5a-k** in, 4T1, GL261-luc2, MDA-MB-231 MIAPaCa-2, and WiDr cell lines.

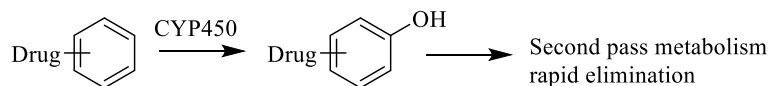
Compound	4T1	GL261-luc2	MDA-MB-231	MIAPaCa-2	WiDr
1.5a	1.9±0.4	3.1±0.5	1.8±0.1	11.0±2.0	1.1±0.3
1.5b	1.4±0.4	3.7±0.2	2.1±0.3	30.2±1.0	2.7±0.5
1.5c	0.9±0.4	0.8±0.1	0.5±0.2	4.8±0.4	8.1±0.3
1.5d	1.8±0.4	2.8±1.5	1.2±0.5	5.9±0.5	5.6±0.4
1.5e	>50.0	24.8±1.0	4.9±0.8	>50.0	>50.0
1.5f	4.8±1.7	3.1±0.4	4.3±0.5	3.1±0.4	0.6±0.1
1.5g	1.4±0.1	1.5±0.3	7.0±0.9	4.1±0.2	1.7±1.1
1.5h	1.1±0.2	1.4±0.1	1.3±0.1	5.2±0.5	3.7±1.5
1.5i	3.6±1.2	2.6±0.5	3.7±0.8	4.6±0.8	1.3±0.2
1.5j	>50.0	32.2±4.2	>50.0	>50.0	26.6±0.7
1.5k	5.0±0.4	3.1±1.4	26.4±1.4	6.5±0.7	1.2±0.4

* IC₅₀ values reported in μM, average ± SEM of minimum three separate experimental values.

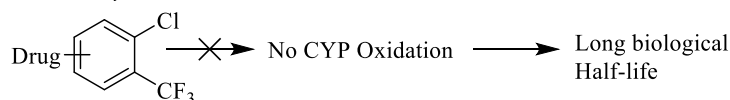
1.2c Synthesis of amido indazole diphenyl ureas as anticancer agents:

Other important considerations of small molecule drug development include metabolic stability and water solubility. Cytochrome P450 (CYP450) enzymes are responsible for a wide variety of oxidation reactions on xenobiotics. Specifically, unsubstituted phenyl rings are highly susceptible to CYP450-mediated oxidation and rapid elimination (**Figure 1.22**). From a structural and metabolic perspective, compound **1.5i** also has multiple sites on the phenyl rings blocked with chlorine and trifluoromethyl which could slow down CYP450 oxidation resulting in metabolic stability (**Figure 1.22**). However, due to the high carbon content and hydrophobic characteristics of compounds, they did not exhibit good water solubility, so we envisioned further modifications to increase solubility.

A *Metabolically Labile*



Metabolically Stable



B

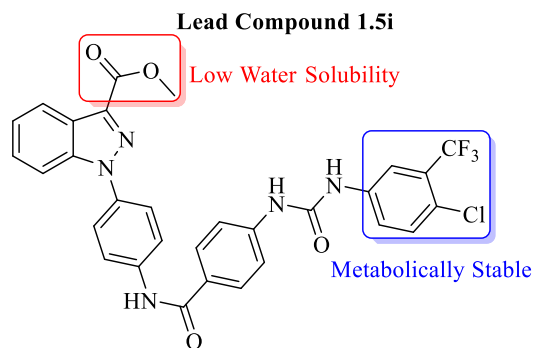
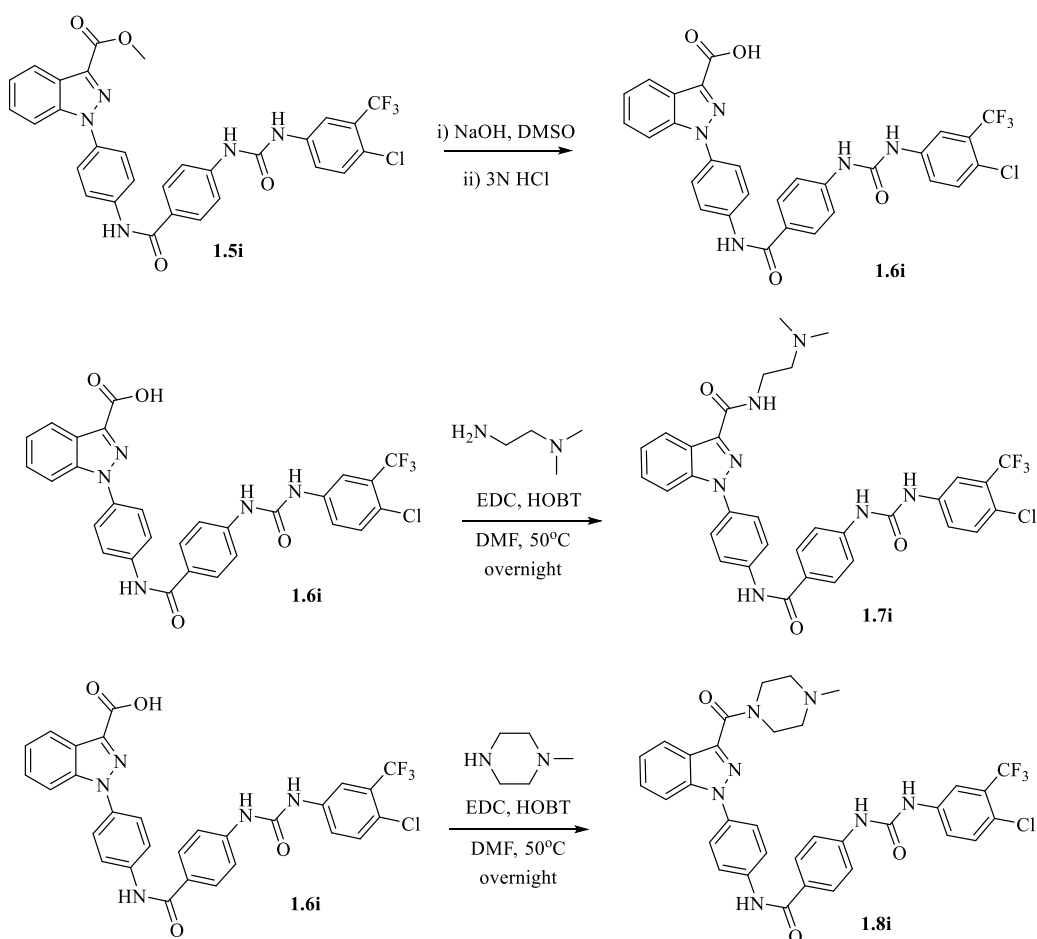


Figure 1.22: A CYP450 mediated metabolism and B lead compound **1.5i** sites of metabolic stability and low water solubility.

In this regard, we hydrolyzed the methyl ester of compound **1.5i** by dissolving it in DMSO and heating in the presence of sodium hydroxide. Upon evaluation of this new compound, we found that the activity of acid **1.6i** was lost in all the cell lines up to a concentration of 50 μM . We hypothesized that the carboxylic acid homolog **1.6i** became ionized limiting its ability to cross the cell membrane. In this regard, we sought to improve the hydrophilicity of compound **1.5i** further by synthesizing two different aminoamide derivatives.



Scheme 1.4: Synthesis of aminoamide appended indazole ureas

The first derivative was prepared by dissolving **1.6i** in DMF and adding EDC/HOBT with N,N-dimethyl ethylene diamine to afford **1.7i**. The second derivative was prepared in a similar fashion instead using N-methylpiperazine, affording **1.8i** (**Scheme 1.4**).

1.2d Cell proliferation study of compounds **1.6i**, **1.7i** and **1.8i** using MTT assay:

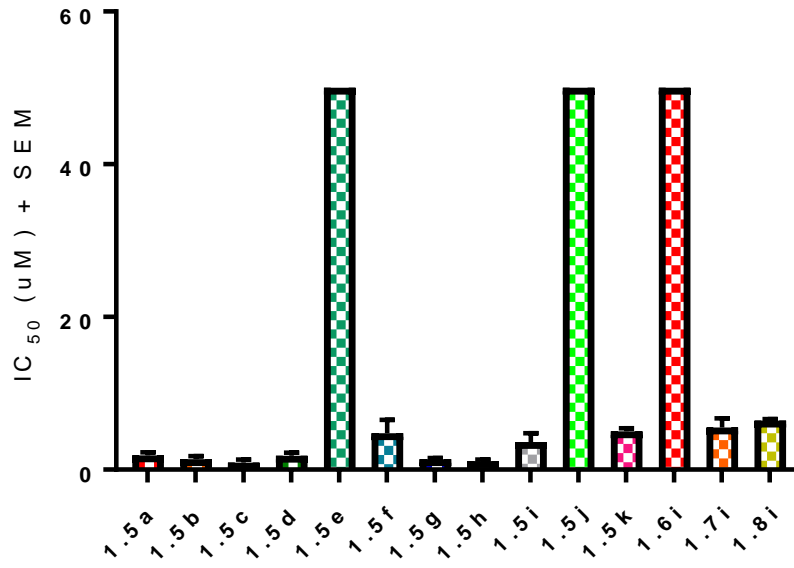
These compounds **1.7i** and **1.8i** exhibited enhanced solubility compared to the parent compound **1.5i**. Evaluation of cell proliferation inhibition resulted in comparable activity on all five cells lines of the parent compound **1.5i** (**Table 1.2**). These amino amide derivatives exhibited improved solubility properties.

Table 1.2: Cell proliferation inhibition of water soluble metabolically stable ureas

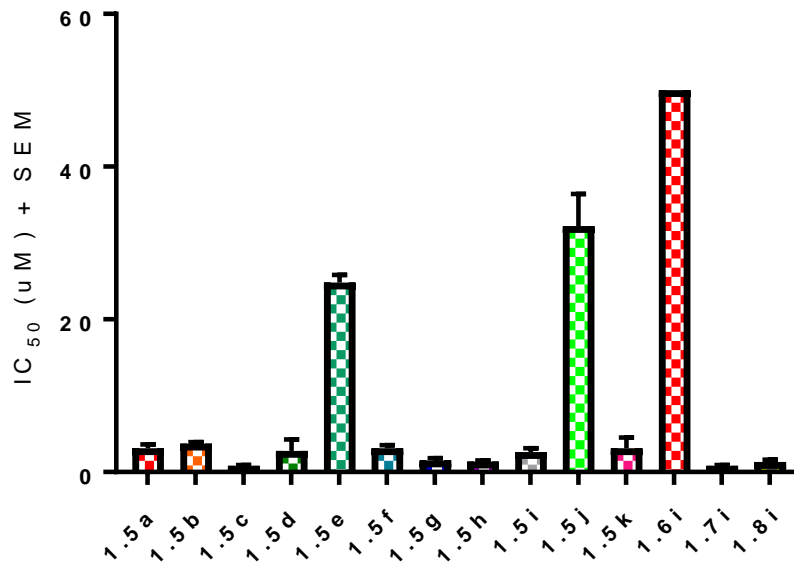
Compound	4T1	GL261-luc2	MDA-MB-231	MIAPaCa-2	WiDr
1.6i	>50.0	>50.0	>50.0	>50.0	>50.0
1.7i	5.5±1.2	0.8±0.1	2.7±0.4	2.8±0.3	1.3±0.1
1.8i	6.4±0.2	1.3±0.3	3.3±0.3	10.2±0.5	3.1±0.7

A comparative analysis of all the synthesized compounds **1.6i-1.8i** were shown in the format of bar graph (**Figure 1.22**).

4 T 1

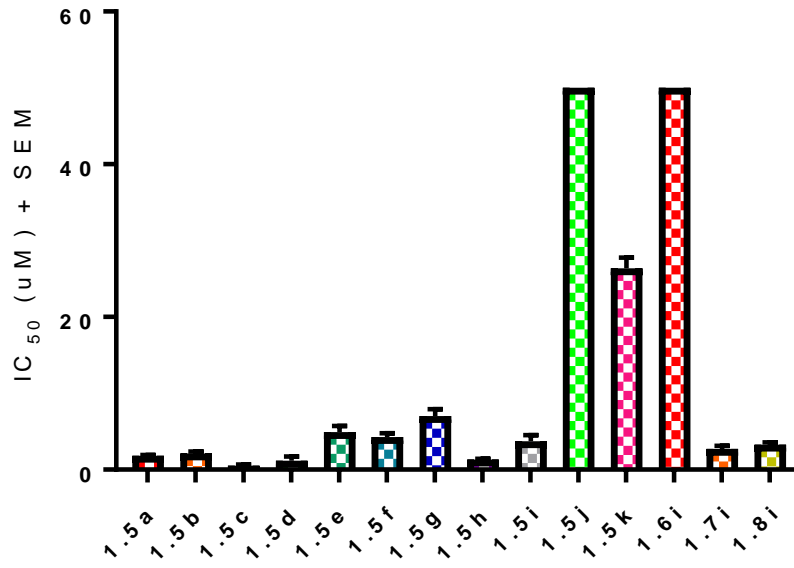


G I 2 6 1 -L u c 2

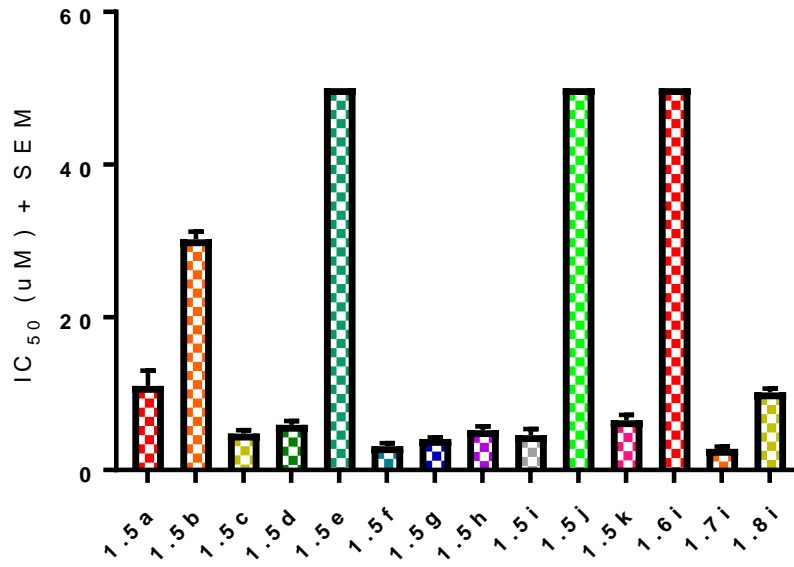


Continued...

M D A - M B - 2 3 1



M I A P a C a - 2



Continued...

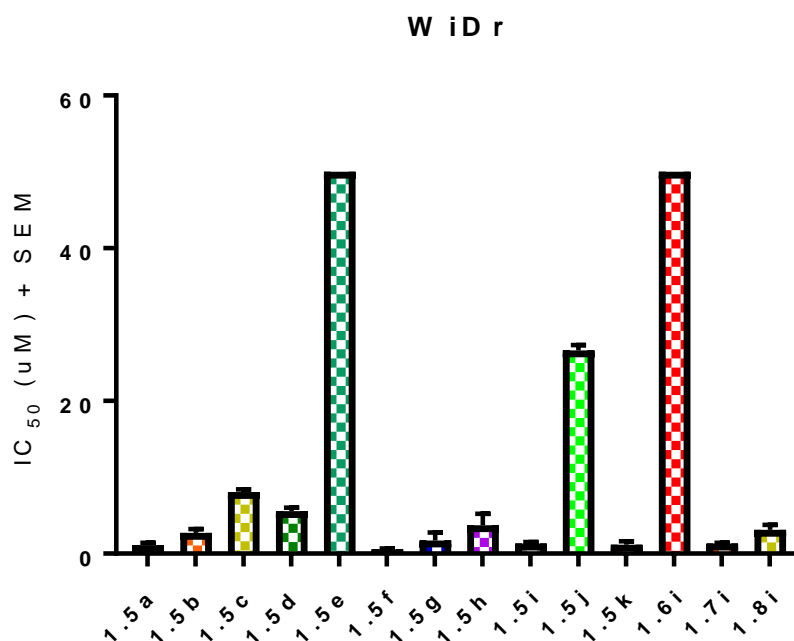


Figure 1.23: Graphical representation of Cell proliferation inhibition in different cell line

1.2e Endothelial Cell Tube Formation Assay:

We hypothesized that our synthesized compounds work by inhibiting angiogenesis similar to that sorafenib and regorafenib. Therefore, we evaluated the ability of compounds **1.5i** and **1.8i** to inhibit the formation of tubes in an endothelial cell line, HUVEC. For this assay, we coated plates with Matrigel Matrix and added compound **1.5i** and **1.8i** at concentrations of 1 μ M and 5 μ M. After a period of 18-24 hours, we added Calcein AM for fluorescent labeling. We then acquired fluorescent images and measured the length of tubes as a measure of the compounds ability to inhibit the formation of new tubes (**Figure 1.24**).

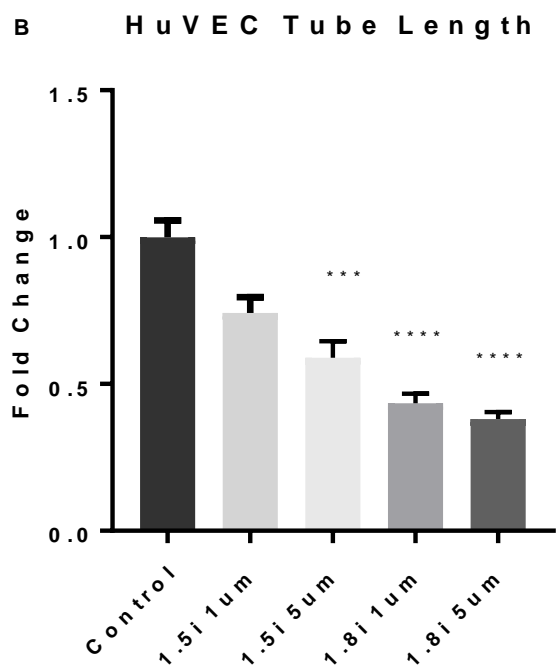
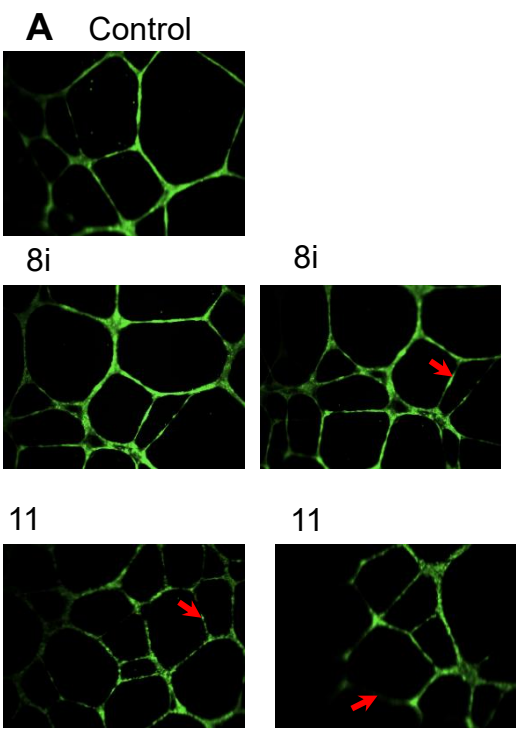


Figure 1.24: Tube formation assay of compounds **1.5i** and **1.8i** in HUVEC cells

1.2f Systemic toxicity evaluation of **1.5i**, **1.7i** and **1.8i** in CD-1 mice

Compounds **1.5i**, **1.7i** and **1.8i** showed inhibition of cellular proliferation at low μM concentrations against five cell lines, inhibition of tube formation in HUVEC cells, and good water solubility. We then evaluated the systemic toxicity of the lead compounds in healthy CD-1 mice. We chose inhibitors **1.5i**, **1.7i** and **1.8i** as lead derivatives (**Figure 1.25**) for the further preclinical development as they were well tolerated in the mice.

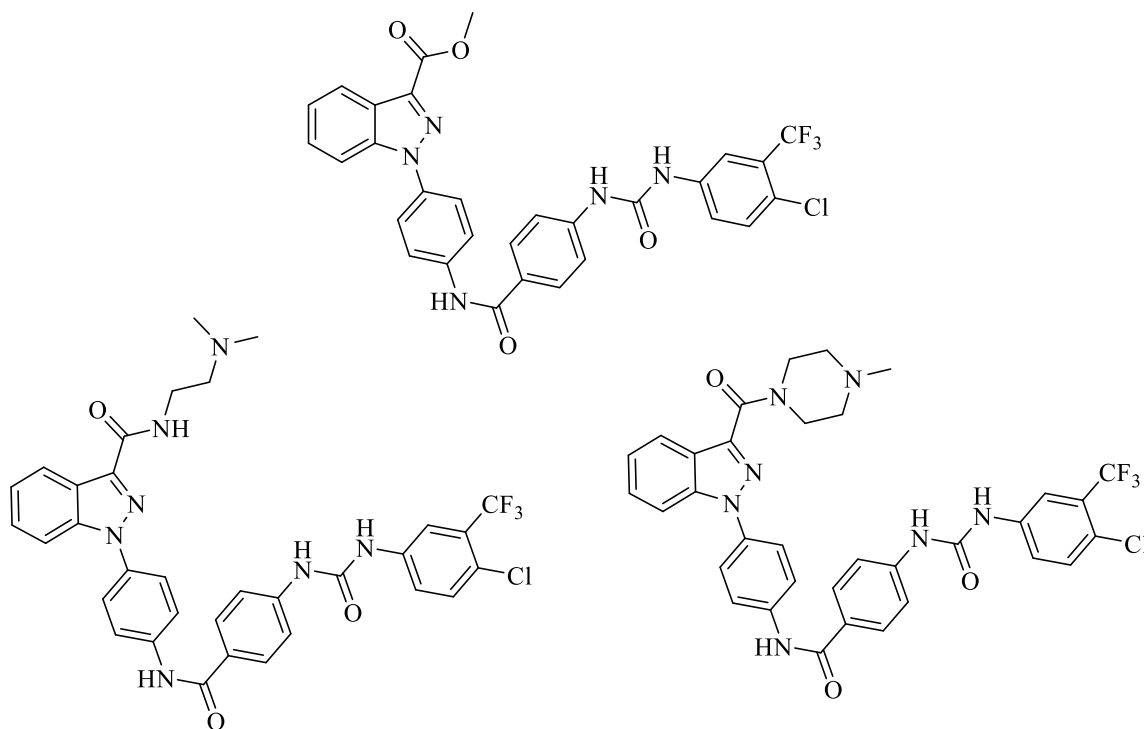


Figure 1.25: Lead candidate compounds **1.5i**, **1.7i** and **1.8i** for further *in vivo* studies

The compounds were dissolved in a formulation comprised of 10% DMSO, 10% PEG, 40% Kolliphor (18.8% wt/volume), and 40% water to achieve a concentration where a dosage of 25 mg/Kg could be given in such a way that a

20g mouse would receive a 0.20mL injection. CD-1 mice were randomly assigned into groups (n = 6 mice per group) with similar average body weights and then were treated with compound **1.5i** at 25 mg/Kg, ip, bid, compound **1.7i** at 25 mg/Kg, ip, bid, compound **1.8i** at 25 mg/Kg, ip, qd, or vehicle (same as vehicle). At the end of the study, the treatment groups did not show any visible toxic effects such as abnormal grooming, hunchback, and morbidity. The treatment groups had no significant differences in body weights compared to control groups (Figure 1.26).

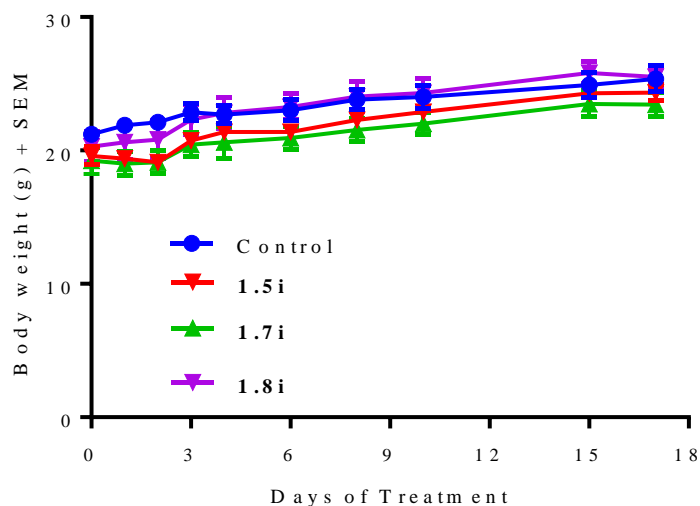


Figure 1.26: Systemic toxicity study of compounds in CD-1 mice

As the lead compounds **1.5i**, **1.7i**, and **1.8i** were well tolerated in mice, we next evaluated these compounds for anticancer efficacy on WiDr xenograft model. For this study, female athymic nude mice were utilized. Mice were injected with 5×10^6 cells suspended in 1:1 mixture of PBS-matrigel. The treatment was initiated after tumors reached a mean volume of 150 mm^3 . Mice were randomly assigned in to groups (n = 6 mice per group) and mice in groups 1-3 were treated

with **1.5i**, **1.7i**, and **1.8i**, respectively, at 25mg/Kg, i.p, once daily, for 14 days. Tumor volume was monitored every 2-3 days (**Figure 1.27**) and starting on day 12, compound **1.8i** showed statistically significant tumor growth reduction of ($P < 0.05$) 47% and 39% compared to control and oxaliplatin, respectively. At the conclusion of the study, mice were euthanized, tumors were resected and weighed. Once again, compound **1.8i** showed significant reduction of ($P < 0.05$) 43% and 38% compared to control and oxaliplatin groups, respectively (**Figure 1.26B**). This data supports the *in vitro* results and our hypothesis about the lability of methyl ester and we did not observe any significant reduction of compounds **1.5i** or **1.8i** by volume or weight.

1.2g *In vivo* anticancer efficacy studies using lead candidate compounds: Anticancer efficacy of compounds 1.5i, 1.7i, and 1.8i in colorectal adeno carcinoma WiDr flank model

We then evaluated the lead candidate compounds **1.5i**, **1.7i**, and **1.8i** for *in vivo* efficacy in colorectal adenocarcinoma WiDr tumor flank model. We selected WiDr cell line because tyrosine kinase inhibitors have been FDA approved for clinical use to treat colorectal cancers and this cell line readily forms aggressive tumors in nude mice. Compound **1.5i** was selected for *in vivo* anticancer efficacy study because of its good cytotoxicity and presumed metabolic stability of the urea. Compound **1.7i** and **1.8i** were also selected due to their increased water solubility and metabolic stability of the amide that

replaced the ester. We also included oxaliplatin, a clinically used anti-cancer agent.

5×10^6 WiDr cells in a 1:1 mixture of Matrigel:PBS were inoculated onto the flank of female BALB/c nude mice. After the average tumor volume reached $\sim 125 \text{ mm}^3$, mice were randomly assigned into 5 groups (n = 6 mice per group). groups 1-3 were treated with **1.5i**, **1.7i**, and **1.8i**, respectively, at 25mg/Kg, i.p, once daily, for 14 days. Group 4, our positive control was treated with oxaliplatin at 10 mg/Kg twice per week for 14 days. Group 5 was assigned as a control group and was treated with our vehicle. Body weights and tumor volume were measured every 2-3 days and after 14 days of treatment, mice were euthanized, and tumors were resected and weighed.

From this study **1.8i** showed a statistically significant reduction of tumor volume ($P < 0.05$) 47% and 39% compared to control and oxaliplatin respectively. At the conclusion of the study, mice were euthanized, tumors were resected and weighed. Once again **1.8i** showed significant reduction of ($P < 0.05$) 43% and 38% control and oxaliplatin respectively. Oxaliplatin was not able to significantly reduce the tumor burden. Supporting our *in vitro* results and hypothesis about the lability of methyl ester, we did not see any significant reduction of compounds **1.5i** or **1.7i** by volume or weight (**Figure 1.27**).

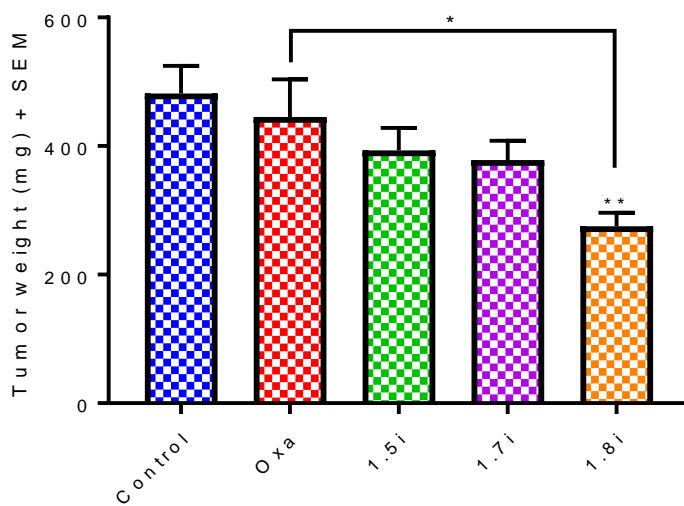
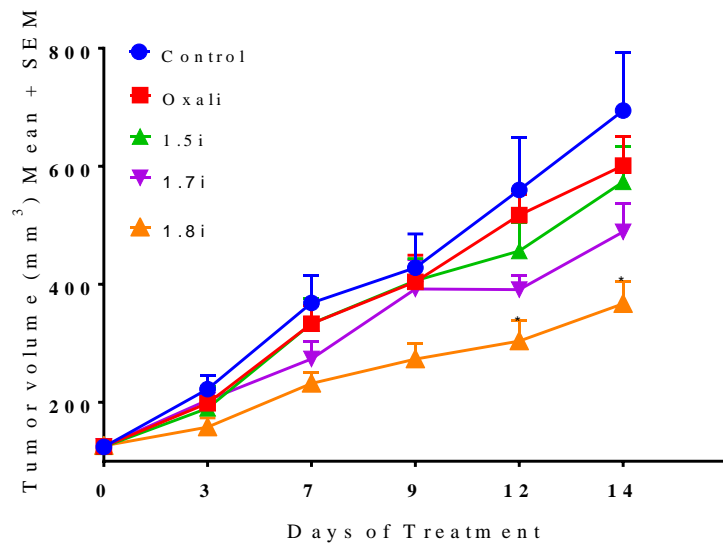


Figure 1.27: Anticancer efficacy study in colorectal adeno carcinoma WiDr flank model. (A) Tumor volumes (B) tumor weights

3.7.3 Anticancer efficacy of lead candidate compound 1.8i in syngeneic 4T1-luc2 flank model:

Since tyrosine kinase inhibitors have FDA approval for multiple cancer types and have been used in the clinic, we evaluated the efficacy of lead

compounds against 4T1 murine tumor model system. 4T1 is an aggressive murine cancer known to be highly metastatic to liver, lungs, bone, and brain. Since compound **1.5i** and **1.7i** did not show significant reduction in WiDr model, we chose compound **1.8i** as a lead candidate for tumor efficacy evaluation in 4T1 model. Once again, compound **1.8i** was compared against a positive and negative control. For the positive control, we chose to use doxorubicin as it is a clinical drug approved for breast cancer treatment.

The flank of female BALB/c mice (4 weeks old) were injected with 1×10^5 cells 4T1 cells. Mice were randomized in to 3 groups (n = 6 mice per group) and due to the aggressiveness of this model, we began treatment of compounds after 48 hours of tumor inoculation. Mice in groups 1 were administered with lead molecule **1.8i** at a dosage of 25 mg/Kg, ip, and doxorubicin was administered at 0.5 mg/Kg, i.p. five days a week as a positive control in group 2. Mice in group 3 were used as a control group and were administered with vehicle. At the end of the study (day-14 of treatment), mice were euthanized, and tumor samples were retrieved and weighed. Compound **1.8i** exhibited a significant reduction in tumor mass compared to vehicle. (**Figure 1.28**).

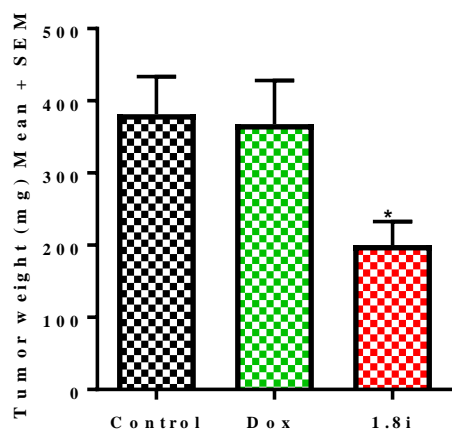


Figure 1.28: Anticancer efficacy study in 4T1 tumor model

1.3 Conclusions

In conclusion, we synthesized several carboxy indazole based diphenyl ureas. Evaluation of these inhibitors showed good cell proliferation inhibition on five cell lines of different cancer types, murine metastatic breast cancer cell line 4T1, murine glioma cell line GL261-luc2, human triple negative breast cancer cell line MDA-MB-231, human pancreatic cancer cell line MIAPaCa-2, and human colorectal adenocarcinoma cell line WiDr. Furthermore, we evaluated lead compounds **1.5i** and **1.8i** for their potential to inhibit tube formation in HUVEC cells. We found that compounds **1.5i** and **1.8i** significantly reduced the length of the tubes. After demonstrating inhibition of cellular proliferation and the ability of

endothelial cells to assemble in tube we translated to in vivo models. For this we first evaluated systemic toxicity in CD-1 mice for compounds **1.5i**, **1.7i**, and **1.8i** and found no significant body weight changes or noticeable behavioral changes. Anticancer efficacy studies in colorectal adenocarcinoma cell line WiDr and metastatic murine breast cancer 4T1 flank models showed that the lead candidate compound **1.8i** provided anticancer efficacy at a clinically relevant dosage of 25mg/Kg ip. Further investigations of these compounds can focus on pharmacokinetic/pharmacodynamic and combination therapies.

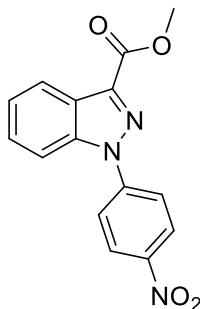
1.4 Experimental

1.4a Chemicals and methods of compound characterization

Indazole methyl carboxylate, 4-fluoronitrobenzene, EDC, and HOBT were acquired from Fisher Scientific, isocyanates, cyanoacetic acid, and piperidine were purchased from Millipore-Sigma, All other chemicals were of reagent grade quality and purchased from Millipore-Sigma. The ^1H - and ^{13}C -NMR spectra were recorded on a Varian Oxford-500 spectrometer. High-resolution mass spectra (HRMS) were recorded using a Bruker BioTOF II ESI mass spectrometer. Elemental analysis (CHN) results were obtained from Atlantic Microlab services.

1.4b Synthesis of methyl 1-(4-nitrophenyl)-1H-indazole-3-carboxylate (1.2):

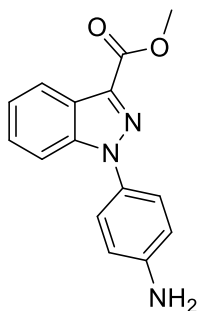
Synthesis of the precursor **1.1** was conducted by taking commercially available methyl 1H-indazole-3-carboxylate (10 mmol) and dissolving it in DMSO 50mL. 1-fluoro-4-nitrobenzene (11 mmol) was added to the solution. Potassium carbonate (30 mmol) was added to the solution, and the mixture was heated to 120 °C for 4hr. After cooling to room temperature, the solution was poured over ice. The resulting pale yellow solid **1.2** was allowed to dry and then stirred in hexanes followed by filtration a second time to afford the pure product.



^1H NMR (500 MHz, DMSO-d_6) δ 8.45 (d, $J = 9$ Hz, 2H), 8.22 (d, $J = 8$ Hz, 1H), 8.14 (d, $J = 9$ Hz, 2H), 8.05 (d, $J = 9$ Hz, 1H), 7.66 (t, $J = 8$ Hz, 1H), 7.51 (t, $J = 8$ Hz, 1H), 3.99 (s, 3H)

^{13}C NMR (126 MHz, DMSO-d_6) δ 162.3, 146.2, 144.2, 139.9, 138.2, 129.3, 125.8, 125.1, 124.6, 123.5, 122.5, 112.2, 52.7

1.4c Synthesis of methyl 1-(4-aminophenyl)-1H-indazole-3-carboxylate: Synthesis of 1.3 was conducted by taking 1.2 (10 mmol) and dissolving it in THF 50mL. Pd/C (0.5 g, 10% Pd) and ammonium formate (30 mmol) was added and the mixture was refluxed for 4hr. After completion of the reaction the mixture was filtered through silica gel and solution was evaporated under reduced pressure to afford the pure product.



^1H NMR (500 MHz, DMSO-d_6) δ 8.16 (d, $J = 8$ Hz, 1H), 7.67 (d, $J = 9$ Hz, 1H), 7.5 (t, $J=7$ Hz, 1H), 7.36 - 7.40 (m, 3H), 6.68 - 6.82 (m, 2H), 5.53 (s, 2H), 3.95 (s, 3H)

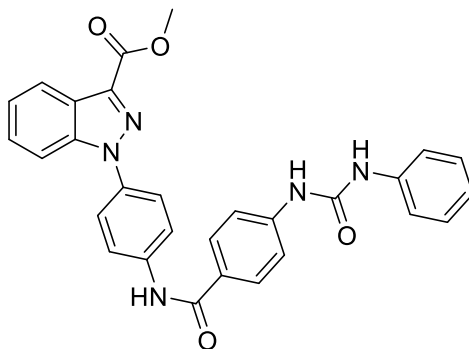
^{13}C NMR (126 MHz, DMSO-d_6) δ 162.9, 149.6, 140.3, 135.0, 127.9, 127.6, 125.4, 124.0, 123.8, 121.8, 114.4, 111.8, 52.2

1.4d Synthesis of 4-(3-phenylureido)benzoic acid (1.4a): Synthesis of 1.4a was conducted by taking 4-Aminobenzoic acid (10 mmol) and dissolving it in THF

(25mL) and a solution of phenyl isocyanate (10mmol) in THF (25mL) was added. After 30-60min the resulting solid was filtered and washed with additional portion of THF (10mL) to afford the pure product.

4-(3-(2-chlorophenyl)ureido)benzoic, 4-(3-(4-tolyl)ureido)benzoic, 4-(3-(4-(trifluoromethyl)phenyl)ureido)benzoic, 4-(3-(4-methoxyphenyl)ureido)benzoic, 4-(3-(4-fluorophenyl)ureido)benzoic, 4-(3-(4-chlorophenyl)ureido)benzoic, 4-(3-(2,4-dichlorophenyl)ureido)benzoic, 4-(3-(4-chloro-3(trifluoromethyl) phenyl)ureido)benzoic, 3,4,5-OCH₃ 4-(3-(3,4,5-trimethoxy phenyl)ureido)benzoic, 4-(3-cyclohexylureido)benzoic acids (1.4a-1.4k) were prepared using the same procedure as above with their corresponding isocyanates.

1.4e Synthesis of methyl 1-(4-(4-(3-phenylureido)benzamido)phenyl)-1H-indazole-3-carboxylate (1.5a): Synthesis of 1.5a was conducted by taking (PABA urea) (10 mmol) and dissolving it in DMF 50mL. triethylamine (30 mmol), EDC (11 mmol), and HOBt (11 mmol). Reaction mixture was stirred for 10 min before the addition of methyl 1-(4-aminophenyl)-1H-indazole-3-carboxylate (1.4a) (10.5 mmol). Reaction was warmed to 60 °C and stirred overnight. After completion of reaction mixture was poured over ice and filtered. Solid was recrystallized in acetone to afford the pure product.

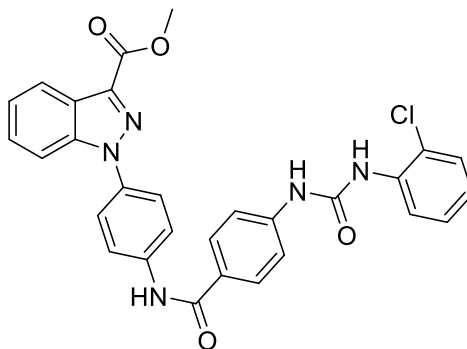


¹H NMR (500 MHz, DMSO-d₆) δ 10.39 (br. s., 1H), 9.06 (br. s., 1H), 8.81 (br. s., 1H), 8.23 (d, *J* = 8 Hz, 1H), 8.08 - 8.11 (m, 2H), 7.99 - 8.02 (m, 2H), 7.90 (d, *J* = 8 Hz, 1H), 7.82 (br. s., 2H), 7.61 - 7.67 (m, 3H), 7.50 (d, *J* = 6 Hz, 3H), 7.33 (d, *J* = 7 Hz, 2H), 7.02 (d, *J* = 6 Hz, 1H), 3.99 (s, 3H)

¹³C NMR (126 MHz, DMSO-d₆) δ 165.6, 162.8, 152.8, 143.6, 140.1, 139.9, 139.7, 136.2, 134.3, 129.4, 129.3, 128.5, 127.9, 124.5, 124.2, 124.1, 122.6, 122.1, 121.5, 118.9, 117.6, 111.9, 52.4

HRMS (ESI) m/z: calc'd for C₂₉H₂₃N₅O₄ [M+H]⁺: 506.1823, found 506.1556

1.4f Synthesis of methyl 1-(4-(4-(3-(2-chlorophenyl))benzamido)phenyl)-1H-indazole-3-carboxylate (1.5b): Synthesis of 1.5b was conducted by taking (paba urea) (10 mmol) and dissolving it in DMF 50mL. triethylamine (30 mmol), EDC (11 mmol), and HOBt (11 mmol). Reaction mixture was stirred for 10 min before the addition of methyl 1-(4-aminophenyl)-1H-indazole-3-carboxylate (1.3) (10.5 mmol). Reaction was warmed to 60 °C and stirred overnight. After completion of reaction mixture was poured over ice and filtered. Solid was recrystallized in acetone to afford the pure product.

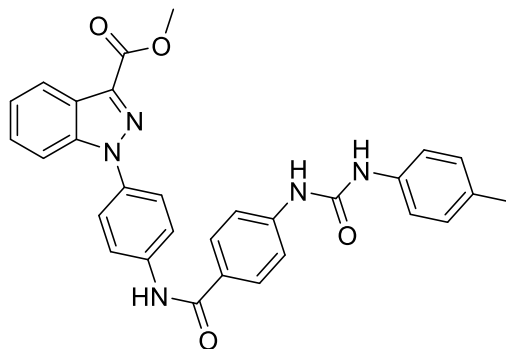


^1H NMR (500 MHz, DMSO- d_6) δ 10.41 (s, 1H), 9.77 (s, 1H), 8.44 (s, 1H), 8.19 (d, $J = 8$ Hz, 1H), 8.22 (d, $J = 8$ Hz, 1H), 8.09 (d, $J = 9$ Hz, 2H), 8.02 (d, $J = 9$ Hz, 2H), 7.88 (d, $J = 9$ Hz, 1H), 7.80 (d, $J = 9$ Hz, 2H), 7.56 - 7.72 (m, 3H), 7.44 - 7.53 (m, 2H), 7.33 (t, $J = 8$ Hz, 1H), 7.07 (t, $J = 8$ Hz, 1H), 3.99 (s, 3H)

^{13}C NMR (126 MHz, DMSO- d_6) δ 165.6, 162.8, 152.4, 143.3, 140.1, 139.7, 136.2, 136.1, 134.3, 129.7, 129.5, 128.4, 128.3, 128.1, 124.4, 124.2, 124.1, 124.1, 122.7, 122.1, 122.0, 121.5, 117.7, 111.9, 52.4

HRMS (ESI) m/z : calc'd for $\text{C}_{29}\text{H}_{22}\text{ClN}_5\text{O}_4$ $[\text{M}+\text{H}]^+$: 540.1433, found 540.1127

1.4g Synthesis of methyl 1-(4-(4-(3-(4-tolyl)benzamido)phenyl)-1H-indazole-3-carboxylate (1.5c): Synthesis of 1.5c was conducted by taking (paba urea) (10 mmol) and dissolving it in DMF 50mL. triethylamine (30 mmol), EDC (11 mmol), and HOBT (11 mmol). Reaction mixture was stirred for 10 min before the addition of methyl 1-(4-aminophenyl)-1H-indazole-3-carboxylate (1.3) (10.5 mmol). Reaction was warmed to 60 °C and stirred overnight. After completion of reaction mixture was poured over ice and filtered. Solid was recrystallized in acetone to afford the pure product.

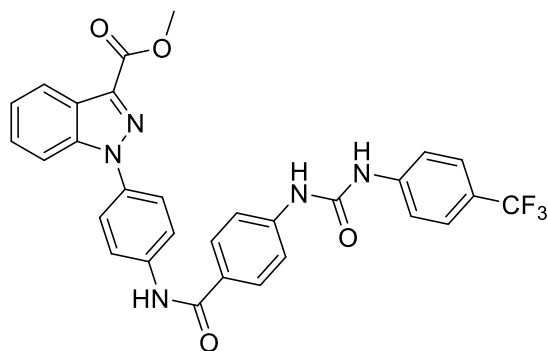


^1H NMR (500 MHz, DMSO- d_6) δ 10.37 (s, 1H), 9.00 (s, 1H), 8.69 (s, 1H), 8.22 (d, $J = 8$ Hz, 1H), 8.08 (d, $J = 9$ Hz, 2H), 7.98 (d, $J = 9$ Hz, 2H), 7.88 (d, $J = 8$ Hz, 1H), 7.80 (d, $J = 9$ Hz, 2H), 7.55 - 7.67 (m, 3H), 7.43 - 7.50 (m, 1H), 7.37 (d, $J = 8$ Hz, 2H), 7.11 (d, $J = 8$ Hz, 2H), 3.99 (s, 3H), 2.26 (s, 3H)

^{13}C NMR (126 MHz, DMSO- d_6) δ 165.6, 162.8, 152.8, 143.7, 140.1, 139.7, 137.3, 136.2, 134.3, 131.5, 129.7, 129.4, 128.5, 127.8, 124.5, 124.2, 124.1, 122.1, 121.5, 119.0, 117.6, 111.9, 52.4, 20.8

HRMS (ESI) m/z : calc'd for $\text{C}_{30}\text{H}_{25}\text{N}_5\text{O}_4$ $[\text{M}+\text{H}]^+$: 520.1979, found 520.1707

1.4h Synthesis of methyl 1-(4-(4-(3-(4-(trifluoromethyl))benzamido)phenyl)-1H-indazole-3-carboxylate)phenyl)-1H-indazole-3-carboxylate (1.5d): Synthesis of 1.5d was conducted by taking (paba urea) (10 mmol) and dissolving it in DMF 50mL. triethylamine (30 mmol), EDC (11 mmol), and HOBT (11 mmol). Reaction mixture was stirred for 10 min before the addition of methyl 1-(4-aminophenyl)-1H-indazole-3-carboxylate (1.3) (10.5 mmol). Reaction was warmed to 60 °C and stirred overnight. After completion of reaction mixture was poured over ice and filtered. Solid was recrystallized in acetone to afford the pure product.

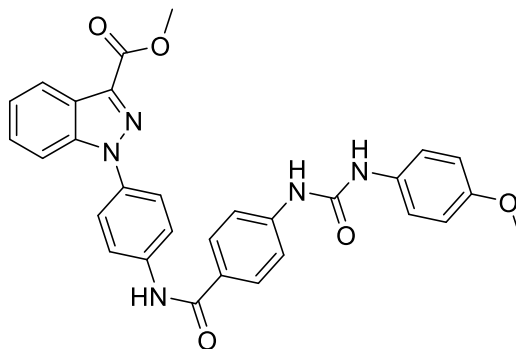


^1H NMR (500 MHz, DMSO- d_6) δ 10.40 (s, 1H), 9.22 (s, 1H), 9.18 (s, 1H), 8.22 (d, $J = 8$ Hz, 1H), 8.08 (d, $J = 9$ Hz, 2H), 8.00 (d, $J = 9$ Hz, 2H), 7.88 (d, $J = 9$ Hz, 1H), 7.80 (d, $J = 9$ Hz, 2H), 7.62 - 7.72 (m, 6H), 7.59 (t, $J = 7$ Hz, 1H), 7.47 (t, $J = 7$ Hz, 1H), 3.99 (s, 3H)

^{13}C NMR (126 MHz, DMSO- d_6) δ 165.6, 162.8, 152.6, 143.7, 143.2, 140.1, 139.7, 136.2, 134.3, 129.4, 128.5, 128.3, 126.6, 126.1, 126.1, 124.3 (q), 122.6 (q), 122.1, 121.5, 118.5, 117.9, 111.9, 52.4

HRMS (ESI) m/z : calc'd for $\text{C}_{30}\text{H}_{22}\text{F}_3\text{N}_5\text{O}_4$ $[\text{M}+\text{H}]^+$: 574.1697, found 574.1376

1.4i Synthesis of methyl 1-(4-(4-(3-(4-methoxyphenyl)benzamido)phenyl)-1H-indazole-3-carboxylate)phenyl)-1H-indazole-3-carboxylate (1.5e): Synthesis of 1.5e was conducted by taking (PABA urea) (10 mmol) and dissolving it in DMF 50mL. triethylamine (30 mmol), EDC (11 mmol), and HOBt (11 mmol). Reaction mixture was stirred for 10 min before the addition of methyl 1-(4-aminophenyl)-1H-indazole-3-carboxylate (1.3) (10.5 mmol). Reaction was warmed to 60 °C and stirred overnight. After completion of reaction mixture was poured over ice and filtered. Solid was recrystallized in acetone to afford the pure product.

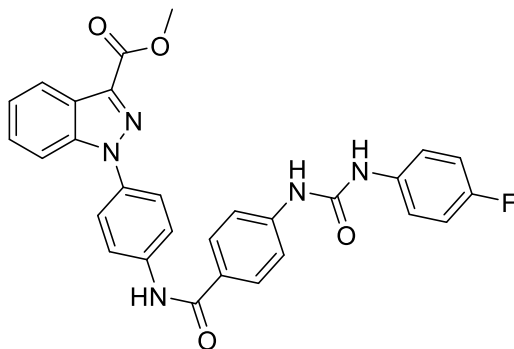


^1H NMR (500 MHz, DMSO- d_6) δ 10.37 (s, 1H), 8.97 (s, 1H), 8.61 (s, 1H), 8.22 (d, $J = 8$ Hz, 1H), 8.08 (d, $J = 9$ Hz, 2H), 7.98 (d, $J = 8$ Hz, 2H), 7.88 (d, $J = 9$ Hz, 1H), 7.80 (d, $J = 9$ Hz, 2H), 7.55 - 7.66 (m, 3H), 7.46 (t, $J = 8$ Hz, 1H), 7.35 - 7.42 (m, 2H), 6.90 (d, $J = 8$ Hz, 2H), 3.99 (s, 3H), 3.73 (s, 3H)

^{13}C NMR (126 MHz, DMSO- d_6) δ 165.7, 162.8, 155.2, 152.9, 143.8, 140.1, 139.7, 136.2, 134.3, 132.8, 129.4, 128.4, 127.7, 124.4, 124.2, 124.1, 122.1, 121.5, 120.7, 117.5, 114.5, 111.9, 55.7, 52.4

HRMS (ESI) m/z : calc'd for $\text{C}_{30}\text{H}_{25}\text{N}_5\text{O}_5$ $[\text{M}+\text{H}]^+$: 536.1928, found 536.1628

1.4j Synthesis of methyl 1-(4-(4-(3-(4-fluorophenyl))benzamido)phenyl)-1H-indazole-3-carboxylate (1.5f): Synthesis of 1.5f was conducted by taking (PABA urea) (10 mmol) and dissolving it in DMF 50mL. triethylamine (30 mmol), EDC (11 mmol), and HOBt (11 mmol). Reaction mixture was stirred for 10 min before the addition of methyl 1-(4-aminophenyl)-1H-indazole-3-carboxylate (1.3) (10.5 mmol). Reaction was warmed to 60 °C and stirred overnight. After completion of reaction mixture was poured over ice and filtered. Solid was recrystallized in acetone to afford the pure product.

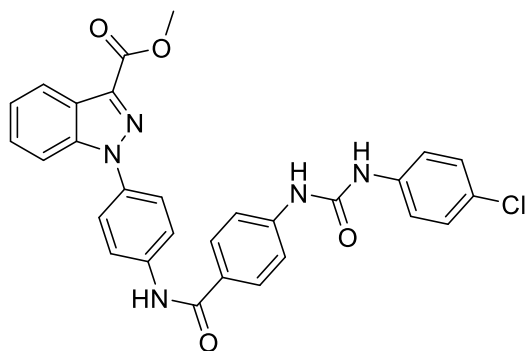


^1H NMR (500 MHz, DMSO- d_6) δ 10.38 (s, 1H), 9.05 (s, 1H), 8.83 (s, 1H), 8.22 (d, $J = 8$ Hz, 1H), 8.07 (d, $J = 9$ Hz, 2H), 7.98 (d, $J = 9$ Hz, 2H), 7.88 (d, $J = 9$ Hz, 1H), 7.80 (d, $J = 9$ Hz, 2H), 7.55 - 7.67 (m, 3H), 7.40 - 7.53 (m, 3H), 7.09 - 7.21 (m, 2H), 3.99 (s, 3H)

^{13}C NMR (126 MHz, DMSO- d_6) δ 165.6, 162.8, 158.9, 157.0, 152.9, 143.6, 140.1, 139.7, 136.2, 134.3, 129.4, 128.5, 127.9, 124.5, 124.2, 124.1, 122.1, 121.5, 120.7, 120.7, 117.7, 115.9, 115.7, 111.9, 52.4

HRMS (ESI) m/z : calc'd for $\text{C}_{29}\text{H}_{22}\text{FN}_5\text{O}_4$ $[\text{M}+\text{H}]^+$: 524.1729, found 524.1447

1.4k Synthesis of methyl 1-(4-(4-(3-(4-chlorophenyl))benzamido)phenyl)-1H-indazole-3-carboxylate (1.5g): Synthesis of 1.5g was conducted by taking (PABA urea) (10 mmol) and dissolving it in DMF 50mL. triethylamine (30 mmol), EDC (11 mmol), and HOBt (11 mmol). Reaction mixture was stirred for 10 min before the addition of methyl 1-(4-aminophenyl)-1H-indazole-3-carboxylate (1.3) (10.5 mmol). Reaction was warmed to 60 °C and stirred overnight. After completion of reaction mixture was poured over ice and filtered. Solid was recrystallized in acetone to afford the pure product.

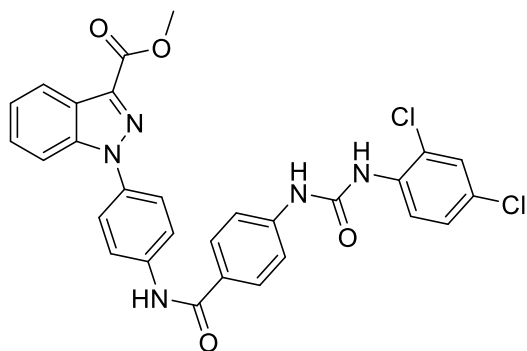


^1H NMR (500 MHz, DMSO- d_6) δ 10.38 (s, 1H), 9.08 (s, 1H), 8.94 (s, 1H), 8.21 (d, $J = 8$ Hz, 1H), 8.08 (d, $J = 9$ Hz, 2H), 7.99 (d, $J = 8$ Hz, 2H), 7.87 (d, $J = 8$ Hz, 1H), 7.79 (d, $J = 9$ Hz, 2H), 7.63 (d, $J = 9$ Hz, 2H), 7.59 (t, $J = 8$ Hz, 1H), 7.49 - 7.55 (m, 2H), 7.42 - 7.48 (m, 1H), 7.35 (d, $J = 9$ Hz, 2H), 3.98 (s, 3H)

^{13}C NMR (126 MHz, DMSO- d_6) δ 165.6, 162.8, 152.7, 143.4, 140.1, 139.7, 138.9, 136.2, 134.3, 129.4, 129.1, 128.4, 128.1, 126.1, 124.4, 124.2, 124.1, 122.1, 121.5, 120.4, 117.8, 111.9, 52.4

HRMS (ESI) m/z : calc'd for $\text{C}_{29}\text{H}_{22}\text{ClN}_5\text{O}_4$ $[\text{M}+\text{H}]^+$: 540.1433, found 540.1137

1.4l Synthesis of methyl 1-(4-(4-(3-(2,4-dichlorophenyl))benzamido)phenyl)-1H-indazole-3-carboxylate (1.5i): Synthesis of 1.5i was conducted by taking (PABA urea) (10 mmol) and dissolving it in DMF 50mL. triethylamine (30 mmol), EDC (11 mmol), and HOBt (11 mmol). Reaction mixture was stirred for 10 min before the addition of methyl 1-(4-aminophenyl)-1H-indazole-3-carboxylate (1.3) (10.5 mmol). Reaction was warmed to 60 °C and stirred overnight. After completion of reaction mixture was poured over ice and filtered. Solid was recrystallized in acetone to afford the pure product.

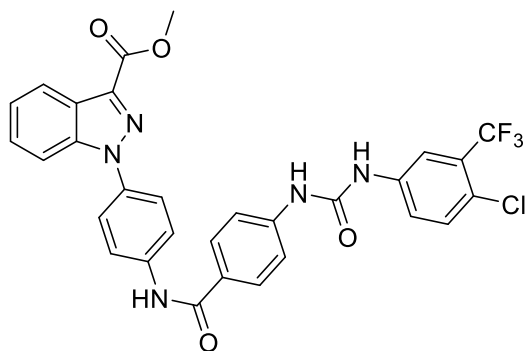


^1H NMR (500 MHz, DMSO- d_6) δ 10.40 (s, 1H), 9.85 (s, 1H), 8.57 (s, 1H), 8.18 - 8.24 (m, 2H), 8.05 - 8.11 (m, 2H), 8.01 (d, J = 9 Hz, 2H), 7.88 (d, J = 9 Hz, 1H), 7.77 - 7.82 (m, 2H), 7.61 - 7.67 (m, 3H), 7.55 - 7.61 (m, 1H), 7.44 - 7.49 (m, 1H), 7.41 (d, J = 9 Hz, 1H), 3.98 (s, 3H)

^{13}C NMR (126 MHz, DMSO- d_6) δ 165.6, 162.8, 152.3, 143.1, 140.1, 139.7, 136.2, 135.4, 134.3, 129.5, 129.1, 128.5, 128.4, 128.2, 126.9, 124.5, 124.2, 124.1, 123.4, 122.8, 122.1, 121.5, 117.8, 111.9, 52.4

HRMS (ESI) m/z : calc'd for $\text{C}_{29}\text{H}_{21}\text{Cl}_2\text{N}_5\text{O}_4$ $[\text{M}+\text{H}]^+$: 574.1043 , found 574.0724

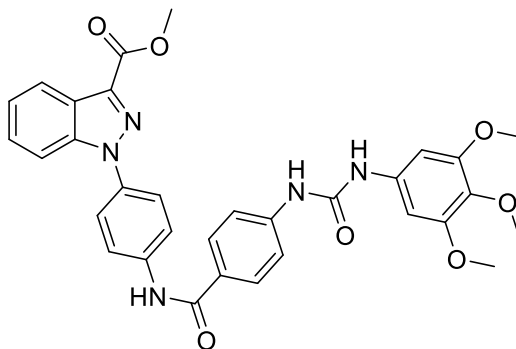
1.4m Synthesis of methyl 1-(4-(4-(3-phenylureido)benzamido)phenyl)-1H-indazole-3-carboxylate (1.5i) Synthesis of **1.5i** was conducted by taking (PABA urea) (10 mmol) and dissolving it in DMF 50mL. triethylamine (30 mmol), EDC (11 mmol), and HOBt (11 mmol). Reaction mixture was stirred for 10 min before the addition of methyl 1-(4-aminophenyl)-1H-indazole-3-carboxylate (**1.3**) (10.5 mmol). Reaction was warmed to 60 °C and stirred overnight. After completion of reaction mixture was poured over ice and filtered. Solid was recrystallized in acetone to afford the pure product.



^1H NMR (500 MHz, DMSO- d_6) δ 10.40 (s, 1H), 9.28 (s, 1H), 9.22 (s, 1H), 8.18 - 8.24 (m, 1H), 8.14 (s, 1H), 8.08 (d, J = 8 Hz, 2H), 8.00 (d, J = 8 Hz, 2H), 7.88 (d, J = 8 Hz, 1H), 7.80 (d, J = 8 Hz, 2H), 7.54 - 7.71 (m, 5H), 7.46 (t, J = 8 Hz, 1H), 3.98 (s, 3H)

^{13}C NMR (126 MHz, DMSO- d_6) δ 165.6, 162.8, 152.7, 143.1, 140.1, 139.7, 139.5, 136.2, 134.3, 132.5, 129.4, 128.5-127.1(q), 124.4 (q), 124.2, 124.1, 123.7, 123.1, 122.2, 122.1, 121.5, 120.0, 118.1, 117.4, 117.4, 111.9, 52.4

1.4n Synthesis of methyl 1-(4-(4-(3-(4-chloro-3-(trimethoxy)phenyl) benzamido) phenyl)-1H-indazole-3-carboxylate (1.5j): Synthesis of 1.5j was conducted by taking (PABA urea) (10 mmol) and dissolving it in DMF 50mL. triethylamine (30 mmol), EDC (11 mmol), and HOBt (11 mmol). Reaction mixture was stirred for 10 min before the addition of methyl 1-(4-aminophenyl)-1H-indazole-3-carboxylate (1.3) (10.5 mmol). Reaction was warmed to 60 °C and stirred overnight. After completion of reaction mixture was poured over ice and filtered. Solid was recrystallized in acetone to afford the pure product.

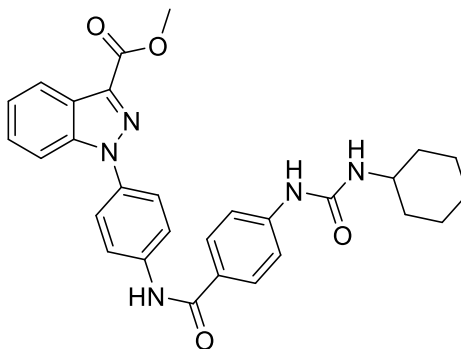


^1H NMR (500 MHz, DMSO- d_6) δ 10.37 (s, 1H), 8.99 (s, 1H), 8.74 (s, 1H), 8.22 (d, $J = 8$ Hz, 1H), 8.07 (d, $J = 9$ Hz, 2H), 7.98 (d, $J = 9$ Hz, 2H), 7.88 (d, $J = 8$ Hz, 1H), 7.80 (d, $J = 9$ Hz, 2H), 7.55 - 7.66 (m, 3H), 7.40 - 7.51 (m, 1H), 6.82 (s, 2H), 3.97 (s, 3H), 3.76 (s, 6H), 3.61 (s, 3H)

^{13}C NMR (126 MHz, DMSO- d_6) δ 165.6, 162.8, 153.4, 152.7, 143.5, 140.1, 139.7, 136.2, 136.0, 134.3, 133.2, 129.4, 128.4, 127.9, 124.4, 124.2, 124.1, 122.1, 121.5, 117.7, 111.9, 96.7, 60.6, 56.2, 52.4

HRMS (ESI) m/z : calc'd for $\text{C}_{32}\text{H}_{29}\text{N}_5\text{O}_7$ $[\text{M}+\text{H}]^+$: 596.2140 , found 596.1865

1.4o Synthesis of methyl 1-(4-(4-(3-cyclohexylureido))benzamido)phenyl)-1H-indazole-3-carboxylate (1.5k): Synthesis of 1.5k was conducted by taking (PABA urea) (10 mmol) and dissolving it in DMF 50mL. triethylamine (30 mmol), EDC (11 mmol), and HOBT (11 mmol). Reaction mixture was stirred for 10 min before the addition of methyl 1-(4-aminophenyl)-1H-indazole-3-carboxylate (1.3) (10.5 mmol). Reaction was warmed to 60 °C and stirred overnight. After completion of reaction mixture was poured over ice and filtered. Solid was recrystallized in acetone to afford the pure product.

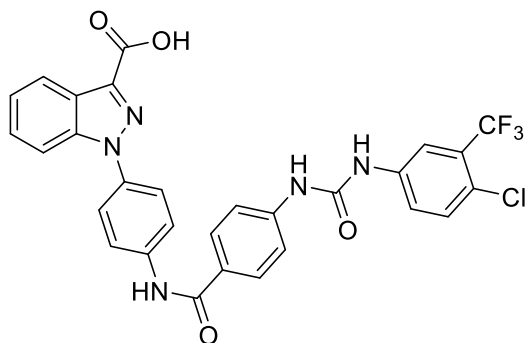


^1H NMR (500 MHz, DMSO- d_6) δ 10.32 (s, 1H), 8.68 (s, 1H), 8.21 (d, J = 8 Hz, 1H), 8.07 (d, J = 9 Hz, 2H), 7.93 (d, J = 9 Hz, 2H), 7.87 (d, J = 8 Hz, 1H), 7.78 (d, J = 9 Hz, 2H), 7.50 - 7.61 (m, 3H), 7.37 - 7.48 (m, 1H), 6.23 (d, J = 8 Hz, 1H), 3.98 (s, 3H), 3.43 - 3.55 (m, 1H), 2.08 (s, 1H), 1.77 - 1.86 (m, 2H), 1.68-1.50 (m, 3H), 1.25 - 1.38 (m, 2H), 1.13 - 1.24 (m, 3H)

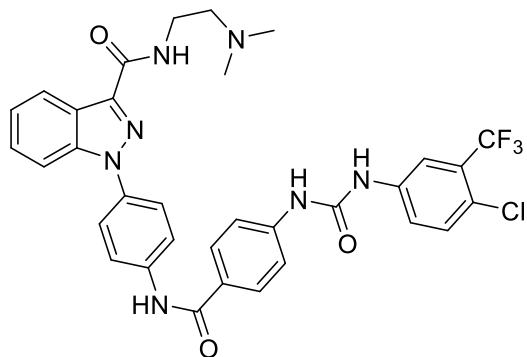
^{13}C NMR (126 MHz, DMSO- d_6) δ 165.7, 162.8, 154.5, 144.4, 140.1, 139.8, 136.1, 134.2, 129.3, 128.4, 127.0, 124.4, 124.2, 124.1, 122.1, 121.4, 116.9, 111.9, 52.4, 48.2, 33.3, 25.7, 24.8

HRMS (ESI) m/z: calc'd for $\text{C}_{29}\text{H}_{29}\text{N}_5\text{O}_4$ $[\text{M}+\text{H}]^+$: 512.2292, found 512.2034

1.4p Synthesis of 1-(4-(4-(3-(4-chloro-3-(trifluoromethyl)phenyl)ureido)benzamide)phenyl)-1H-indazole-3-carboxylic acid (**1.6i**): Synthesis of **1.6i** was conducted by taking (**1.5i**) (5 mmol) and dissolving it in DMSO 30mL. 2.5 M NaOH (5mL) was added and the reaction mixture was heated. Upon completion of hydrolysis reaction mixture was poured over ice and acidified with 3 M HCl dropwise. Solid was filtered and recrystallized with acetone to afford the pure product



1.4q Synthesis of 1-(4-(4-(3-(4-chloro-3-(trifluoromethyl)phenyl)ureido)benzamido)phenyl)-N-(2-(dimethylamino)ethyl)-1H-indazole-3-carboxamide (**1.7i**): Synthesis of **1.7i** was conducted by taking **1.6i** (2 mmol) and dissolving it in DMF 10mL. Triethylamine (2.2 mmol), EDC (2.2 mmol), and HOBt (2.2 mmol) was added to the solution. The reaction mixture was stirred for 10 min before the addition of N,N'-Dimethylethylenediamine (2.5 mmol). Reaction was warmed to 60 °C and stirred overnight. After completion of reaction, the mixture was poured over ice and filtered. Resulting solid was recrystallized in ethyl acetate.

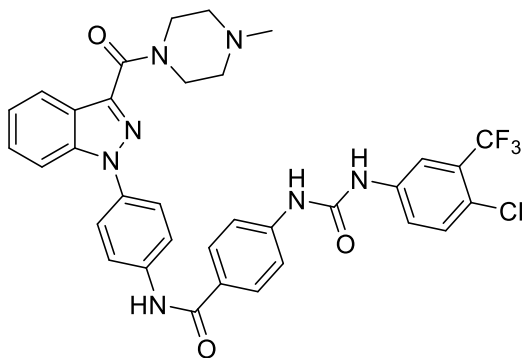


^1H NMR (500 MHz, DMSO- d_6) δ 10.37 (s, 1H), 9.39 (s, 1H), 9.31 (s, 1H), 8.36 (t, $J = 6$ Hz, 1H), 8.30 (d, $J = 8$ Hz, 1H), 8.13 (s, 1H), 8.05 (d, $J = 8$ Hz, 2H), 7.99 (d, $J = 8$ Hz, 2H), 7.77 - 7.84 (m, 4H), 7.60 - 7.69 (m, 4H), 7.54 (t, $J = 8$ Hz, 1H), 7.37 (t, $J = 8$ Hz, 1H), 3.41 - 3.47 (m, 2H), 2.45 - 2.51 (m, 2H), 2.21 (s, 6H)

^{13}C NMR (126 MHz, DMSO- d_6) δ 165.5, 162.1, 152.7, 143.1, 140.1, 139.6, 139.4, 139.3, 134.6, 132.5, 129.3, 128.4, 128.3, 124.0, 123.7(q), 123.6, 123.5, 123.0(q), 122.7, 121.4, 118.0, 117.4, 117.4, 111.4, 58.5, 45.5, 36.9

HRMS (ESI) m/z: calc'd for $\text{C}_{33}\text{H}_{29}\text{ClF}_3\text{N}_7\text{O}_3$ $[\text{M}+\text{H}]^+$: 664.2045, found 664.1690

1.4r 4-(3-(4-chloro-3-(trifluoromethyl)phenyl)ureido)-N-(4-(3-(4-methyl piperazine-1-carbonyl)-1H-indazol-1-yl)phenyl)benzamide (**1.8i**): Synthesis of **1.8i** was conducted by taking (**1.6i**) (2 mmol) and dissolving it in DMF 10mL. Triethylamine (2.2 mmol), EDC (2.2 mmol), and HOBt (2.2 mmol) was added to the solution. The reaction mixture was stirred for 10 min before the addition of N methyl piperazine (2.5 mmol). Reaction was warmed to 60 °C and stirred overnight. After completion of reaction, the mixture was poured over ice and filtered. Resulting solid was recrystallized in ethyl acetate.



^1H NMR (500 MHz, DMSO- d_6) δ 10.37 (s, 1H), 9.32 (s, 1H), 9.26 (s, 1H), 8.14 (d, $J = 1.95$ Hz, 1H), 8.02 - 8.09 (m, 3H), 8.02 - 8.03 (m, 1H), 7.99 (d, $J = 8.79$ Hz, 2H), 7.85 (d, $J = 8.30$ Hz, 1H), 7.78 (d, $J = 8.79$ Hz, 2H), 7.61 - 7.71 (m, 5H), 7.55 (t, $J = 7.56$ Hz, 1H), 7.32 - 7.40 (m, 1H), 3.97 (br. s., 2H), 3.76 (br. s., 2H), 3.34 (br. s., 1H), 2.33 - 2.46 (m, 4H), 2.22 (s, 3H)

^{13}C NMR (126 MHz, DMSO- d_6) δ 165.6, 161.8, 152.7, 143.1, 140.1, 139.6, 139.3, 139.1, 134.7, 132.5, 129.3, 128.5, 128.4, 127.3(q), 127.1, 123.8, 123.3, 122.4, 122.2, 121.6, 118.1, 117.4, 111.3, 55.7, 54.9, 47.0, 46.1, 42.3, 31.2

HRMS (ESI) m/z: calc'd for $\text{C}_{34}\text{H}_{29}\text{ClF}_3\text{N}_7\text{O}_3$ $[\text{M}+\text{H}]^+$: 676.2045, found 676.1673

1.4s Cell lines and culture conditions

4T1 cells were purchased from Caliper Life Sciences and were cultured in RPMI-1650 supplemented with FBS (10%) and penicillin-streptomycin (50 U/mL, 50 $\mu\text{g}/\text{mL}$).

GL261-luc2 cells were purchased from Perkin-Elmer and cultured in DMEM supplemented with geneticin G418 (50 $\mu\text{g}/\text{mL}$), FBS (10%) and penicillin-streptomycin (50 U/mL, 50 $\mu\text{g}/\text{mL}$).

MDA-MB-231 cells were purchased from ATCC and were cultured in DMEM supplemented with FBS (10%, Atlanta Biologicals) and penicillin-streptomycin (50 U/mL, 50 $\mu\text{g}/\text{mL}$, Invitrogen).

MIAPaCa-2 cells were purchased from ATCC and were cultured in DMEM supplemented with FBS (10%, Atlanta Biologicals), Horse serum (1% Atlanta Biologicals), and penicillin-streptomycin (50 U/mL, 50 $\mu\text{g}/\text{mL}$, Invitrogen).

WiDr cells were purchased from ATCC and were cultured in MEM supplemented with FBS (10%) and penicillin-streptomycin (50 U/mL, 50 $\mu\text{g}/\text{mL}$).

HUVEC cells were purchased from ATCC and were cultured in F-12K supplemented with heparin (0.1mg/mL), endothelial grown supplement (1%)and FBS (10%)

1.4t MTT assay

Cells (5×10^3 cells/well) were cultured in 96-well plates and incubated for 18-24 hours. Stock solution of compound was made up at 100 mM concentration in DMSO. The final concentration of DMSO in the wells were $< 0.01\%$. Concentration range of compounds from 100 μM to 0.1 μM was tested by adding 2x concentration of test compound to the first well and then the serial dilutions by going from well to well. All the compounds were tested in duplicates. After 72 hours of treatment, 10 μL of MTT (5 mM in 1x PBS) was added into the wells and the cells were incubated for a period of 4 hours. At this point, the conversion of MTT to formazan was quenched by the addition of 100 μL of SDS (1 g of SDS dissolved in 0.01 N HCl) and the cells were incubated for further 4 hours. The absorbance was recorded at 570 nm using BioTek Synergy 2 plate reader. The absorbance is directly proportional to the cell viability. % Survival was calculated using the formula

$$\% \text{ survival} = (\text{absorbance of test compound} / \text{absorbance of control}) \times 100\%.$$

IC₅₀ was calculated using GraphPad Prism software, by plotting a dose-response curve with log[concentration] on x-axis and % survival on y-axis and analyzing via nonlinear regression with variable slope.

1.4u Endothelial Cell Tube Formation Assay

Culture plates were coated with Corning Matrigel Matrix (10mg/mL). HUVEC cells were plated at 4×10^5 cell/mL with 300 μL /well. Compound 1.5i and 1.8i were added to wells each at concentrations of 1 μM and 5 μM . Cells were then allowed to incubate for a period of 18-24 hours. Media was then gently

aspirated as to not disrupt the formation of tubes and then washed with 750 μ L of HBSS 2x. Cells were labeled by adding 300 μ L/well of 8 μ g/mL Corning Calcein AM in HBSS and incubate plates for 30 to 40 minutes at 37°C, 5% CO₂. Once again cells were washed with HBSS. Cells were then imaged on a fluorescence microscope and tube length was measured.

1.4v *Ethical Considerations for animal studies*

The experimental procedures involving animals that were conducted at the University of Minnesota Duluth were in compliance with the U.S. National Institutes of Health Guide for Care and Use of Laboratory Animals and approved by the Institutional Animal Care and Use Committee at the University of Minnesota (UMN).

1.4w *General procedure for systemic toxicity evaluation*

Mice were procured from Charles River, and acclimatized at room temperature for a period of 7 days. The mice were weighed and randomized into groups (n = 6 mice per group) based on same average weights. Mice were housed as two mice per cage. Treatment was started via i.p. and body weights were monitored for a period of 14-21 days. At the end of the study, mice were euthanized using CO₂.

1.4x *Anticancer efficacy of compound 1.5i, 1.7i, and 1.8i in WiDr flank model*

5×10^6 WiDr cells were suspended in a mixture of 1:1 matrigel-PBS (100 μ L). These cells were then injected subcutaneously onto the right flank of athymic nude mice and tumors were measured via calipers and the tumor volume was calculated using the formula

$$V = \frac{1}{2} \times a \times b^2$$

where 'a' is the long diameter of the tumor and 'b' is the short diameter of the tumor. Mice were assigned into groups (n = 8 mice per group) when the average tumor volume reached ~100-200 mm³ and the treatment was initiated and continued for a period of 21 days. Tumor volume was recorded every 2-3 days and at the end of the study, mice were euthanized, and tumors were resected and weighed. The tumor growth inhibition amount was determined using the formula

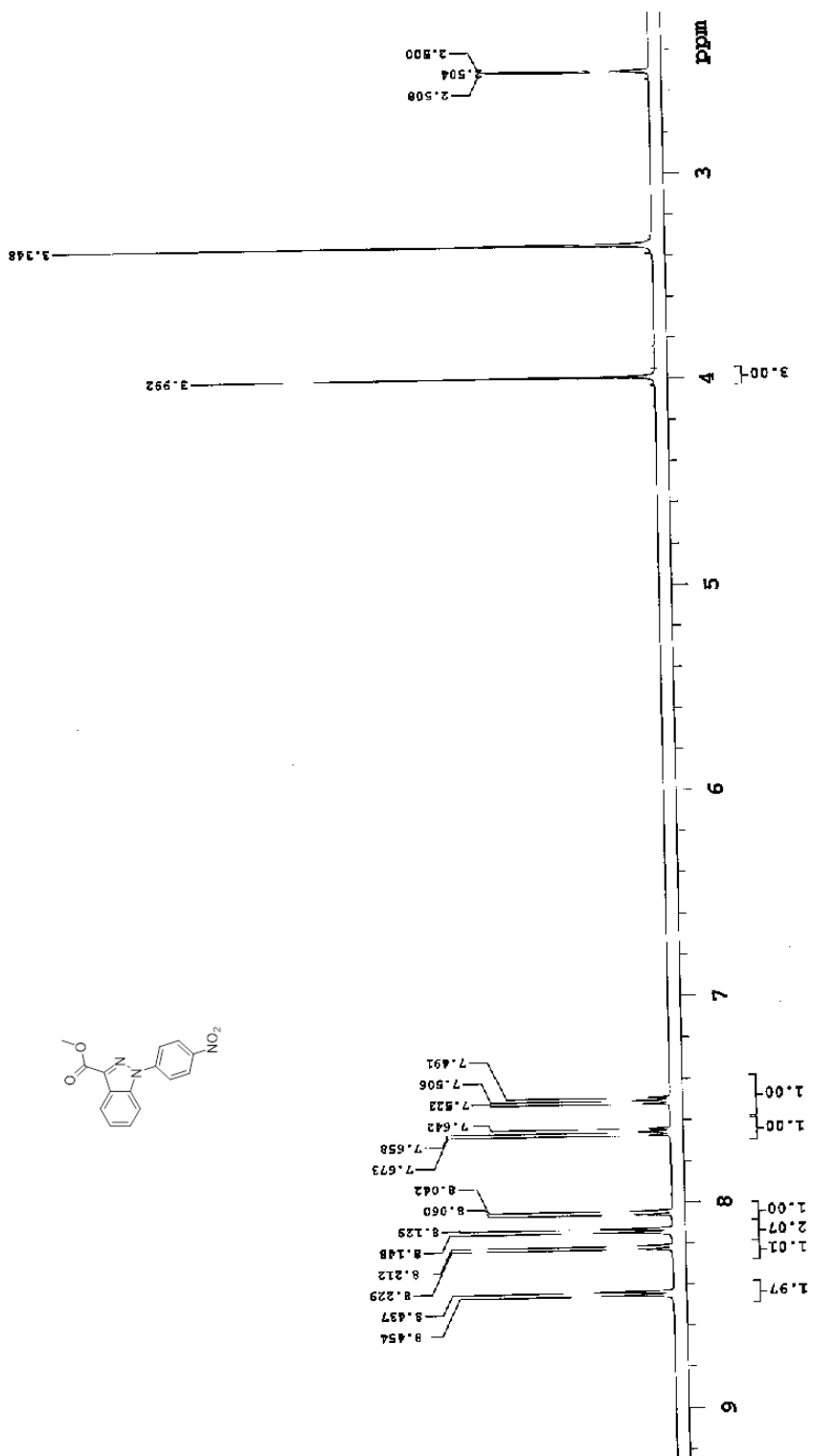
$$\% \text{ inhibition} = \frac{(C-T)}{C} \times 100$$

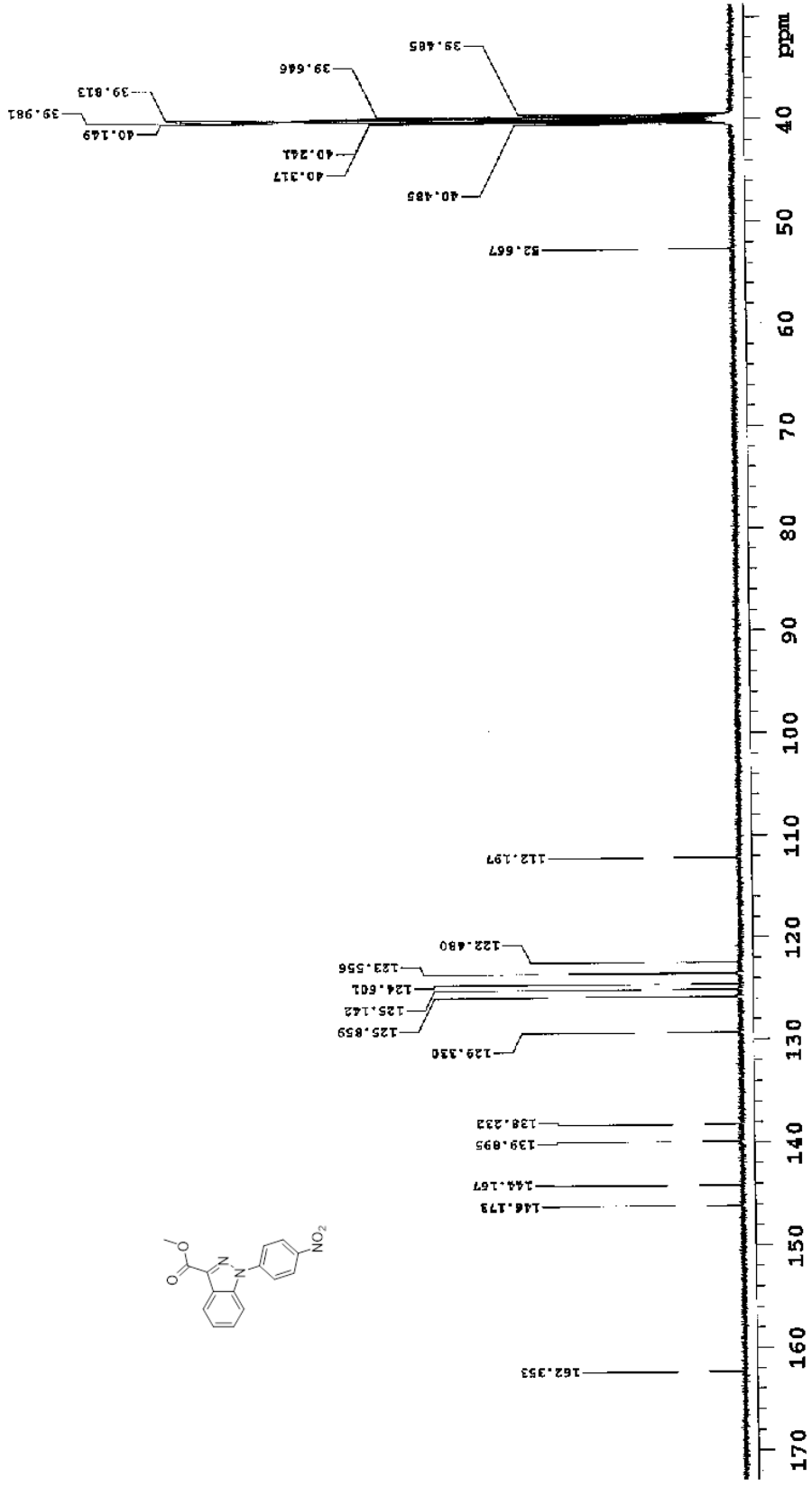
where C is average tumor weight of the control group and T is the average tumor weight of the test group.

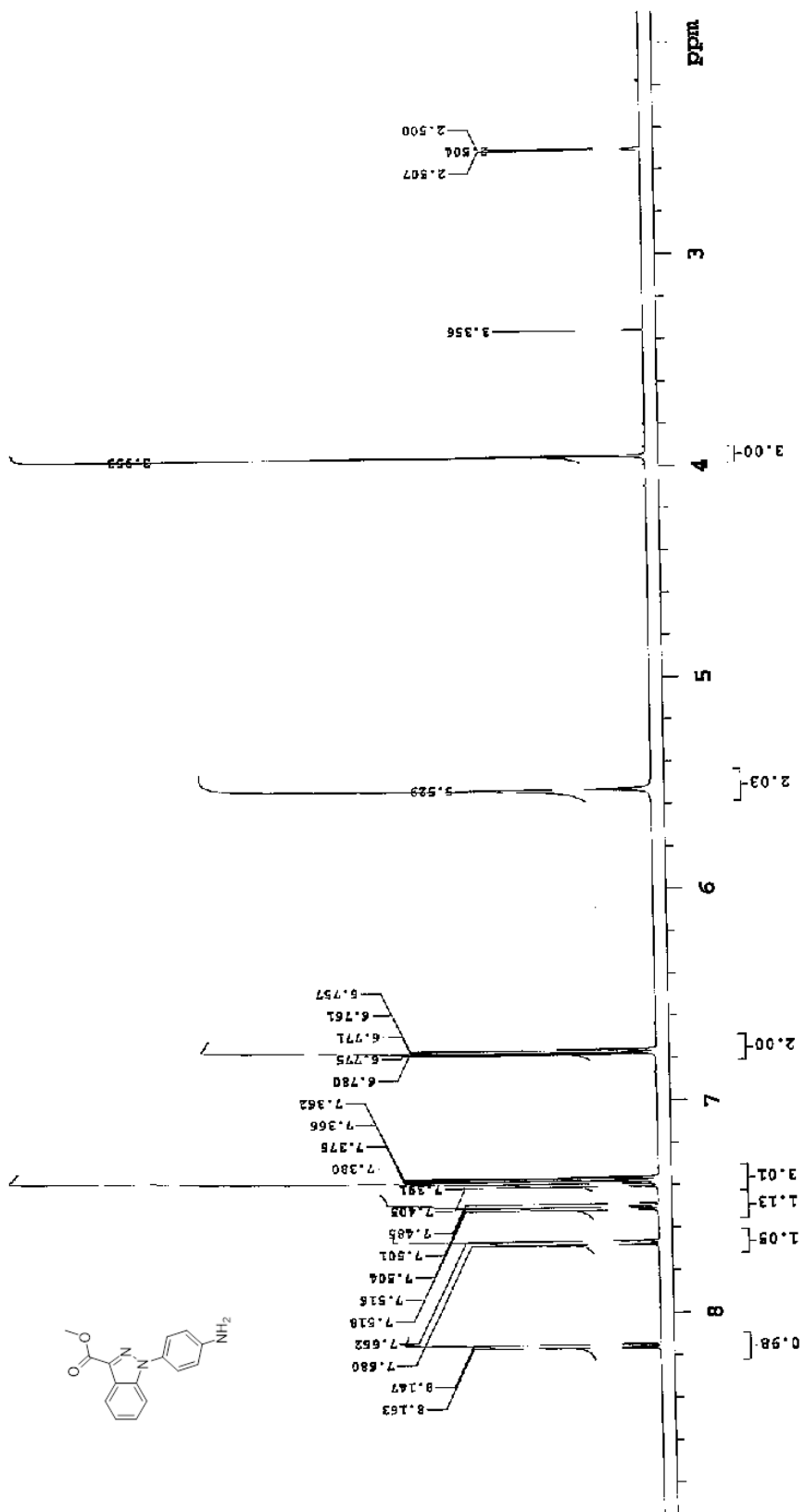
1.4y Anticancer efficacy of compound 1.8i in 4T1 flank model:

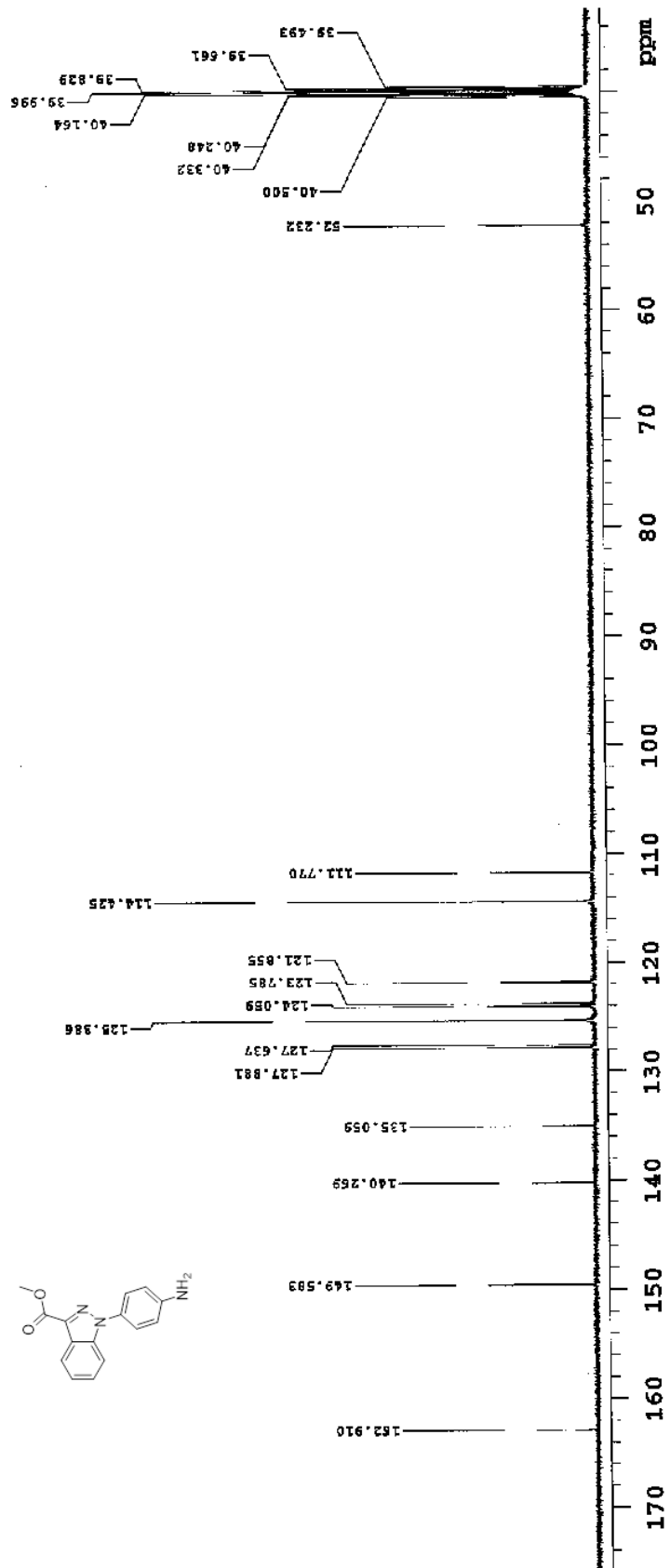
5 x 10⁴ 4T1 cells were suspended in a mixture of 1:1 matrigel-PBS (100μL). These cells were then injected subcutaneously onto the right flank of Balb/C mice and tumors were measured via calipers. Volumes and measurements were carried out the same as the WiDr efficacy model described above.

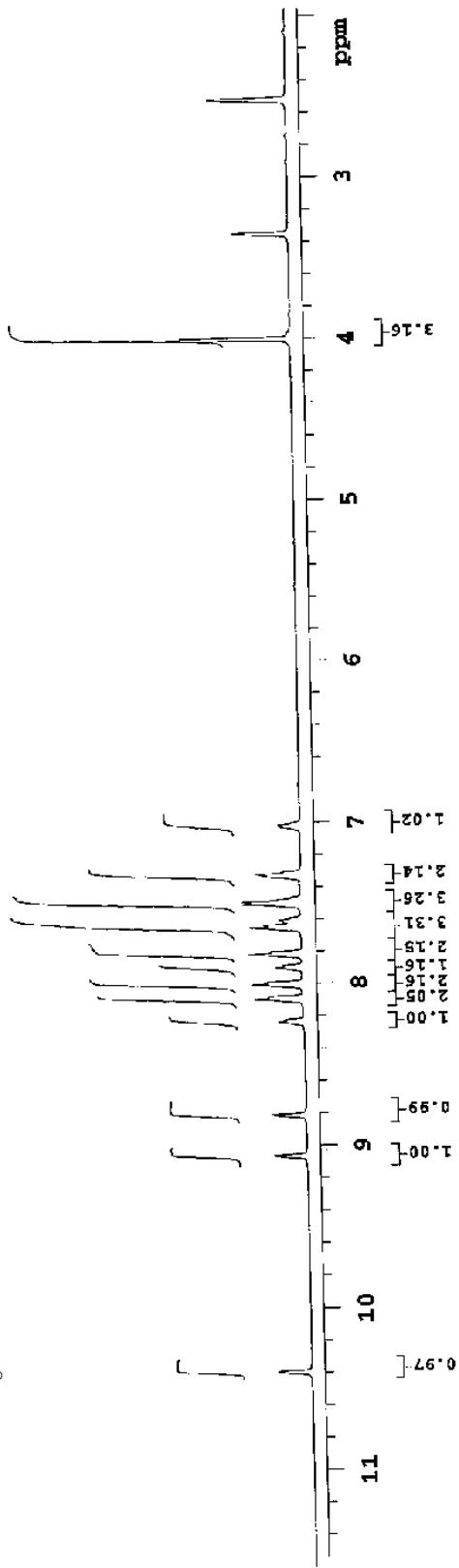
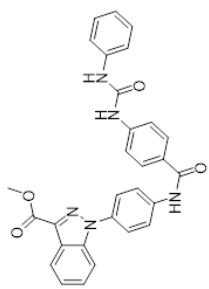
1.5 NMR Spectra

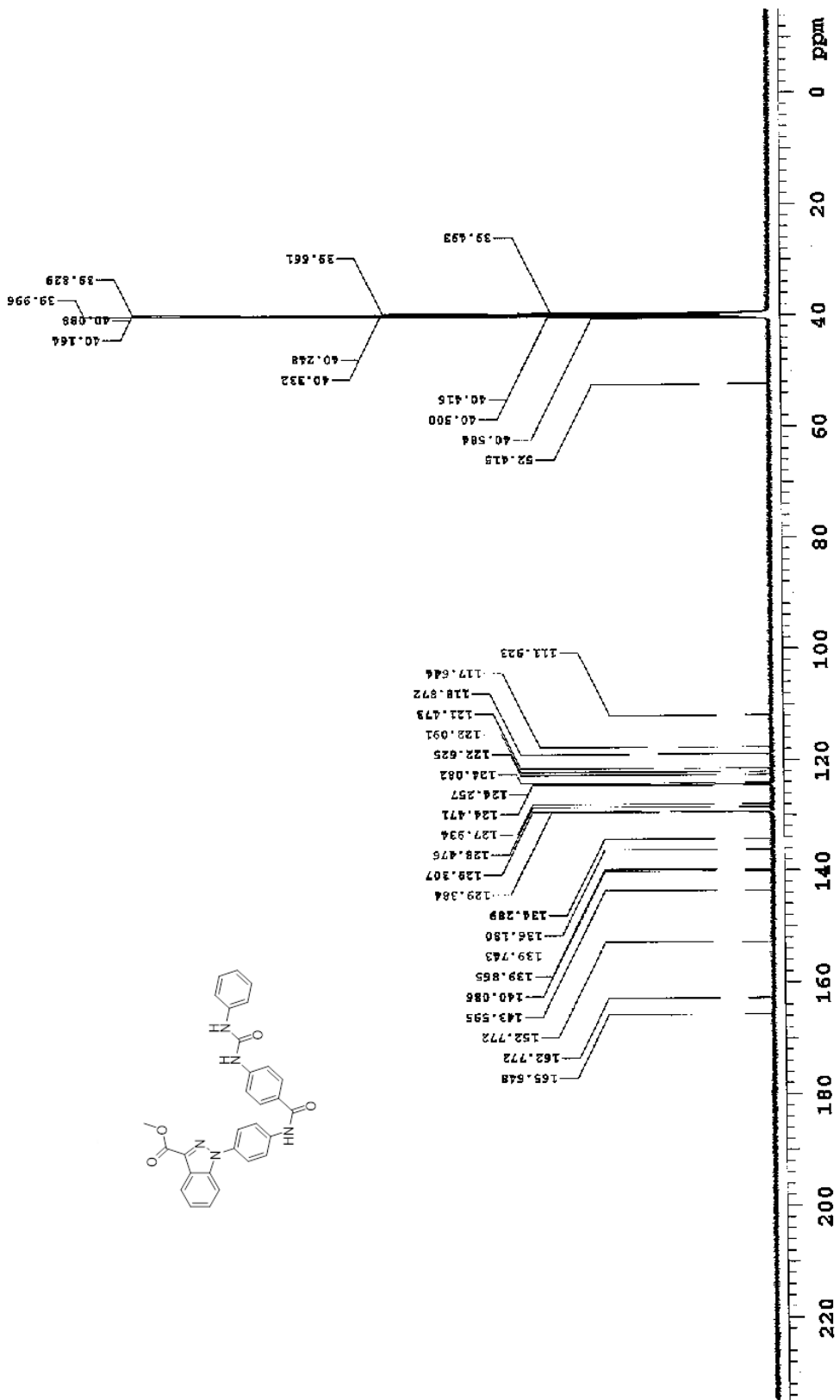


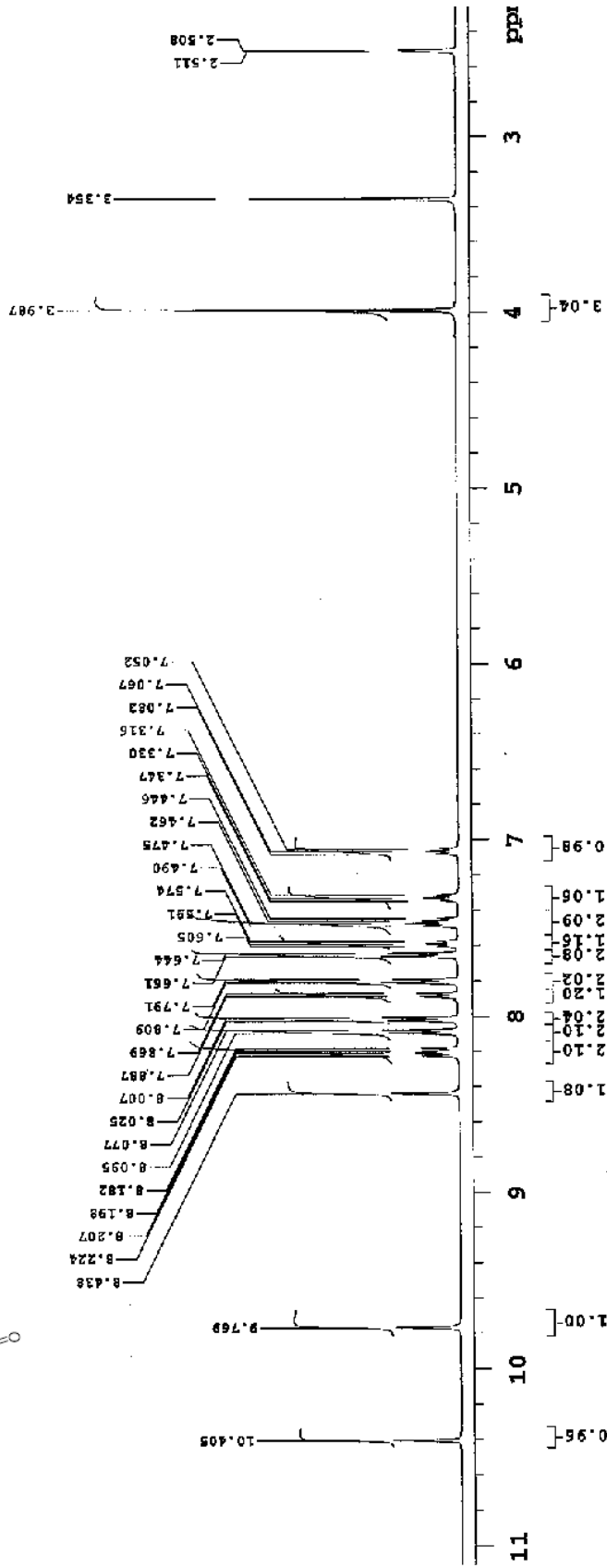
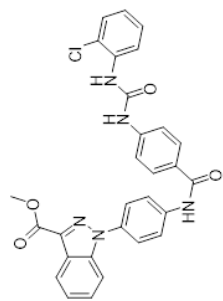


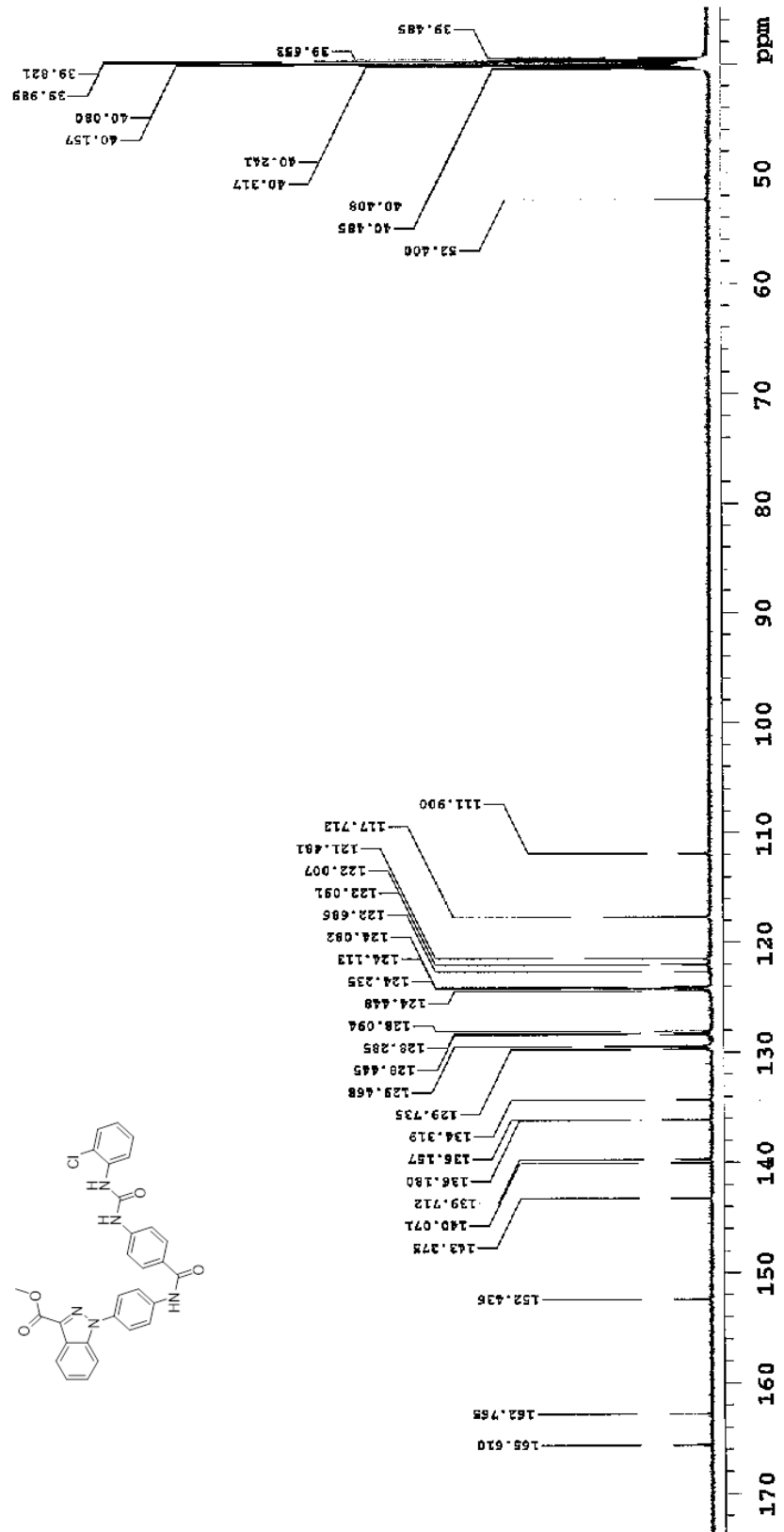


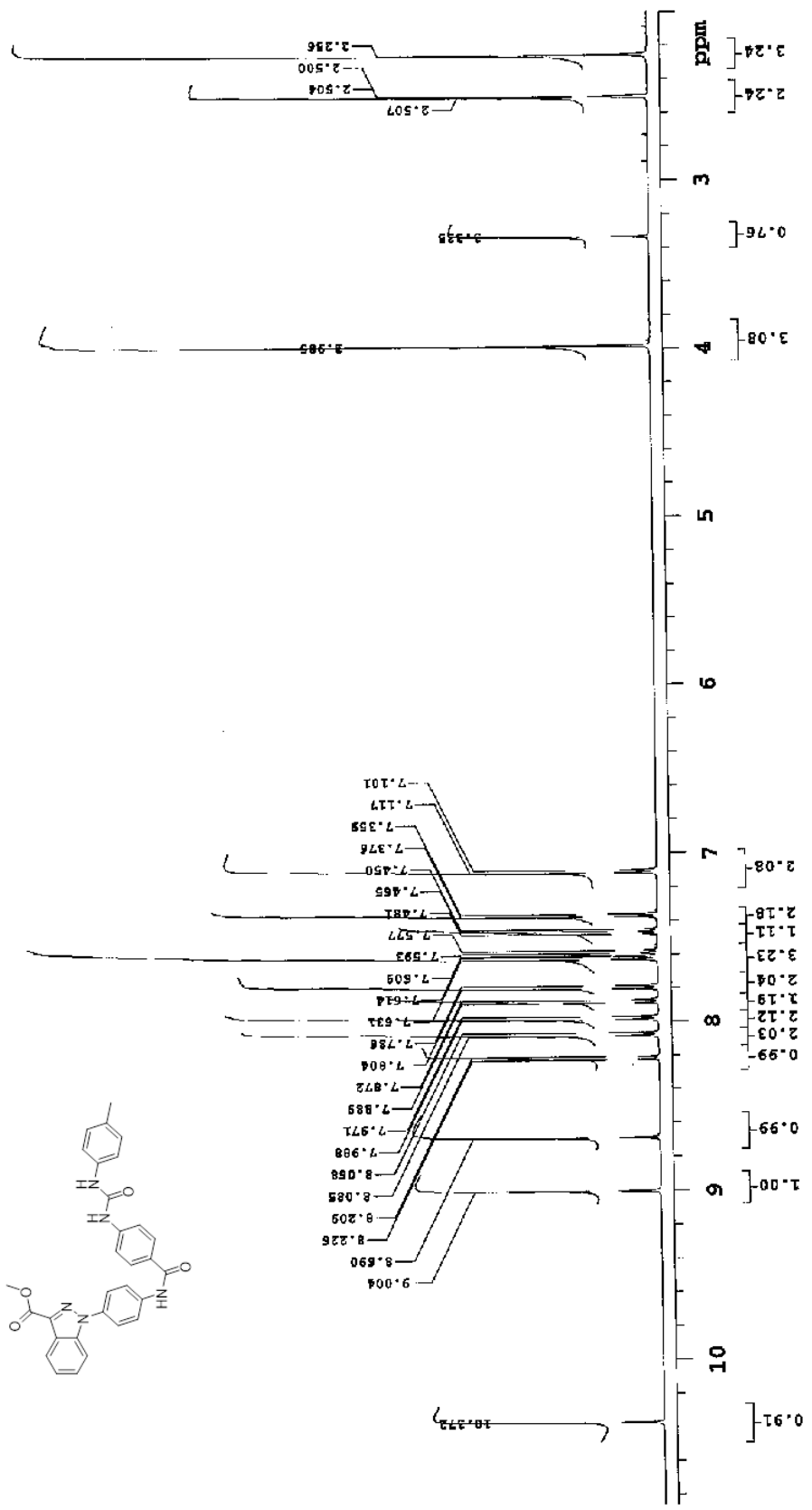


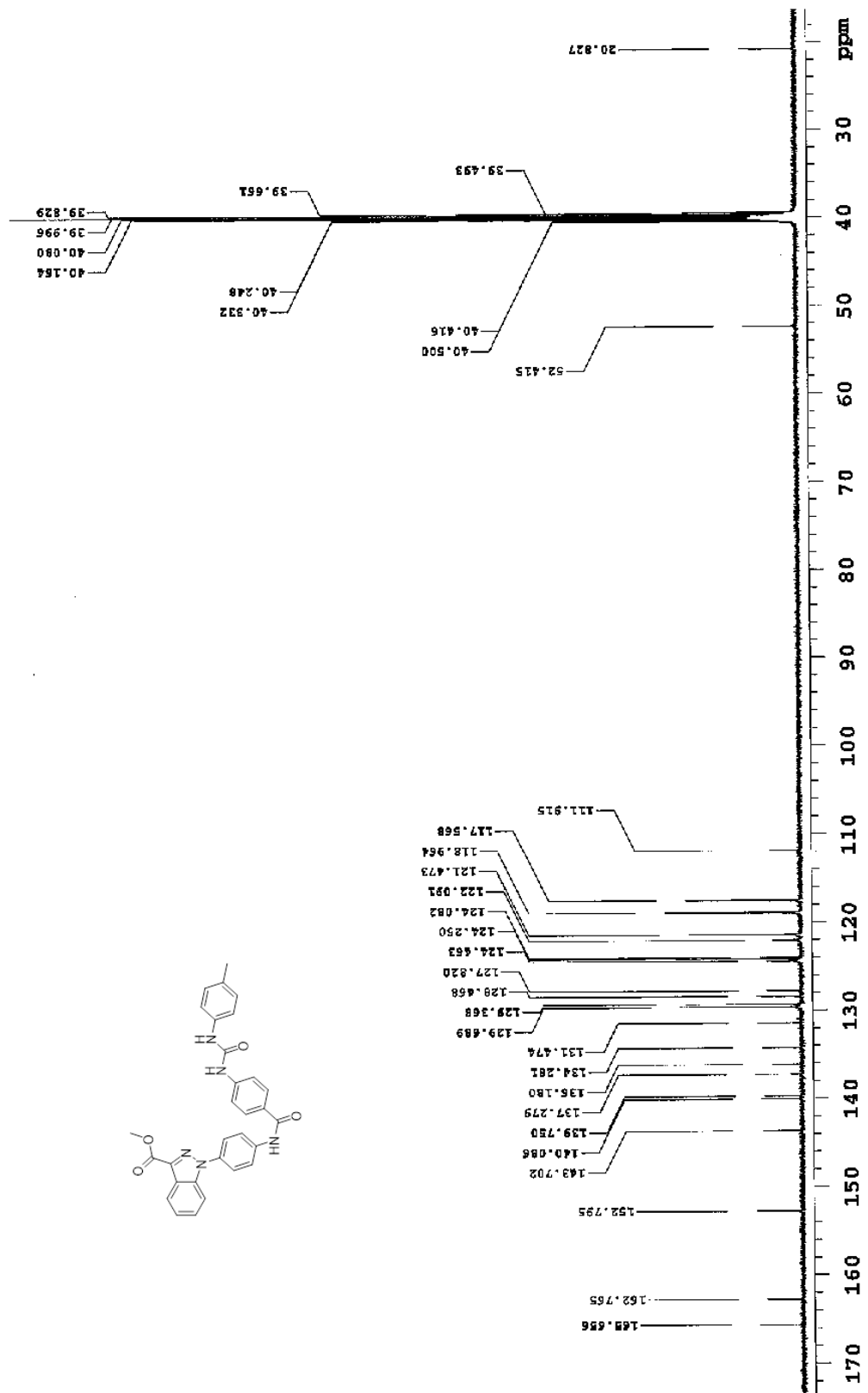


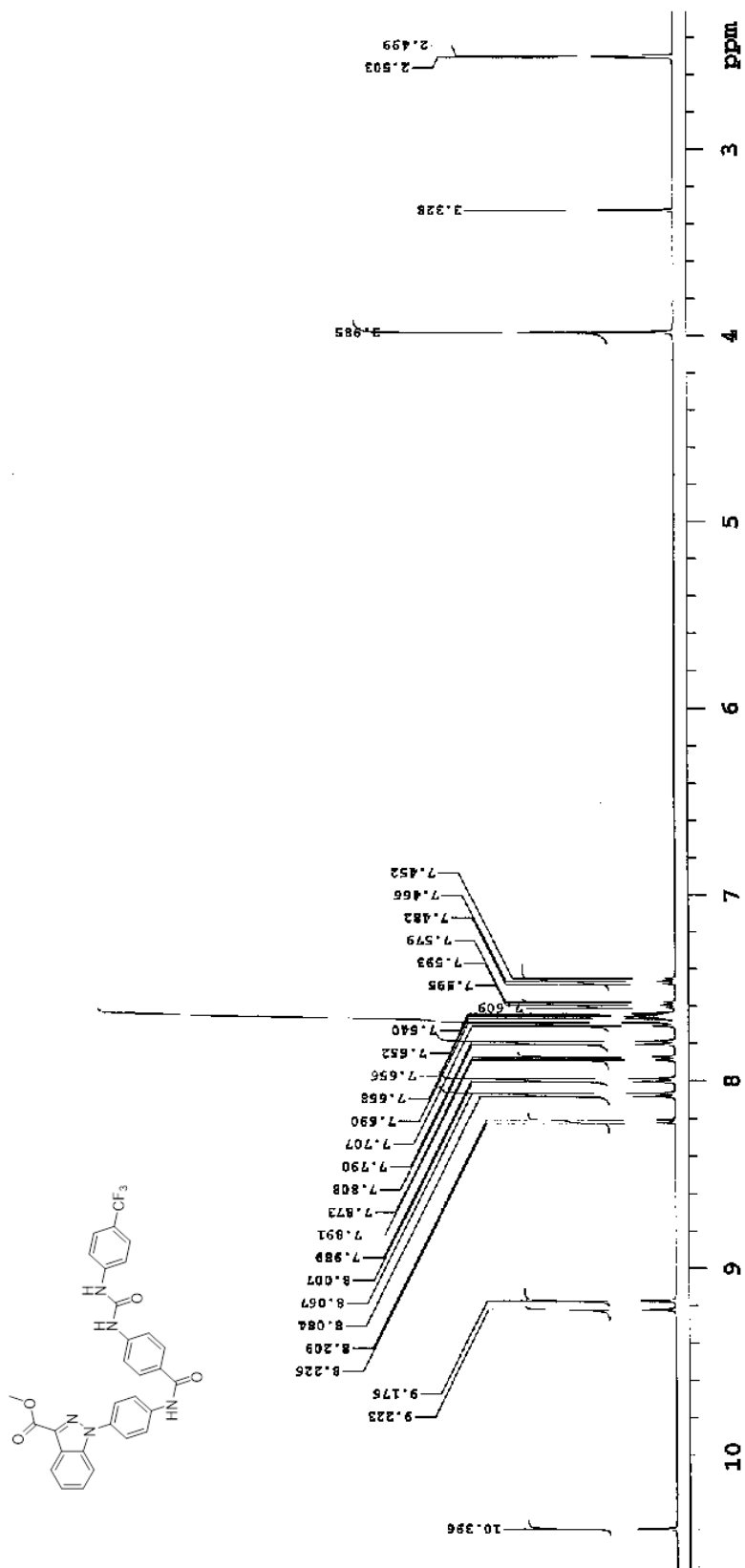


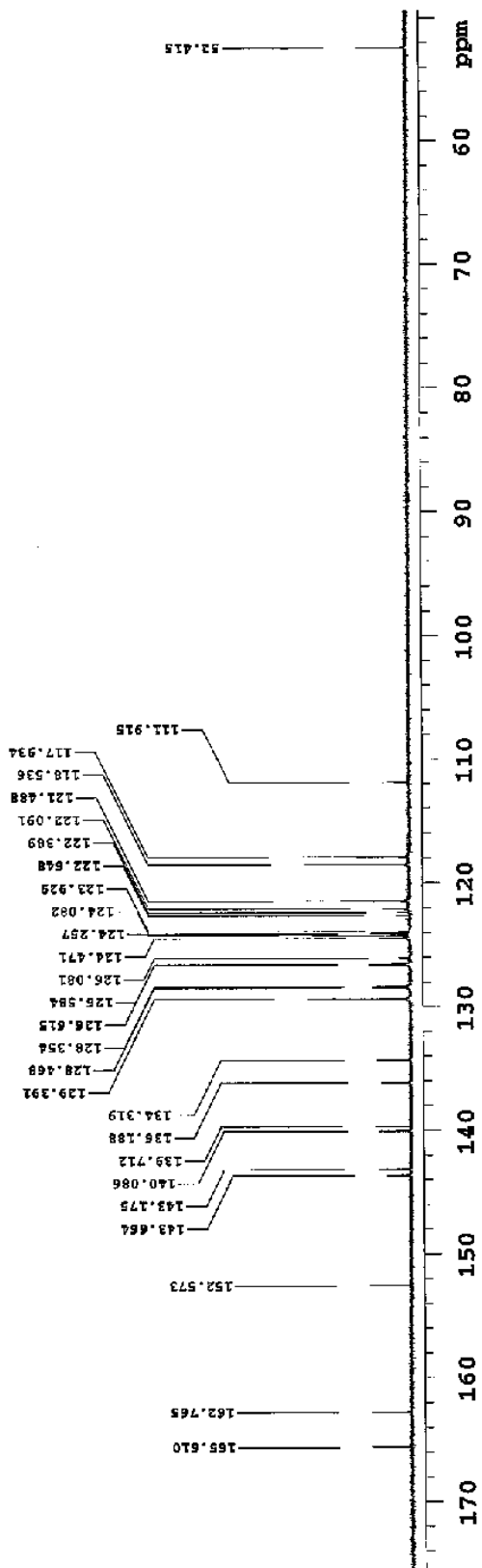
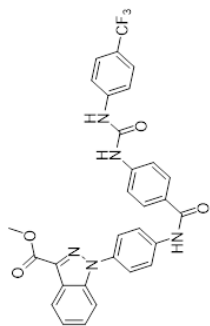


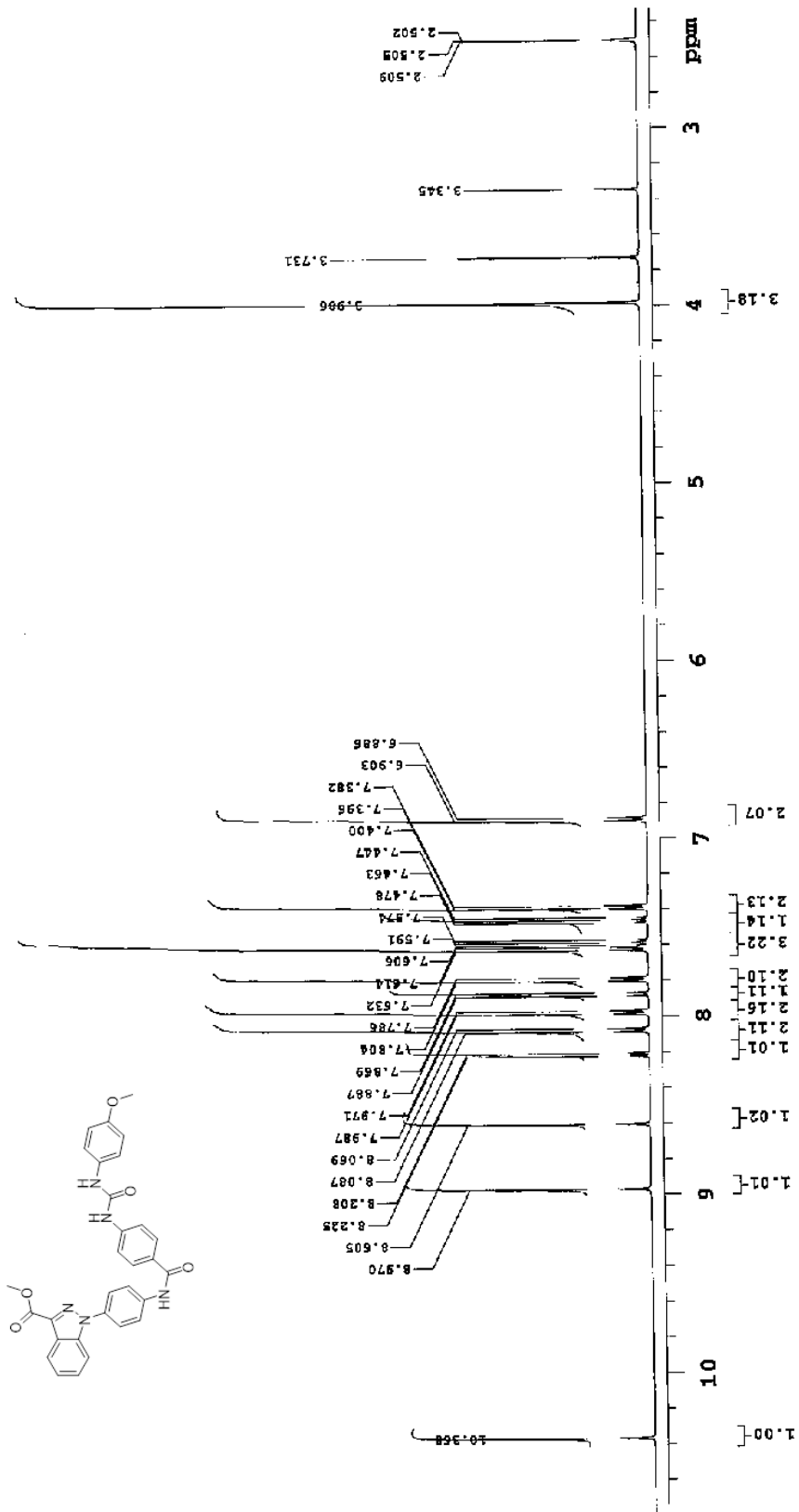


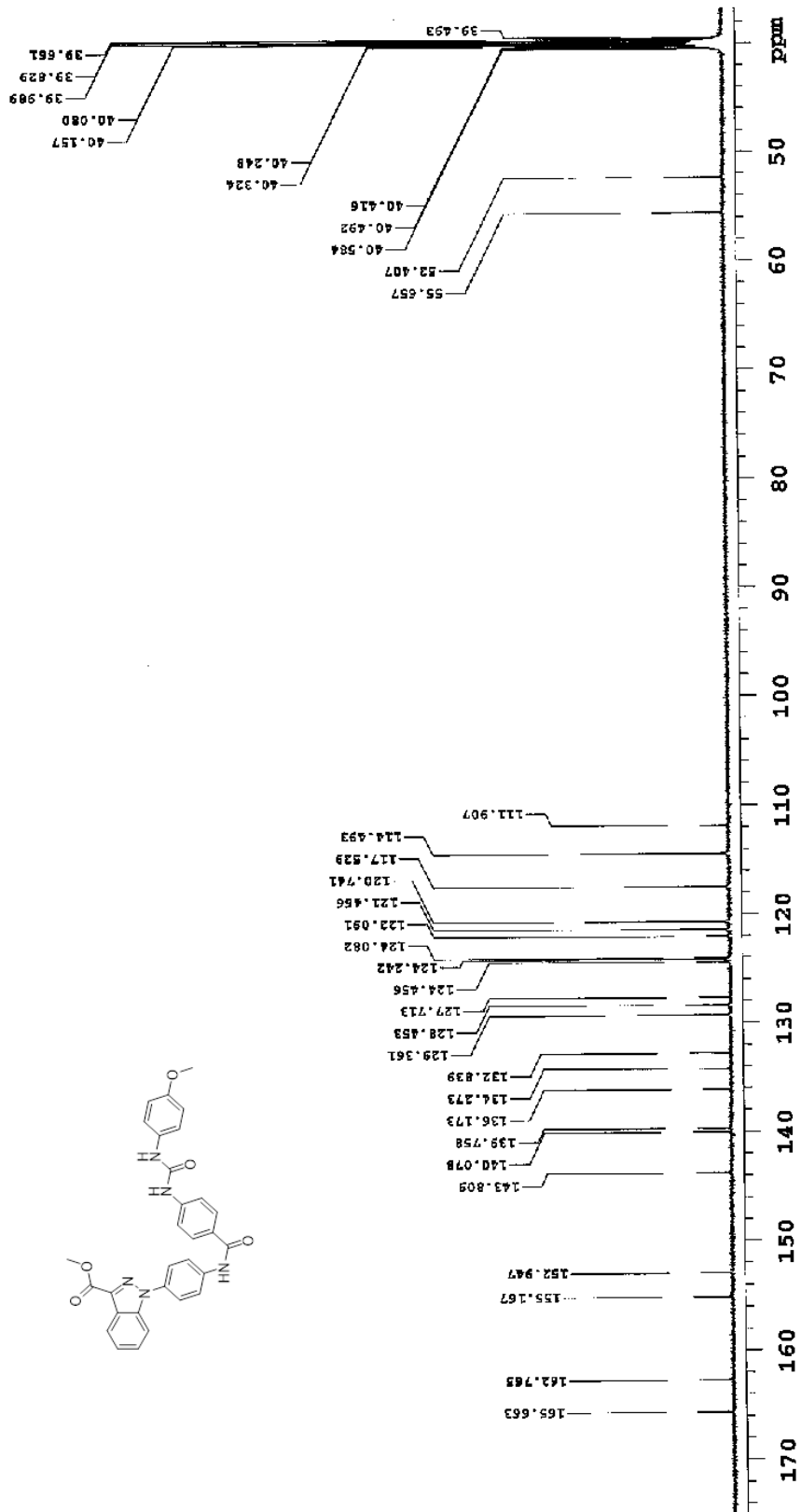


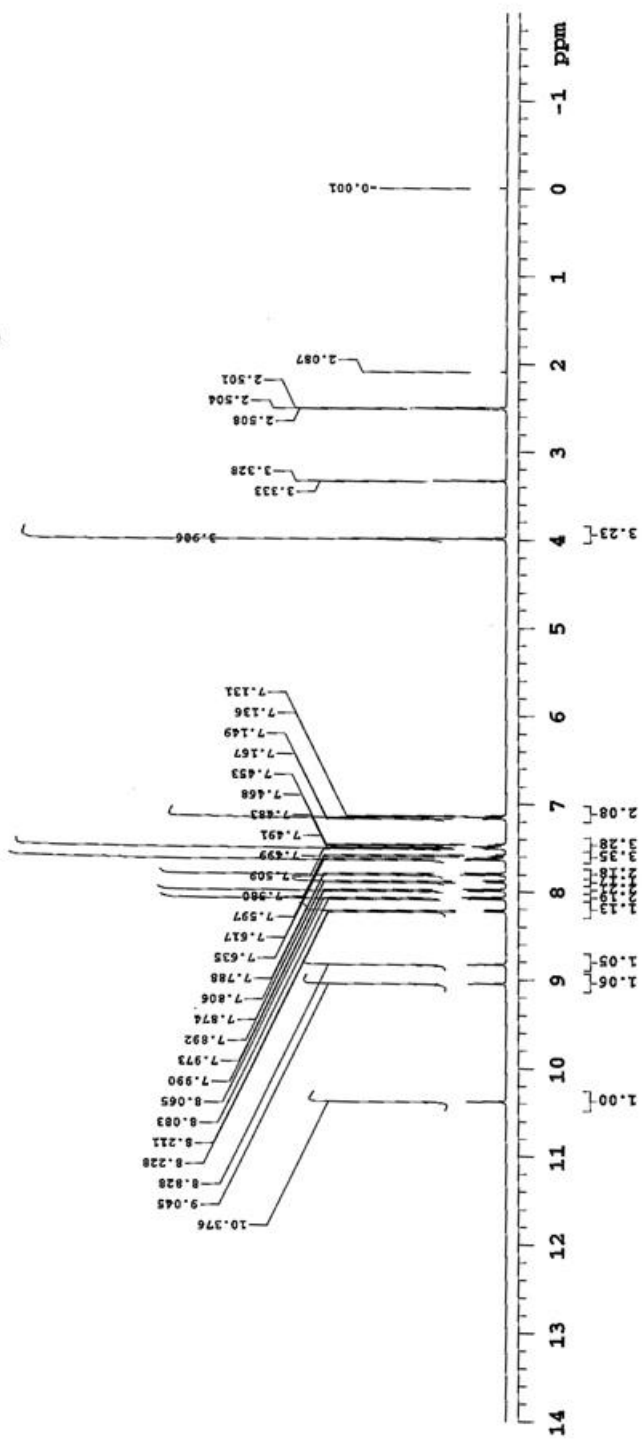
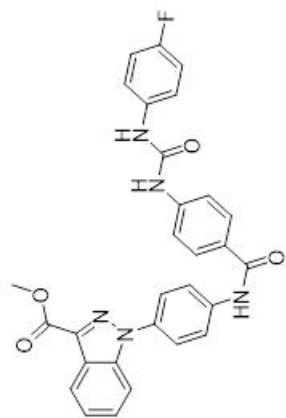


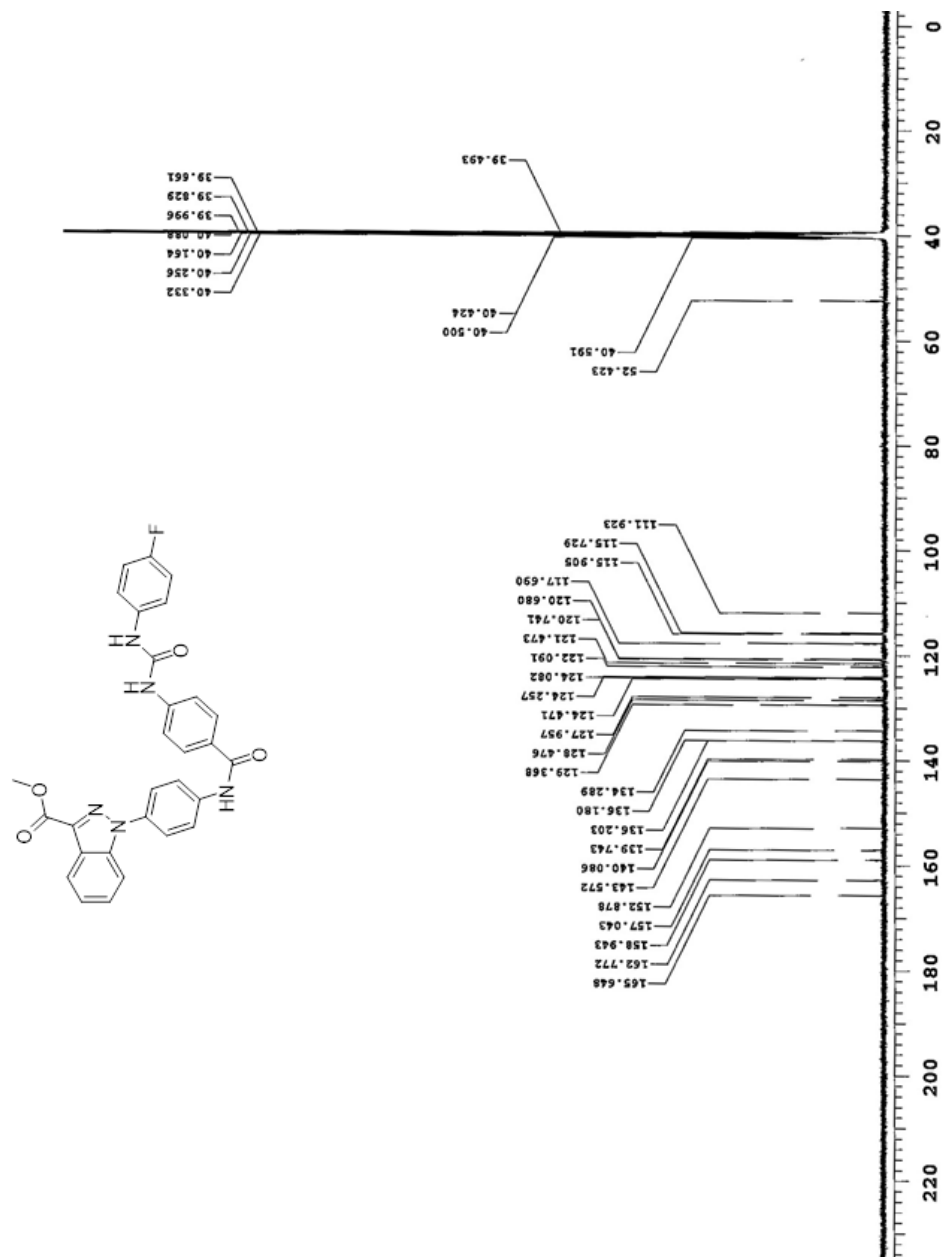


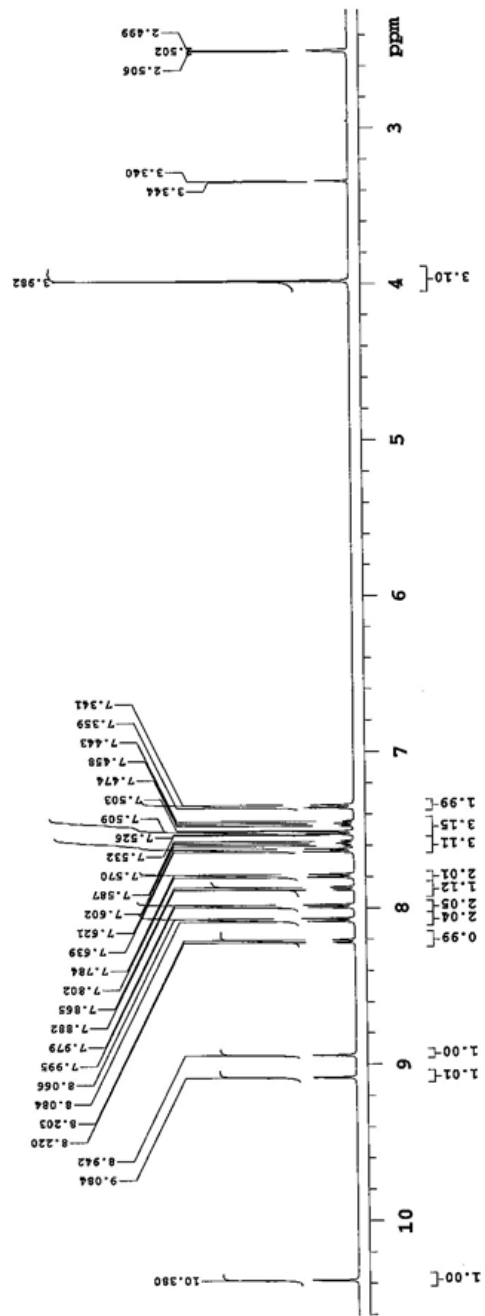
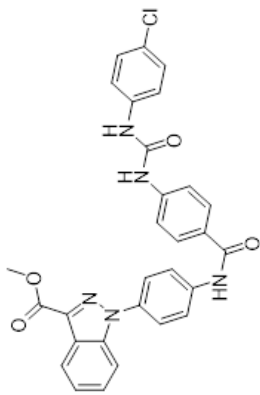


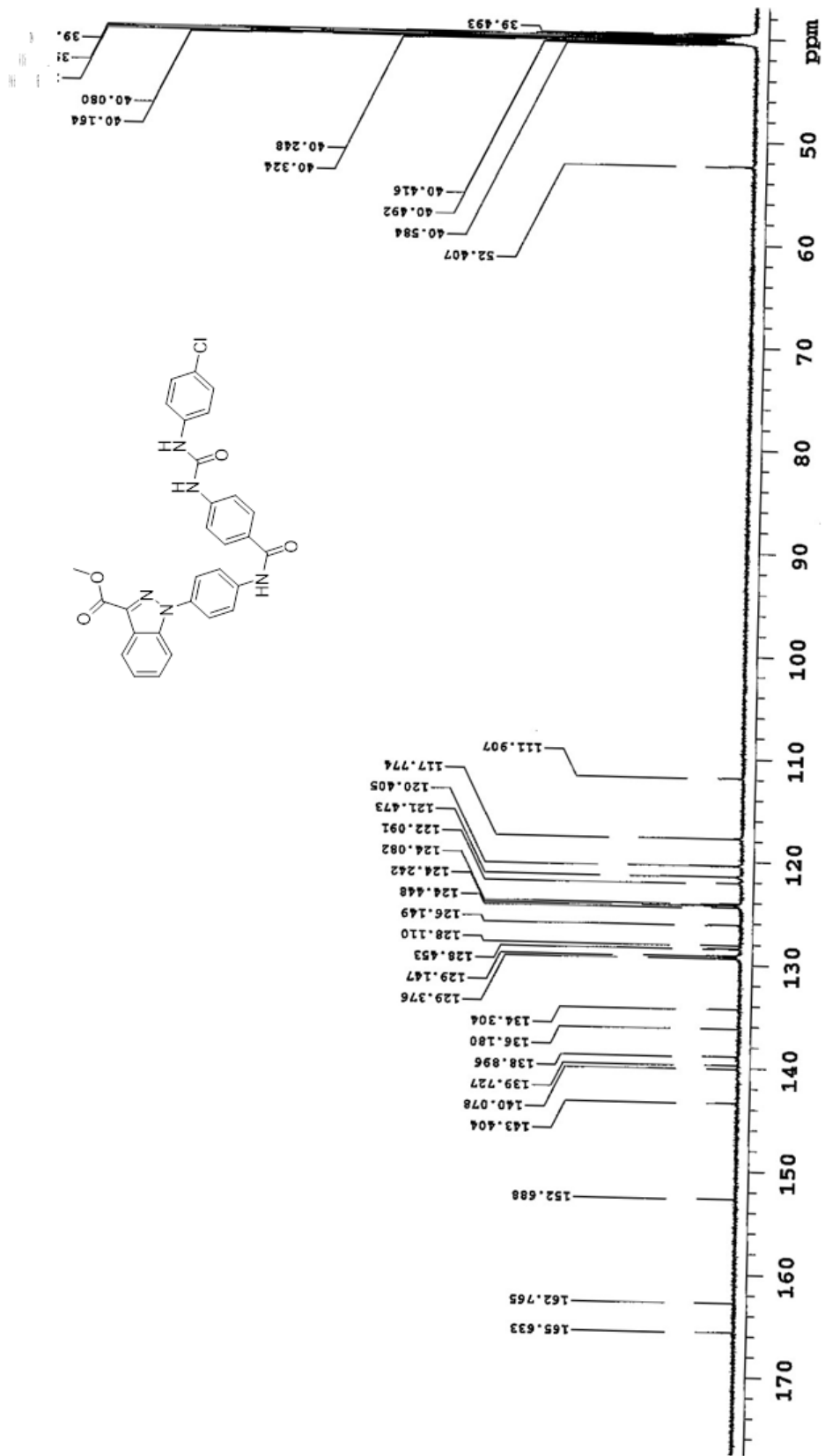


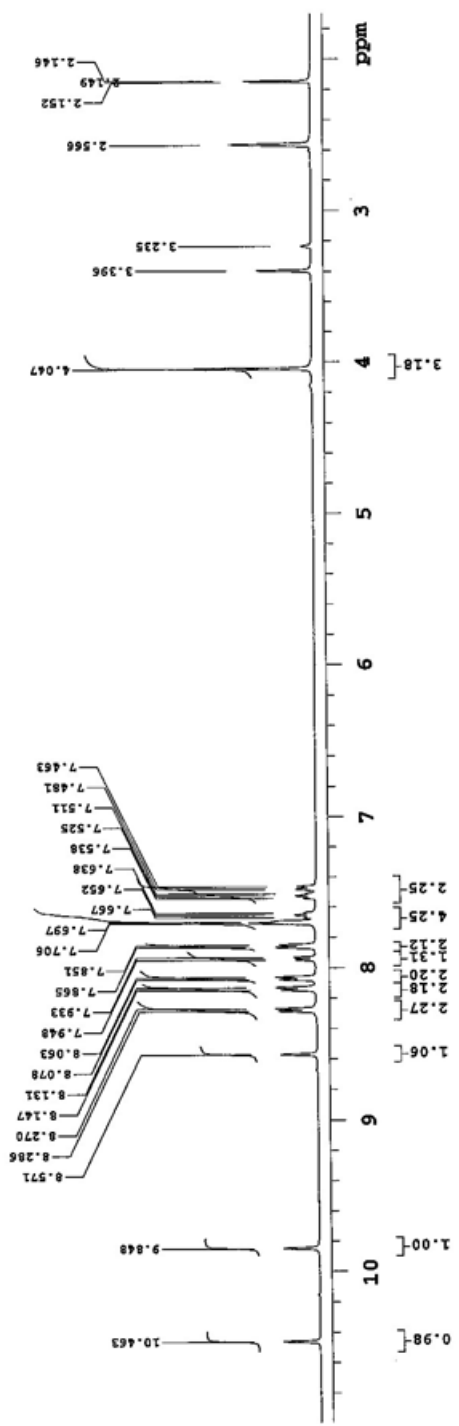
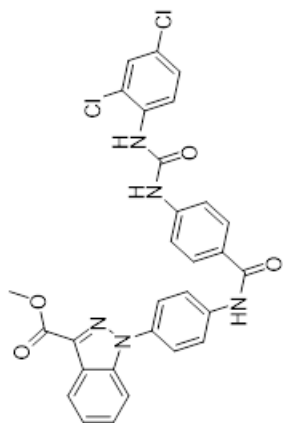


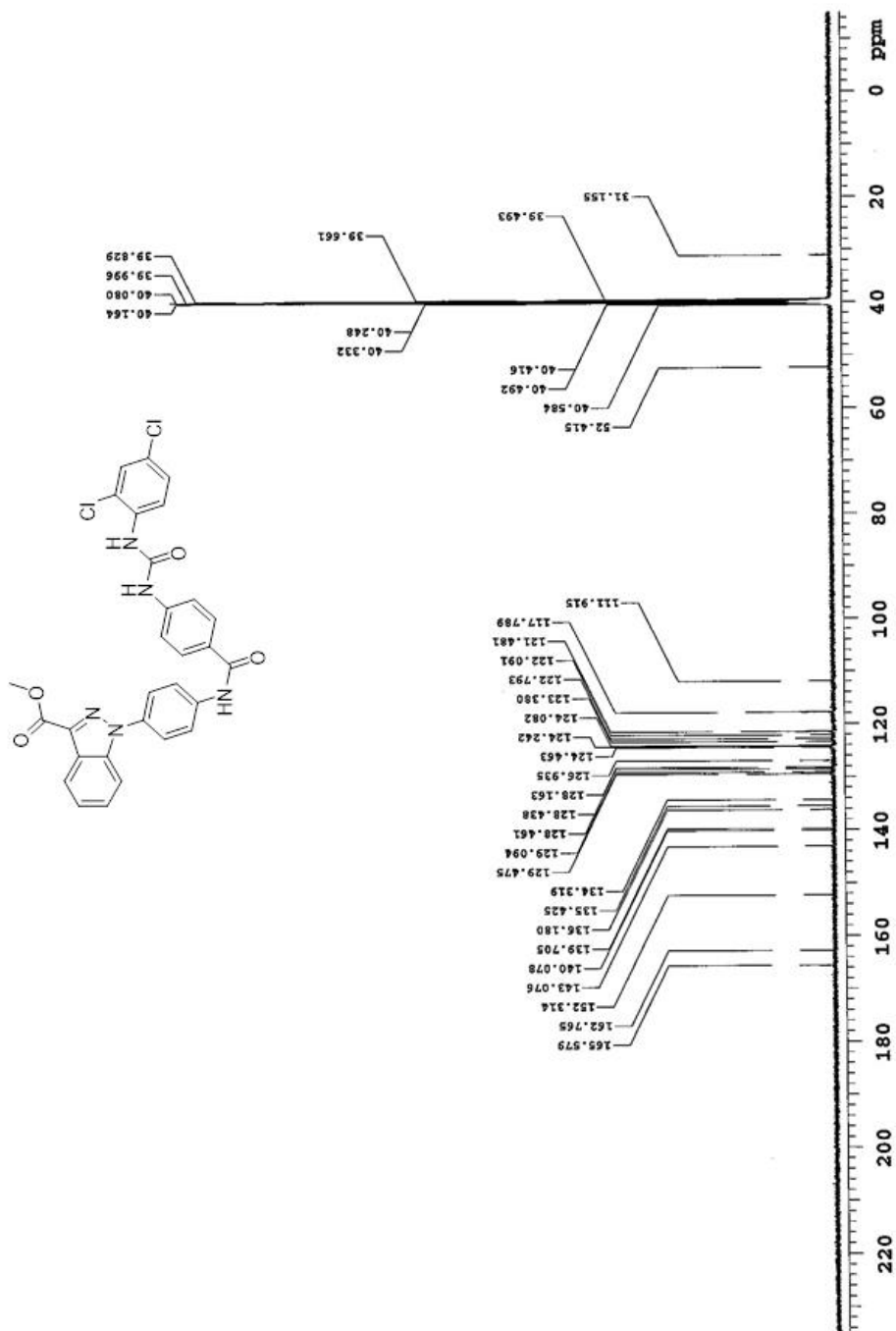


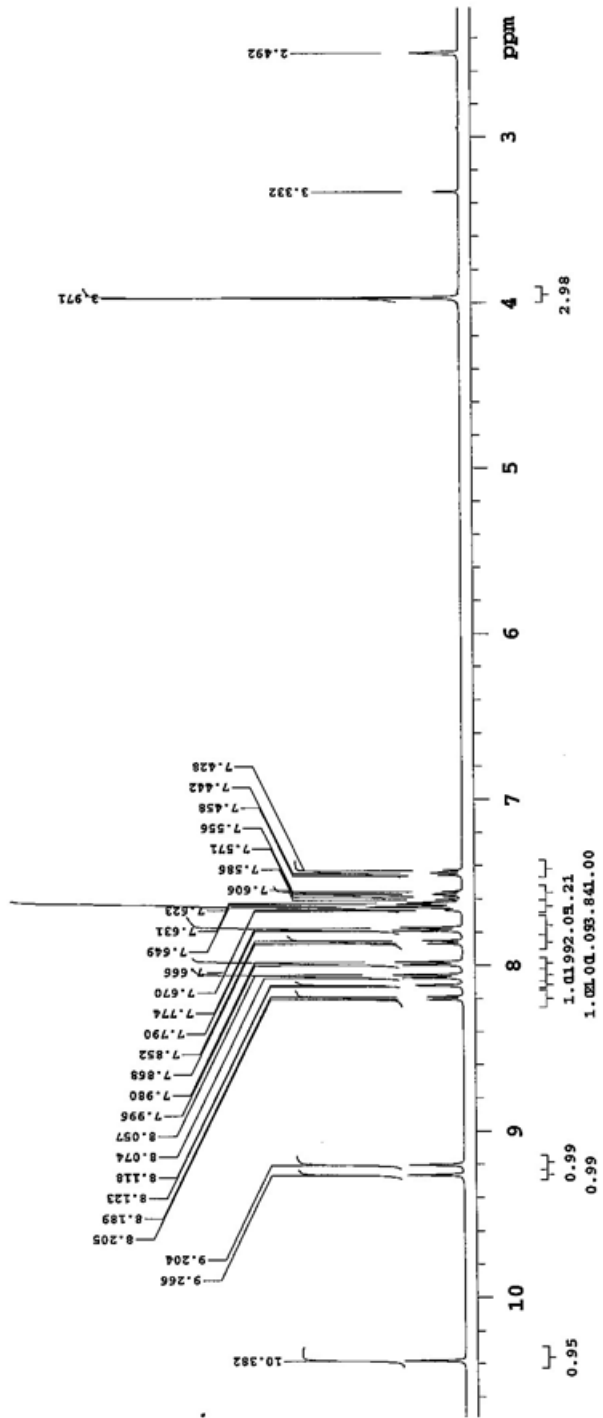
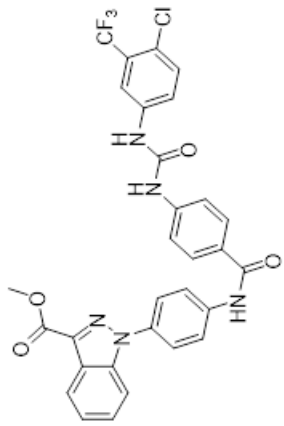


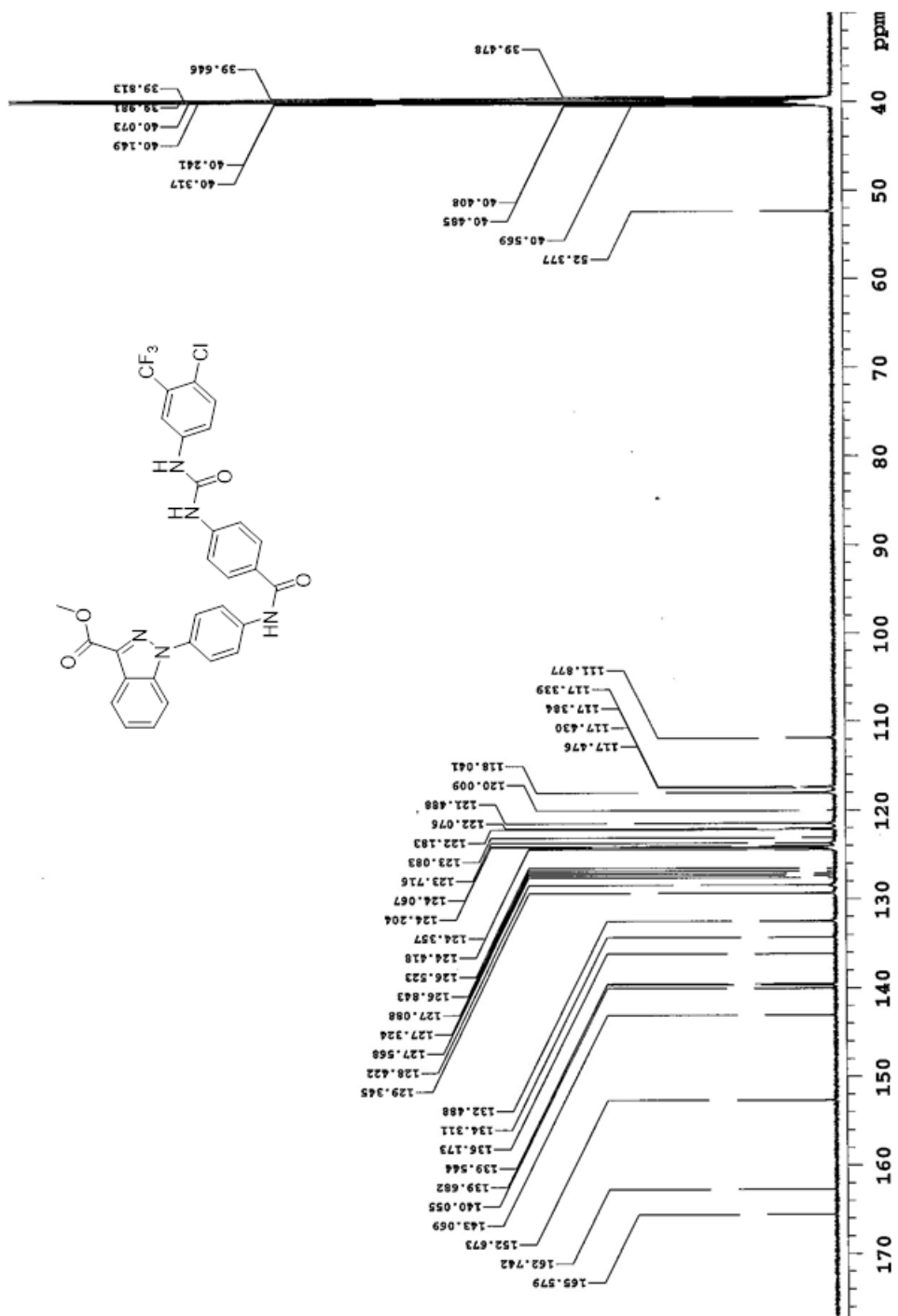


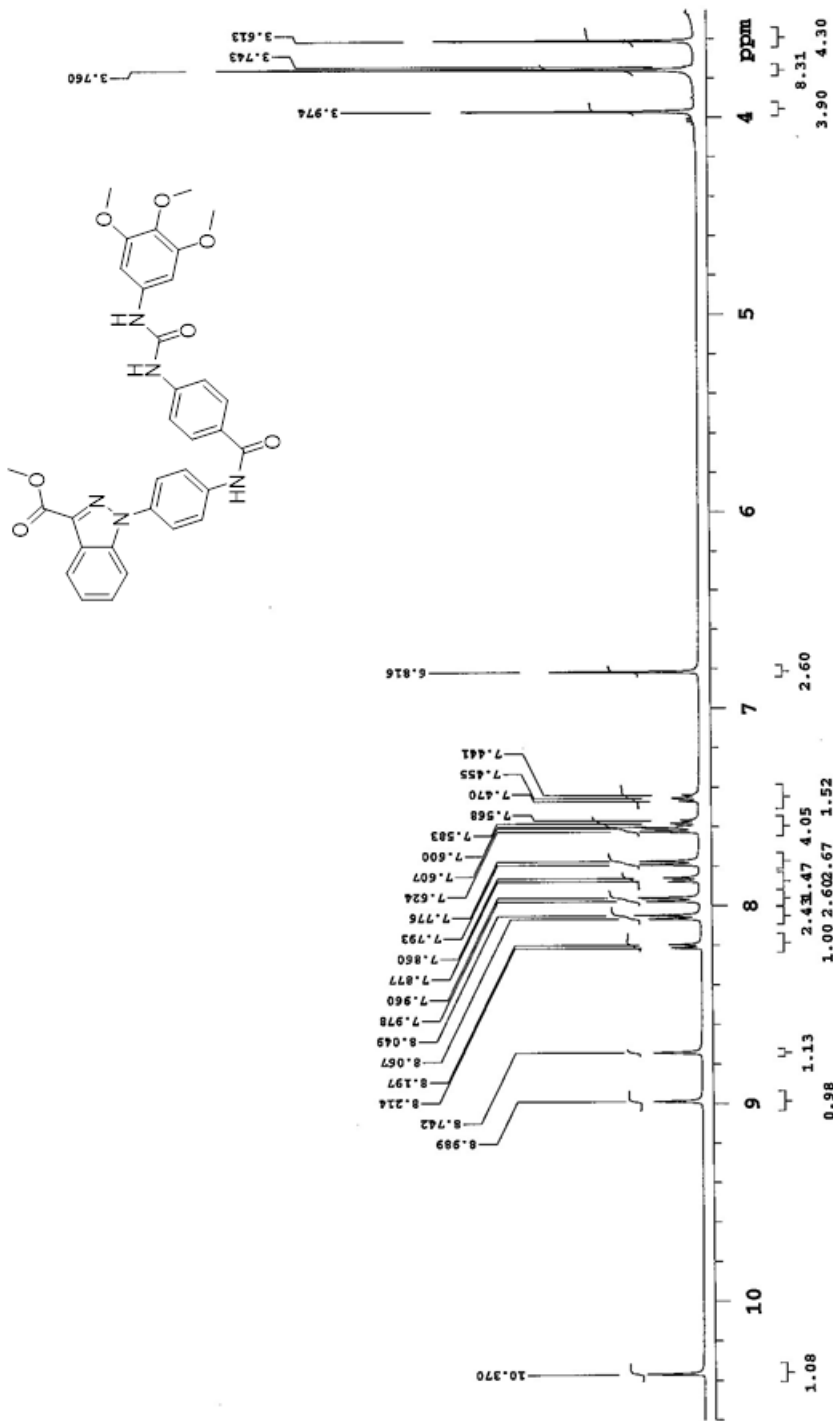


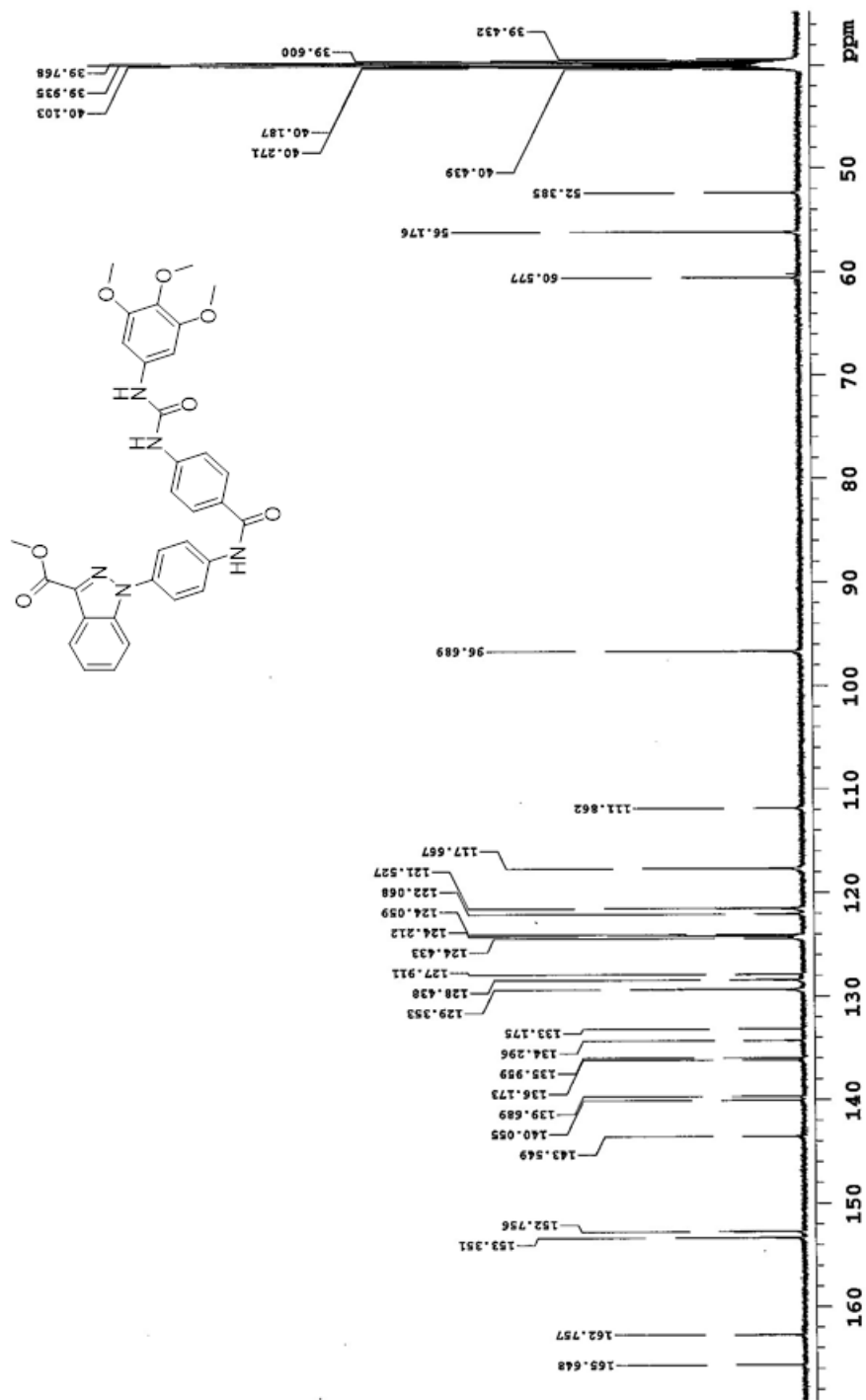


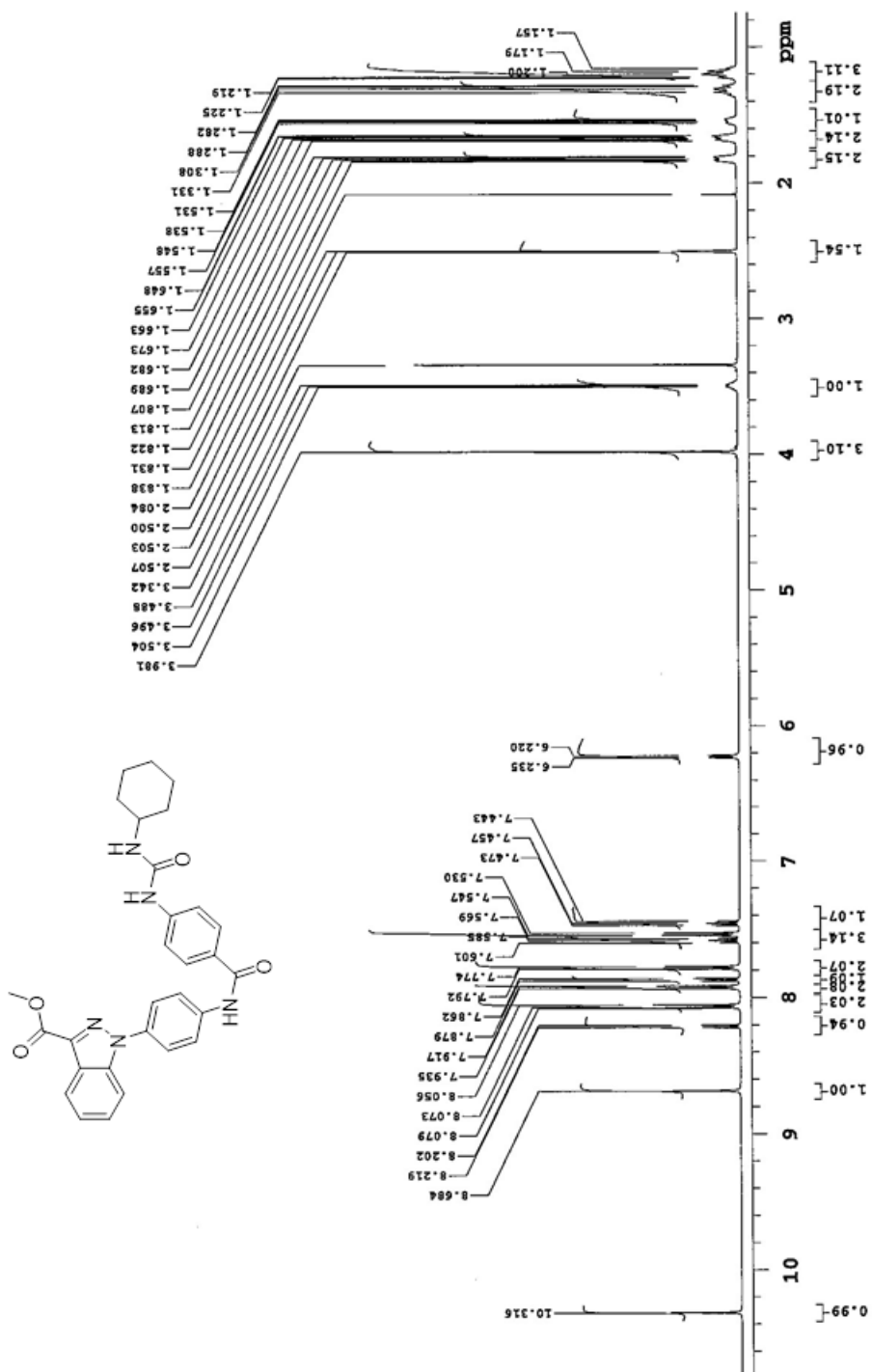


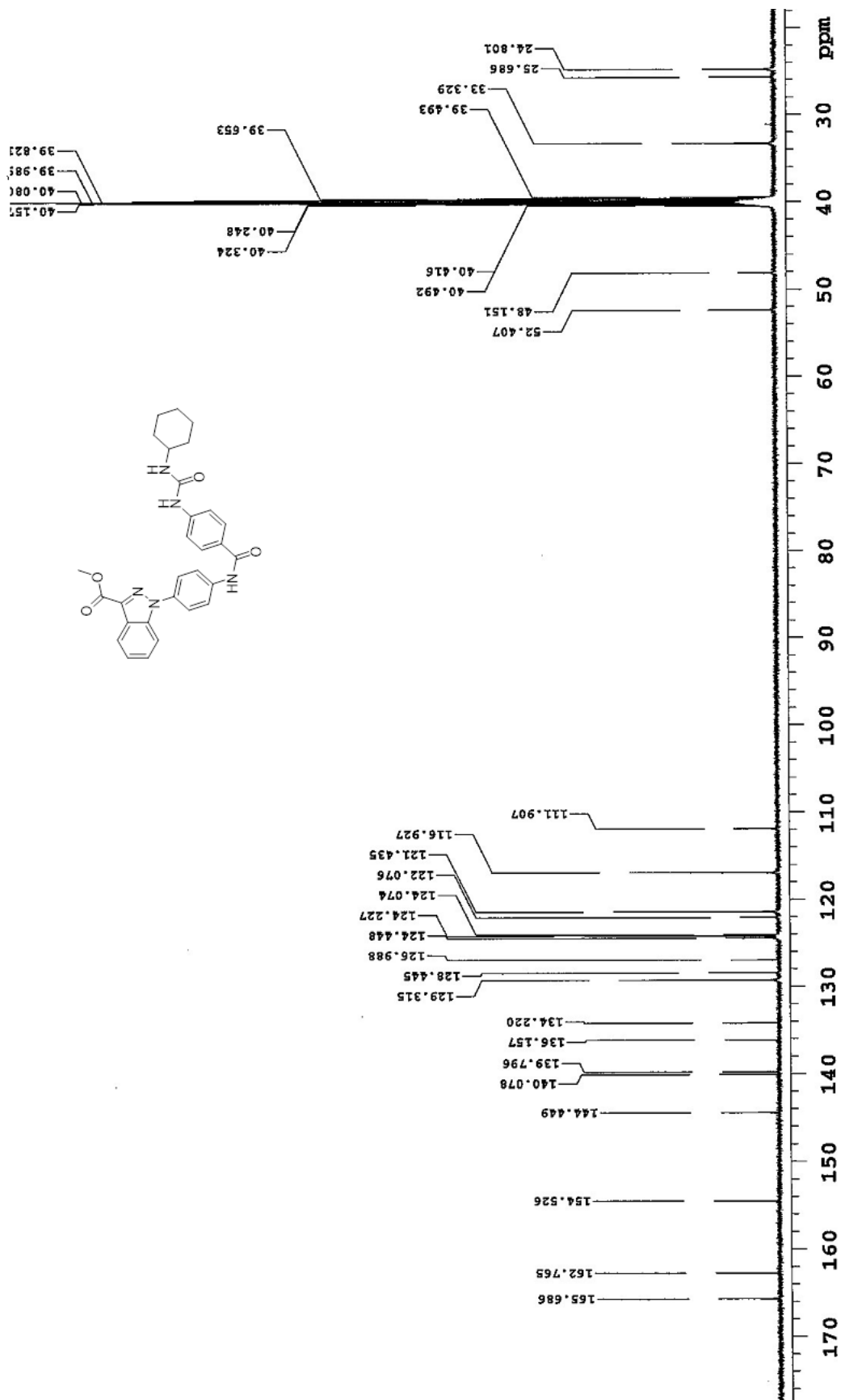


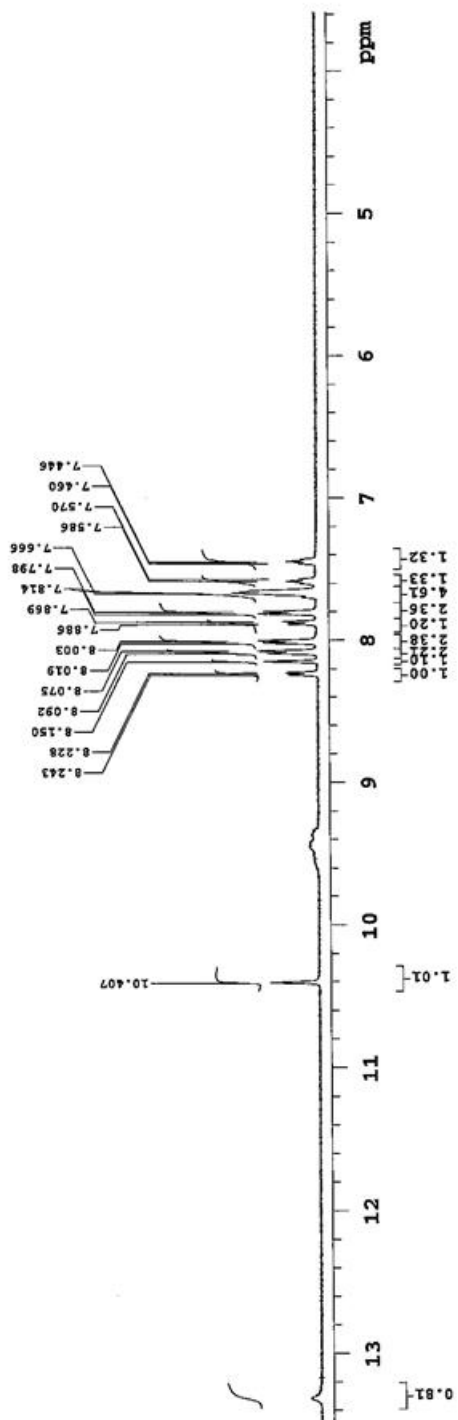
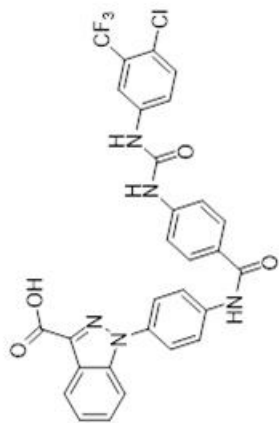


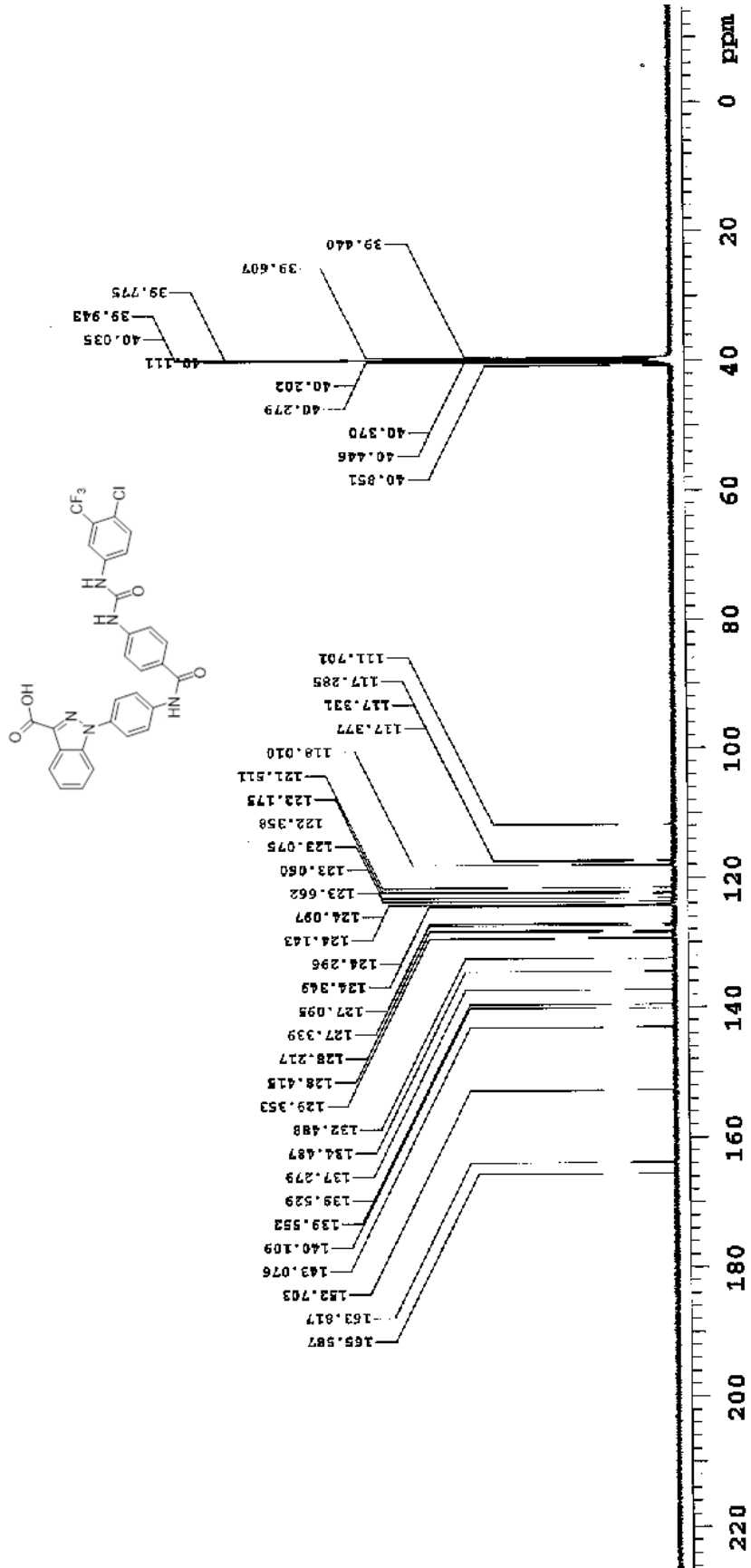


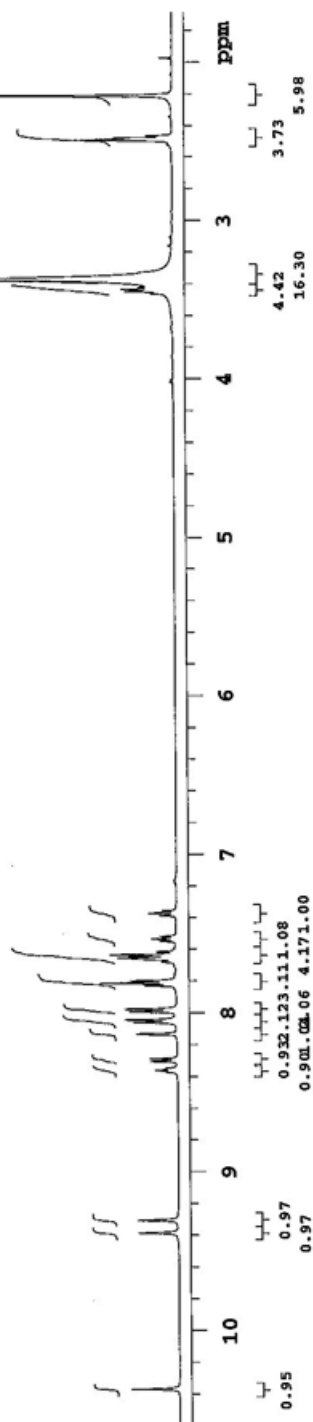
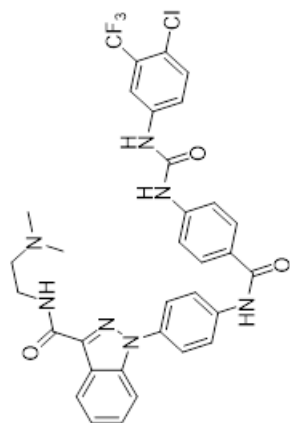


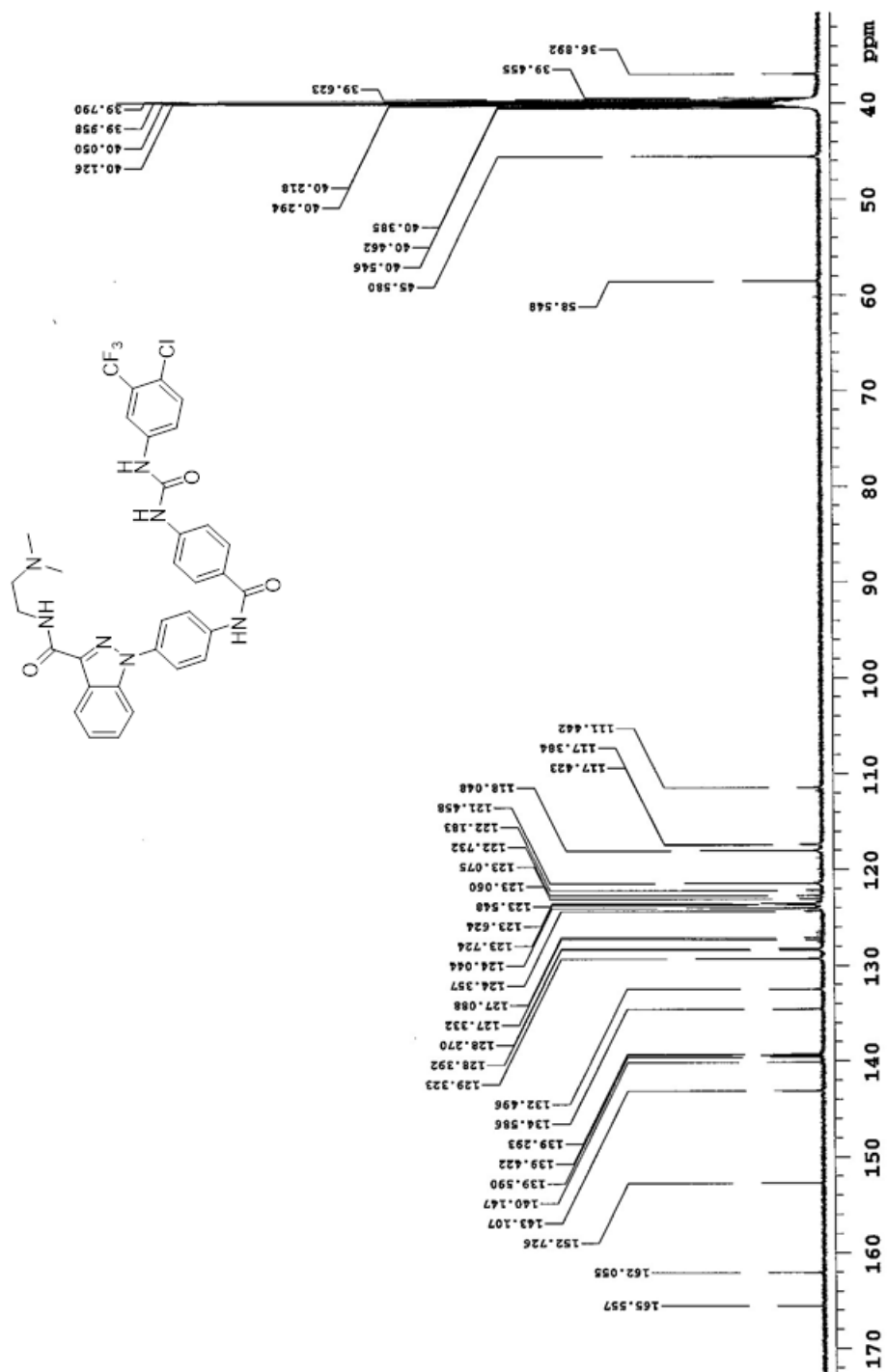


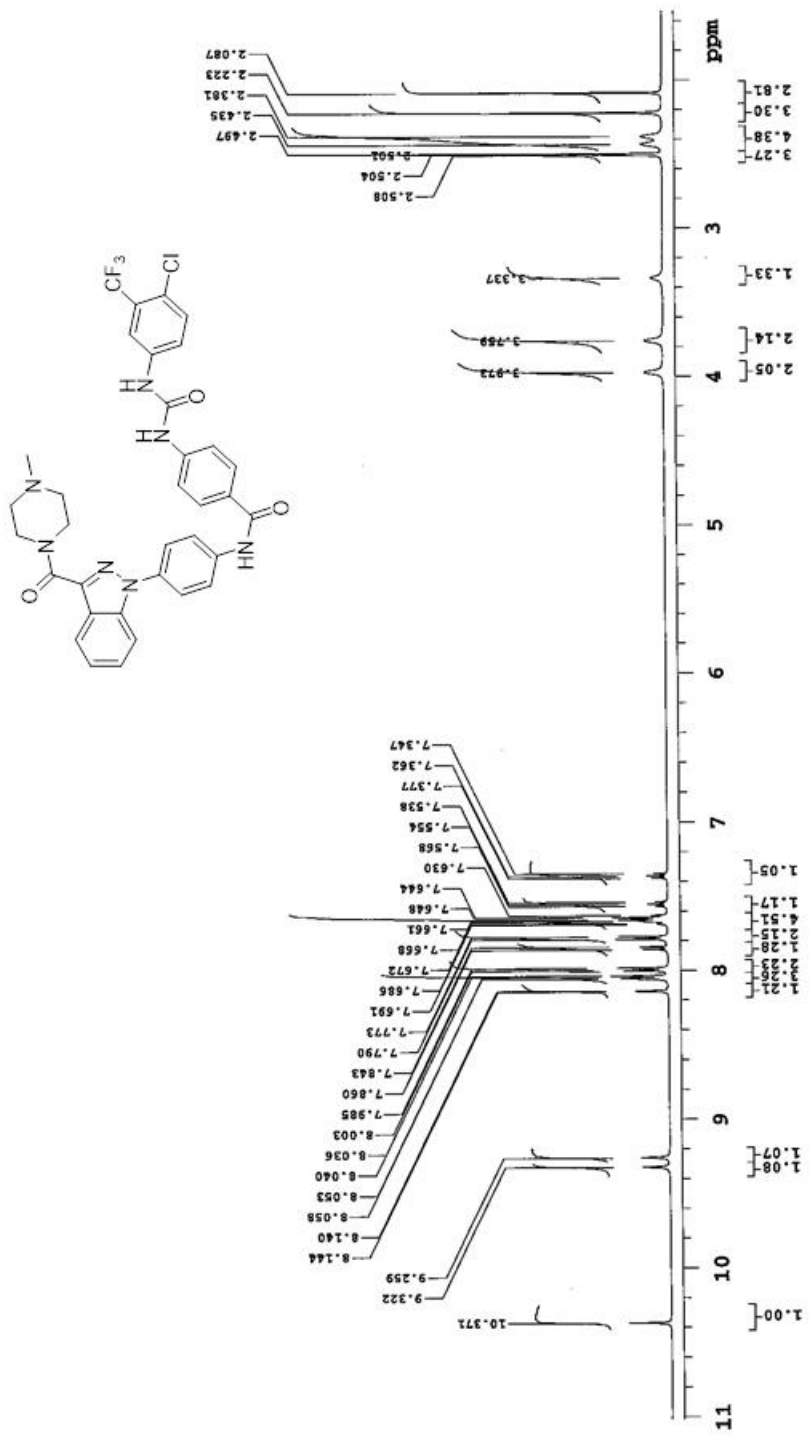


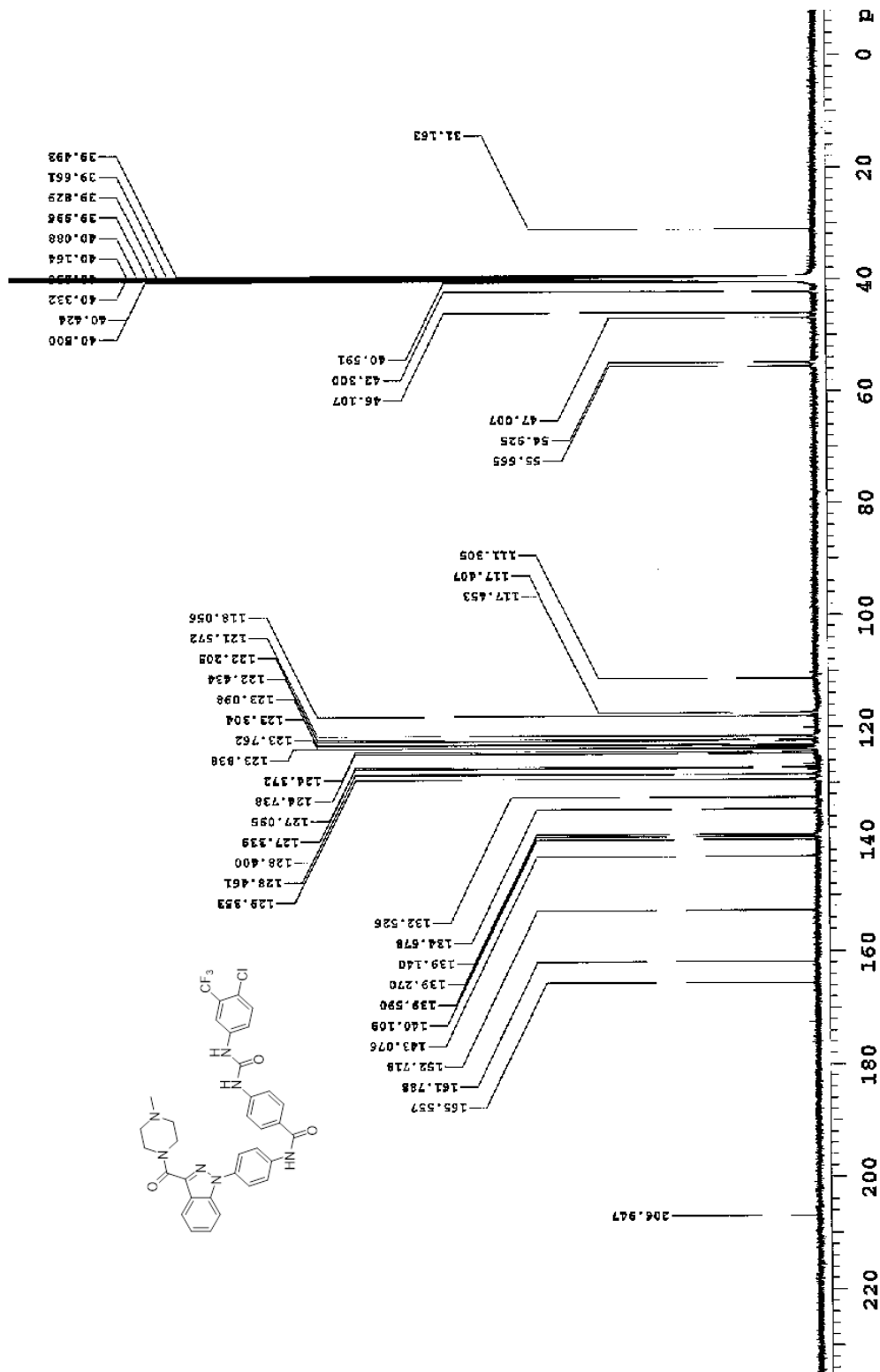












Chapter 2: Synthesis and Evaluation of Piperazinyll Curcuminoid Based Quaternary Salts as Anticancer Agents

2.1 Introduction

2.1a Natural products as medicinal agents

Evolution has allowed nature to design an infinite number of organic compounds that can be studied and used for medicinal purposes. In nature, species were driven to evolve for survival that results in highly specialized compounds for signaling, protection, and mating. Such compounds found in nature have been repurposed extensively as medicinal agents in the past few decades.⁷⁵ Natural products are chemicals produced by living organisms and can be found in nature. The repurposing includes the use of natural products as antibiotics, antiparasitics, anti-cancer, analgesics, and anesthesia.⁷⁶⁻⁷⁸ Flavonoids are a sub group of natural products that are polyphenolic compounds and can readily be found in fruits, vegetables, wine, and tea. Flavonoids are readily extracted from common foods such as peanuts, dark chocolate, green tea and turmeric.⁷⁶⁻⁷⁸ Flavonoids have been given high interest due to their supposed protective role in cancer prevention which includes pro-oxidant activity, mitochondrial toxicity, and interactions with drug-metabolizing enzymes.^{77,79}

2.1b Turmeric and its anticancer agent curcumin

Curcumin has been one of the most studied natural products. Curcumin is the yellow spice derived from the roots, rhizome, of the plant *Curcuma longa*.⁷⁷ The roots are commonly known as turmeric which has been widely used in Asia for thousands of years in food as a preservative, a coloring agent, and has also been

used as medicine for treating wide variety of diseases.⁷⁶⁻⁷⁸ Extracts of turmeric contain flavonoid mimicking three curcuminoids are namely curcumin, demethoxycurcumin, and bisdemethoxycurcumin. Curcuminoids are often extracted with ethanol and can range from 2-8% of the total composition.⁷⁶

2.1c Chemical properties of curcumin

The molecular formula of curcumin was first reported in the early 19th century by Vogel and Pellatie and nearly a century later was identified by Lampe and Milobedzka. Curcumin is a crystalline solid that does not dissolve in water but can be solubilized in many organic solvents. Curcumin has high absorbance and fluoresces under the right conditions. Maximum absorbance is between 425 and 430 nm in methanol. In aqueous mediums curcumin does not have fluorescence, however, upon conjugation with ions, lipids, and proteins it can exhibit high fluorescence. This unique property is extremely helpful in visualizing the localization and uptake of curcumin in cells.⁷⁷

Curcumin is a bis α,β -unsaturated β -ketone that can exist as either bis keto or keto enol forms (**Figure 2.1**). In acidic or neutral conditions, the bis keto dominates and under basic conditions, the enolate form is more prevalent. As a result, it is a potent proton donor from pH 3-7 and at pH > 8, it acts as an electron donor.⁷⁵

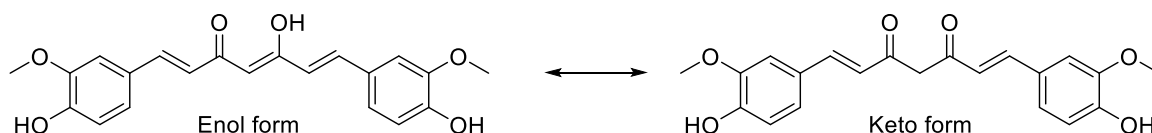


Figure 2.1: Curcumin in its keto and enol form

2.1d Curcumin as a therapeutic agent

Curcumin has been reported as a promising natural product in the treatment of wide variety of diseases due to its pleotropic effects with no reported side effects even at high concentrations.⁸⁰ Curcumin has been traditionally used in prevention and treatment of several conditions and diseases. Curcumin has been shown to have hepato- and nephro-protective, thrombosis suppressing, myocardial infarction-protective properties.⁸¹ Other properties that make curcumin the most interesting natural product is due to its strong antioxidant, antimicrobial, anticarcinogenic and anti-inflammatory properties (**Figure 2.2**).^{77,82-84}

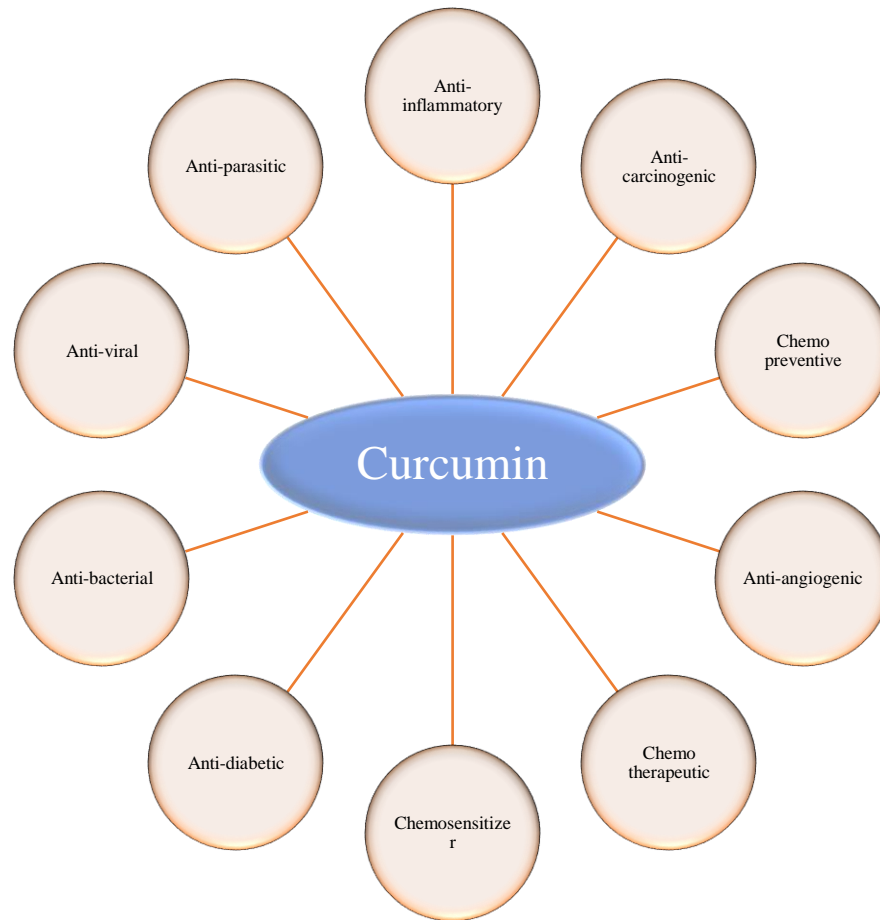


Figure 2.2 Therapeutic properties of curcumin

Curcumin has shown suppression of nuclear transcription factor NF- κ B, down regulation of cyclooxygenase-2 (cox2), decrease in cellular nitric oxide (NO), decrease in cell surface adhesion molecules, and decrease in inflammatory cytokines IL-1-8.^{77,85,86} NF- κ B is an inducible transcription factor that regulates genes expression involved in inflammation, cell proliferation and cell survival.^{75,78,82,83,87} Cox-2 is responsible for the formation of prostanoids including thromboxane and prostaglandins such as prostacyclin. Cox is often overexpressed in cancer and have multifaceted roles in carcinogenesis, chemoresistance, and metastasis.⁸⁸ NO is a water soluble free radical gas with

many roles in pathogenesis of cancer. NO has been suggested to modulate different cancer-related events including angiogenesis, apoptosis, cell cycle, invasion, and metastasis.^{77,89} Cytokines are often released in response to cellular stress that include infection, inflammation, and carcinogenesis.^{77,86} Carcinogenesis results in stress due to the need of additional nutrients and building blocks for continued proliferation. Cancer-associated cytokines have numerous different roles including promotion of angiogenesis, immunoprotection, increased invasiveness, motility, and metastasis.^{1,85} Together, these effects of curcumin makes it an intriguing natural product to pursue as an anti-cancer agent **(Figure 2.3)**.

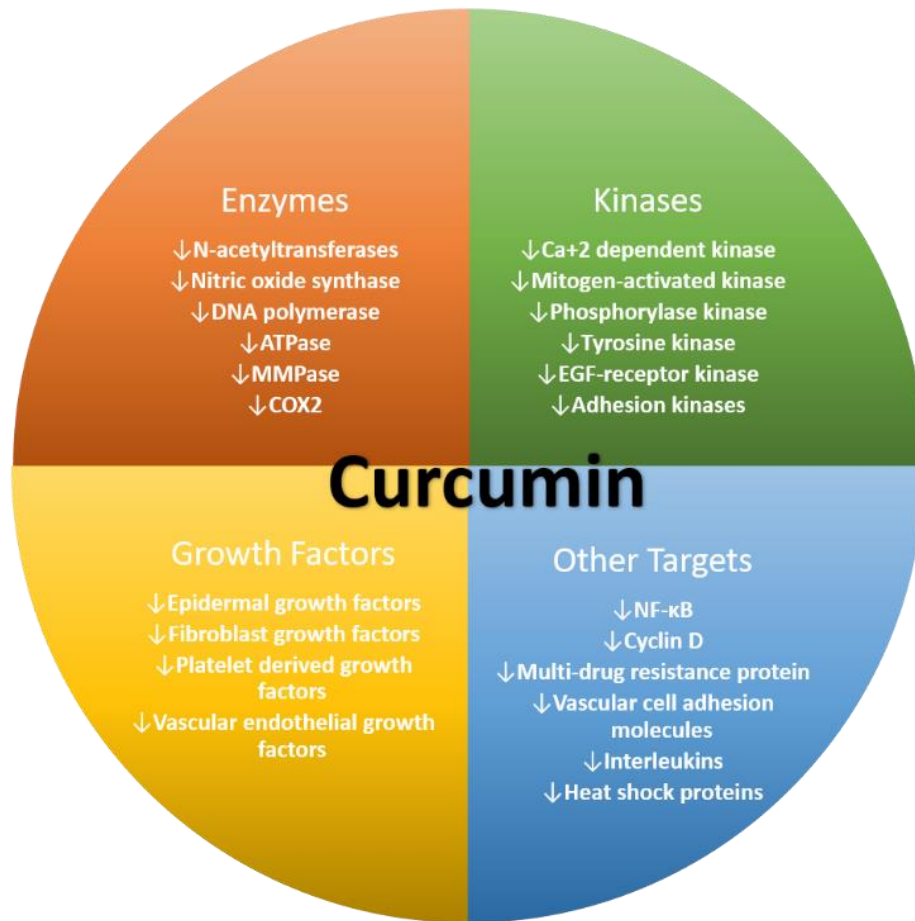


Figure 2.3: Multiple modes of biological activity of curcumin

Owing to all the biological properties of curcumin in *in vitro*, there has been a large interest in understanding the pharmaceutical properties of curcumin. In this regard, numerous pharmacokinetic studies have been performed and revealed that curcumin undergoes rapid and extensive metabolism. Bioavailability of curcumin is extremely limited due to metabolic instability, poor water solubility, and rapid elimination.⁹⁰⁻⁹² Curcumin is highly susceptible to glucuronidation and sulfation of the phenols making it a readily excretable compound (**Figure 2.4**). As a result, clinical studies with curcumin have been conducted at very high doses of up to 12 grams daily.^{90,93} While these high doses did not show toxic effects, mild

side effects such as diarrhea and nausea were observed.^{90,93} However it is highly impractical and medically not recommended to administer 12 grams of therapeutic in either acute or chronic setting. Efforts to increase the bioavailability include nanoformulations, and formulations with phosphatidylcholine.^{86,94}

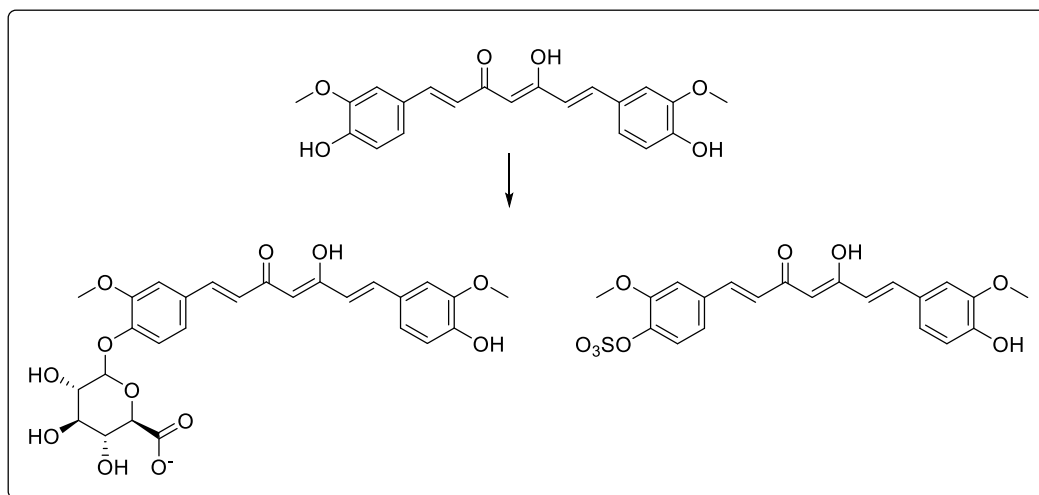


Figure 2.4: Metabolites of curcumin

Numerous modification sites are present in the in curcumin that have been modified to increase the anti-inflammatory, antioxidant, antimalarial, and anticarcinogenic effects, increase solubility, and improve pharmacological properties (**Figure 2.5**). However, the existing modifications have been met with little clinical success and as a result further development is needed. Some of the modification on curcumin template to improve its potency by extensive manipulation by various groups are presented below.

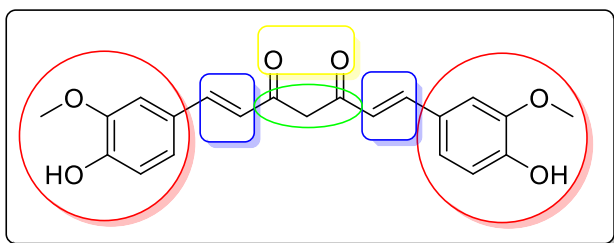
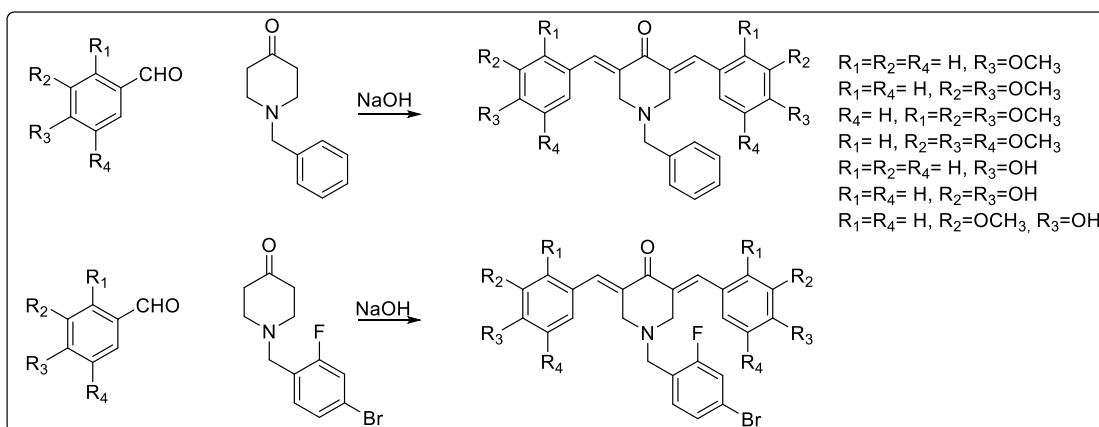


Figure 2.5 Modification sites of curcumin, red circle highlights aromatic substitution, blue α , β unsaturation, green diketo and yellow denotes carbonyl

Zhou et al. synthesized a series of curcuminoid compounds containing benzyl piperidone (**Scheme 2.1**). They evaluated the ability of the synthesized compounds to inhibit proliferation on human prostate cancer PC-3, pancreas cancer BxPC-3, colon cancer HT-29 and lung cancer cells H1299. Compounds showed increased activity compared to native curcumin. In fact, the lead compound was found to be ~40 times more potent than curcumin on all the tested cell lines. Toxicity of the remaining compounds showed IC_{50} values ranging from 0.41 to 17.67 μ M.⁹⁵



Scheme 2.1: Synthesis of piperidone curcuminoids as anticancer agents

Ferrari et al. synthesized a series of ester and carboxylic acid modified curcuminoids in an attempt to improve chemical stability and anti-cancer activity (**Figure 2.6**). Compounds were evaluated for activity against different tumorigenic cell lines human ovarian carcinoma cells, A2780, and A2780/CP, and human colon carcinoma cells HCT116 and LoVo. Results showed improved toxicity of compared to curcumin, with the esters being more active than acids.⁹⁶

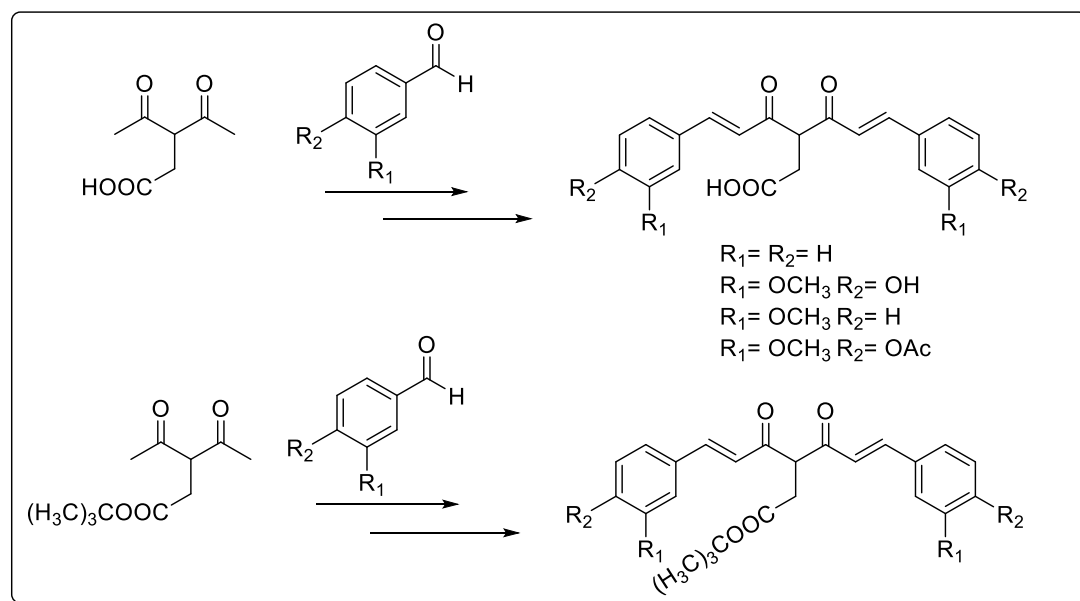
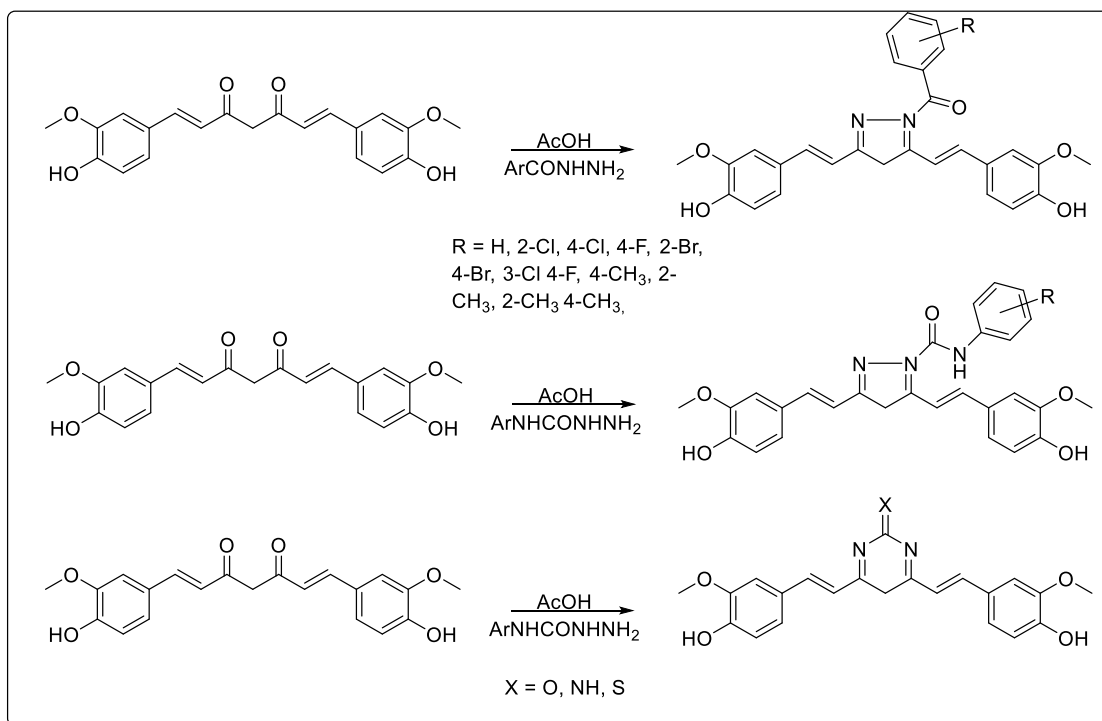


Figure 2.6: Synthesis of carboxylic and ester based curcuminoids

Ahsan et al. synthesized a novel class of heterocyclic azole-based curcumin analogs (**Scheme 2.2**). Compounds were synthesized to yield three different types, pyrazole amide, pyrazole urea, and pyrimidinone. Compounds were tested against a NCI 60 cell line panel at five doses. Many of the compounds exhibited greater activity compared to curcumin with toxicity in low micro concentrations. Pyrazole based curcuminoids are being further developed as potential anticancer agents.⁹⁷



Scheme 2.2: Synthesis of azole based curcuminoids

Shim et al. reported the synthesis of a class of semisynthetic hydrazinocurcuminoids. The lead compound (**Figure 2.7**) was found to inhibit bovine aortic endothelial cells (BAECs) at a nanomolar concentration.⁹⁸

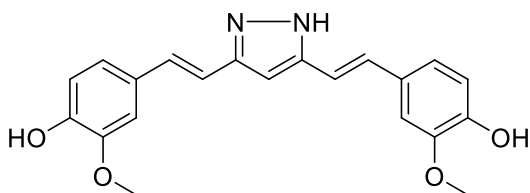


Figure 2.7: Structure of hydrazinocurcuminoid

Ishida et al. reported the synthesis of several curcuminoids with substitutions on the central carbon. Furthermore, they evaluated the in vitro cytotoxicity on a panel of human cancer cell lines. The most potent compound was shown in **Figure 2.8**. This compound showed proliferation inhibition across multiple cell lines including

HOS, bone osteosarcoma 1A9, breast cancer with IC₅₀ values in low micromolar range.⁹⁹

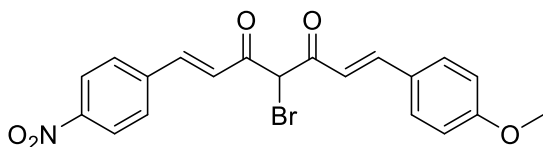


Figure 2.8: Structure of lead candidate compound with substitution on central carbon

Adams et al. synthesized a series of novel curcuminoids with modified diketo component. Modifications included mono ketone, cyclic ketone, and reduced monoketone (**Figure 2.9**). Compounds were evaluated for anticancer and antiangiogenic activities. Screening showed that the curcuminoids containing the cyclic ketone had increased *in vitro* anticancer and antiangiogenic activity compared with the diketone structure of curcumin.⁹⁵

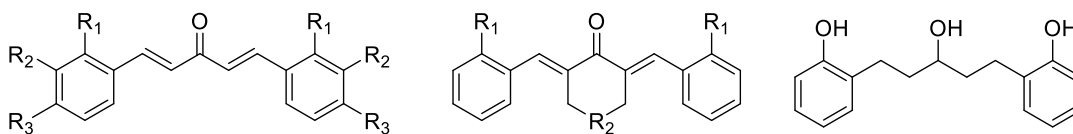


Figure 2.9: structure of modified mono ketones and alcohols of curcuminoid origin

2.1e Curcumin formulations

As mentioned above, curcumin is a natural product with a diverse set of medicinal properties. The metabolic lability of curcumin has led to an effort to formulate curcumin to increase clinical potential. Formulations of curcumin focus on improving the bioavailability and currently, there are several well studied

formulations. It has been found that NovaSol®, CurcuWin®, and LongVida® exhibited over 100-fold higher bioavailability relative to reference unformulated curcumin. As a result, these are the leading formulations of curcumin being developed further.

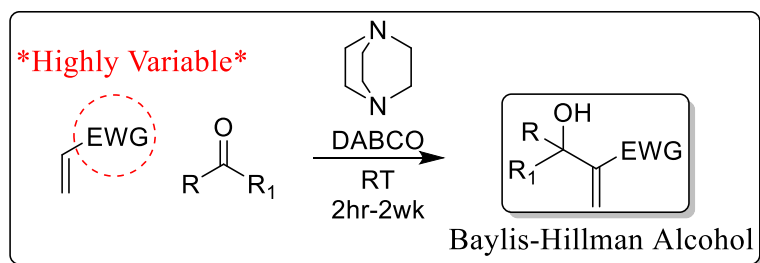
CurcuWin® is currently being developed by OmniActive Health Technologies. CurcuWin® is a novel formulation of curcumin comprised of 20%–28% turmeric powder, 63%–75% polyvinyl pyrrolidone, 10%–40% cellulosic derivatives and 1–3% natural antioxidants that allows for increased water solubility and bioavailability. Studies found the relative bioavailability was 130–140 times higher than unformulated curcumin.¹⁰⁰

NovaSol® is a liquid micelle formulation of curcumin being developed by Frutarom. NovaSol® curcumin micelles were formulated of 7% curcumin powder (6% curcumin) and 93% Tween-80. This micellation of curcumin showed ~185 times the relative bioavailability compared to native curcumin.¹⁰¹

LongVida® is currently being developed by Verdure Sciences. LongVida® is a solid lipid curcumin particle based formulation. Advantages of this formulation prevents curcumin from rapid degradation and excretion resulting in an increased half-life. LongVida® currently is comprised between 20% and 30%, however further modifications are in the works adjusting the composition percentages. LongVida® also contains soy lecithin containing purified phospholipids, docosahexaenoic acid, stearic acid and ascorbic acid.¹⁰²

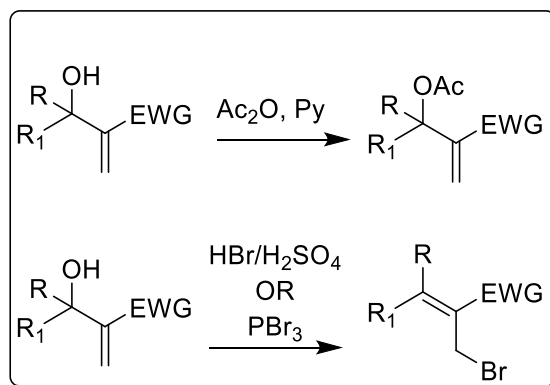
2.1f Baylis-Hillman reaction

One of the robust reaction that we intended to utilize for the synthesis of novel curcuminoid based derivatives is Baylis-Hillman reaction. Baylis-Hillman reactions are highly atom efficient and have little to no waste or byproducts generated.^{103–105} Another interesting feature is that this reaction is solvent free thus making it environmentally benign. Baylis-Hillman reaction involves condensation of aldehydes and electron deficient ketones with different unsaturated systems to produce functionalized allylic alcohols (**Scheme 2.3**).



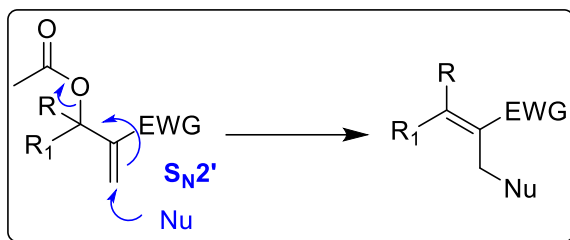
Scheme 2.3: Baylis-Hillman reaction.

These alcohols can be readily converted to leaving groups such as acetates and bromides with acetic anhydride and HBr/H₂SO₄ respectively (**Scheme 2.4**).



Scheme 2.4: Conversion of Baylis-Hillman alcohols to acetates and bromides

The acetates of product BH alcohols can be isomerized with various nucleophiles in S_N2' fashion to provide further functionalized structural synthons (**Scheme 2.5**).



Scheme 2.5: S_N2' capability of BH acetates.

The BH alcohols can also be converted into allyl bromides by reacting them with HBr/H_2SO_4 or PBr_3 (**Scheme 2.4**). The bromides have increased versatility where nucleophilic substitutions can occur in three different ways, S_N2 , allylic rearrangement in S_N2' mode, and 1,4-addition reaction (**Figure 2.10**).

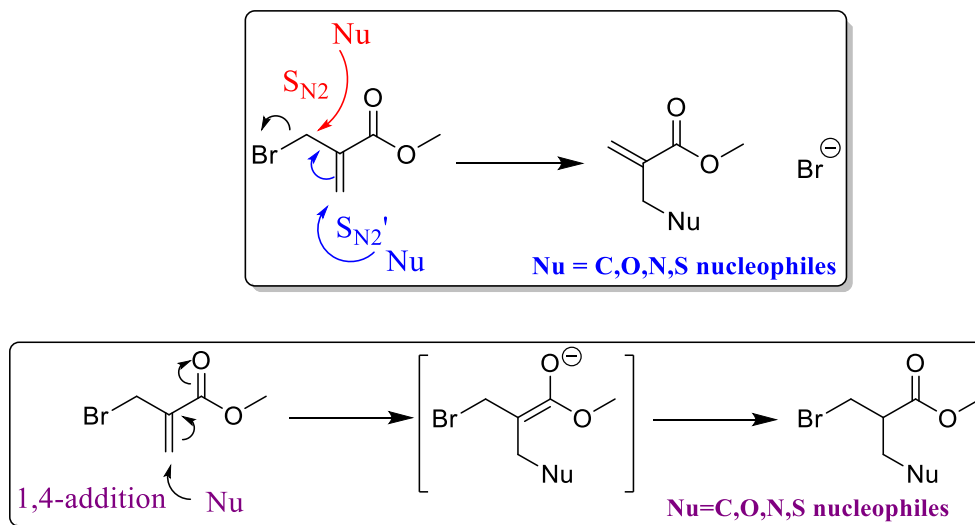
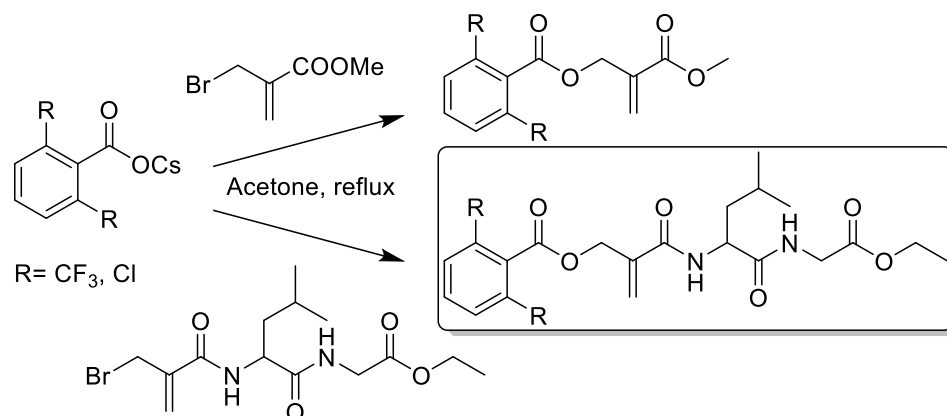


Figure 2.10: S_N2 , S_N2' , and 1,4 addition capabilities of Baylis-Hillman bromides.

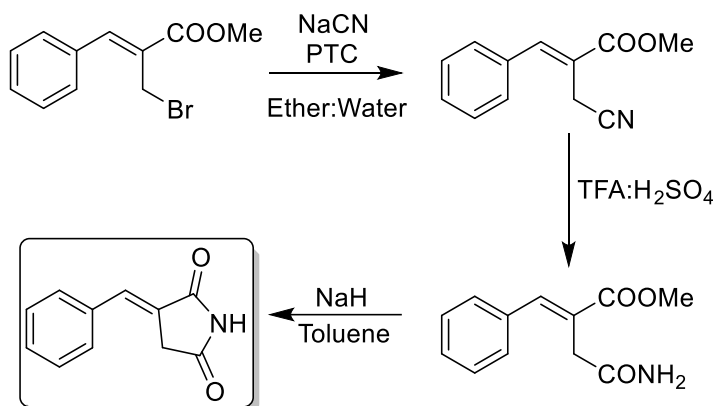
Below are some of the literature methods where Baylis-Hillman reaction was utilized in synthesizing biologically relevant molecules.

Klossowski et al. reported the synthesis of novel peptidomimetic inhibitors of thioredoxin–thioredoxin reductase system via O-alkylation of substituted cesium benzoates with α -methylbromo acrylamides derivatives to provide target compound in **Scheme 2.6**. *In vitro* cell proliferation inhibition showed IC₅₀ values between 3.4-25 μ M for many of the derivatives on numerous cell lines. Furthermore, *in vivo* evaluation of these derivatives showed significant tumor growth reduction against EMT6, breast cancer cells.¹⁰⁶



Scheme 2.6: Synthesis of BH bromide derived peptidomimetics.

Baylis Hillman bromides were utilized in the synthesis of 3-benzylidene-pyrrolidine-2,5-dione via nucleophilic displacement of bromide with sodium cyanide in S_N2 fashion. After substitution, nitriles were converted to amides and subsequent cyclization under basic conditions to obtain 3-benzylidene-pyrrolidine-2,5-dione product (**Scheme 2.7**).¹⁰⁷



Scheme 2.7: Synthesis of 3-benzylidene-pyrrolidine-2,5-dione using BH bromide

Spyvee, M., et al. further developed of 3-benzylidene-pyrrolidine-2,5-diones into a class of selective notch inhibitors. Compounds were evaluated for anticancer activity on numerous cell lines both notch dependent and independent. Results showed activity selectively towards notch dependent cell lines. Furthermore, compound 1-134-83 (**Figure 2.11**) was evaluated *in vivo* against esophageal adenocarcinoma, OE19, and showed significant tumor reduction at dosages of 15mg/Kg.¹⁰⁸

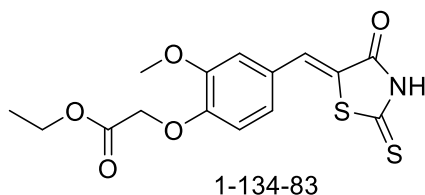
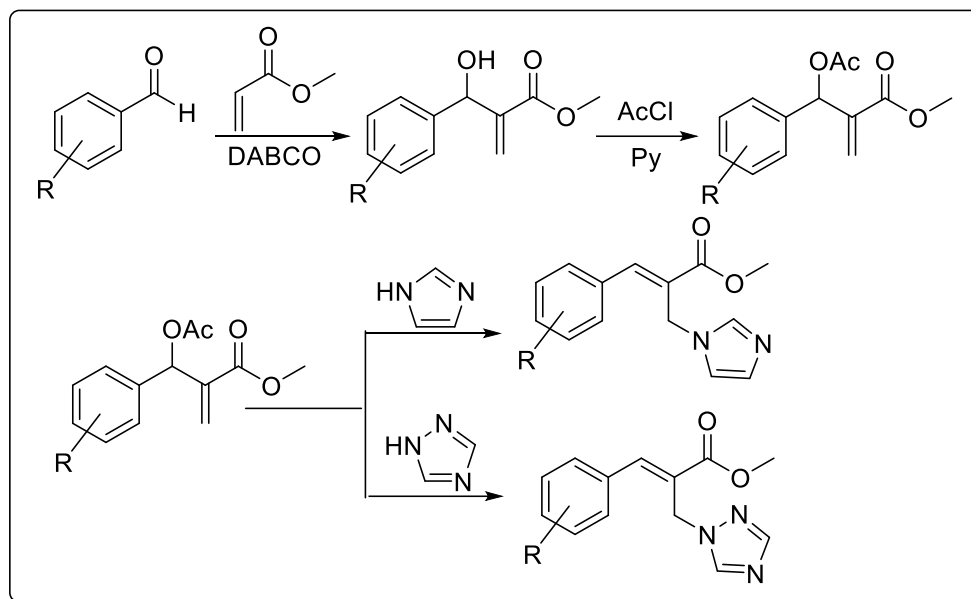


Figure 2.11: structure of 1-134-83

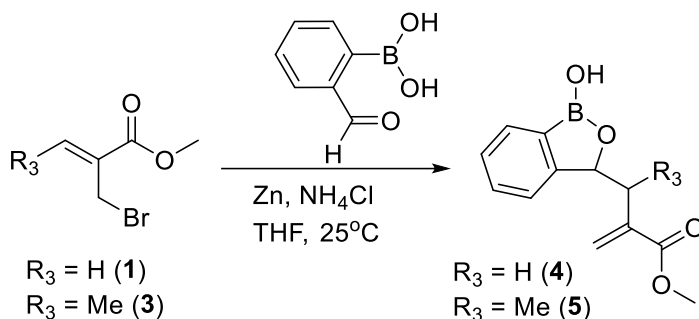
Nelson et al. synthesized Baylis-Hilman substituted imidazoles and triazoles for their antifungal activity against *C. neoformans* (**Scheme 2.8**). Several halogenated aromatic imidazole and triazole derivatives exhibited promising anti-fungal activity against *C. neoformans* (~8-13 $\mu\text{g/mL}$). The active

molecules exhibited little to no cytotoxicity when tested on proliferating breast cancer cell line MCF-7 (up to 50 μ M).¹⁰⁹



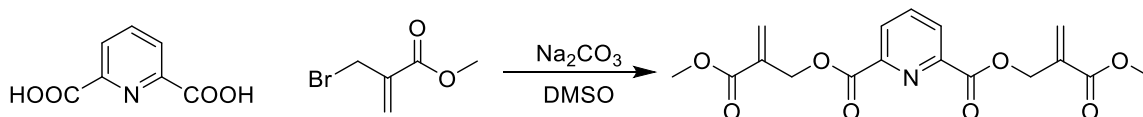
Scheme 2.8: Synthesis of Baylis-Hilman substituted imidazoles and triazoles

Extending the chemical applications of Baylis Hillman, Mereddy et al. carried out Zn based Barbier allylations on *o*-formyl phenyl boronic acids to synthesize functionalized benzoxaboroles as potential antimicrobial and antifungal agents.¹¹⁰ The reaction took place in a highly diastereoselective (*syn*) manner with BH bromide to obtain diastereometrically pure compound (**Scheme 2.9**). Activity of the synthesized compounds was limited on gram positive *Streptococcus thermophilus* and gram negative *Pseudomonas aeruginosa* bacteria, *Candida albicans* fungus, *Mycobacterium smegmatis*, and *Mycobacterium tuberculosis*.¹¹⁰



Scheme 2.9: Synthesis of functionalized benzoxaboroles from BH bromides.

Ronayne et al. previously synthesized a library of compounds with the Baylis-Hillman template as potential DNA alkylators. The reported synthesis produces benzoates, naphthoates, and nicotinates from the corresponding carboxylic acids and Baylis-Hillman bromides. The Compound shown was chosen as the lead (**Scheme 2.9**). It exhibited good activity on multiple cell lines including MDA-MB-231 (4 μM), 4T1 (6 μM), and MIAPaCa-2 (3 μM). Furthermore, this compound demonstrated an ability to bind to cellular nucleophiles due to increased nuclear disorganization and DNA damage. *In vitro* results were then translated to *in vivo* systems where this compound showed statistically significant tumor reduction in triple negative breast cancer (TNBC) MDA-MB-231 xenograft model at a dose of 20mg/Kg.¹¹¹



Scheme 2.9: Synthetic schemes for biologically active Baylis Hillman derived symmetrical curcumin-like template

2.1g Quaternary ammonium salts

To improve the water solubility, we intended to introduce quaternary ammonium salts in the curcuminoid template. Quaternary ammonium salts are an important class of compounds with unique chemical and biological properties. Quaternary ammonium salts are a group of organic compounds that contain a positively charged nitrogen atom on lipophilic backbones.¹¹²⁻¹¹⁴ Chemically, quaternary ammonium compounds are soluble in both aqueous as well as organic mediums, allowing for their use as phase transfer catalysts.¹¹²⁻¹¹⁴ Tuning of the solubility is easily obtainable through modification of carbon chain length. Commercially, these compounds are produced as surfactants, cleaners, and fabric softeners.¹¹²⁻¹¹⁴ Biologically, the polar ammonium component and the nonpolar chain group allows them to interact with cellular membranes.¹¹²⁻¹¹⁴ Medicinally, quaternary ammonium compounds have been used as antibacterials, antivirals, anticancer, muscle relaxants and spermicides. High throughput screening of quaternary ammonium salts showed that over 60% show disruption of mitochondrial activity with a majority illustrating disruption of complex 1.¹¹²⁻¹¹⁴

A small literature review on various quaternary ammonium salts and their biological relevance are presented below.

Benzalkonium chloride is a quaternary ammonium salt that functions as a cationic surfactant (**Figure 2.12**).¹¹⁵ Utility of benzalkonium chloride varies but has three primary uses as a biocide, a cationic surfactant, and as a phase transfer agent. As a biocide benzalkonium chlorides primarily cause dissociation of cellular membrane lipid bilayers.¹¹⁵ They also play a role in disruption of

respiratory and metabolic activities. As a result, benzalkonium chlorides have been investigated for use in hand sanitizers.¹¹⁵

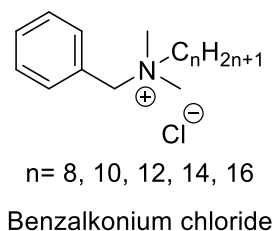


Figure 2.12: Structural template for various alky chain containing benzalkonium chlorides

Cetyl-pyridinium chloride (**Figure 2.13**) is a cationic quaternary ammonium compound used in some types of mouthwashes, toothpastes, lozenges, throat sprays, breath sprays, and nasal sprays. It is an antiseptic that kills bacteria and other microorganisms.¹¹⁵ It has been shown to be effective in preventing dental plaque and reducing gingivitis. It has also been used as an ingredient in certain pesticides.¹¹⁵ Recently, it has been investigated as a potential mitochondrial disrupting agent for the use of cancer.¹¹⁵

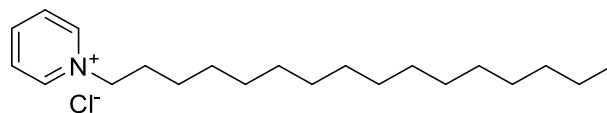


Figure 2.13: Structure of Cetylpyridinium chloride

ESC8 is a quaternary ammonium salt derivative of estrogen (**Figure 2.14**). First synthesized by Sinha et al., it has been shown to induce apoptosis in cancer cells through mitochondrial damage. The modification of including the ammonium salt has increased toxicity to hormone negative breast cancers while

keeping selective toxicity to cancer cells.¹¹⁶ They showed cell death occurred through intrinsic and extrinsic apoptotic pathways in response to mitochondrial function at low concentrations. Furthermore, they illustrated translatability to *in vivo* models with statistically significant reduction in tumor volume of TNBC MDA-MB-231 xenograft model at doses as low as 10mg/Kg.¹¹⁶

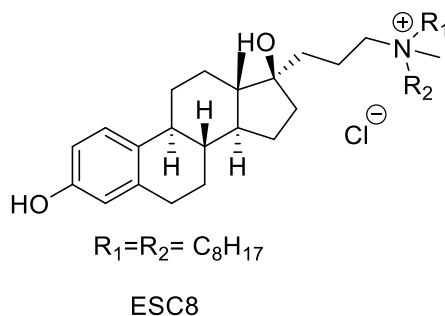


Figure 2.14: Structure of ESC8

2.1h Mitochondrial targeting agents with Quaternary salts

Several types of cancers have shown significantly increased mitochondrial membrane potential compared to normal cells. One explanation for increased mitochondrial potential is the higher energetic demands of cancerous cells. From a therapeutic aspect, this increased potential allows for the development of specific mitochondrial-targeting compounds. Of specific interest is the disruption of the mitochondrial potential. Currently several classes of compounds have been shown to disrupt mitochondrial potential including triphenylphosphoniums, guanidiniums, triethylammoniums, pyridiniums, 3-phenylsulfonylfuroxans, 2,3-dimethylbenzo thiazoliums, rhodamine 19, rhodamine 123 and dequalinium

(Figure 2.15).¹¹⁷ A conserved feature of these classes of compounds are they contain a lipophilic moiety connected to a delocalizable cation.

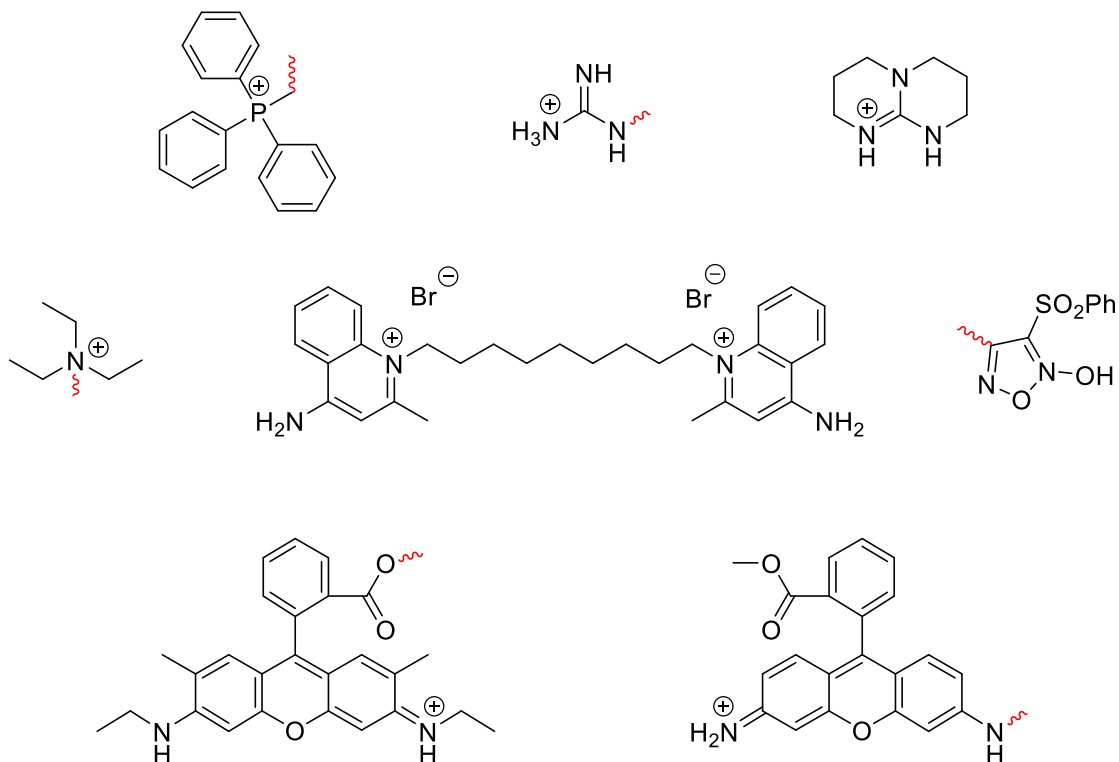


Figure 2.15: Examples of mitochondrial targeting agents.

2.2 Results and Discussion

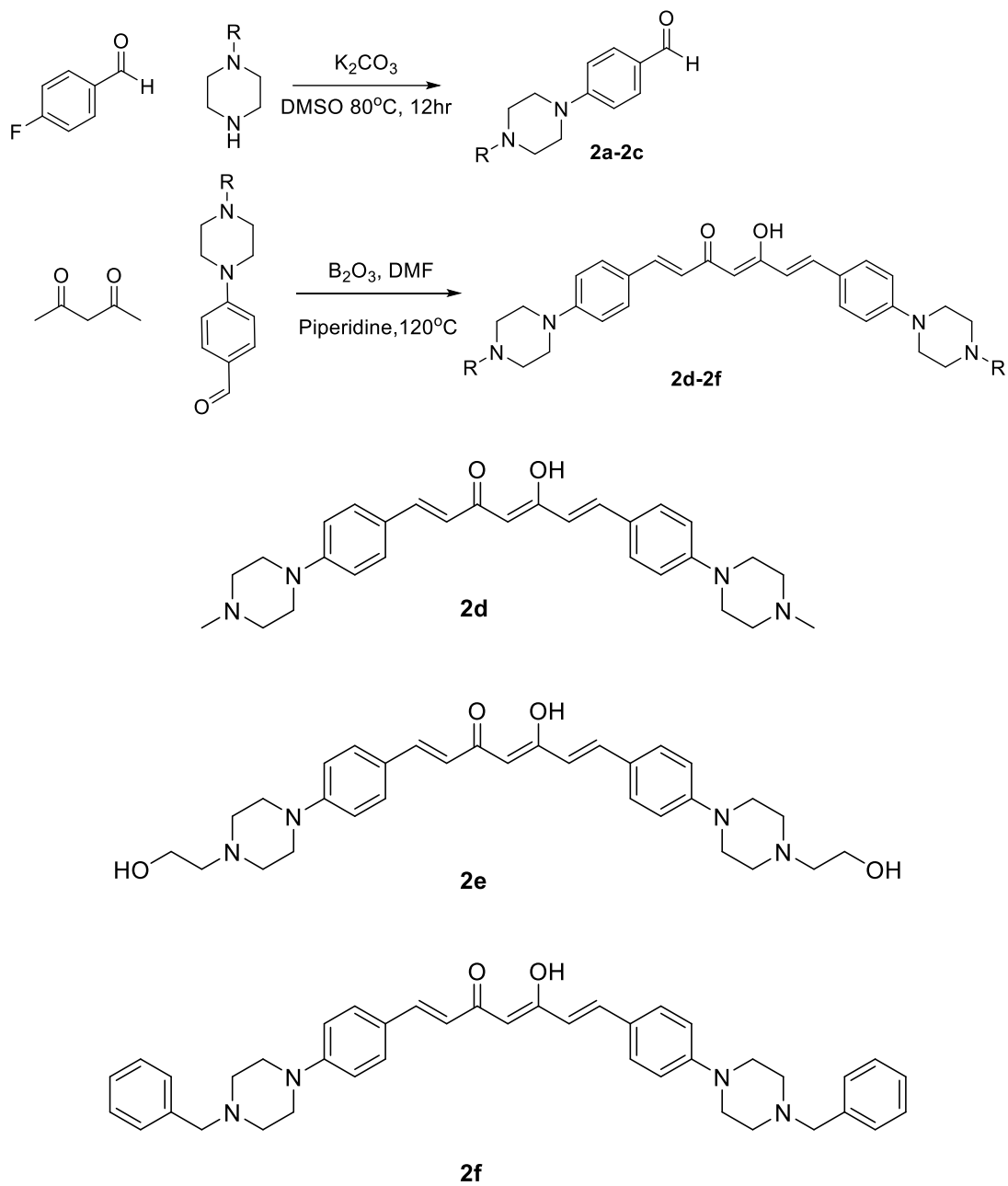
2.2a Synthesis of piperazine substituted curcumin analogs

For modification of phenol, we intended to include a functional group that not only maintained electron donating properties, but also allowed for further modifications. In this regard, we chose to substitute the phenolic group with piperazines. In addition to allowing for further modifications, piperazines also help to increase water solubility. To introduce the piperazine unit, we first started with *ipso* substitution of 4-fluoro benzaldehyde with different N-substituted

piperazines to obtain corresponding piperizinyl benzaldehydes. These piperazinyl benzaldehydes were further condensed with 2,4-pentanedione in the presence of boron oxide, triethylborate, and piperadine to yield corresponding curcuminoids **2d-2f**. (**Scheme 2.10**)

Owing to the relevance of curcumin, we endeavored the synthesis of curcumin analogs. Since the solubility is one of the major hurdles, solubility enhancing piperazine curcuminoids were synthesized. Initial synthesis of piperazinyl benzaldehydes were achieved by ipso substitution of fluoro benzaldehyde with three different piperazines namely *N*-methyl piperazine, *N*-ethanol piperazine and *N*-benzyl piperazine. The usual reaction conditions involve refluxing aldehyde along with piperazine and potassium carbonate in DMSO solvent. The pure aldehydes were obtained by diluting the reaction in water and filtration of the resulting solid product.

Synthesis of piperazines appended curcumins started by heating 1,4-pentanedione and boric anhydride at high temperature in DMF. This process of heating deactivates the central carbon by forming borate adduct on 1,4-pentanedione. The reaction was cooled to 120°C and corresponding aldehyde was added followed by dropwise addition of an amine base piperidine in DMF. Upon the completion of the reaction, solid product was obtained by adding cold water. This was filtered, washed and recrystallized in ethyl acetate and methanol. (**Scheme 2.10**).



Scheme 2.10. Structures of synthesized piperizinyl curcumin analogs.

2.2b Cell proliferation/cytotoxicity study of compounds 2d-2f

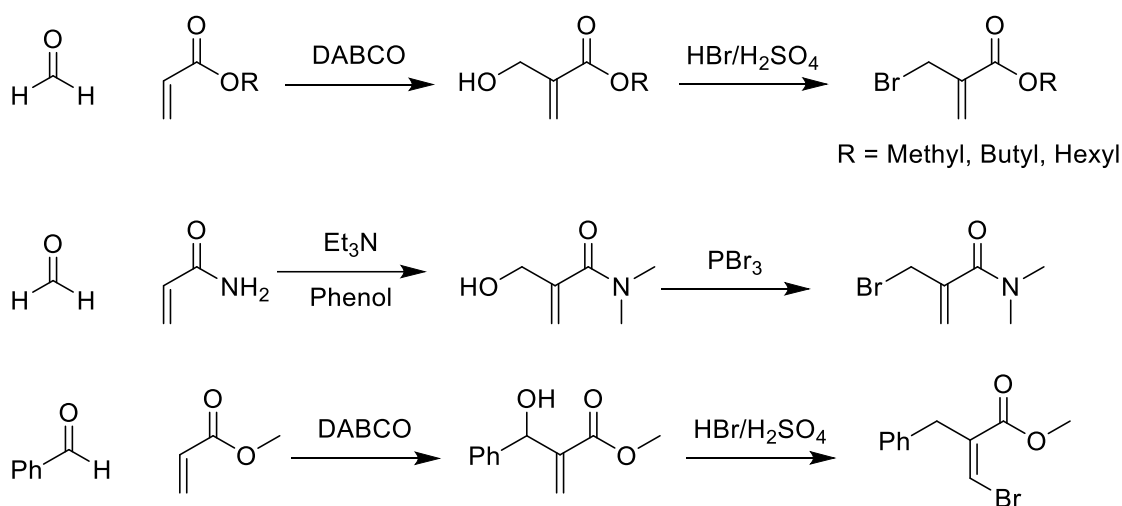
We hypothesized that these modifications would increase water solubility and potency. Therefore, we first evaluated these compounds for their ability to inhibit cell proliferation. Initial cell proliferation studies of the synthesized compounds **2d-2f** were carried out using 3-(4,5-dimethylthiazol-2-yl)-2,5-diphenyltetrazolium bromide (MTT) assay. This colorimetric assay measures the reduction of MTT to formazan by cellular mitochondrial reductase as a measure of cell viability. For this assay, we utilized three cell lines including, murine metastatic breast cancer cell line 4T1, human breast cancer cell line MDA-MB-231, and human pancreatic cell line MIAPaCa-2. The new compounds **2d-2f** did not exhibit toxicity up to 100 μM , whereas the parent compound curcumin has activity on these cell lines between 10 and 20 μM .

2.2c Design of novel water soluble curcuminoids as potential anticancer agents

Although curcumin has a lot of potential as therapeutic, it suffers from several drawbacks to be a lead compound for clinical applications. Inhibitory concentrations on molecular targets only exist at high micromolar concentrations. Curcumin is extremely limited in its bioavailability and metabolic stability. Therefore, modifications of curcumin should address the metabolically vulnerable sites, increase potency, water solubility, and absorption. In this regard, we modified curcumin's free phenol groups to increase metabolic stability and

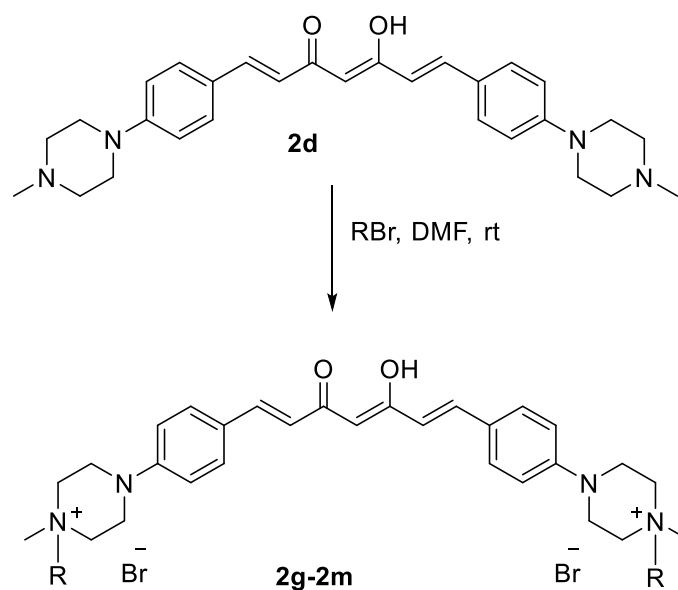
incorporated quaternary ammonium salts for solubility, and introduced Michael acceptors for increased potency.

Our initial modifications helped to increase water solubility and metabolic stability but resulted in reduced potency. To help achieve increased potency, we envisioned the inclusion of Michael acceptors on our curcuminoid scaffold. Michael acceptors are known to be good covalent linkers and can irreversibly bind to proteins, mitochondria, and DNA. In this regard, we developed novel Michael acceptors with high structural tunability using a Baylis-Hillman reaction template. This reaction is simple to perform, and by reacting an aldehyde with electron withdrawing group substituted ethylenes such as acrylates, and acrylamides in the presence of a nucleophilic base 1,4-diazabicyclo[2.2.2]octane (DABCO) provides functionalized allyl alcohols in one step. Furthermore, conversion of allylic alcohols to allylic bromides was achieved with either PBr_3 or $\text{H}_2\text{SO}_4/\text{HBr}$ (**Scheme 2.11**).



Scheme 2.11: Synthesis of Baylis Hillman bromides

As previously mentioned, we envisioned the inclusion of these Michael acceptors to our curcumin scaffold. To achieve this, we utilized our N-methyl curcuminoids as a representative example. To incorporate the bromides, the curcuminoid was dissolved in DMF and reacted with the corresponding bromide to obtain quaternary ammonium piperazinyl curcuminoids. Our design included acrylates of varying lengths to investigate the role of lipophilicity played in potency of the synthesized derivatives. We also intended to evaluate the necessity of our functionalized group in exhibiting SN2 and SN2' reactivity and generated quaternary ammonium salts with allyl and benzyl bromides in this regard (**Scheme 2.12, Figure 2.16**).



Scheme 2.12. Synthesis of quaternary ammonium curcuminoids

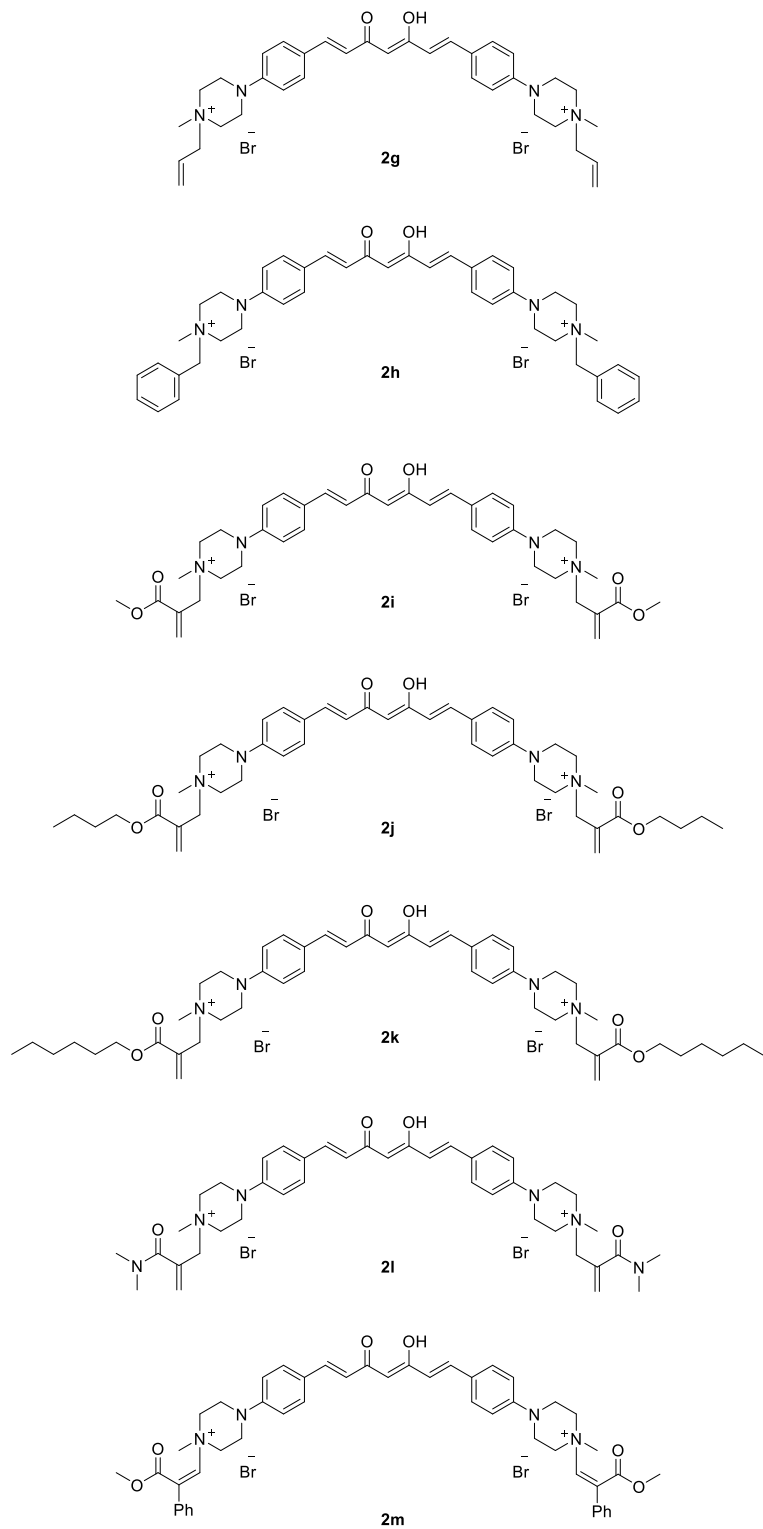


Figure 2.16. Structures of synthesized quaternary ammonium curcuminoids.

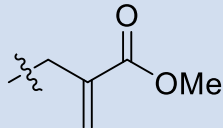
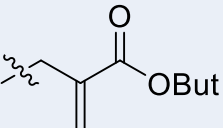
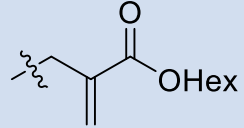
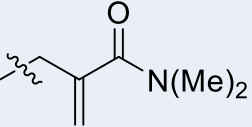
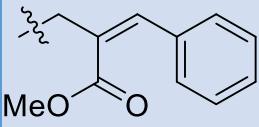
2.2d Cell proliferation/cytotoxicity study of compounds 2g-2m

We hypothesized that the inclusion of functionalized allyl bromides to our modified piperazinyll curcuminoids in the form of quaternary ammonium salts would increase potency and further increase solubility with SN_2 and SN_2' capability.

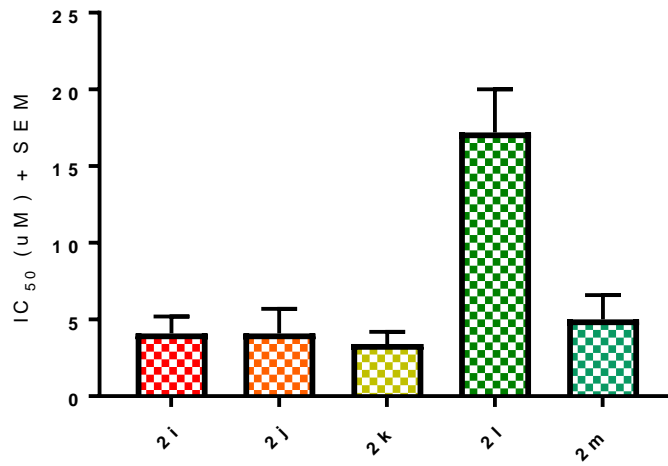
Cell proliferation studies of the synthesized compounds **2g-2m** were carried out using *in vitro* cell proliferation using 3-(4,5-dimethylthiazol-2-yl)-2,5-diphenyltetrazolium bromide (MTT) assay. This colorimetric assay measures the reduction of MTT to formazan by cellular mitochondrial reductase as a measure of cell viability. For this assay, we utilized three cell lines including, murine metastatic breast cancer cell line 4T1, human breast cancer cell line MDA-MB-231, and human pancreatic cell line MIAPaCa-2. The new compounds **2g** and **2h** containing simple allyl and benzyl salts did not exhibit cell proliferation inhibition up to 100 μ M concentration, similar to piperazine curcuminoids **2d-2f**, whereas the ammonium salts containing Baylis-Hillman groups exhibited good activity (**Table 2.1**). Compound **2i** exhibited the most potent cell proliferation inhibition properties with IC_{50} values of 3.6, 2.7, and 4.1 μ M on MDA-MB-231, MIAPaCa-2, and 4T1 cell lines, respectively. We also observed that with an increase in the carbon chain on the acrylates, the activity was also decreased. To further investigate the structure activity of our functionalized curcuminoids, we included a phenyl group on the olefin which resulted in decreased activity (**Table 2.1**, **Figure 2.17**). Lastly, in the modification to include acrylamide instead of acrylates, the activity was substantially decreased. It is still noteworthy that all the

functionalized allylic salts still resulted in increased potency compared to curcumin.

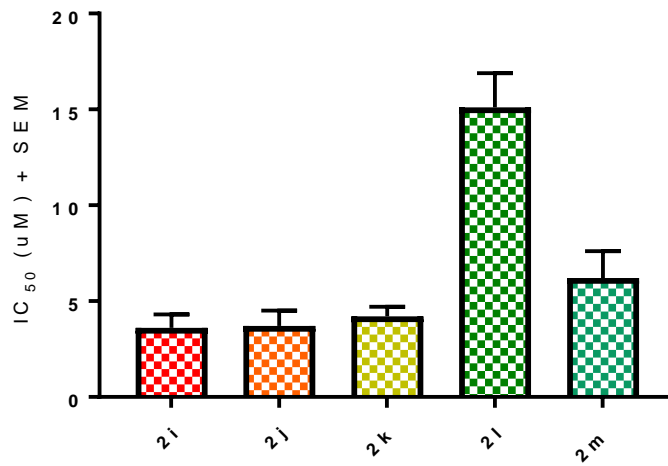
Table 2.1: Cell proliferation inhibition activity of **2g-2m** in MDA-MB-231, MIAPaCa-2 and 4T1 cell lines

Sl. No	R	MDA-MB-231 (μM)	MIAPaCa-2 (μM)	4T1 (μM)
2g	Allyl	>100	>100	>100
2h	Benzyl	>100	>100	>100
2i		3.6 \pm 0.7	2.7 \pm 0.5	4.1 \pm 1.1
2j		3.7 \pm 0.8	4.4 \pm 0.4	4.1 \pm 1.6
2k		4.2 \pm 0.5	4.2 \pm 0.7	3.4 \pm 0.8
2l		15.1 \pm 1.8	14.2 \pm 0.4	17.2 \pm 2.8
2m		6.2 \pm 1.4	4.1 \pm 0.3	5.0 \pm 1.6

4 T 1



M D A - M B - 2 3 1



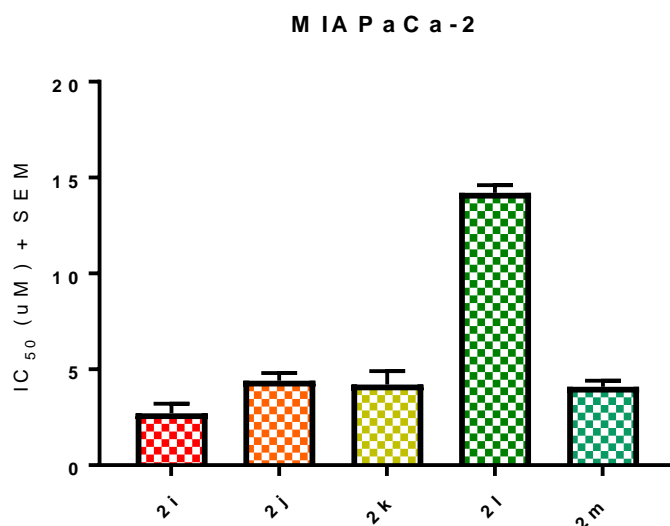
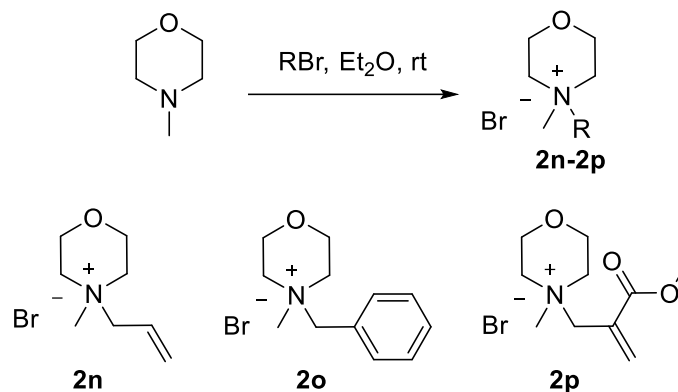


Figure 2.17. Cell proliferation inhibition of compounds **2i-2m** on 4T1, MDA-MB-231, and MIAPaCa-2

To demonstrate the necessity of the curcuminoid scaffold, we synthesized analogous quaternary ammonium salts utilizing a chemically simple template of N-methylmorpholine. For this purpose, N-methylmorpholine was dissolved in diethyl ether and the corresponding bromide was added (**Scheme 2.13**). The resulting morpholino quaternary ammonium salts **2n-2p** were obtained in good yields (**Scheme 2.13**). *In vitro* cell proliferation inhibition of these compounds did not indicate any significant activity up to 100 μ M concentration. We attribute this to highly polar nature due to low carbon content and their inability to cross lipophilic bilayers of the cells to cause any cytotoxicity.



Scheme 2.13. Synthesis of morpholino quaternary ammonium salts.

2.2e Florescence microscopy study of compound **2i** in MIAPaCa-2 cells

The lead compound **2i** exhibited good inhibition of cellular proliferation against multiple cancer cell lines and has fluorescent properties. Previously mentioned was the ability of quaternary ammonium salts to cause mitochondrial dysfunction and damage. In this regard, we planned to use fluorescence microscopy to 1) see if our compound enters the cell 2) localizes in the mitochondria and 3) causes mitochondrial disruption. To test the ability of the compound **2i** to cross the cell membrane and induce mitochondrial damage, we utilized MIAPaCa-2 cell line and studied fluorescence by labeling mitochondria with MitoTracker Red. MitoTracker Red is dependent upon mitochondrial potential and thus a change in fluorescent properties could be indicative of mitochondrial damage. The images were obtained using Nikon epifluorescence microscope. These studies indicated that in MIAPaCa-2 cells, compound **2i** is localized in the mitochondria and surrounding areas (**Figure 2.18**). It also shows

that there is mitochondrial disruption as the mitochondria become less defined and organized when exposed to compound. For a comparison, we also treated cells with curcumin. However mitochondrial damage was not detected utilizing this method.

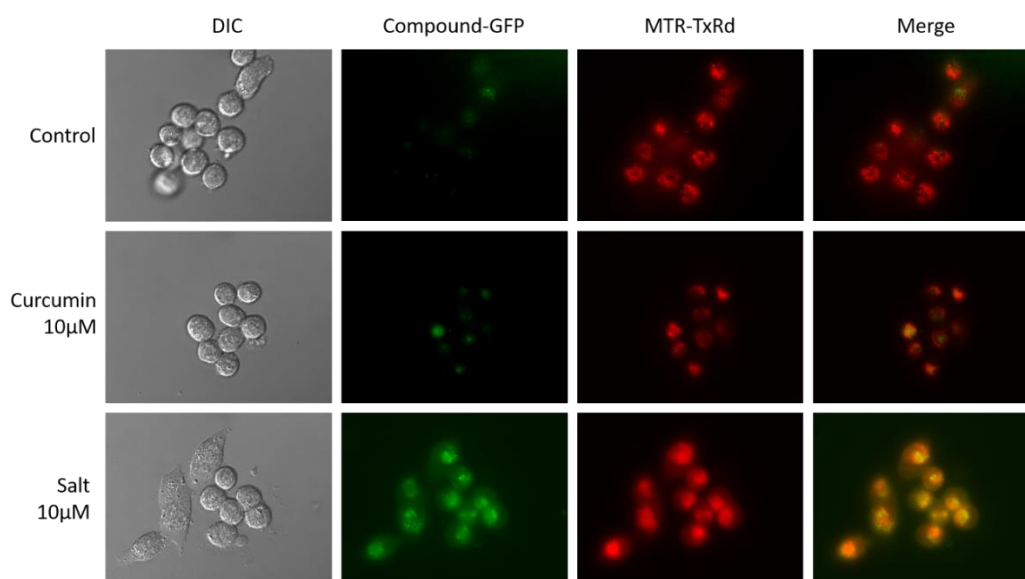


Figure 2.18. Fluorescence microscopy of MIAPaCa-2 cells treated with parent curcumin (10uM) and lead candidate **2i** salt (10uM) for 24 hours. Note candidate **2i** exhibited fluorescent characteristics when excited using a GFP filter set.

2.2f Systemic toxicity evaluation of compound **2i** in CD-1 mice

Compound **2i** showed enhanced inhibition of cancer cellular proliferation at low μM concentrations against three cell lines and exhibits increased water solubility compared to the natural product curcumin. Therefore, we chose to evaluate the systemic toxicity of the lead compound **2i** in healthy CD-1 mice.

Compound **2i** was dissolved in a 10% DMSO-saline solution. Toxicity study was carried out with mice randomly assigned into 2 groups (n = 6 mice per group) with similar average body weights. First group was treated with compound **2i** at 30 mg/Kg, ip, bid for the first 7 days and the dosage was increased to 50mg/Kg ip bid for an additional 7 days. The control group was administered with vehicle (10% DMSO-saline solution). At the end of the study, the treatment group did not show any visible toxic effects such as abnormal grooming, hunchback, morbidity and did not exhibit significant differences in body weights compared to the control group (**Figure 2.19**).

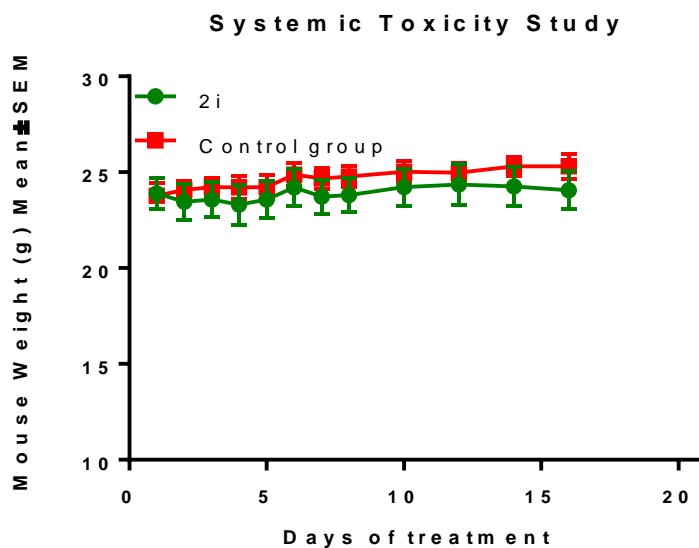


Figure 2.19: Systemic toxicity study of compound **2i**

2.2g Anticancer efficacy of compound **2i** in pancreatic cancer MIAPaCa-2 xenograft model in athymic nude mice

We then evaluated the lead candidate compound **2i** for *in vivo* efficacy in pancreatic cancer, MIAPaCa-2 tumor flank model. We selected MIAPaCa-2 cell line because this compound showed good *in vitro* activity and it is a well-established model. Compound **2i** was selected for *in vivo* anticancer efficacy study because of its good cytotoxicity and water solubility. We also included gemcitabine, a clinically used chemotherapeutic agent for pancreatic cancer as a positive control.

5×10^6 MIAPaCa-2 cells in a 1:1 mixture of Matrigel:PBS were inoculated onto the flank of female athymic nude mice. After the average tumor volume reached $\sim 225 \text{ mm}^3$, mice were randomly assigned into 4 groups (n = 6 mice per group). Group 1 was treated with compound **2i** at a dose of 40mg/Kg i.p bid. **2i**, group 2 was administered gemcitabine at 100mg/Kg, i.p, twice weekly, group 3 received the same dosages of compound **2i** and gemcitabine as a combination for 21 days. Group 4 was assigned as a control group and was treated with vehicle (10% DMSO). Body weights and tumor volume were measured every 2-3 days and after 14 days of treatment, mice were euthanized, and tumors were resected and weighed.

From this study, **2i** showed a statistically significant reduction of tumor volume ($P < 0.05$) 43% compared to control. This reduction was same as that of the clinically used gemcitabine. At the end of, the study, mice were euthanized, tumors were resected and weighed. Compound **2i** showed tumor reduction by 42% compared to control as a single agent and a reduction of 57% in combination with gemcitabine (**Figure 2.20**).

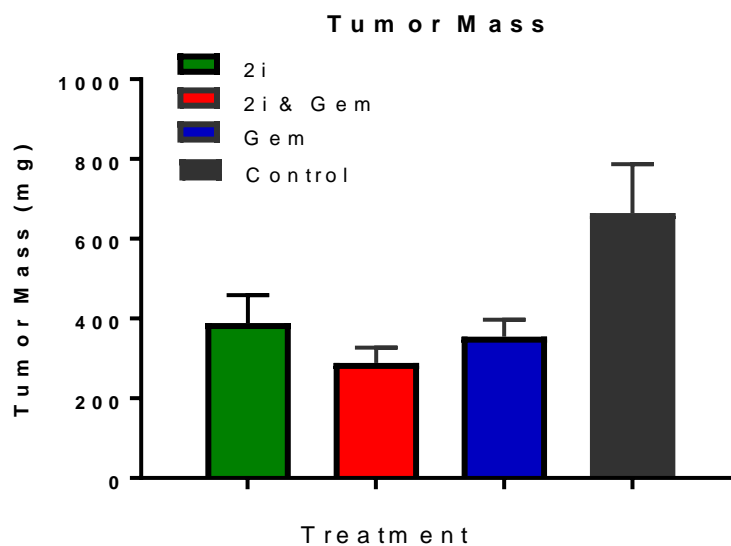
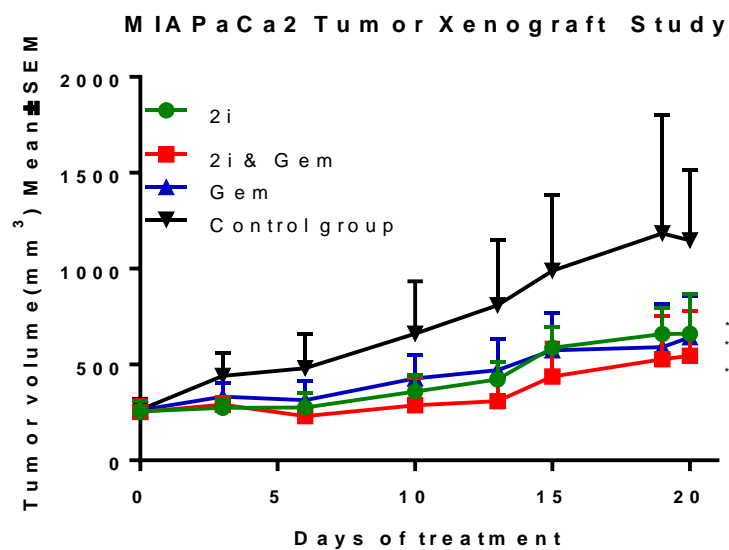


Figure 2.20: Tumor growth inhibition study of **2i** in MIAPaCa-2 flank xenograft study

2.3 Conclusions

In conclusion, we modified a natural product curcumin to increase its potency and solubility. Evaluation of these curcuminoids showed good cell proliferation inhibition on three cell lines of different cancer types, murine

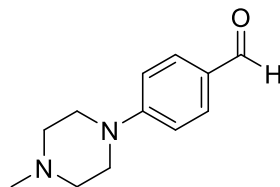
metastatic breast cancer cell line 4T1, human TNBC cell line MDA-MB-231, and human pancreatic cancer cell line MIAPaCa-2. After demonstrating inhibition of cellular proliferation, we translated these results in to *in vivo* models. For this, we first evaluated systemic toxicity in CD-1 mice for compound **2i** and found no significant body weight changes.

Anticancer efficacy studies in pancreatic cancer cell line MIAPaCa-2 showed that the lead candidate compound **2i** reduced the tumor burden at a dosage of 40mg/Kg ip bid as a single agent. Compound **2i** showed greater reduction when given with clinically used gemcitabine. Further investigations of these compounds can focus on pharmacokinetic/pharmacodynamic properties and combination therapies.

2.4 Experimental

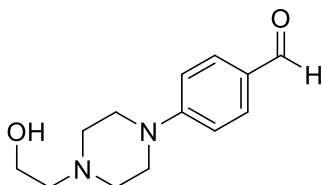
Synthesis of 4-(4-methylpiperazin-1-yl)benzaldehyde

To a solution of 4-fluorobenzaldehyde (10 mmol) in 20 mL DMSO, was added N-Methylpiperazine (40 mmol), potassium carbonate (20 mmol), and heated for 12hrs at 80 °C. Upon the completion of the reaction, the reaction mixture was extracted with ethyl acetate and water. The organic layer was dried with anhydrous Mg_2SO_4 and evaporated to obtain 4-(4-methylpiperazin-1-yl)benzaldehyde.



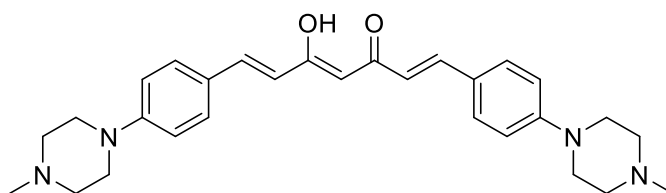
Synthesis of 4-(4-(2-hydroxyethyl)piperazin-1-yl)benzaldehyde

To a solution of 4-fluorobenzaldehyde (10 mmol) in 20 mL DMSO, was added 2--hydroxyethylpiperazine (40 mmol), potassium carbonate (20 mmol), and heated for 12hrs at 80 °C. Upon the completion of the reaction, the reaction mixture was extracted with ethyl acetate and water. The organic layer was dried with anhydrous Mg_2SO_4 and evaporated to obtain 4-(4-(2-hydroxyethyl)piperazin-1-yl)benzaldehyde.



Synthesis of (1E,4Z,6E)-5-hydroxy-1,7-bis(4-(4-methylpiperazin-1-yl)phenyl)hepta-1,4,6-trien-3-one:

To a solution of acetylacetone (10 mmol) in DMF (5 mL) was added boric anhydride (10 mmol) and the reaction mixture was heated at 170 °C for 0.5 h. The reaction was then cooled to 120 °C and 4-(4-methylpiperazin-1-yl)benzaldehyde (20 mmol) was added. A 1:1 mixture of piperidine (10 mmol) in DMF was then added drop wise and the reaction was stirred for 2 h. Upon the completion of the reaction (TLC), cold water (20 mL) was added and the solid was filtered and washed with water (3 × 20 mL). 5 was obtained as the pure compound upon recrystallization in ethyl acetate–methanol mixture.

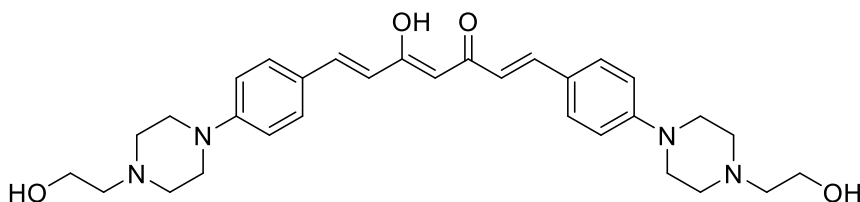


(1E,4Z,6E)-5-hydroxy-1,7-bis(4-(4-methylpiperazin-1-yl)phenyl)hepta-1,4,6-trien-3-one ¹H NMR (500 MHz, CDCl₃): δ ppm 7.59 (d, J = 15 Hz, 2H), 7.46 (d, J = 10 Hz, 4H), 6.88 (d, J = 10 Hz, 4H), 6.46 (d, J = 15 Hz, 2H), 5.75 (s, 1H), 3.32 (t, J = 5 Hz, 8H), 2.58 (t, J = 5 Hz, 8H), 2.36 (s, 6H); ¹³C NMR (125 MHz, CDCl₃): δ ppm 183.27, 152.12, 140.19, 129.61, 125.82, 120.68, 115.03, 101.16, 54.73, 47.71, 45.97.

HRMS (ESI) m/z: calc'd for C₂₉H₃₆N₄O₂ [M]⁺: 472.2838, found [M+H]⁺: 473.2763

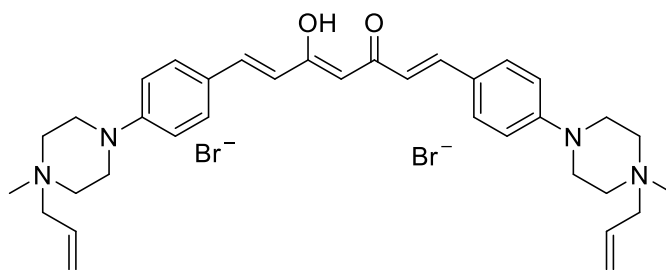
Synthesis of (1E,4Z,6E)-5-hydroxy-1,7-bis(4-(4-(2-hydroxyethyl)piperazin-1-yl)phenyl)hepta-1,4,6-trien-3-one

To a solution of acetylacetone (10 mmol) in DMF (5 mL) was added boric anhydride (10 mmol) and the reaction mixture was heated at 170 °C for 0.5 h. The reaction was then cooled to 120 °C and 4-(4-(2-hydroxyethyl)piperazin-1-yl)benzaldehyde (20 mmol) was added. A 1:1 mixture of piperidine (10 mmol) in DMF was then added drop wise and the reaction was stirred for 2 h. Upon the completion of the reaction (TLC), cold water (20 mL) was added and the solid was filtered and washed with water (3 × 20 mL). (1E,4Z,6E)-5-hydroxy-1,7-bis(4-(4-(2-hydroxyethyl)piperazin-1-yl)phenyl)hepta-1,4,6-trien-3-one as the pure compound upon recrystallization in ethyl acetate–methanol mixture.



Synthesis of (1E,4Z,6E)-1,7-bis(4-(4-allyl-4-methylpiperazin-1-yl)phenyl)-5-hydroxyhepta-1,4,6-trien-3-one, bromide salt

To a solution of (1E,4Z,6E)-5-hydroxy-1,7-bis(4-(4-methylpiperazin-1-yl)phenyl)hepta-1,4,6-trien-3-one (10 mmol) in DMF (60 mL) was added the allyl bromide (50 mmol) and the reaction mixture was stirred at RT for 1 hour. Upon the completion of the reaction, acetone (20 mL) was added and the resulting dibromide salt of (1E,4Z,6E)-5-hydroxy-1,7-bis(4-(4-methylpiperazin-1-yl)phenyl)hepta-1,4,6-trien-3-one was filtered.

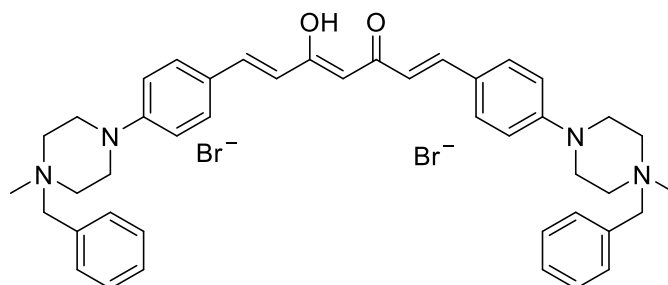


Synthesis of (1E,4Z,6E)-1,7-bis(4-(4-benzyl-4-methyl-4H-piperazin-1-yl)phenyl)-5-hydroxyhepta-1,4,6-trien-3-one, bromide salt

To a solution of (1E,4Z,6E)-5-hydroxy-1,7-bis(4-(4-methylpiperazin-1-yl)phenyl)hepta-1,4,6-trien-3-one (10 mmol) in DMF (60 mmol) was added the benzyl bromide (50 mmol) and the reaction mixture was stirred at RT for 1 hour. Upon the completion of the reaction, acetone (20 mL) was added and the resulting dibromide salt of (1E,4Z,6E)-5-hydroxy-1,7-bis(4-(4-methylpiperazin-1-yl)phenyl)hepta-1,4,6-trien-3-one was filtered.

^1H NMR (500 MHz, $\text{DMSO-}d_6$) δ ppm 7.65 (d, $J=9$ Hz, 4H), 7.55 (d, $J=16$ Hz, 2H), 7.05 (d, $J=9$ Hz, 4H), 6.75 (d, $J=16$ Hz, 2H), 6.11-6.04 (m, 3H), 5.70-5.65 (m, 4H), 4.16 (d, $J=13$ Hz, 4H), 3.77-3.36 (m, 16H), 3.12 (s, 6H)

^{13}C NMR (126 MHz, $\text{DMSO-}d_6$) δ ppm 183.5, 151.1, 140.5, 130.3, 128.5, 126.1, 125.7, 121.3, 115.7, 101.6, 65.0, 58.6, 46.6, 41.6



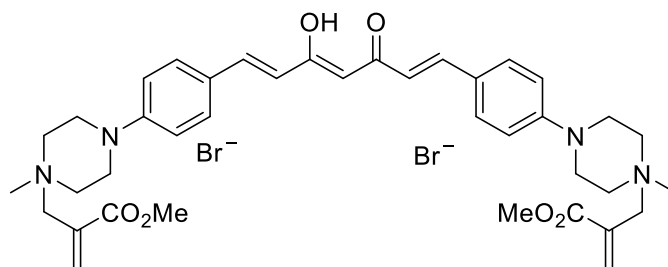
^1H NMR (500 MHz, $\text{DMSO-}d_6$) δ ppm 2.86 (br. s., 5 H) 3.43 (br. s., 8 H) 3.60 (d, $J=13$ Hz, 3 H) 3.86 (s, 5 H) 4.66 (br. s., 3 H) 6.02 (s, 1 H) 6.73 (d, $J=15$ Hz, 1 H) 6.96 (d, $J=8$ Hz, 3 H) 7.46 - 7.57 (m, 9 H) 7.60 (br. s., 9 H) 8.37 (s, 2 H);

^{13}C NMR (126 MHz, $\text{DMSO-}d_6$) δ ppm 39.7, 41.3, 45.5, 53.4, 58.1, 59.2, 79.7, 115.3, 120.8, 126.1, 129.7, 134.0, 140.5, 150.9, 152.0, 167.4, 183.5

HRMS (ESI) m/z : calc'd for $\text{C}_{51}\text{H}_{58}\text{N}_4\text{O}_6$ [$M/2$]: 411.2178, found 411.2202

Synthesis of dimethyl 2,2'-((((1E,3Z,6E)-3-hydroxy-5-oxohepta-1,3,6-triene-1,7-diyl)bis(4,1-phenylene))bis(1-methyl-1λ4-piperazine-4,1-diyl))bis(methylene)) diacrylate, bromide salt

To a solution of (1E,4Z,6E)-5-hydroxy-1,7-bis(4-(4-methylpiperazin-1-yl)phenyl)hepta-1,4,6-trien-3-one (10 mmol) in DMF (60 mmol) was added the alkyl bromide (50 mmol) and the reaction mixture was stirred at RT for 1 hour. Upon the completion of the reaction, acetone (20 mL) was added and the resulting in corresponding ammonium bromide was filtered.



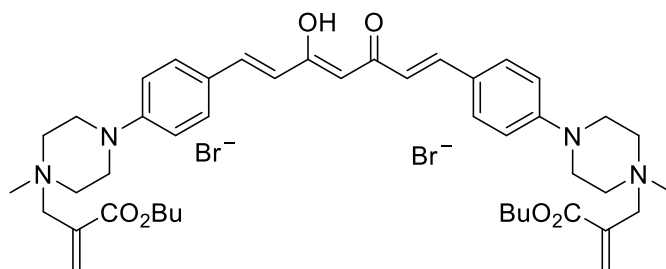
^1H NMR (500 MHz, $\text{DMSO-}d_6$) δ ppm 8.33 (s, 1H), 7.63 (d, $J = 9$ Hz, 4H), 7.55 (d, $J = 16$ Hz, 2H), 7.06 (d, $J = 9$ Hz, 4H), 6.85 (s, 2H), 6.75 (d, $J = 16$ Hz, 2H), 6.50 (s, 2H), 6.04 (s, 1H), 4.42-3.85 (m, 10H), 3.78-3.49 (m, 16H), 3.10 (s, 6H)

^{13}C NMR (126 MHz, $\text{DMSO-}d_6$) δ 183.5, 166.1, 162.8, 151.1, 141.7, 140.5, 130.3, 128.8, 126.1, 121.3, 115.4, 62.6, 59.2, 53.2, 45.8, 41.4

HRMS (ESI) m/z : calc'd for $\text{C}_{39}\text{H}_{50}\text{N}_4\text{O}_6$ $[\text{M}]^+$: 830.2077, found $\text{C}_{39}\text{H}_{50}\text{N}_4\text{O}_6$ $[\text{M}-2\text{Br}]^+$: 335.1716

Synthesis of dibutyl 2,2'-((((1E,3Z,6E)-3-hydroxy-5-oxohepta-1,3,6-triene-1,7-diyl)bis(4,1-phenylene))bis(1-methyl-1λ4-piperazine-4,1-diyl))bis(methylene))diacrylate, bromide salt

To a solution of (1E,4Z,6E)-5-hydroxy-1,7-bis(4-(4-methylpiperazin-1-yl)phenyl)hepta-1,4,6-trien-3-one (10 mmol) in DMF (60 mmol) was added the alkyl bromide (50 mmol) and the reaction mixture was stirred at RT for 1 hour. Upon the completion of the reaction, acetone (20 mL) was added and the resulting dibromide salt, dibutyl 2,2'-((((1E,3Z,6E)-3-hydroxy-5-oxohepta-1,3,6-triene-1,7-diyl)bis(4,1-phenylene))bis(1-methyl-1λ4-piperazine-4,1-diyl))bis(methylene))diacrylate was filtered.



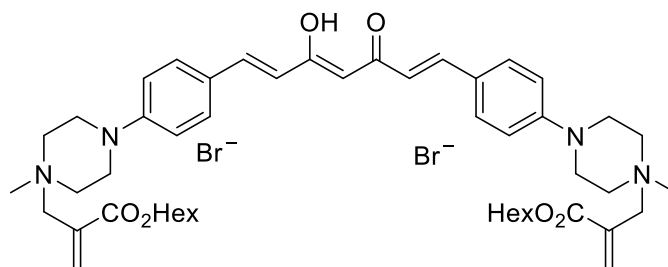
^1H NMR (500 MHz, $\text{DMSO-}d_6$) δ ppm 7.62 (d, $J= 8$ Hz, 4H), 7.54 (d, $J= 16$ Hz, 2H), 7.03 (d, $J= 8$ Hz, 4H), 6.84 (s, 2H), 6.73 (d, $J= 16$ Hz, 2H), 6.49 (s, 2H), 6.04 (s, 1H), 4.42 (s, 4H), 4.17 (t, $J= 7$ Hz, 4H), 3.84 (d, $J= 12$ Hz, 4H), 3.55-3.52 (m, 12H), 3.07 (s, 6H), 1.65-1.60 (m, 4H), 1.38-1.34 (m, 4H), 0.90 (t, $J=8$ Hz, 6H)

^{13}C NMR (126 MHz, $\text{DMSO-}d_6$) δ ppm 183.6, 165.7, 151.1, 141.5, 140.5, 130.3, 129.0, 126.1, 121.3, 115.4, 101.6, 65.7, 62.6, 59.2, 45.8, 41.4, 30.5, 19.1, 14.1

HRMS (ESI) m/z : calc'd for $\text{C}_{45}\text{H}_{62}\text{N}_4\text{O}_6$ [$M/2$]: 377.2335, found 377.2273

Synthesis of dihexyl 2,2'-((((1E,3Z,6E)-3-hydroxy-5-oxohepta-1,3,6-triene-1,7-diyl)bis(4,1-phenylene))bis(1-methyl-1λ4-piperazine-4,1-diyl))bis(methylene))diacrylate, bromide salt

To a solution of (1E,4Z,6E)-5-hydroxy-1,7-bis(4-(4-methylpiperazin-1-yl)phenyl)hepta-1,4,6-trien-3-one (10 mmol) in DMF (60 mmol) was added the alkyl bromide (50 mmol) and the reaction mixture was stirred at RT for 1 hour. Upon the completion of the reaction, acetone (20 mL) was added and the resulting dibromide salt, dihexyl 2,2'-((((1E,3Z,6E)-3-hydroxy-5-oxohepta-1,3,6-triene-1,7-diyl)bis(4,1-phenylene))bis(1-methyl-1λ4-piperazine-4,1-diyl))bis(methylene))diacrylate was filtered.



^1H NMR (500 MHz, $\text{DMSO-}d_6$) δ ppm 7.63 (d, $J=8$ Hz, 4 H), 7.55 (d, $J=16$ Hz, 2H), 7.05(d, $J=8$ Hz, 4H), 6.84 (s, 2H), 6.75 (d, $J=16$ Hz, 2H), 6.53 (s, 2H) 6.05 (s, 1H), 4.46 (s, 4H), 4.17 (t, $J=7$ Hz, 4H), 3.85 (d, $J=11$ Hz, 4H), 3.55-3.53 (m, 12H), 3.10 (s, 6H), 1.66-1.62 (m, 4H), 1.34-1.27 (m, 12H), 0.85 (t, $J=7$ Hz, 6H)

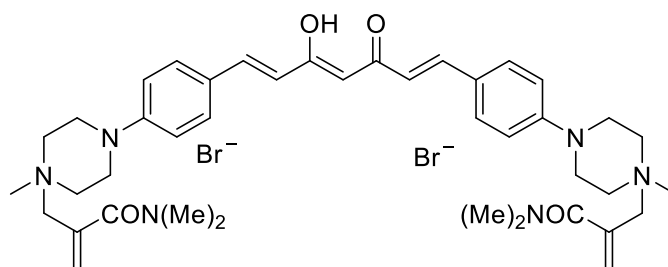
^{13}C NMR (126 MHz, $\text{DMSO-}d_6$) δ ppm 183.6, 165.6, 151.1, 141.4, 140.5, 130.3, 129.0, 126.1, 121.3, 115.4, 105.0, 66.0, 62.7, 59.2, 45.9, 41.4, 31.3, 28.4, 25.5, 22.4, 14.4

HRMS (ESI) m/z : calc'd for $\text{C}_{49}\text{H}_{70}\text{N}_4\text{O}_6$ [$M/2$]: 405.2642, found 405.2637

Synthesis of 2,2'-((((1E,3Z,6E)-3-hydroxy-5-oxohepta-1,3,6-triene-1,7-diyloxybis(4,1-phenylene))bis(1-methyl-1,4-piperazine-4,1-diyloxybis(methylene))bis(N,N-dimethylacrylamide), bromide salt

To a solution of (1E,4Z,6E)-5-hydroxy-1,7-bis(4-(4-methylpiperazin-1-yl)phenyl)hepta-1,4,6-trien-3-one (10 mmol) in DMF (60 mmol) was added the alkyl bromide (50 mmol) and the reaction mixture was stirred at RT for 1 hour. Upon the completion of the reaction, acetone (20 mL) was added and the resulting

dibromide salt, 2,2'-((((1E,3Z,6E)-3-hydroxy-5-oxohepta-1,3,6-triene-1,7-diyl)bis(4,1-phenylene))bis(1-methyl-1λ4-piperazine-4,1-diyl))bis(methylene))bis(N,N-dimethylacrylamide) was filtered.



^1H NMR (500 MHz, $\text{DMSO-}d_6$) δ ppm 7.64 (d, $J=8\text{Hz}$, 4H), 7.55 (d, $J=16\text{ Hz}$, 2H), 7.05 (d, $J=8\text{Hz}$, 4H), 6.75 (d, $J=16\text{ Hz}$, 2H), 6.11 (s, 2H), 6.04 (s, 1H), 5.94 (s, 2H), 4.44 (s, 4H), 3.81-3.78 (m, 4H), 3.60-3.10 (m, 24H), 2.92 (s, 6H)

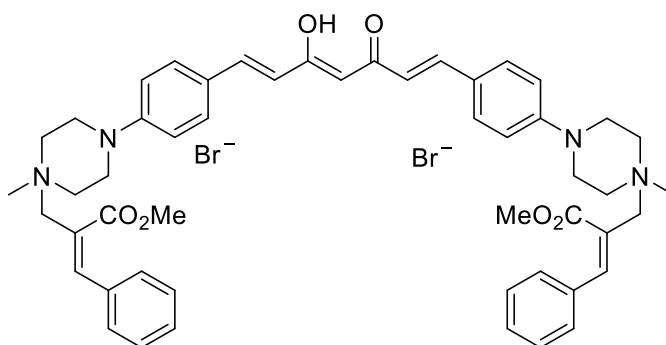
^{13}C NMR (126 MHz, $\text{DMSO-}d_6$) δ ppm 183.5, 168.4, 151.0, 140.5, 132.4, 132.3, 130.3, 126.1, 121.3, 115.4, 101.6, 64.9, 59.1, 46.5, 41.4, 35.4

HRMS (ESI) m/z: calc'd for $\text{C}_{41}\text{H}_{56}\text{N}_6\text{O}_4$ [$\text{M}/2$]: 348.2181, found 348.2060

Synthesis of dimethyl 2,2'-((((1E,3Z,6E)-3-hydroxy-5-oxohepta-1,3,6-triene-1,7-diyl)bis(4,1-phenylene))bis(1-methyl-1λ4-piperazine-4,1-diyl))bis(methylene)) (2Z,2'Z)-bis(3-phenylacrylate)

To a solution of (1E,4Z,6E)-5-hydroxy-1,7-bis(4-(4-methylpiperazin-1-yl)phenyl)hepta-1,4,6-trien-3-one (10 mmol) in DMF (60 mmol) was added the alkyl bromide (50 mmol) and the reaction mixture was stirred at RT for 1 hour. Upon the completion of the reaction, acetone (20 mL) was added and the resulting

dibromide salt, dimethyl 2,2'-((((1E,3Z,6E)-3-hydroxy-5-oxohepta-1,3,6-triene-1,7-diyl)bis(4,1-phenylene))bis(1-methyl-1 λ 4-piperazine-4,1-diyl))bis(methylene)) (2Z,2'Z)-bis(3-phenylacrylate) was filtered.



dimethyl 2,2'-((((1E,3Z,6E)-3-hydroxy-5-oxohepta-1,3,6-triene-1,7-diyl)bis(4,1-phenylene))bis(1-methyl-1 λ 4-piperazine-4,1-diyl))bis(methylene)) (2Z,2'Z)-bis(3-phenylacryl)

^1H NMR (500 MHz, DMSO- d_6) δ 8.37 (s, 2H), 7.39 - 7.71 (m, 17H), 6.96 (d, J = 8 Hz, 4H), 6.73 (d, J = 16 Hz, 2H), 6.02 (br. s., 1H), 4.66 (s, 4H), 3.86 (s, 6H), 3.60 (d, J = 13 Hz, 6H), 3.10-3.49 (m, 4H), 2.86 (s, 6H), 2.49 (s, 6H)

^{13}C NMR (126 MHz, DMSO- d_6) δ 183.5, 167.4, 152.0, 150.9, 140.5, 134.1, 130.5, 130.2, 129.7, 126.2, 121.4, 120.8, 115.3, 101.6, 59.2, 53.4, 45.4, 41.3

HRMS (ESI) m/z : calc'd for $\text{C}_{51}\text{H}_{58}\text{N}_4\text{O}_6$ [$M/2$]: 411.2178, found 411.2202

2.4b Cell lines and culture conditions

4T1 cells were purchased from Caliper Life Sciences and were cultured in RPMI-1650 supplemented with FBS (10%) and penicillin-streptomycin (50 U/mL, 50 $\mu\text{g/mL}$).

MDA-MB-231 cells were purchased from ATCC and were cultured in DMEM supplemented with FBS (10%, Atlanta Biologicals) and penicillin-streptomycin (50 U/mL, 50 µg/mL, Invitrogen).

MIAPaCa-2 cells were purchased from ATCC and were cultured in DMEM supplemented with FBS (10%, Atlanta Biologicals), Horse serum (1% Atlanta Biologicals), and penicillin-streptomycin (50 U/mL, 50 µg/mL, Invitrogen).

2.4c MTT assay

Cells (5×10^3 cells/well) were cultured in 96-well plates and incubated for 18-24 hours. Stock solution of compound was made up at 100 mM concentration in DMSO. The final concentration of DMSO in the wells were < 0.01%. Concentration range of compounds from 100 µM to 0.1 µM was tested by adding 2x concentration of test compound to the first well and then the serial dilutions by going from well to well. All the compounds were tested in duplicates. After 72 hours of treatment, 10 µL of MTT (5 mM in 1x PBS) was added into the wells and the cells were incubated for a period of 4 hours. At this point, the conversion of MTT to formazan was quenched by the addition of 100 µL of SDS (1 g of SDS dissolved in 0.01 N HCl) and the cells were incubated for further 4 hours. The absorbance was recorded at 570 nm using BioTek Synergy 2 plate reader. The absorbance is directly proportional to the cell viability. % Survival was calculated using the formula

$$\% \text{ survival} = (\text{absorbance of test compound} / \text{absorbance of control}) \times 100\%.$$

IC₅₀ was calculated using GraphPad Prism software, by plotting a dose-response curve with log[concentration] on x-axis and % survival on y-axis and analyzing via nonlinear regression with variable slope.

2.4d *Florescence microscopy study*

The cells (2 mL) were seeded at a concentration of 5×10^4 cells/mL in a 2 cm MatTek (MatTek Corp, #P35G010C) culture dish with glass bottom and were incubated at 37°C in 5% CO₂ atmosphere for 48 hours. The growth medium was removed and 2 mL of fresh growth medium with compound **2i** was added to the culture dish. The cells were incubated for a period of one hour, and the medium was aspirated and washed once with 5% FBS in 1X PBS solution, and further 2 mL of 5% FBS was added to the culture dish. The cells were then imaged to observe the localization of compound in the cells. In the case of MitoTracker Red CMXRos (Invitrogen, M7512), the compound was incubated for 45 minutes, and a 20 µL solution of mitotracker red (100 nM) was added to the cells and further incubated for 15 minutes and cells were washed and replaced with 5% FBS solution for imaging.

2.4e *Ethical Considerations for animal studies*

The experimental procedures involving animals that were conducted at the University of Minnesota Duluth were in compliance with the U.S. National Institutes of Health Guide for Care and Use of Laboratory Animals and approved

by the Institutional Animal Care and Use Committee at the University of Minnesota (UMN).

2.4f General procedure for systemic toxicity evaluation

Mice were procured from Charles River, and acclimatized at room temperature for a period of 7 days. The mice were weighed and randomized into groups (n = 6 mice per group) based on same average weights. Mice were housed as two mice per cage. Treatment was started via i.p. and body weights were monitored for a period of 14-21 days. At the end of the study, mice were euthanized using CO₂.

2.4g Anticancer efficacy of compound 2i in MIAPaCa-2 flank model

5 x 10⁶ MIAPaCa-2 cells were suspended in a mixture of 1:1 matrigel-PBS (100µL). These cells were then injected subcutaneously onto the right flank of athymic nude mice and tumors were measured via calipers and the tumor volume was calculated using the formula

$$V = \frac{1}{2} \times a \times b^2$$

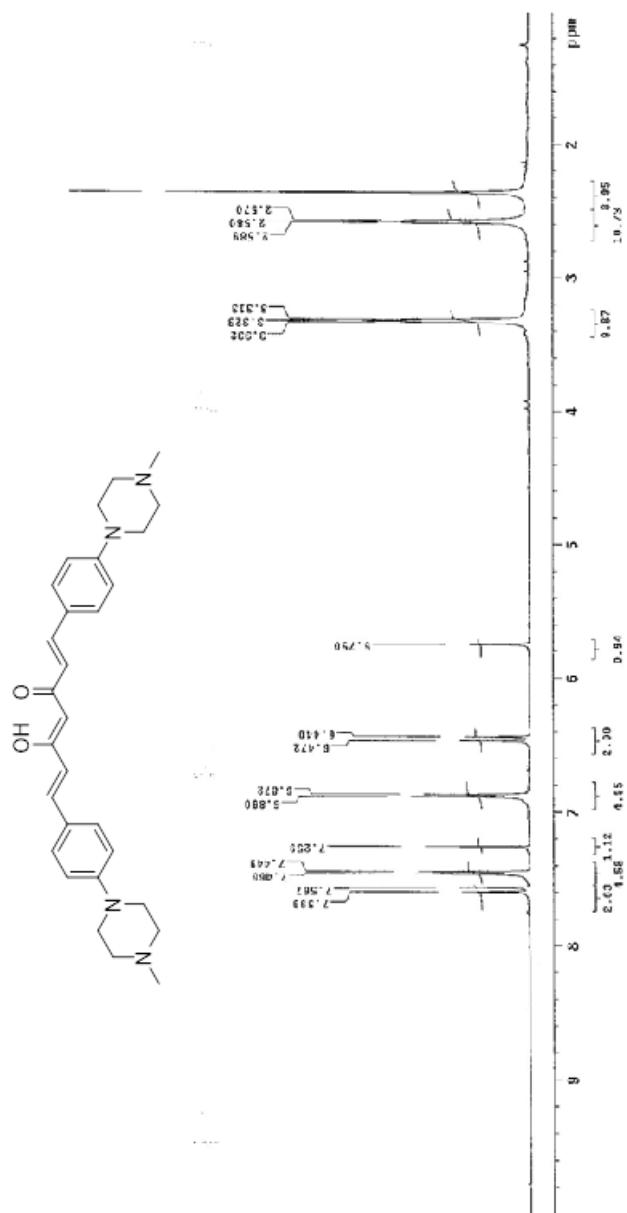
where 'a' is the long diameter of the tumor and 'b' is the short diameter of the tumor. Mice were assigned into groups (n = 8 mice per group) when the average tumor volume reached ~100-200 mm³ and the treatment was initiated and continued for a period of 21 days. Tumor volume was recorded every 2-3 days and at the end of the study, mice were euthanized, and tumors were resected

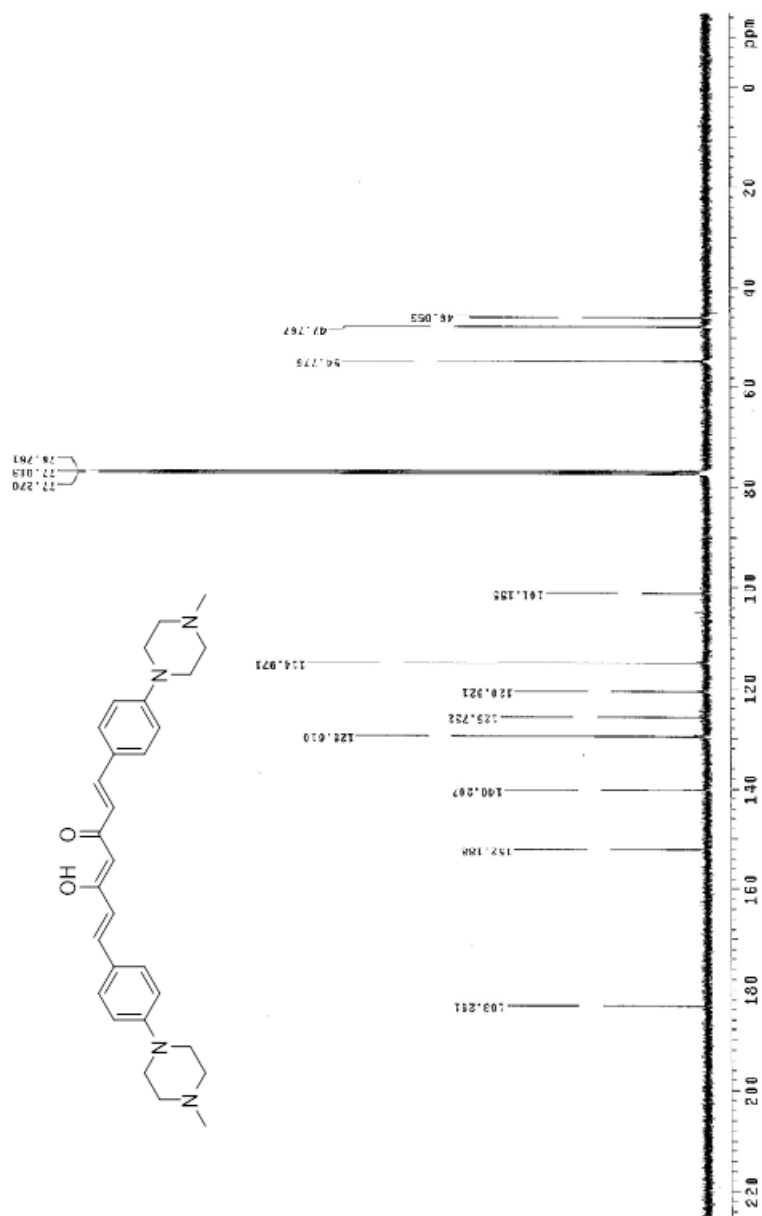
and weighed. The tumor growth inhibition amount was determined using the formula

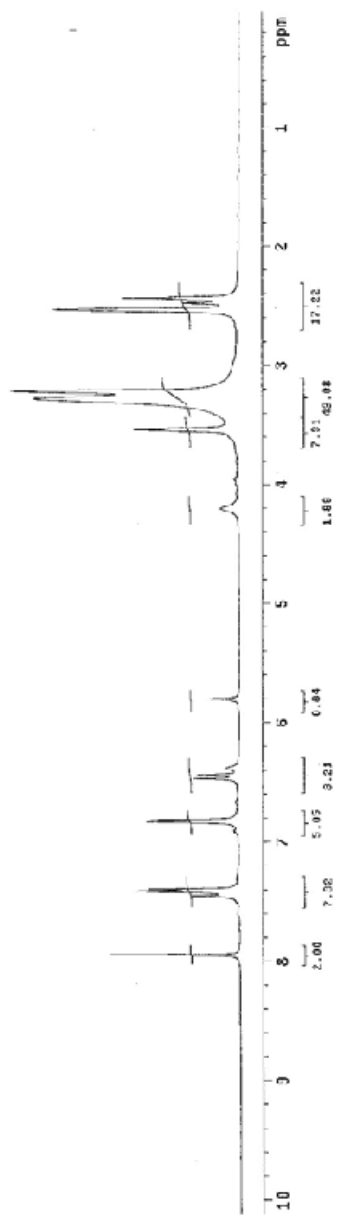
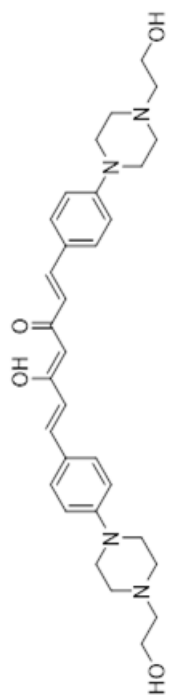
$$\% \textit{inhibition} = \frac{(C-T)}{C} \times 100$$

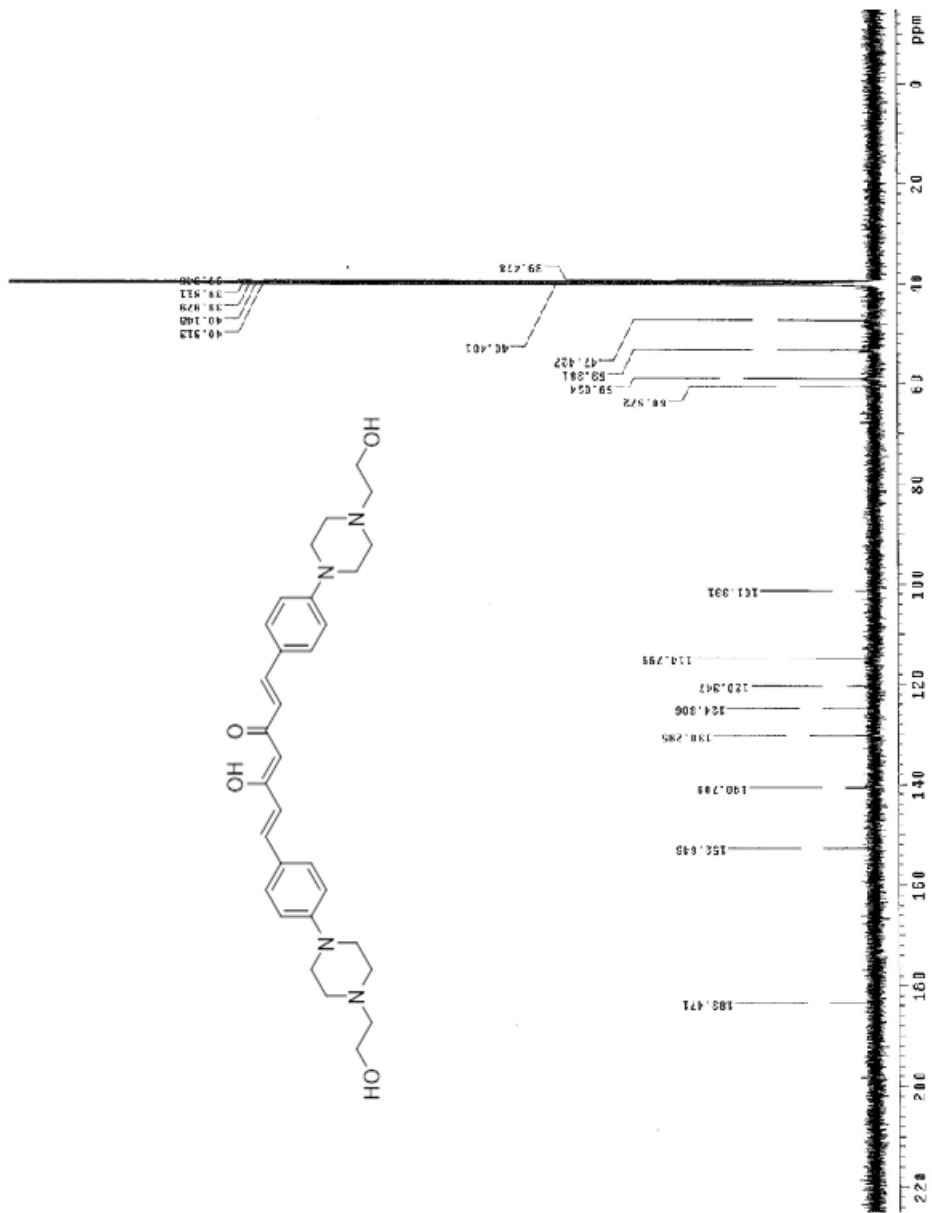
where C is average tumor weight of the control group and T is the average tumor weight of the test group.

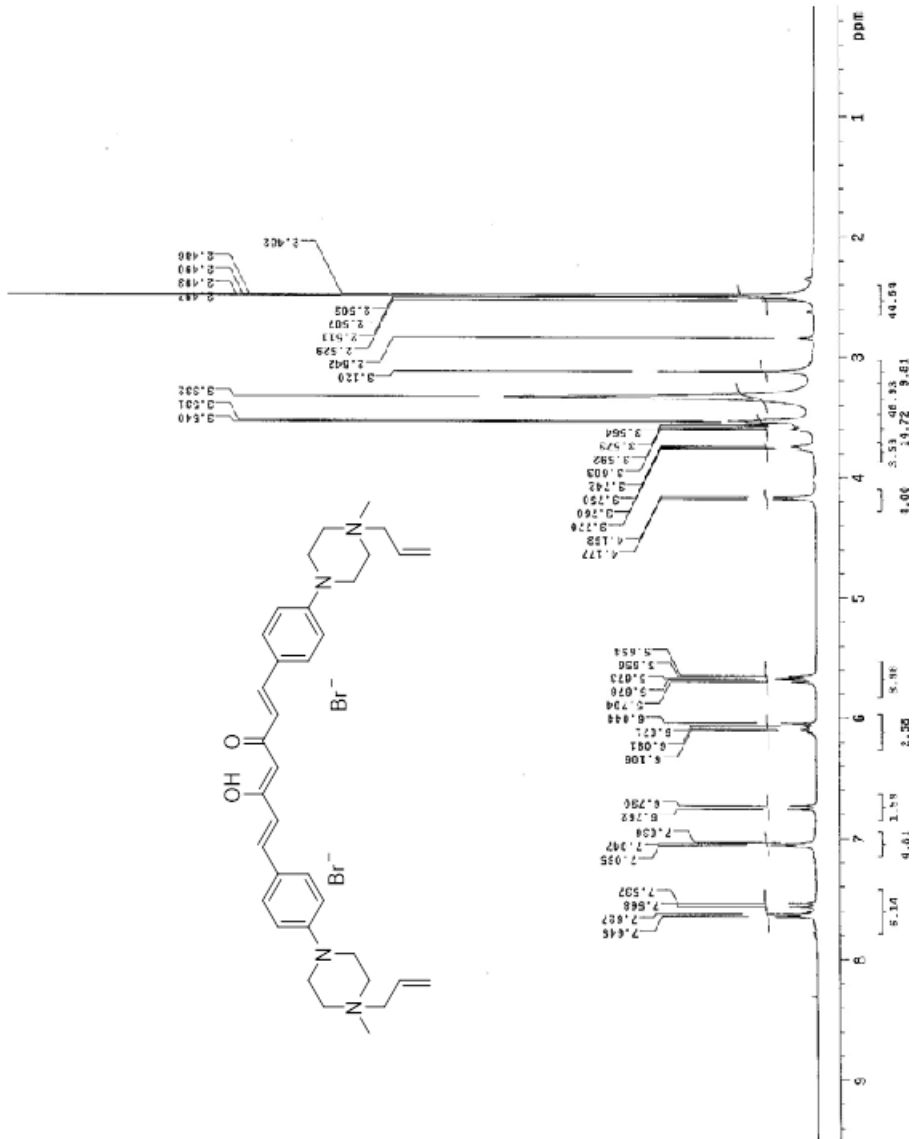
2.5 NMR Spectra

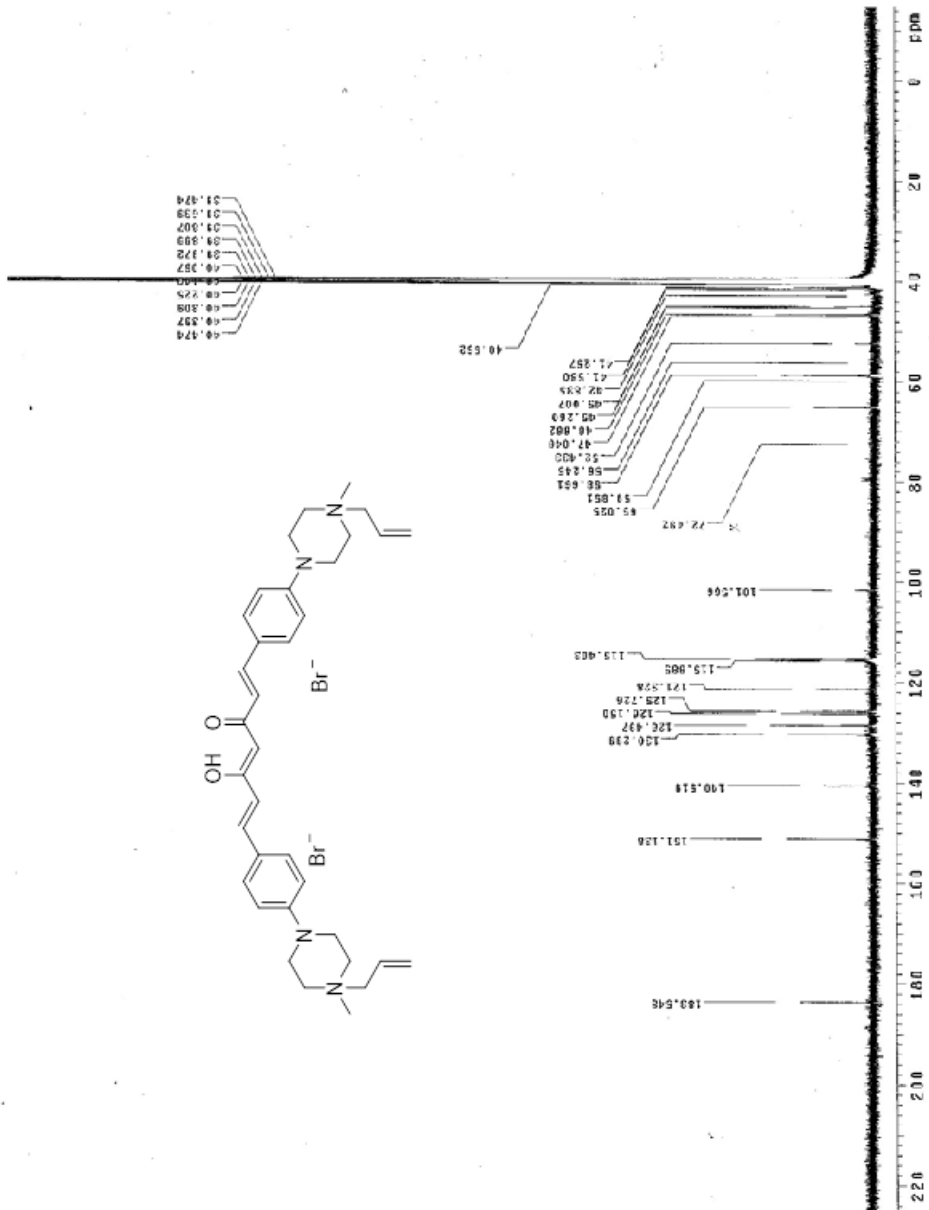


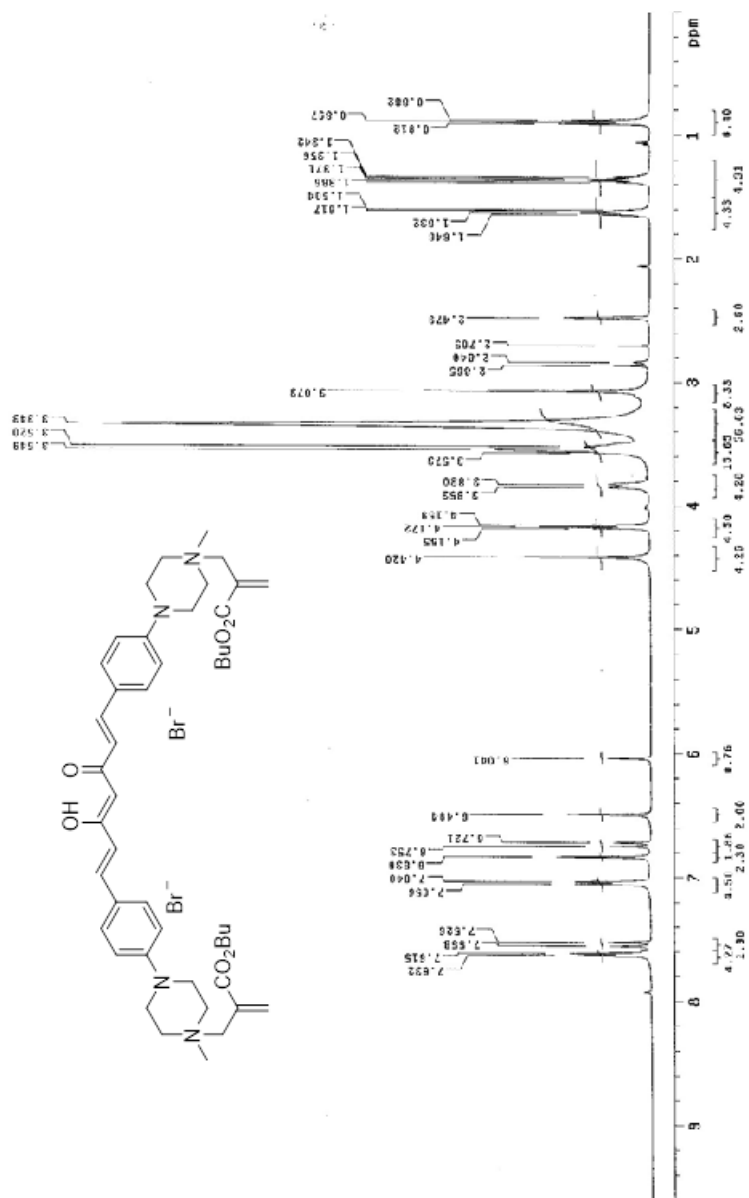


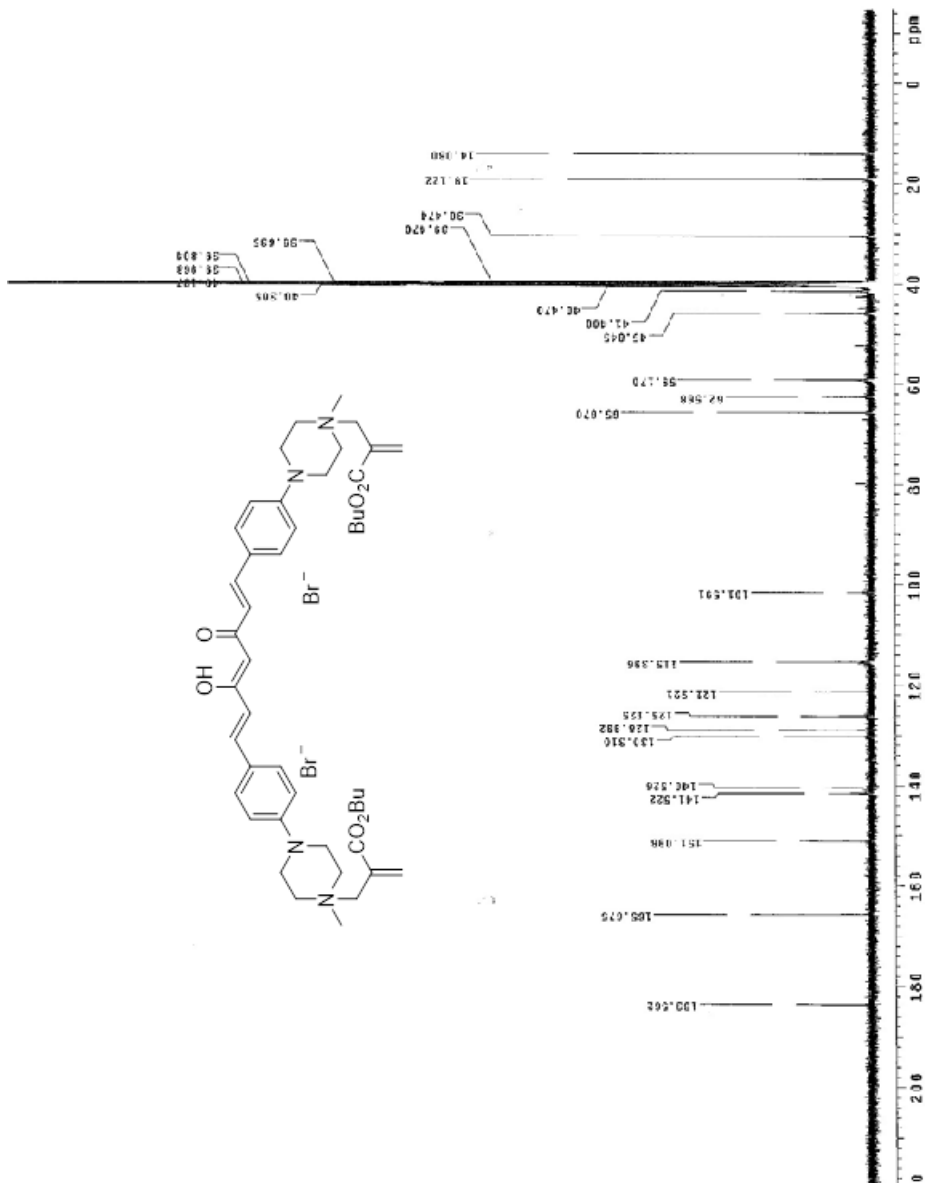


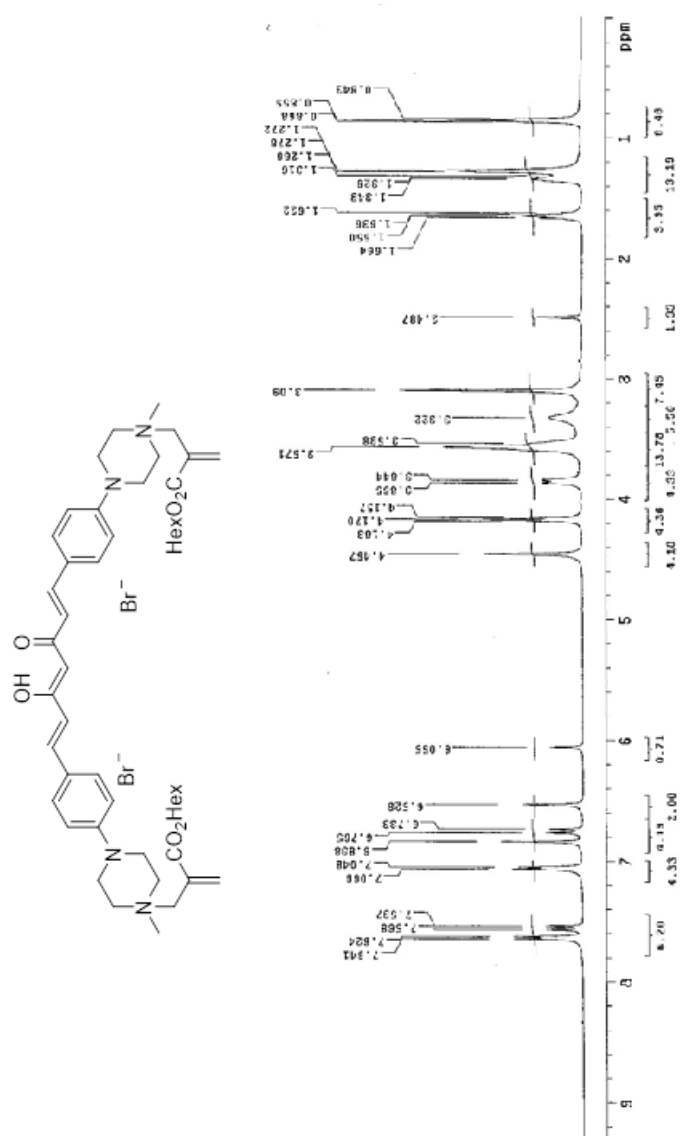


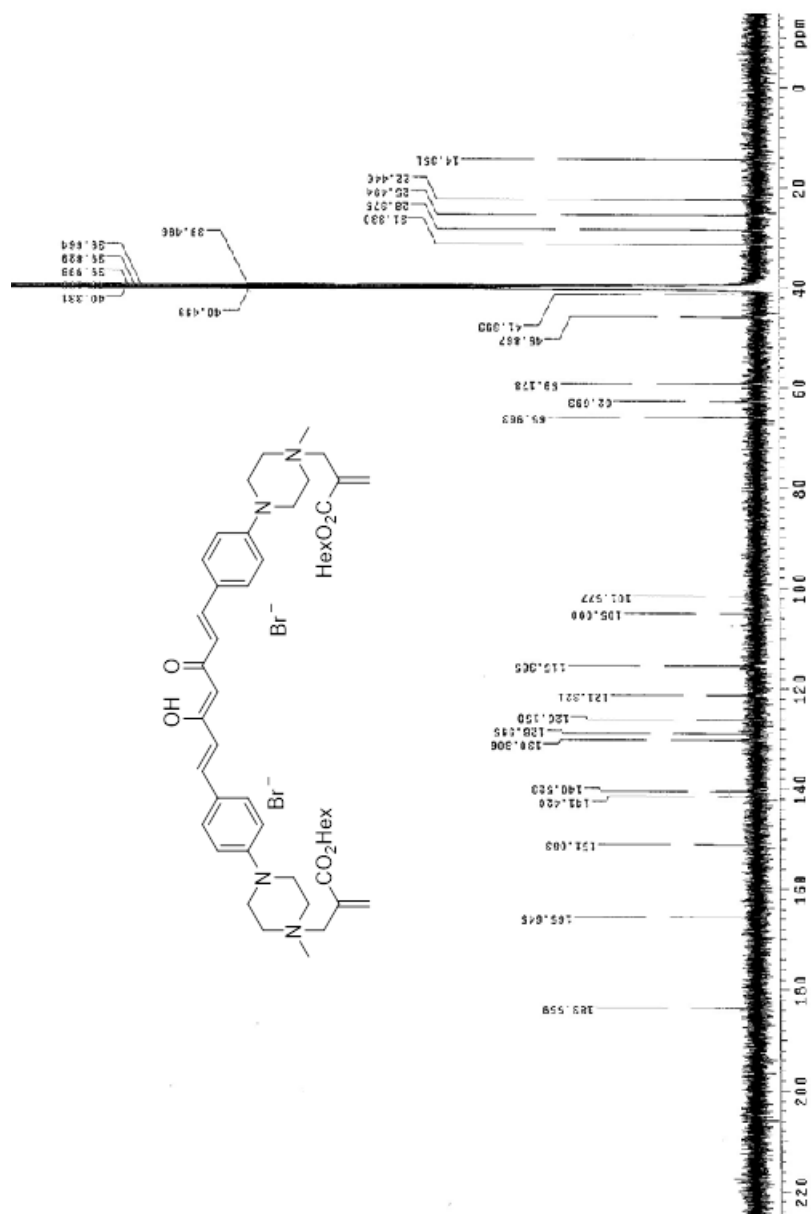


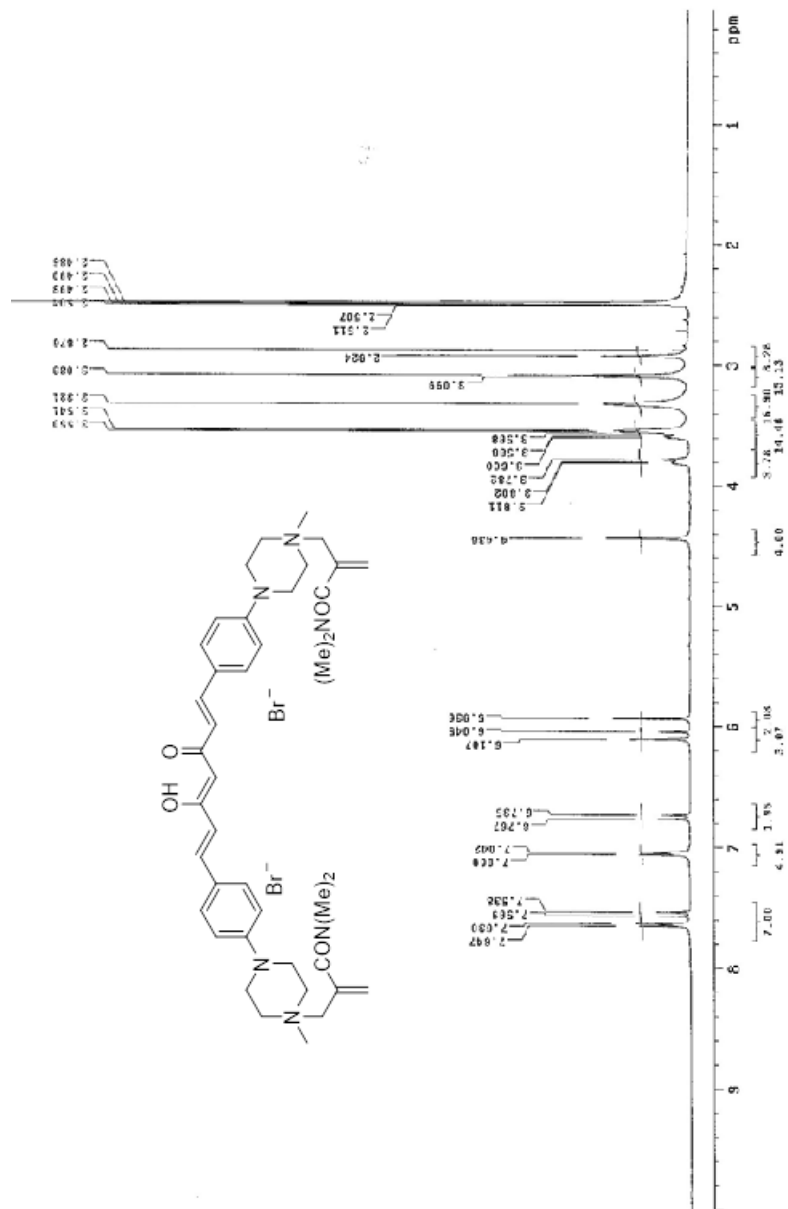


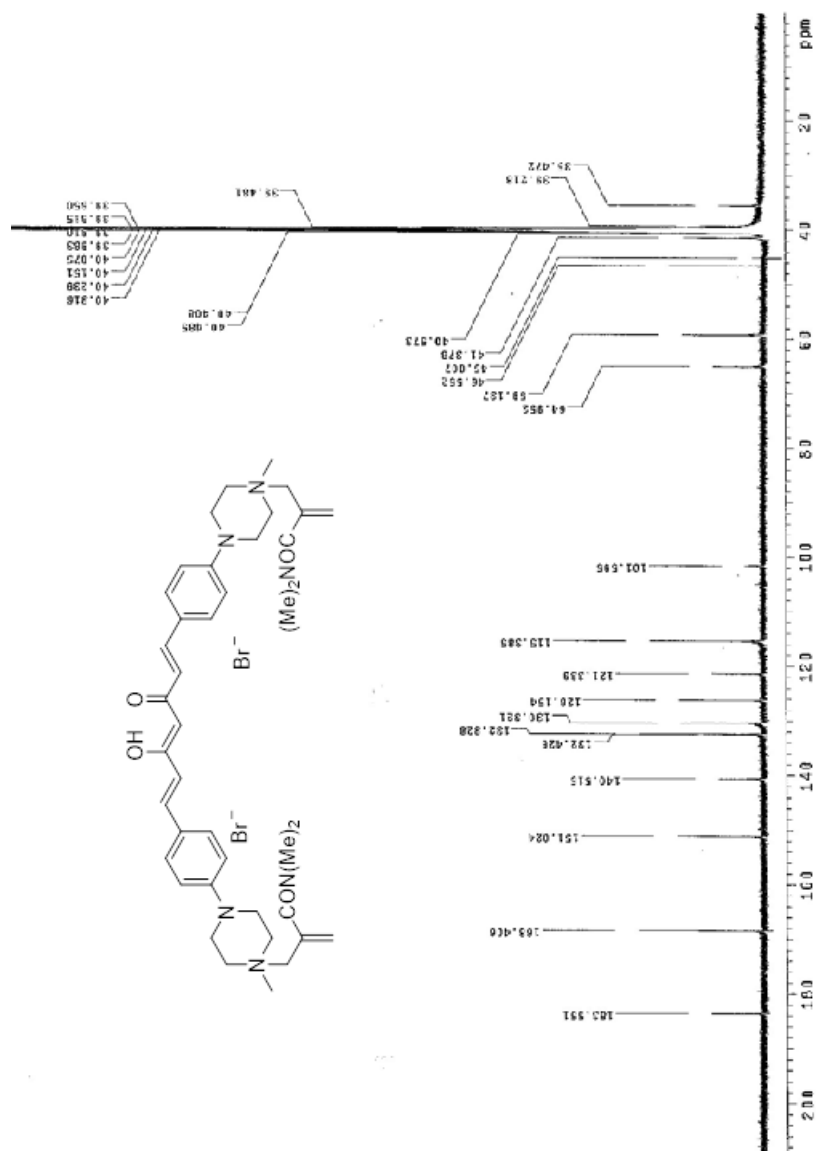


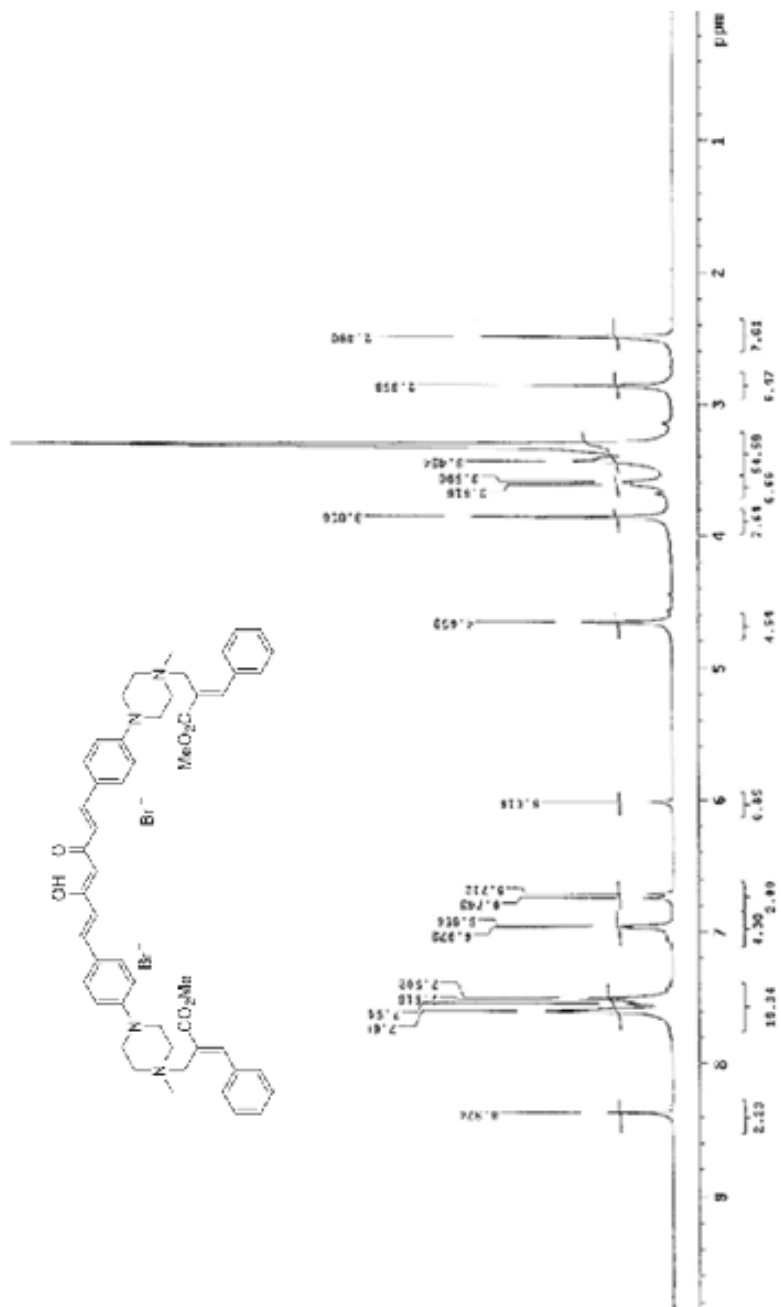


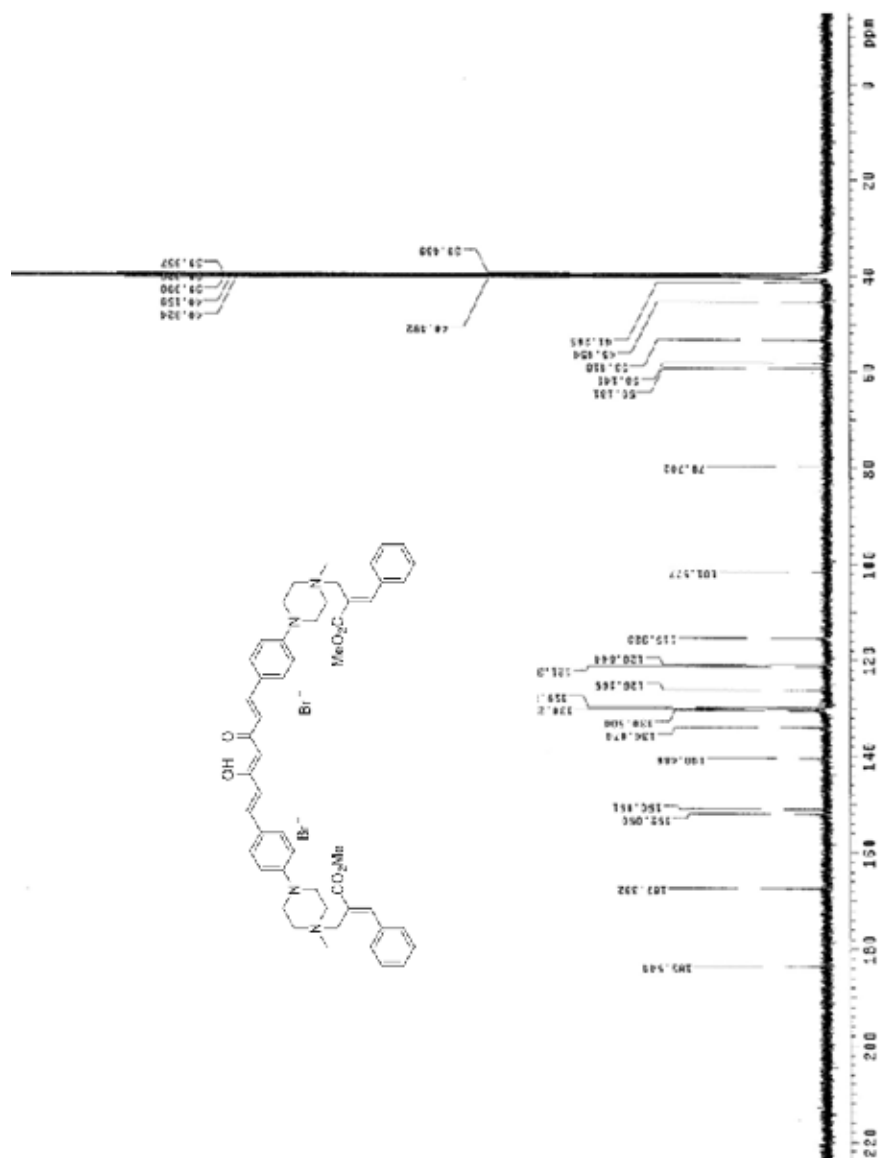












CHAPTER 3: Synthesis and Biological Evaluation of Chalcone Appended Cyanoacrylic acids as Anticancer Agents

3.1 Introduction

3.1a Evolution of hallmarks of cancer: A focus on tumor metabolism

In the chapter 1, Hanahan and Weinberg's summary of major hallmarks of cancer was discussed with the focus on angiogenesis and cell signaling. The focus of this chapter will be on tumor metabolism or more specifically, cellular energetics. Mutational events and the heterogenous nature of tumors result in changes to their cellular metabolism.^{1,118,119} These changes in cellular metabolism play a major role in tumorigenesis. Several studies have shown and demonstrated altered cellular metabolism in solid tumors.^{119,120,129,121–128} As a result, the development of therapeutics combating the metabolism of cancer cells are highly useful.

3.1b Glycolysis and its relation to Warburg effect

Cellular energy is produced through several different metabolic pathways including aerobic glycolysis, mitochondrial oxidative phosphorylation (OxPhos), glutaminolysis, fatty acid metabolism, etc.^{117,130–134} In cancer cells, the balance of these processes is heavily altered, with many advanced stage tumors relying on glycolysis.^{131,135,136} Glycolysis is a process of metabolism which involves the conversion of glucose to lactate and pyruvate. The highly proliferative nature of cancerous tumors gives rise to differences in spatial oxygen availability. These spatial differences result in different tumor cell populations being oxygen rich

(aerobic) and some being oxygen deficient (hypoxic).^{118,137} Hypoxic tumor cells consume large quantities of glucose producing lactic acid and pyruvic acid as by-products.^{120,127,138} The inefficiency of glycolysis results in one mole of glucose yielding only two moles of ATP. However, the increased rate of glycolysis in hypoxic cells allows for sufficient energy production to sustain cell proliferation (**Figure 3.1**).^{120,127,138} The glycolytic by-products do not go to waste as nearby aerobic cancer cells take up these products to efficiently generate energy through mitochondrial oxidative phosphorylation, a process that produces 30-36 moles of ATP per mole of starting glucose. As a result, a metabolic symbiosis occurs where hypoxic cells take up glucose and provide glycolytic by-products for aerobic cells. Overall this cellular specialization results in a very efficient means of energy production and is essential to tumor progression. The cellular specialization arising from differences in oxygen availability, has led to great clinical barriers in tumor treatment and results in failed treatment, patient relapse and mortality.^{132,133,139}

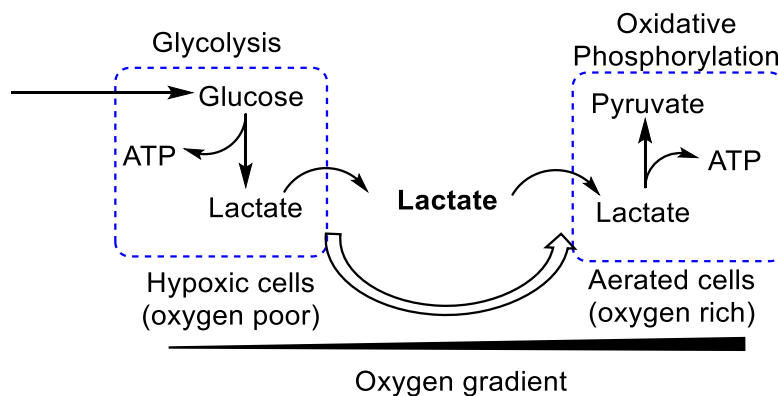


Figure 3.1: Metabolic symbiosis and Warburg effect in cancer cells

3.1c Monocarboxylic acid transporters (MCTs) and their importance in metabolism

MCTs are a class of proton-linked plasma membrane transporters belonging to the SLC16 gene family. The primary role of MCTs is to shuttle small molecules such as lactic acid, pyruvic acid and other ketone bodies across biological membranes of cells. The MCT family is comprised of 14 known isoforms with varying affinities to each of these molecules^{140,141}. MCT1 and MCT4 have been known to be highly involved in metabolic processes. MCT1 is encoded by *SLC16A1* gene and it is a 40 kDa protein consisting of 12 transmembrane domains which are assumed to have hydrophobic α -helical segments. MCT1 has intracellular N-terminal and C-terminal with loops spanning across the cellular transmembrane. Although the crystal structure of MCT1 is unknown, a few homology models have been proposed. MCT1 is ubiquitously distributed throughout the body and is overexpressed in many cancer types, making it an intriguing therapeutic target. MCT1 plays a major role in the export of lactic acid out of hypoxic cells where MCT4 can import lactic acid to nearby aerobic cells.¹⁴⁰ Shuttling of lactic acid outside of the highly glycolytic cells via MCT1 will prevent apoptosis from cellular acidosis, and give substrates for aerobic cells to generate energy from. Similarly, MCT4s role in the import of lactate plays an essential role in relieving the acidic environment from hypoxic regions and providing the fuel for the aerobic cells.¹⁴¹ Due to their importance in the influx and efflux of metabolites for energy production, MCT1 and MCT4 can be considered as important targets

for cancer treatment.¹⁴²⁻¹⁴⁷ Inhibition of MCT1 and/or MCT4 results in the decrease of intracellular pH leading to cell acidosis, and eventually, aerobic cells will not receive lactic acid for OxPhos which can result in the suppression of tumor growth.¹⁴²⁻¹⁴⁷

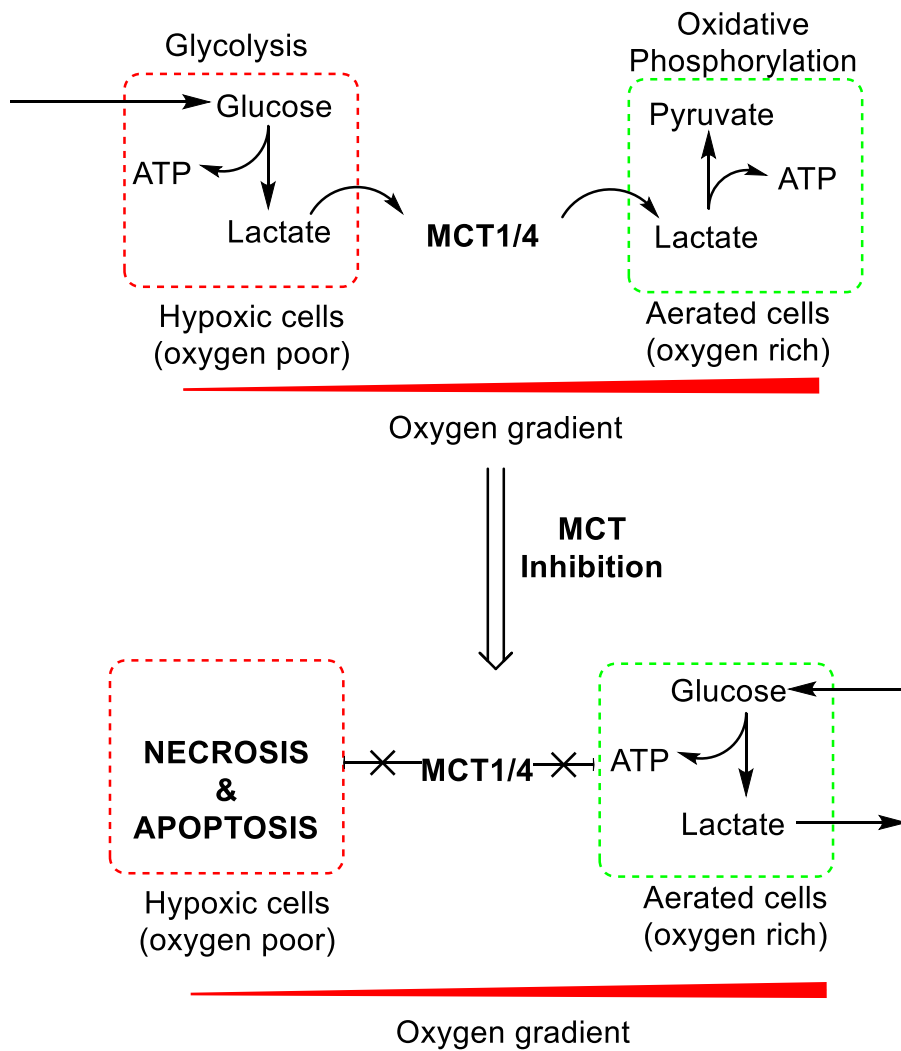


Figure 3.2: Inhibition of MCT1 and/or MCT4 leads to a decrease in tumor growth

3.1d Mitochondrial pyruvate carriers

Mitochondrial pyruvate carriers (MPCs) are on the inner mitochondrial membrane and function to connect glycolysis to OxPhos. MPCs are responsible for carrying pyruvate from the cytosol to the mitochondria.^{135,148} The loss of MPC activity has been found to promote glycolysis or Warburg-like metabolic profile in various tumor models.^{135,148} Overexpression of MPC has been correlated with negative patient outcomes in several tumor types. Inhibition of MPC results in an increase of mitochondrial ROS and triggering of apoptosis pathway.^{135,148–151}

3.1e CHC as MCT1 inhibitor

Since Hanahan and Weinberg reported cellular energetics as a hallmark of cancer, there has been a huge interest in developing glycolysis inhibitors as anticancer therapies. In this regard, α -cyano-4-hydroxy cinnamic acid (CHC, **Figure 3.3**) was first reported to be an inhibitor of MCT1. Since then, CHC has also been reported as a plant growth regulator and a mitochondrial pyruvate carrier inhibitor.¹³³

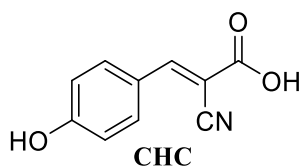
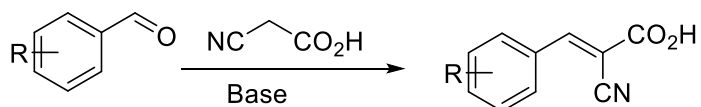


Figure 3.3: Chemical structure of MCT1 inhibitor CHC.

CHC was able to inhibit the growth of U87-MG glioblastoma cells injected into rats.¹⁵² For this study, tumors were implanted and allowed to grow for fourteen days. At which point an osmotic pump was implanted and CHC was directly given to the tumor site. Half of the mice that received treatment were able to survive for 120 days, illustrating that CHC can significantly increase the survival of glioma *in vivo*. Histological analysis showed treated tumors underwent necrosis while healthy brain tissue surrounding the tumor were unaffected. Several more recent studies have demonstrated CHC's ability in reducing tumor burden in wide variety of cancers.^{149,153–156} These results support the hypothesis that MCT inhibitors can be used as therapeutic agents for the treatment of cancers.

3.1f SAR studies on CHC

Previous work in our lab involved the synthesis and evaluation of novel MCT1/4 inhibitors as potential anticancer agents. To generate a large library of CHC derivatives, Mereddy's lab took a variety of benzaldehydes and performed Knoevenagel condensation with cyanoacetic acid (**Scheme 3.1**).^{156,157}



IC₅₀: 1-50 μM

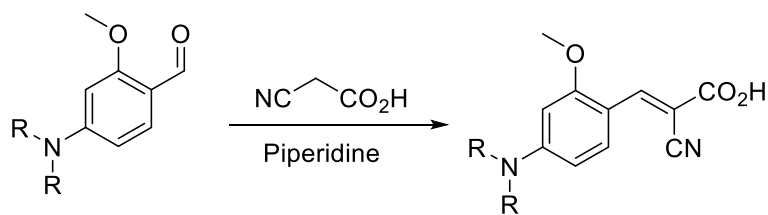
R= OMe, OEt, Br, Cl, F, NO₂, CN, Me, Et, iPr, tButyl, etc.

NR'₂

Where R'=Me, Eth, Propyl, Butyl, Pentyl,
phenyl, benzyl, pyrrolidinyl, piperidinyl, etc.

Scheme 3.1: Knoevenagel condensation of substituted benzaldehydes with cyanoacetic acid to form CHC based derivatives.

Initial modifications of the benzaldehydes included substitution of *p*-hydroxyl group in CHC with electron withdrawing groups such as halides, CN, and NO₂ and electron donating groups such as methoxy, 3,4-methylenedioxy, alkyl, and *N,N*-dialkyl groups. Testing of these compounds for MCT1 inhibition showed that the *N,N*-dialkyl derivatives were the most potent. The potency of the *N,N*-dialkyl derivatives was dependent upon chain length, such that increasing chain length from methyl to butyl increased activity, however further extension resulted in a loss of activity. Similarly, we found that the substitution on nitrogen with phenyl and benzyl groups also resulted in good activity.^{156,157} After optimization of the para position, we investigated substitutions in ortho position. In this case methoxy group was introduced (**Scheme 3.2**).



R=Me, Eth, Propyl, Butyl, Pentyl,
phenyl, benzyl, pyrrolidinyl, piperidinyl, etc.

Scheme 3.2: A representative scheme for the synthesis of the library of *N,N*-dialkyl amino CHC derivatives.

Lactate uptake inhibition studies showed inclusion of a methoxy group further enhanced activity against MCT1 and MCT4 (**Scheme 3.2** and **Figure 3.4**). Modifications of the cyano, carboxylic acid, and α,β -unsaturation resulted in a loss of activity (data not shown). Furthermore, these derivatives were able to significantly reduce the tumor burden of various tumor models *in vivo*.^{156,157}

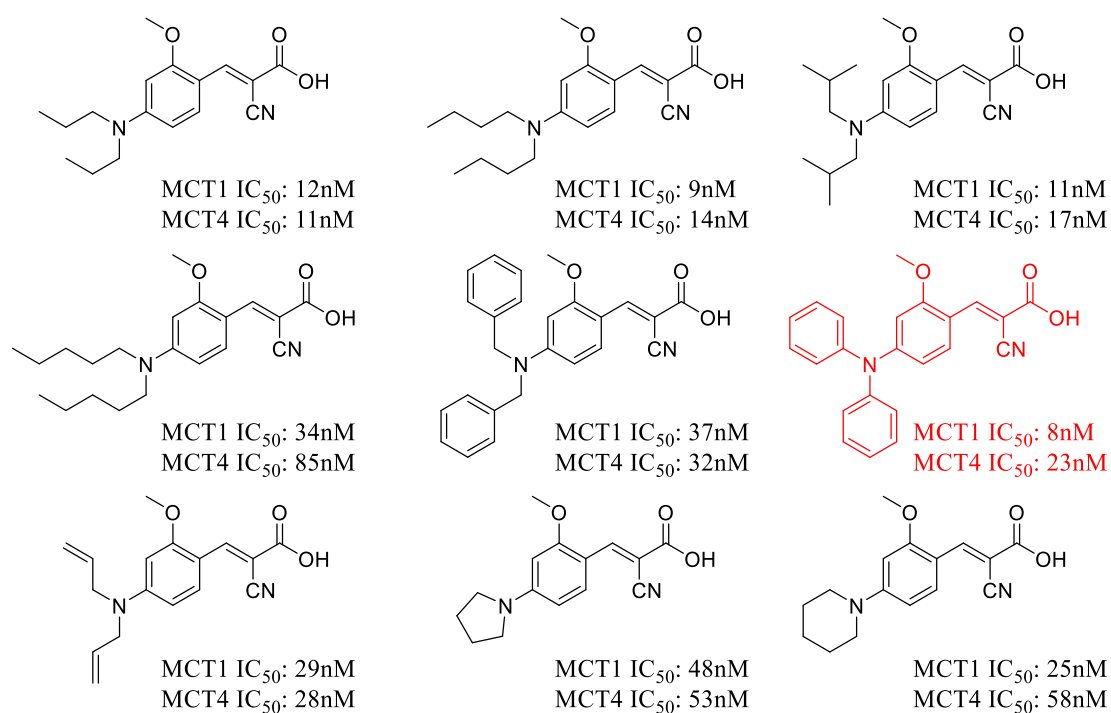


Figure 3.4: The SAR study of the *N,N*-dialkyl/diaryl substituted CHC derivatives

3.1g Other MCT1 inhibitors

Utilizing MCT1 as a potential target for therapeutic intervention is actively being investigated by other labs for the development of chemotherapeutics. AstraZeneca has developed a series of MCT1 inhibitors and selected AZD3965 as a lead compound.^{158–162} AZD3965 was shown to be selective towards MCT1

and has no activity towards MCT4 (**Figure 3.5**).^{158–162} The MCT1 efficacy was evaluated using L-lactate transport study on rat erythrocytes and xenopus oocytes. Furthermore, AZD3965 was tested *in vivo* with COR-L103 which was isolated from human lung small cell carcinoma. AZD3965 also exhibited significant tumor growth inhibition in other tumor models. Dosing of AZD3965 at 100mg/kg compound exhibited ~60% tumor growth inhibition.^{158–162} It is now currently in phase-I clinical trials for diffuse large B-cell lymphoma, Burkitt lymphoma, and other solid tumors.

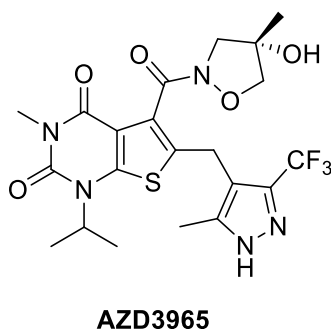
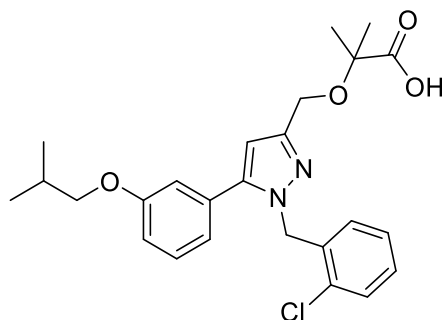


Figure 3.5: Structure of AZD3965

3.1j Pyrazole methylpropanoic acid derivatives as MCT4 inhibitors

Not only have compounds been developed for the inhibition of MCT1 but interest in developing selective MCT4 inhibitors has arose. SAR studies have identified therapeutics that are selective to MCT4 transporters.¹⁴² One class of reported MCT4 inhibitors are 2-((1-(2-chlorobenzyl)-5-(3-substituted phenyl)-1H-pyrazol-3-yl)methoxy)-2-methylpropanoic acids (**Figure 3.6**). These derivatives exhibited excellent specificity towards MCT4 activity. These pyrazole derivatives exhibited potent MCT4 inhibition in low nM range.¹⁴²

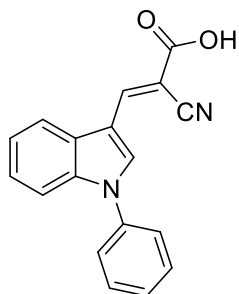


isobutyl substituted pyrazole methyl propanoic acid

Figure 3.6: Lead MCT4 inhibitor 2-((1-(2-chlorobenzyl)-5-(3-substituted phenyl)-1H-pyrazol-3-yl)methoxy)-2-methylpropanoic acids

3.1k UK-5099 as mitochondrial pyruvate carrier inhibitor

UK-5099 (**Figure 3.7**) is currently being developed as a mitochondrial pyruvate carrier inhibitor and is known to have activity against mitochondrial pyruvate carriers and MCTs. Potency of UK-5099 was found to be 50nM. As result of the good potency studies evaluating mitochondrial function have been carried out. Studies reported that 150 μ M UK-5099 significantly reduced mitochondrial ATP.^{135,149}



UK-5099

Figure 3.7: Structure of UK-5099

3.1I Chalcones as a therapeutic agent

Chalcones, or 1,3-diphenyl-2-propen-1-ones, are a very important class of flavonoids. Chalcones are yellow to orange open-chain precursors for biosynthesis of flavonoids and isoflavonoids and in nature occur mainly as polyphenolic compounds.^{163,164} They exist as either trans (E, 1) or cis (Z, 2) isomers having two aromatic rings that are joined by a three-carbon α,β -unsaturated carbonyl system (**Figure 3.8**).

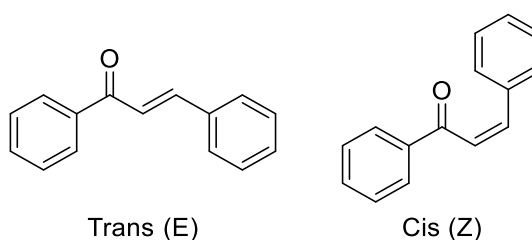


Figure 3.8: Structural template of chalcones

Thermodynamically the E isomer is more stable and thus is the predominant form found in nature.¹⁶⁴ Chalcones have been found to have many therapeutic properties such as anti-inflammatory, anti-microbial, anti-protozoal, anti-malarial, anti-hypertensive, anti-oxidant, anti-cancer, and anti-fungal, etc. (**Figure 3.9**).^{165,166}



Figure 3.9 Biological activities of Chalcones

Clinically, chalcones have been utilized; For example, metochalcone was approved as a choleric drug and sofalcone an anti-ulcer agent (**Figure 3.10**).^{163,167}

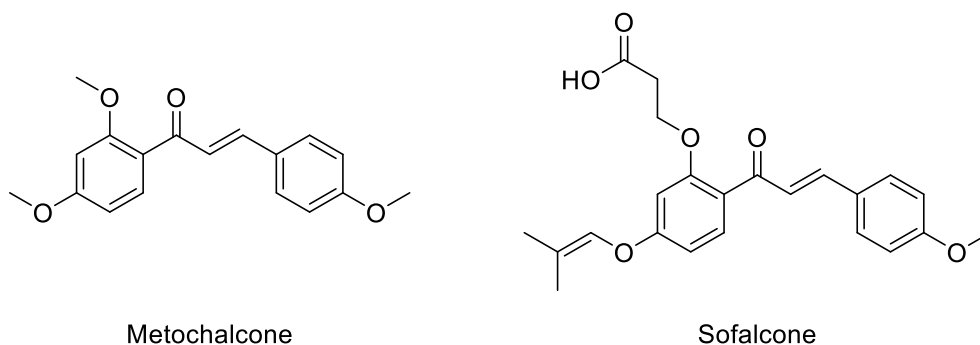
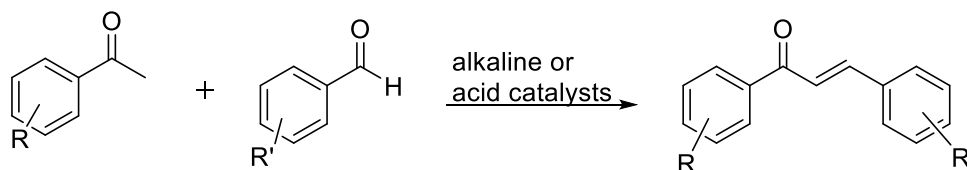


Figure 3.10: Examples of clinically explored chalcones

3.1m Synthesis of Chalcones

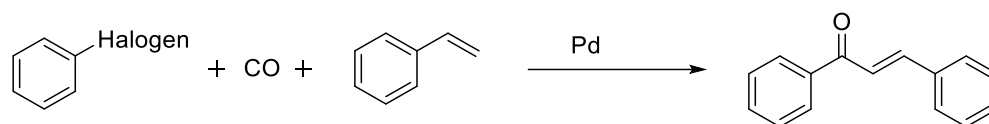
Claisen-Schmidt condensation

The simple chemistry of chalcones allows several different substitutions and a wide variety of methods for their synthesis. Typically, chalcone synthesis is carried out with a condensation reaction of two aromatic carbonyl systems. Claisen-Schmidt condensation is one of the most common methods due to the availability of substituted aldehydes and ketones. In this reaction, chalcones are formed by condensation of benzaldehyde and acetophenone derivatives in the presence of alkaline or acid catalysts in liquid solvent at 50–100 °C for several hours (**Scheme 3.3**).¹⁶⁸



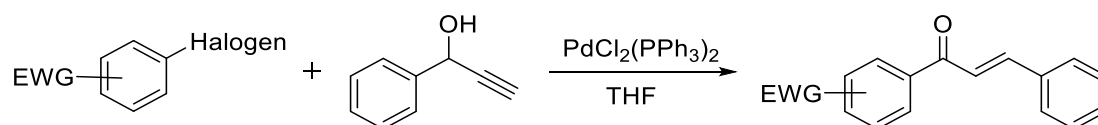
Scheme 3.3: The Claisen-Schmidt condensation to synthesize chalcones

Carbonylative Heck coupling: In the carbonylative Heck coupling reaction chalcones are synthesized with the use of palladium catalyst causing the reaction conditions to be more expensive. Palladium catalyzes the vinylation of phenyl halides with styrenes in the presence of carbon monoxide (**Scheme 3.4**).¹⁶⁹



Scheme 3.4: Carbonylative Heck coupling reaction to synthesize chalcones

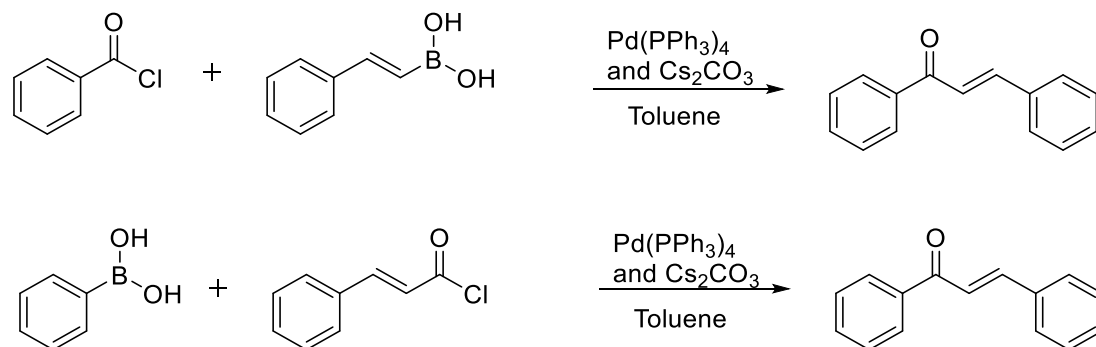
Sonogashira Isomerization coupling: The Sonogashira isomerization coupling method offers less versatility due to the requirement of electron deficient phenyl halides. In this reaction, electron deficient phenyl halides are reacted with phenyl substituted propargyl alcohols in the presence of $\text{PdCl}_2(\text{PPh}_3)_2$ and microwave irradiation. Like the carbonylative Heck coupling, this method tends to be more expensive and limited in scope (**Scheme 5**).¹⁶⁹



Scheme 3.5: Sonogashira isomerization coupling to synthesize chalcones

Suzuki-Miyaura Coupling reaction: Suzuki-Miyaura coupling reaction involves the reaction of boronic acids with acid chlorides. The versatility of this reaction is conserved with the boronic acid existing as either the phenyl boronic acid or as the styryl boronic acid. Similarly, the acid chloride can be prepared as either the benzoyl chloride or the cinnamoyl chloride. Once again this reaction requires the

use of a palladium catalyst ($\text{Pd(PPh}_3)_4$) increasing the cost of the reaction
(**Scheme 3.6**).¹⁷⁰



Scheme 3.6: Suzuki-Miyaura coupling reaction to synthesize chalcones

3.1n Chalcones as natural product and drug candidates:

Xanthoangelol: Xanthoangelol is a chalcone isolated from Japanese herb *Angelica keiskei*, that exhibits versatile biological and pharmacological activities, including anti-inflammatory, anti-microbial, anti-platelet, antioxidant, and antidiabetic. Recently, xanthoangelol has been recognized for its anti-cancer activity towards a variety of cancer types including osteosarcoma, leukemia, and neuroblastoma (**Figure 3.11**).^{164,171} Xanthoangelol has been shown to inhibit the phosphorylation of Stat3 in LM8 osteosarcoma models in mice which resulted in suppressed growth and metastasis. In neuroblastoma and leukemia cell lines IMR-32 and Jurkat respectively, xanthoangelol induced apoptosis through the activation of caspase-3.^{164,171} Xanthoangelol is also being studied as an aurora kinase inhibitor and EGFR inhibitor.¹⁷²

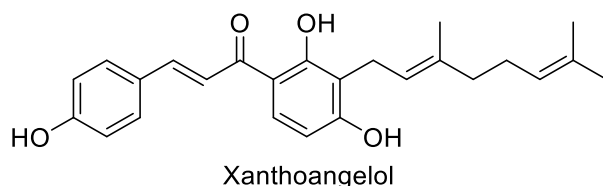


Figure 3.11: Structure of Xanthoangelol

3.1o Chalcones as anticancer agents TUB091 and TUB099: Canela, et al. reported the synthesis and biological evaluation of novel tubulin binding chalcones. They selected TUB091 as a lead derivative and TUB099 as a peptide-based prodrug (**Figure 3.12**). These lead compounds showed tubulin binding, vascular-targeting, anti-tumor, and anti-metastatic activities on numerous cell lines. TUB091 and TUB099 was able to inhibit the proliferation of endothelial and tumor cell lines in the 1-4nM range.^{164,173} CAM assays showed the ability of lead compounds to inhibit endothelial cell migration, angiogenesis, and disruption of immature capillary networks while leaving mature vasculature intact. Furthermore, TUB099 significantly reduced the primary growth of mouse melanoma B16-F10-luc2 and human triple negative breast cancer MDA-MB-231 cells in mice through intratumorally and intraperitoneal administration.^{164,173} Immunohistological analysis with Ki67 and CD31 provided evidence TUB099 was able to have antiproliferative effects in both models.

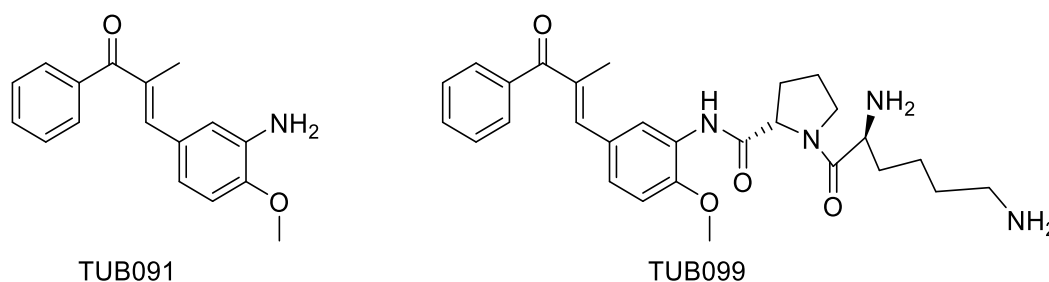
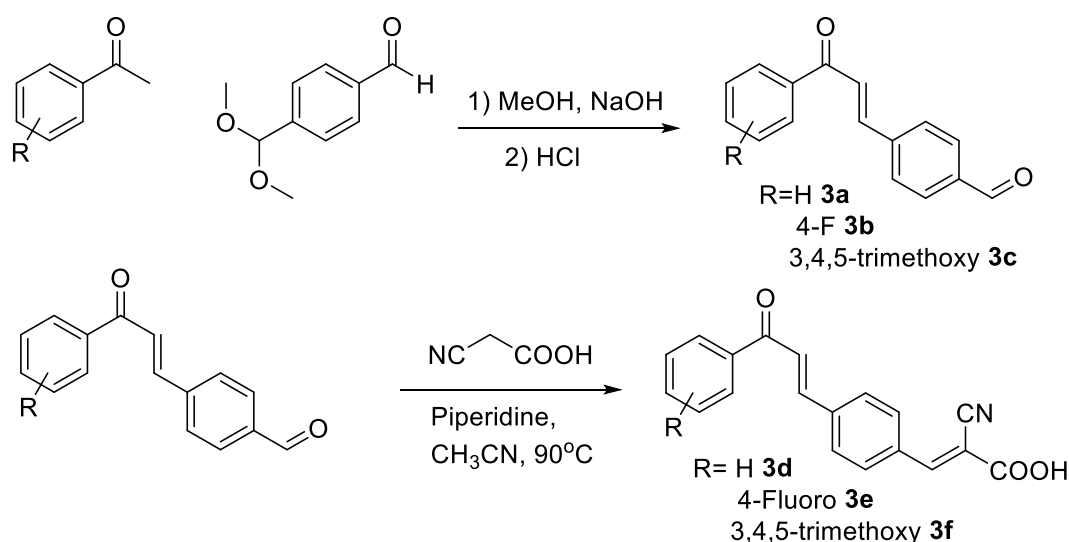


Figure 3.12: Structure of TUB091 and TUB099

3.2 Results and Discussion:

3.2a Synthesis of Chalcone appended cyanoacrylic acid

The phenylacrylic acids were synthesized starting from commercially available substituted acetophenones. For this purpose, we utilized acetophenone, 1-(4-fluorophenyl)ethan-1-one and 1-(3,4,5-trimethoxyphenyl)ethan-1-one. The first step involved condensation of methyl ketones with an acetal protected aldehyde, 4-(dimethoxymethyl)benzaldehyde in the presence of a base, followed by the deprotection of acetal to obtain the corresponding acetophenone-benzaldehydes **3a-3c**. The aldehydes were then condensed with cyanoacetic acid via Knoevenagel condensation to get the corresponding chalcone cyanoacrylic acids **3d-3f** (**Scheme 3.7**).



Scheme 3.7: Synthesis of chalcone substituted cyanocinnamic acids **3d-3f**

As we reported previously, presence of doubly activated cyanoacrylic acid unit make these compounds powerful 1,4-acceptors but due to the presence of highly acidic hydrogen they act as rapid reversible inhibitors. We envisioned that introduction of an α,β -unsaturated system similar to that of a chalcone will make

these compounds irreversible inhibitors also with metabolic inhibition properties (Figure 3.13).

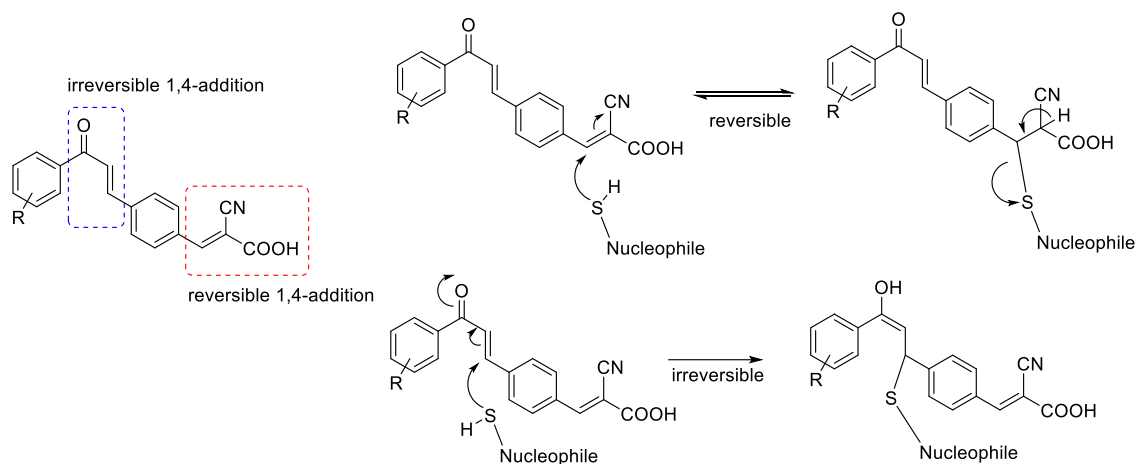


Figure 3.13: Reversible and irreversible units in chalcone cyanoacrylate structure.

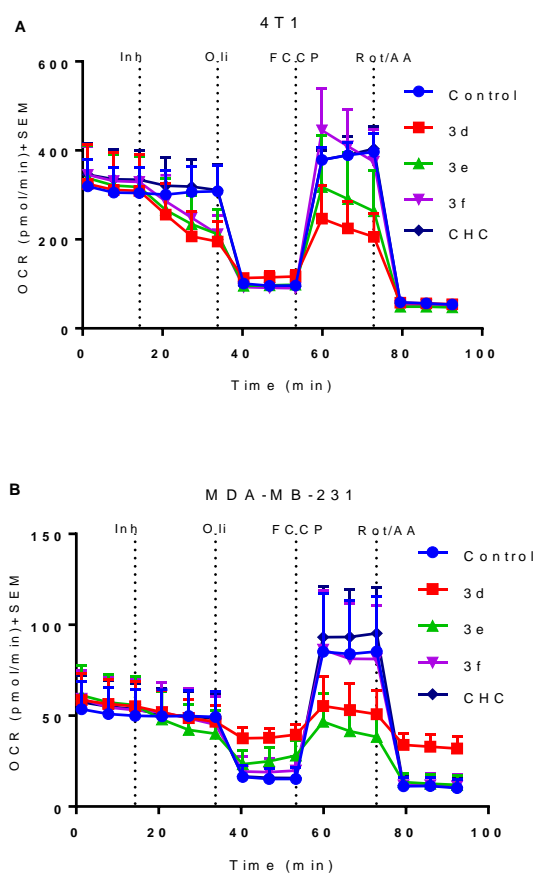
3.2b *In vitro* MTT based cell proliferation inhibition

These chalcone cyanoacrylate acids **3d-3f** were tested for cell proliferation inhibition properties using MTT based assay against MDA-MB-231, WiDr, 4T1 cell lines and found to be not significantly active up to 50 μM concentration.

3.2c Seahorse XFe96® analyzer

The compounds **3d-3f** were then evaluated for extracellular flux analysis using Seahorse XFe96® analyzer at 100 μM concentration. For this purpose, 4T1, MDA-MB-231, and WiDr and cell lines were subjected to mitochondrial stress test (MST) and glycolytic stress test (GST) according to the manufacturer's protocol. For MST, oxygen consumption rate (OCR) was recorded and the following parameters were calculated using wave software based on the OCR

values in the presence of different mitochondrial inhibitors: maximal respiration, ATP production, proton leak and spare respiratory capacity. Compounds were dissolved in DMSO which was used as a negative control. The candidate compounds **3d** and **3e** altered OCR values significantly compared to control in all these three cell lines (**Figure 3.14**).



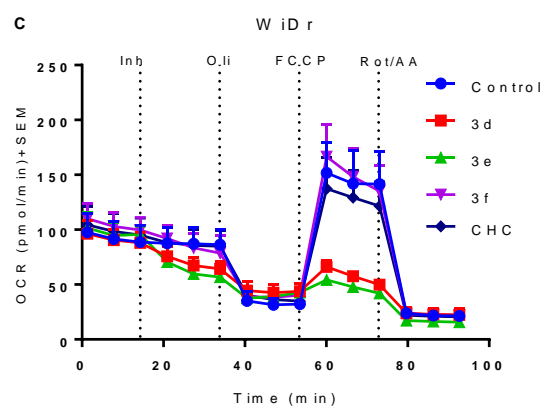


Figure 3.14: Mitochondrial stress test in (A) 4T1, (B) MDA-MB-231 and (C) WiDr cell lines using compounds **3d-3e**. The OCR values were calculated using wave software. The average+SEM values of at least three independent experimental values were calculated.

To measure maximal oxygen consumption rate, cells were treated with a proton uncoupler, FCCP. FCCP eliminates the proton gradient, perturbing the mitochondrial membrane potential. As a result, the electron transport chain works to oxidize substrates rapidly to return the membrane potential in the mitochondria, which requires a large consumption of oxygen. Thus, the maximum oxygen consumption rate that the mitochondria can utilize could be measured. In 4T1 cell line, compound **3d** significantly reduced maximal oxygen consumption, whereas in MDA-MB-231 cell line, compounds **3d** and **3e** significantly reduced this parameter. Compounds **3e** and **3f** significantly decreased maximal respiration compared to the control in WiDr cell line (**Figure 3.15**).

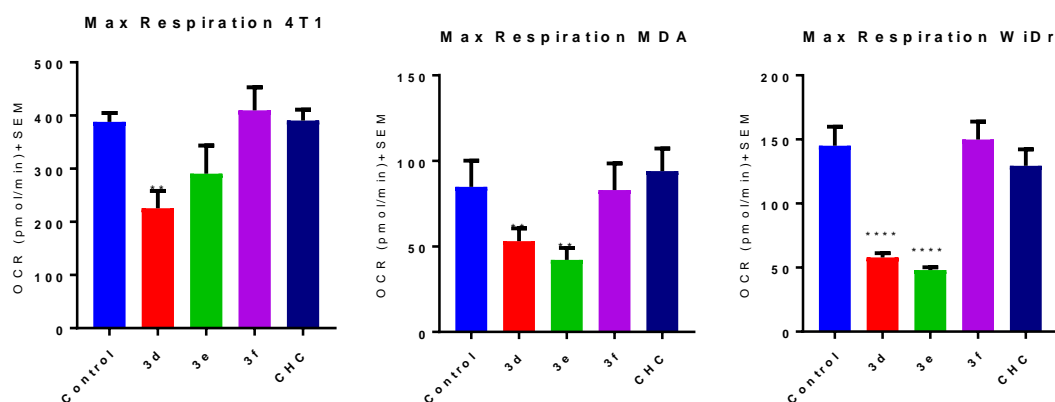


Figure 3.15: Maximal respiration in (A) 4T1, (B) MDA-MB-231 and (C) WiDr cell lines using compounds **3d-3f**. The OCR values were calculated using wave software. The average+SEM values of at least three independent experimental values were calculated.

ATP production from mitochondria can be determined by observing the difference in OCR before and after the addition of an ATP synthase inhibitor, oligomycin A. In MDA-MB-231 cell line, all the candidate compound **3d** significantly reduced ATP production, whereas in 4T1 and WiDr cell line, no significant change was observed (**Figure 3.16**). These results suggest that these compounds may affect the mitochondria by interfering with ATP synthase and suppress mitochondrial OxPhos.

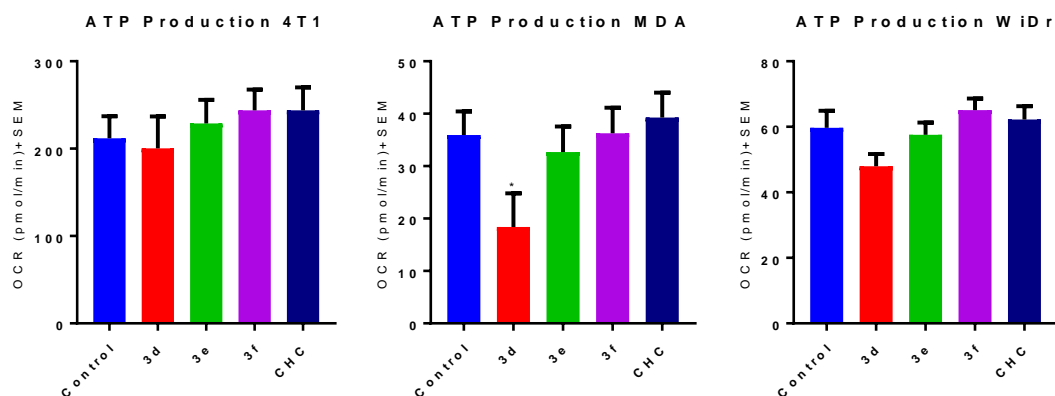


Figure 3.15: Maximal respiration in (A) 4T1, (B) MDA-MB-231 and (C) WiDr cell lines using compounds **3d-3f**. The OCR values were calculated using wave software. The average+SEM values of at least three independent experimental values were calculated.

After the addition of oligomycin, proton leak can also be determined. Proton leak is the sum of the oxygen consumption from processes outside of ATP synthase. Cells with damaged mitochondria have greater amounts of proton leak as they are forced to use less efficient pathways to generate ATP. In 4T1 and WiDr cell lines, compounds **3d-3f** did not show significant changes in proton leak, whereas in MDA-MB-231 cell line, candidate compound **3d** significantly increased proton leak compared to the control (**Figure 3.17**). These results illustrate that compound **3d** disrupts the mitochondria proton flux in highly glycolytic cells MDA-MB-231.

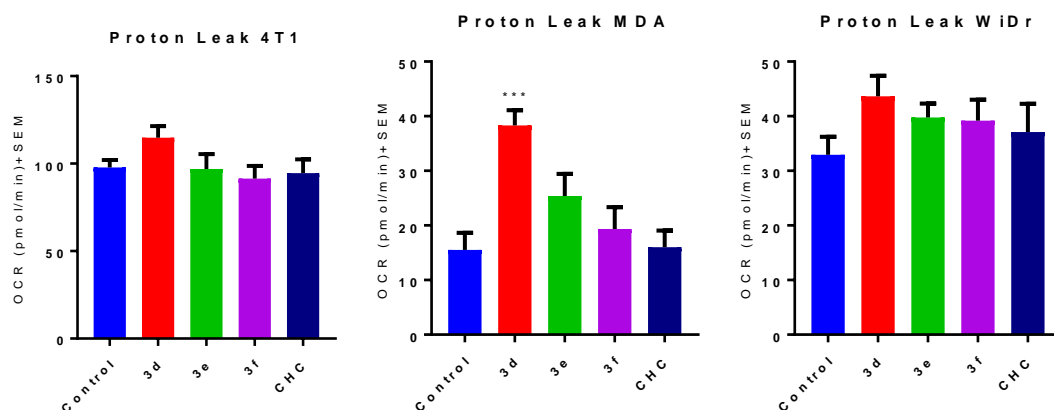


Figure 3.17: Proton leak in (A) 4T1, (B) MDA-MB-231 and (C) WiDr cell lines using compounds **3d-3f**. The OCR values were calculated using wave software. The average+SEM values of at least three independent experimental values were calculated.

Spare respiratory capacity is calculated from the difference between basal oxygen consumption and the consumption of ATP synthase proton uncoupled mitochondria. Relevance of measuring spare respiratory capacity explains the capability of the cell to respond to an energetic demand. In all cell lines, candidate compounds **3d** and **3e** significantly reduced this spare respiratory capacity compared to the control (**Figure 3.18**). These results show that these compounds may limit the capability of cells to produce energy under mitochondrial stress.

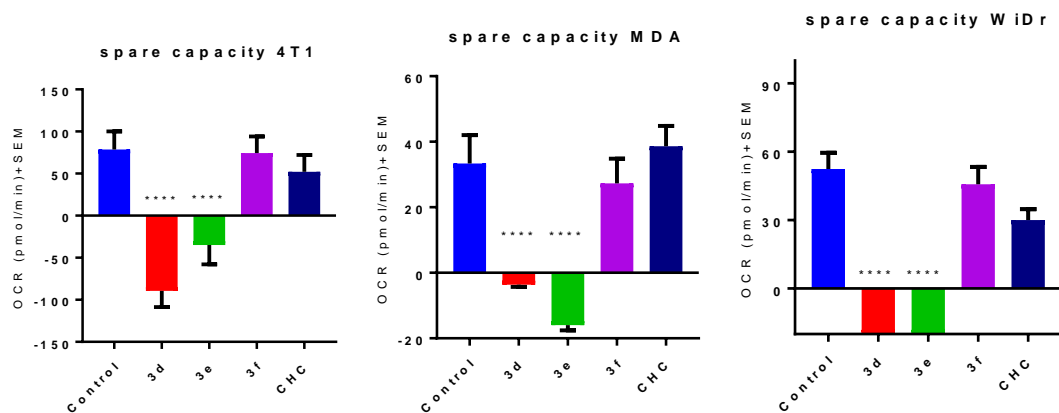
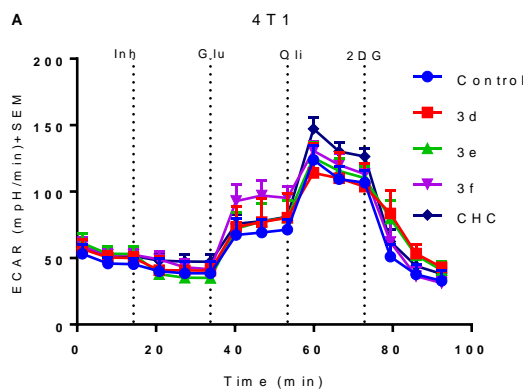


Figure 3.18: Spare respiratory capacity in (A) 4T1, (B) MDA-MB-231 and (C) WiDr cell lines using compounds **3d-3f**. The OCR values were calculated using wave software. The average+SEM values of at least three independent experimental values were calculated.

Glycolysis stress test in MDA-MB-231 and WiDr cell lines: The glycolysis stress test allows us to evaluate glycolysis, glycolytic capacity and glycolytic reserve. Measuring the extracellular acidification rate (ECAR) of glucose deprived cells allows us to determine basal levels of ECAR. We can then add glucose to the cells and measure the ECAR. Glycolysis is defined by this change in ECAR. For example, if our test compound inhibits glycolysis, we will see a smaller change in ECAR before and after addition of glucose. To force the cells to undergo higher rates of glycolysis, we can treat cells with an ATP synthase inhibitor, oligomycin A and measure the change in ECAR. Since cells have the same energetic demand and mitochondrial function has been inhibited this results in the cells undergoing glycolysis at maximum capacity or glycolytic capacity. If our compound is active, we expect to see a decrease in the ECAR. The final drug

delivery port is injected with glycolysis inhibitor 2-deoxy-glucose. With this addition, ECAR is reduced to basal levels and the difference between glycolysis and glycolytic capacity can be defined as glycolytic reserve, which indicates the flexibility of cells to overcome stressful conditions.

Glycolytic stress test ECAR were measured in real-time, and the following parameters were calculated as a result: glycolysis, glycolytic capacity and glycolytic reserve. Like the mitochondrial stress test, compounds were dissolved in DMSO and as such was used as a negative control. The compounds were tested at 100 μ M concentration. Although compounds **3e** and **3f** only minimally altered ECAR in MDA-MB-231 cell line, in WiDr cell line, these compounds **3d** and **3e** significantly altered the ECAR compared to control (**Figure 3.19**). All the test compounds did not exhibit any effect on ECAR in 4T1



cell line.

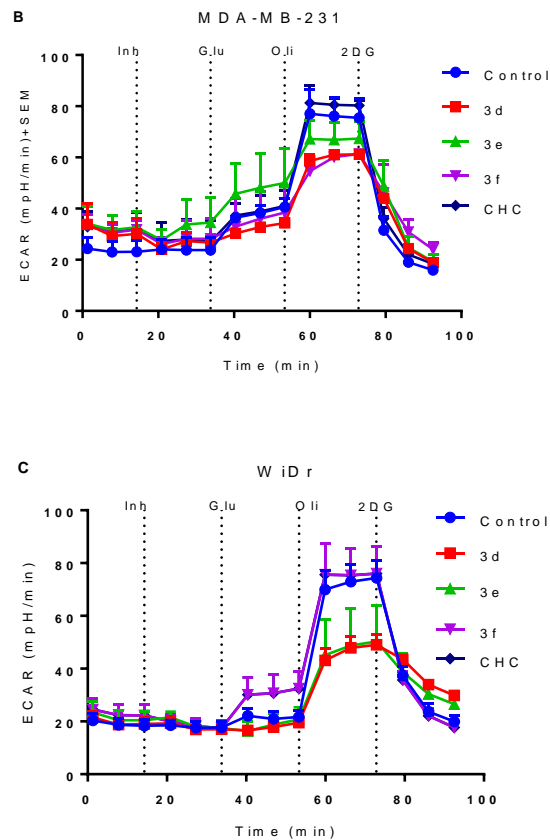


Figure 3.19: Glycolytic stress test in (A) 4T1, (B) MDA-MB-231 and (C) WiDr cell lines using compounds **3d-3f**. The ECAR values were calculated using wave software. The average+SEM values of at least three independent experimental values were calculated.

Glycolysis is the cells ability to convert glucose to pyruvate. To measure glycolysis basal extracellular acidification rates in the absence of glucose is compared to after the addition of glucose. As glucose is converted extracellular acidification rate should increase showing the cells ability to perform glycolysis. In 4T1 cell line, none of the compounds showed a significant change. In MDA-

MB-231 cell line, compound **3d** and **3f** significantly reduced glycolysis compared to the control (**Figure 3.20**).

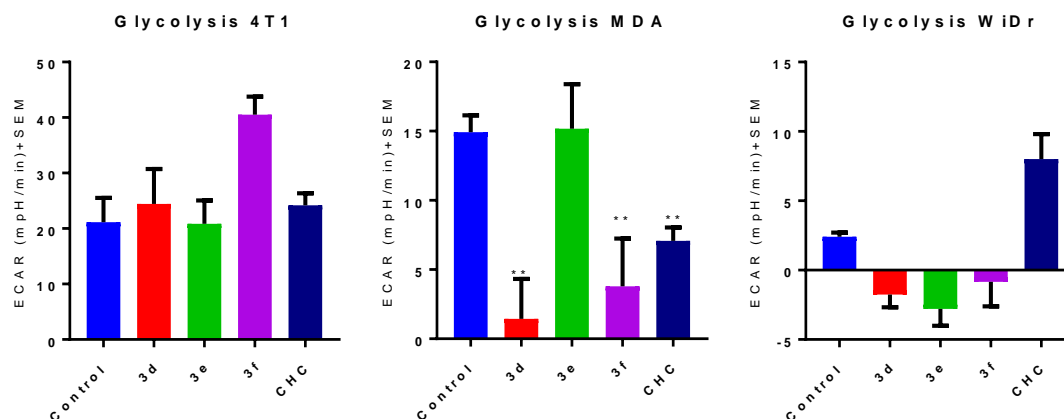


Figure 3.20: Glycolysis in (A) 4T1, (B) MDA-MB-231 and (C) WiDr cell lines using compounds **3d-3f**. The ECAR values were calculated using wave software. The average+SEM values of at least three independent experimental values were calculated.

Glycolytic capacity is the ability of the cells to meet energetic demands after the addition of an ATP synthase inhibitor oligomycin A, which disrupts oxidative phosphorylation. The addition of oligomycin A results in the cell to achieve its theoretical maximum rate of glycolysis. Glycolytic capacity is also the difference between basal level before glucose addition and after the cell is in crisis (**Figure 3.21**). None of the tested compounds showed a significant change in glycolytic capacity.

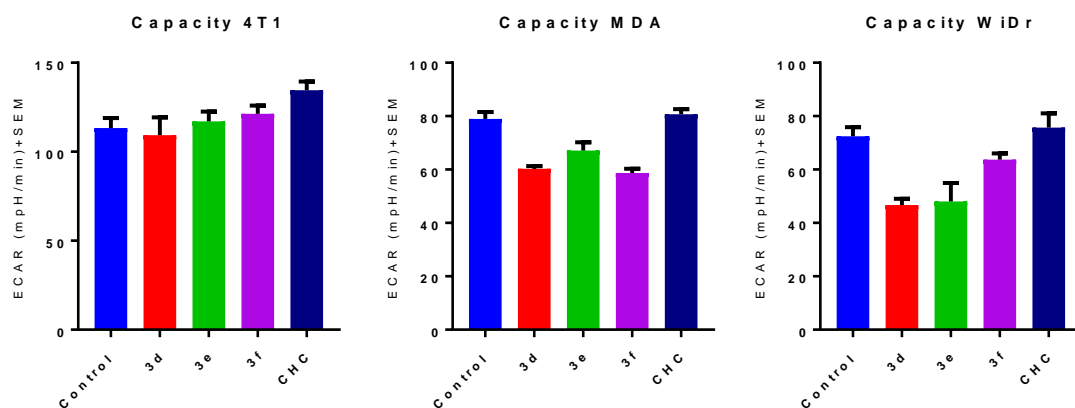


Figure 3.21: Glycolytic capacity in (A) 4T1, (B) MDA-MB-231 and (C) WiDr cell lines using compounds **3d-3f**. The ECAR values were calculated using wave software. The average+SEM values of at least three independent experimental values were calculated.

Glycolytic reserve is the difference of the cells ability to undergo glycolysis under normal conditions and after there is an energetic demand (**Figure 3.22**). Therefore, it is a measurement of how closely the glycolytic function is to the theoretical maximum. None of the tested compounds showed a significant change in glycolytic reserve.

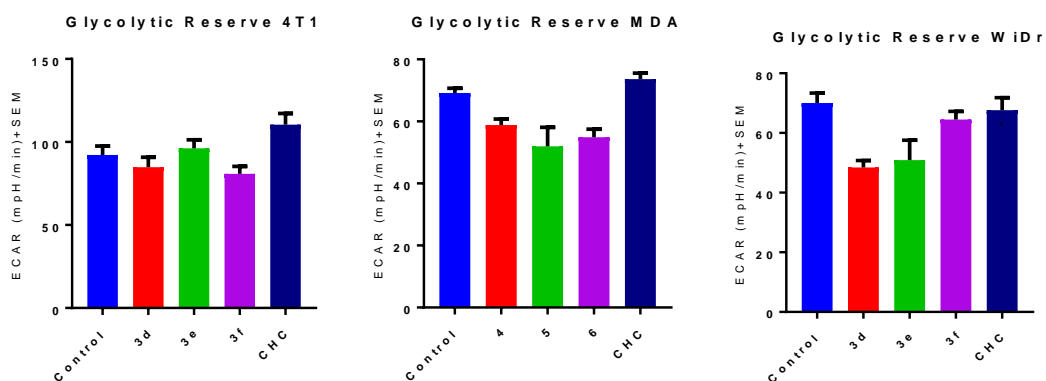


Figure 3.22: Glycolytic reserve in (A) 4T1, (B) MDA-MB-231 and (C) WiDr cell lines using compounds **3d-3f**. The ECAR values were calculated using wave software. The average+SEM values of at least three independent experimental values were calculated.

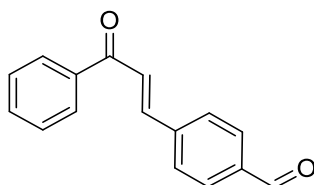
3.3 Conclusions

In conclusion, we have synthesized chalcone based phenylcyanoacrylic acids as potential metabolic inhibitors. These inhibitors were evaluated for their cell proliferation inhibition and these compounds did not show any toxicity in 4T1, MCF7, MDA-MB-231, MIAPaCa2, and WiDr up to a concentration of 100 μ M. However, since we envisioned to generate generally nontoxic compounds as metabolic inhibitors, we evaluated **3d-3f** for their metabolic profile using seahorse XFe96 glycolytic and mitochondrial stress tests. These studies showed that compounds caused mitochondrial dysfunction in 4T1, MDA-MB-231, and WiDr cell lines. Glycolytic stress test showed that compounds had the greatest effect on MDA-MB-231 and WiDr. Further investigation of these compounds will involve determination of the mechanism for which oxidative phosphorylation and glycolysis are affected. A lead compound will be selected and evaluated for metabolic stability, and efficacy as a single agent and in conjunction with other metabolic inhibitors.

3.4 Experimental

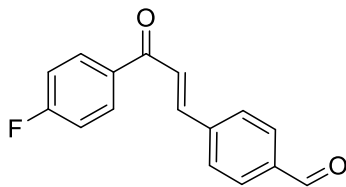
*Synthesis of (E)-4-(3-(phenyl)-3-oxoprop-1-en-1-yl)benzaldehyde **3a***

Acetophenone (10 mmol) was dissolved in methanol (50 mL) and 5 mL 2.5M NaOH was added. 4-(dimethoxymethyl)benzaldehyde was added to the reaction mixture and stirred for ~30 min. TLC showed completion of the reaction and concentrated HCl (2 mL) was added. The reaction mixture was stirred for an additional 30 min at which point the reaction mixture was further diluted with water and subsequently filtered. Product was recrystallized in ethanol to afford the pure product (E)-4-(3-(phenyl)-3-oxoprop-1-en-1-yl)benzaldehyde **3a** in ~75% yield.



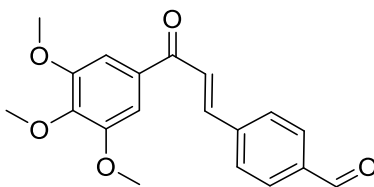
*Synthesis of (E)-4-(3-(4-fluorophenyl)-3-oxoprop-1-en-1-yl)benzaldehyde **3b***

4'-Fluoroacetophenone (10 mmol) was dissolved in methanol (50 mL) and 5 mL 2.5M NaOH was added. 4-(dimethoxymethyl)benzaldehyde was added to the reaction mixture and stirred for ~30 min. TLC showed completion of the reaction and concentrated HCl (2 mL) was added. The reaction mixture was stirred for an additional 30 min at which point the reaction mixture was further diluted with water and subsequently filtered. Product was recrystallized in ethanol to afford the pure product (E)-4-(3-(4-fluorophenyl)-3-oxoprop-1-en-1-yl)benzaldehyde **3b** in ~80% yield.



*Synthesis of (E)-4-(3-oxo-3-(3,4,5-trimethoxyphenyl)prop-1-en-1-yl)benzaldehyde **3c***

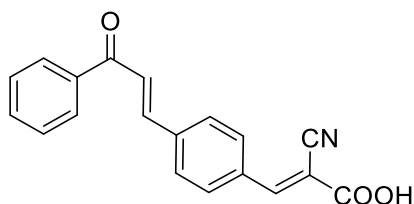
3',4',5'-Trimethoxyacetophenone (10 mmol) was dissolved in methanol (50 mL) and 5 mL 2.5M NaOH was added. 4-(dimethoxymethyl)benzaldehyde was added to the reaction mixture and stirred for ~30 min. TLC showed completion of the reaction and concentrated HCl (2 mL) was added. The reaction mixture was stirred for an additional 30 min at which point the reaction mixture was further diluted with water and subsequently filtered. Product was recrystallized in ethanol to afford the pure product (E)-4-(3-oxo-3-(3,4,5-trimethoxyphenyl)prop-1-en-1-yl)benzaldehyde **3c** in ~80% yield.



*Synthesis of (E)-2-cyano-3-(4-((E)-3-(phenyl)-3-oxoprop-1-en-1-yl)phenyl)acrylic acid **3d***

(E)-4-(3-(4-fluorophenyl)-3-oxoprop-1-en-1-yl)benzaldehyde **3a** (10 mmol) was dissolved in acetonitrile (30 mL) followed by the addition of cyanoacetic acid (11 mmol) and piperidine (11 mmol). The reaction mixture was then refluxed for 2 hours, at which time TLC confirmed the completion of the reaction. The reaction

was then cooled to room temperature and dilute HCl was added. The resulting solid was then filtered and recrystallized to afford the pure product (E)-2-cyano-3-(4-((E)-3-(phenyl)-3-oxoprop-1-en-1-yl)phenyl)acrylic acid **3d** in ~90% yield.

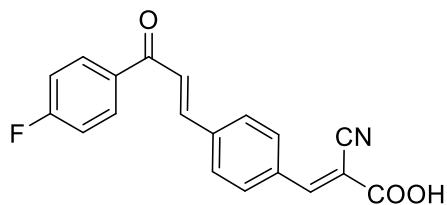


^1H NMR (500 MHz, DMSO- d_6) δ 8.17 (d, $J = 7$ Hz, 2H), 8.08-8.00 (m, 6H), 7.73 - 7.79 (m, 1H), 7.68 (t, $J = 7$ Hz, 1H), 7.58 (t, $J = 8$ Hz, 2H)

^{13}C NMR (126 MHz, DMSO- d_6) δ 189.6, 163.3, 147.9, 143.2, 137.9, 137.5, 135.3, 133.8, 130.4, 129.8, 129.3, 129.1, 124.1, 119.1, 113.1

*Synthesis of (E)-2-cyano-3-(4-((E)-3-(4-fluorophenyl)-3-oxoprop-1-en-1-yl)phenyl) acrylic acid **3e***

(E)-4-(3-(4-fluorophenyl)-3-oxoprop-1-en-1-yl)benzaldehyde **3b** (10 mmol) was dissolved in acetonitrile (30 mL) followed by the addition of cyanoacetic acid (11 mmol) and piperidine (11 mmol). The reaction mixture was then refluxed for 2 hours, at which time TLC confirmed the completion of the reaction. The reaction was then cooled to room temperature and dilute HCl was added. The resulting solid was then filtered and recrystallized to afford the pure product (E)-2-cyano-3-(4-((E)-3-(4-fluorophenyl)-3-oxoprop-1-en-1-yl)phenyl)acrylic acid **3e** in ~90% yield.



$^1\text{H NMR}$ (500 MHz, DMSO- d_6) δ 8.34 (s, 1H), 8.19 - 8.29 (m, 2H), 8.04 - 8.11

(m, 4H), 7.74 (d, $J = 16$ Hz, 1H), 7.32 - 7.43 (m, 2H)

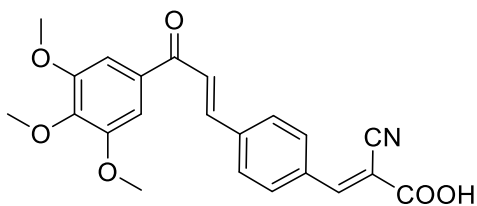
$^{13}\text{C NMR}$ (126 MHz, DMSO- d_6) δ 188.0, 166.6, 164.6, 163.6, 153.8, 142.8,

139.3, 134.4, 134.4, 133.5, 132.2, 132.1, 131.5, 129.9, 124.8, 116.5, 116.4,

116.2, 104.8

*Synthesis of (E)-2-cyano-3-(4-((E)-3-(4-fluorophenyl)-3-oxoprop-1-en-1-yl)phenyl) acrylic acid **3f***

(E)-4-(3-(4-fluorophenyl)-3-oxoprop-1-en-1-yl)benzaldehyde **3c** (10 mmol) was dissolved in acetonitrile (30 mL) followed by the addition of cyanoacetic acid (11 mmol) and piperidine (11 mmol). The reaction mixture was then refluxed for 2 hours, at which time TLC confirmed the completion of the reaction. The reaction was then cooled to room temperature and dilute HCl was added. The resulting solid was then filtered and recrystallized to afford the pure product (E)-2-cyano-3-(4-((E)-3-(4-fluorophenyl)-3-oxoprop-1-en-1-yl)phenyl)acrylic acid **3f** in ~90% yield.



^1H NMR (500 MHz, DMSO- d_6) δ 8.38 (s, 1H), 8.11 - 8.09 (m, 5H), 7.78 (d, J = 20 Hz, 1H), 7.45 (s, 2H), 3.91 (s, 6H), 3.77 (s, 3H)

^{13}C NMR (126 MHz, DMSO- d_6) δ 188.1, 163.6, 153.8, 153.4, 142.7, 142.6, 139.4, 133.5, 133.2, 131.5, 130.0, 124.8, 116.6, 106.8, 104.8, 60.7, 56.7

3.4b Cell lines and culture conditions

4T1 cells were purchased from Caliper Life Sciences and were cultured in RPMI-1650 supplemented with FBS (10%) and penicillin-streptomycin (50 U/mL, 50 $\mu\text{g}/\text{mL}$).

MDA-MB-231 cells were purchased from ATCC and were cultured in DMEM supplemented with FBS (10%, Atlanta Biologicals) and penicillin-streptomycin (50 U/mL, 50 $\mu\text{g}/\text{mL}$, Invitrogen).

WiDr cells were purchased from ATCC and were cultured in MEM supplemented with FBS (10%) and penicillin-streptomycin (50 U/mL, 50 $\mu\text{g}/\text{mL}$).

3.4c MTT assay

Cells (5×10^3 cells/well) were cultured in 96-well plates and incubated for 18-24 hours. Stock solution of compound was made up at 100 mM concentration

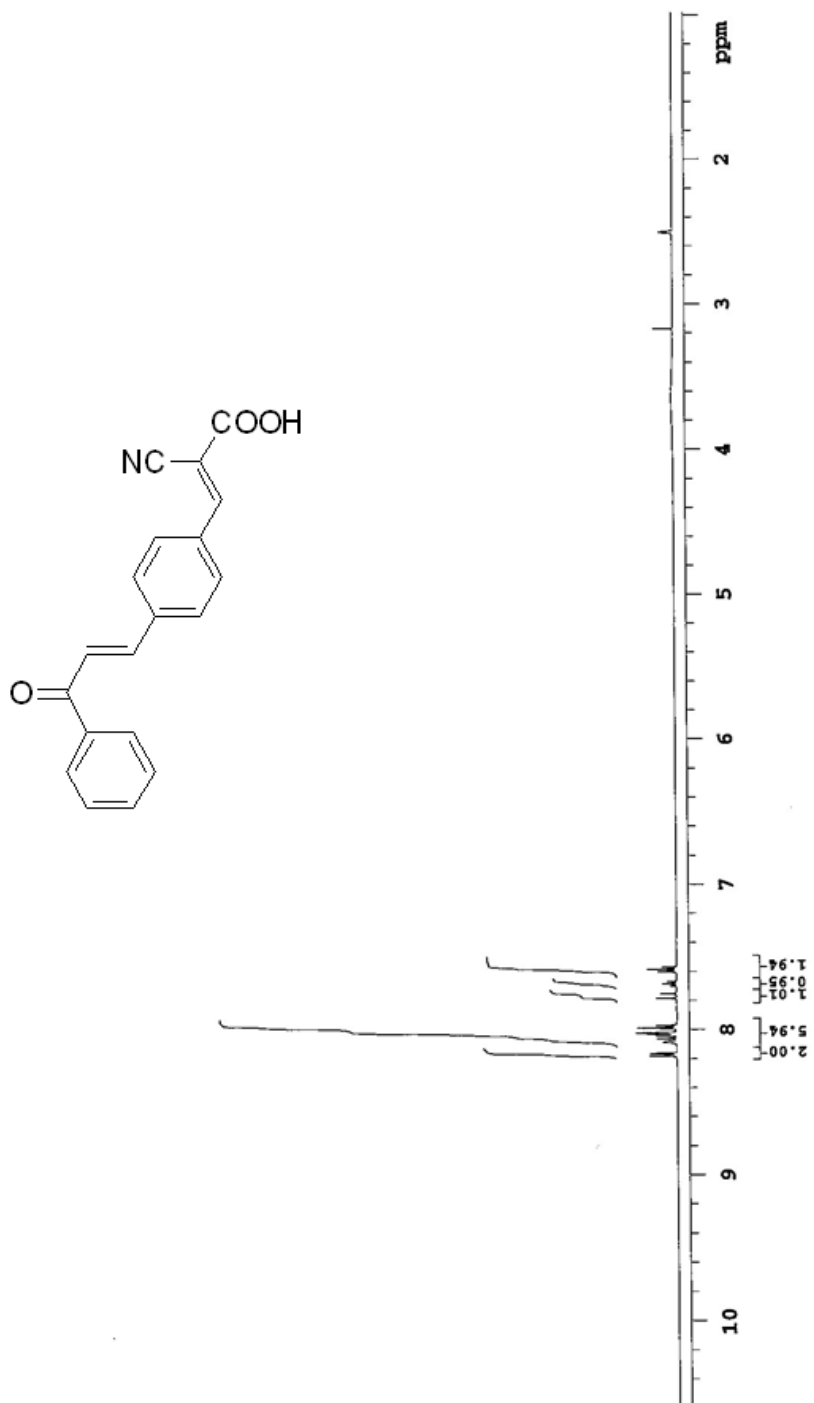
in DMSO. The final concentration of DMSO in the wells were < 0.01%. Concentration range of compounds from 50 μ M to 0.5 μ M was tested by adding 2x concentration of test compound to the first well and then the serial dilutions by going from well to well. All the compounds were tested in duplicates. After 72 hours of treatment, 10 μ L of MTT (5 mM in 1x PBS) was added into the wells and the cells were incubated for a period of 4 hours. At this point, the conversion of MTT to formazan was quenched by the addition of 100 μ L of SDS (1 g of SDS dissolved in 0.01 N HCl) and the cells were incubated for further 4 hours. The absorbance was recorded at 570 nm using BioTek Synergy 2 plate reader. The absorbance is directly proportional to the cell viability. % Survival was calculated using the formula

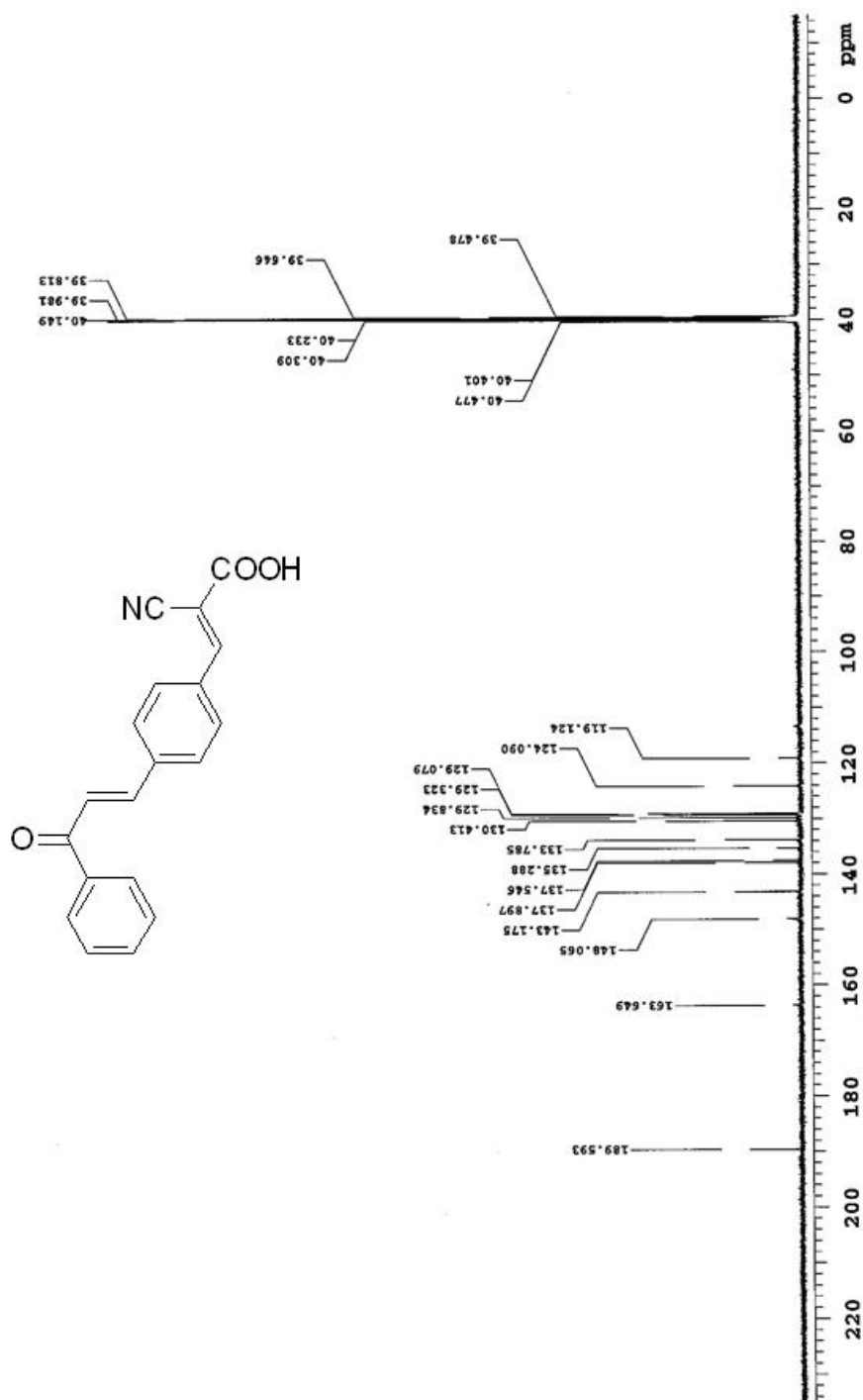
3.4d Seahorse XFe96[®] assessment of glycolysis and mitochondrial respiration

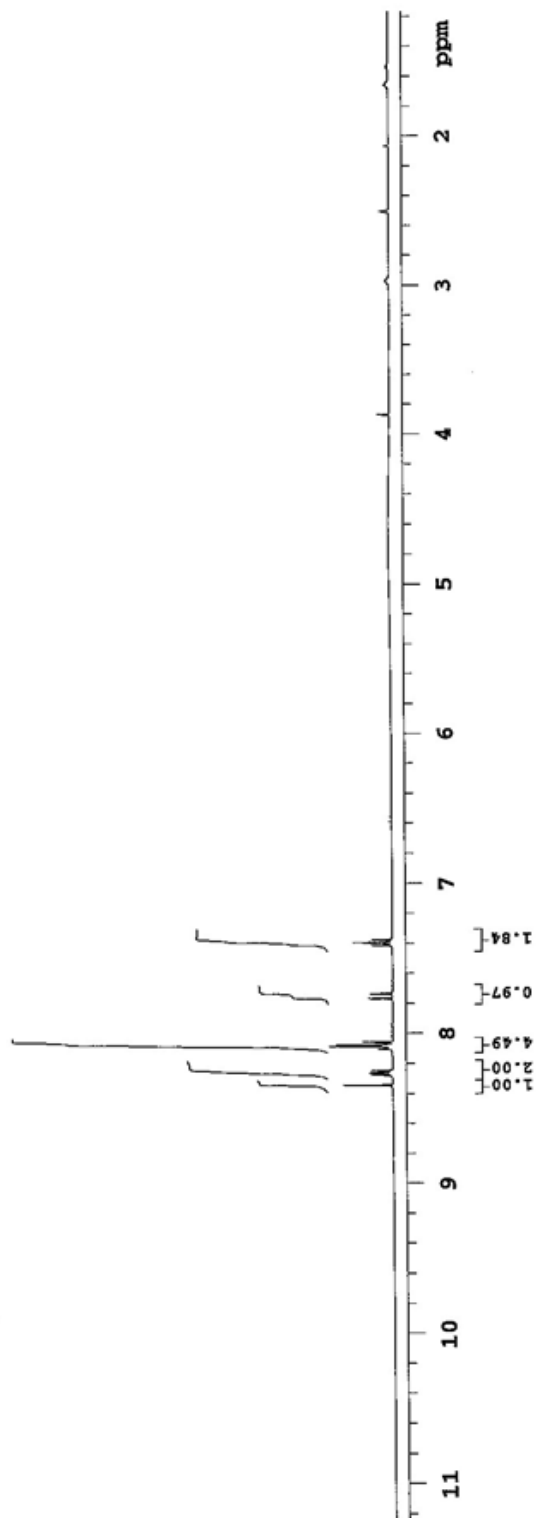
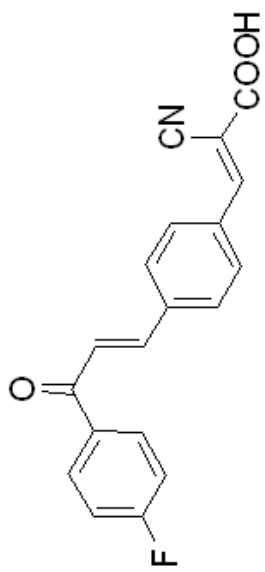
20,000 cells/well were plated in 96-well Seahorse plates (Agilent, part no. 101085-004) and incubated 16-24 hours at 37°C at 5% CO₂. Flux pack sensors (Agilent, part no. 102416-100) were hydrated with XF calibrant solution (Agilent, part no. 100840-000) overnight at 37°C in a non-CO₂ incubator. Serum free assay media were prepared using Seahorse base medium (Agilent, part no. 102353-100) with the addition of glutamine (1mM) and sodium pyruvate (1mM) for glycolysis stress test, whereas for mitochondrial stress test, glucose (10mM), glutamine (1uM), and sodium pyruvate (1mM) were used. The pH of these media was adjusted to 7.4 and warmed to 37°C. An 8X stock concentration of test

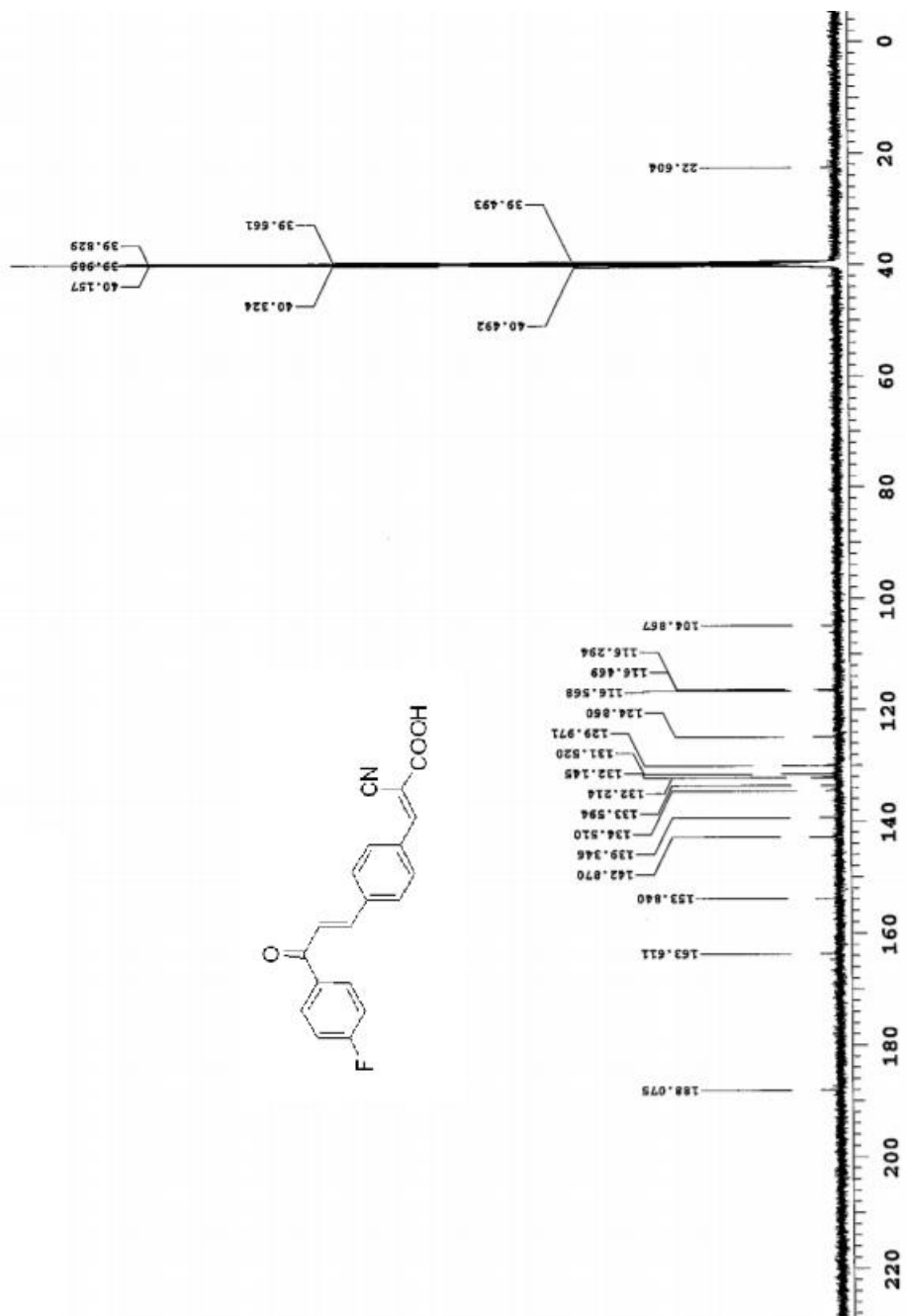
compounds was prepared for microplate injections in port A. Stock solutions of glucose, oligomycin, and 2-deoxyglucose (Chem Impex) were prepared such that their final working concentrations are 10mM, 1 μ M and 50mM, respectively, for glycolysis stress test. For mitochondrial stress test, stock solutions of oligomycin, FCCP, rotenone+antimycin A were prepared such that their final concentrations are 1 μ M, 0.25-1 μ M, and 0.5 μ M, respectively. Under glycolytic stress test, the cells were treated with test compounds, followed by the addition of glucose, oligomycin and 2-deoxyglucose at 14.29, 33.8, 53.35, 72.87 minutes, respectively. Under mitochondrial stress test, cells were treated with test compounds, followed by the addition of oligomycin, FCCP, and rotenone+antimycin A, at 14.29, 33.8, 53.35, 72.87 minutes, respectively. Extracellular acidification rates (ECAR) and oxygen consumption rates (OCR) were recorded in real-time for glycolysis and mitochondrial stress tests, respectively, using a Seahorse XFe96[®] analyzer (Agilent). The parameters related to glycolytic and mitochondrial functions were calculated utilizing the Wave 2.4.0 software (Agilent) according to manufactures protocol.

3.6 NMR Spectra









3.5 References:

1. Hanahan, D. & Weinberg, R. A. Hallmarks of cancer: The next generation. *Cell* **144**, 646–674 (2011).
2. Cruijsen, H. Van, Giaccone, G. & Hoekman, K. Epidermal growth factor receptor and angiogenesis : opportunities for combined anticancer strategies. **888**, 883–888 (2006).
3. Dudley, A. C. & Claesson-Welsh, L. Mechanisms of angiogenesis and lymphangiogenesis. *Tumor Angiogenes.* **1**, 17–34 (2010).
4. Wener Risau. Mechanisms of angiogenesis. *Nature* **386**, 671–674 (1997).
5. Rajabi, M. & Mousa, S. The Role of Angiogenesis in Cancer Treatment. *Biomedicines* **5**, 34 (2017).
6. Lemmon, M. A. & Schlessinger, J. Cell Signaling by Receptor Tyrosine Kinases. *Cell* **141**, 1117–1134 (2010).
7. Hunter, T. & Blume-Jensen, P. Oncogenic kinase signalling. *Nature* **411**, 355 (2001).
8. Cancer, N. R. Nature reviews. **411**, 2001 (2016).
9. Sada, K., Takano, T., Yanagi, S. & Yamamura, H. Structure and Function of Syk Protein-Tyrosine Kinase. *J. Biochem.* **130**, 177–186 (2001).
10. Gilbert, J. A. *et al.* Molecular markers for novel therapeutic strategies in pancreatic endocrine tumors. *Pancreas* **42**, 411–421 (2013).
11. Bianco, R. *et al.* Vascular Endothelial Growth Factor Receptor-1 Contributes to Resistance to Anti-Epidermal Growth Factor Receptor Drugs in Human Cancer Cells. *Clin. Cancer Res.* **14**, 5069–5080 (2008).

12. Hierro, C. & Taberero, J. *Fibroblast Growth Factor Receptor Inhibitors : Enhancing Therapeutic Strategies for Solid Tumors. Targeting Cell Survival Pathways to Enhance Response to Chemotherapy* (Elsevier Inc., 2018). doi:10.1016/B978-0-12-813753-6/00005-6
13. Sonoshita, M. *et al.* kinase inhibitor into new disease space. **14**, (2018).
14. O’Keefe, R. A., Grandis, J. R. & Johnson, D. E. Targeting Members of the Epidermal Growth Factor Receptor Family to Improve Response to Chemotherapy. in *Targeting Cell Survival Pathways to Enhance Response to Chemotherapy* 1–23 (Elsevier, 2019). doi:10.1016/B978-0-12-813753-6.00001-9
15. Bean, J. *et al.* Acquired Resistance to Epidermal Growth Factor Receptor Kinase Inhibitors Associated with a Novel T854A Mutation in a Patient with EGFR-Mutant Lung Adenocarcinoma. *Clin. Cancer Res.* **14**, 7519–7525 (2008).
16. Pao, W. *et al.* EGF receptor gene mutations are common in lung cancers from ‘never smokers’ and are associated with sensitivity of tumors to gefitinib and erlotinib. *Proc. Natl. Acad. Sci.* **101**, 13306–13311 (2004).
17. Byeon, H. K., Ku, M. & Yang, J. Beyond EGFR inhibition: multilateral combat strategies to stop the progression of head and neck cancer. *Exp. Mol. Med.* **51**, 8 (2019).
18. Bhullar, K. S. *et al.* Kinase-targeted cancer therapies: progress, challenges and future directions. *Mol. Cancer* **17**, 48 (2018).
19. Abaan, O. D. *et al.* The exomes of the NCI-60 panel: a genomic resource

- for cancer biology and systems pharmacology. *Cancer Res.* **73**, 4372–82 (2013).
20. Neal, J. W. The SATURN trial: the value of maintenance erlotinib in patients with non-small-cell lung cancer. *Futur. Oncol.* **6**, 1827–1832 (2010).
 21. Li, Z. *et al.* Erlotinib Effectively Inhibits JAK2V617F Activity and Polycythemia Vera Cell Growth. *J. Biol. Chem.* **282**, 3428–3432 (2006).
 22. Maemondo, M. *et al.* Gefitinib or Chemotherapy for Non–Small-Cell Lung Cancer with Mutated EGFR. *N. Engl. J. Med.* **362**, 2380–2388 (2010).
 23. Arora, A. & Scholar, E. M. Role of tyrosine kinase inhibitors in cancer therapy. *J. Pharmacol. Exp. Ther.* **315**, 971–9 (2005).
 24. Gridelli, C. *et al.* Gefitinib as first-line treatment for patients with advanced non-small-cell lung cancer with activating epidermal growth factor receptor mutation: Review of the evidence. *Lung Cancer* **71**, 249–257 (2011).
 25. Bae, J. H. *et al.* The Selectivity of Receptor Tyrosine Kinase Signaling Is Controlled by a Secondary SH2 Domain Binding Site. *Cell* **138**, 514–524 (2009).
 26. Shibuya, M. Vascular Endothelial Growth Factor (VEGF) and Its Receptor (VEGFR) Signaling in Angiogenesis: A Crucial Target for Anti- and Pro-Angiogenic Therapies. *Genes and Cancer* **2**, 1097–1105 (2011).
 27. Jang, J. *et al.* Antitumor Effect of AZD4547 in a Fibroblast Growth Factor Receptor 2–Amplified Gastric Cancer Patient–Derived Cell Model. *Transl.*

- Oncol.* **10**, 469–475 (2017).
28. Aggarwal, C. *et al.* Phase II study of the FGFR inhibitor AZD4547 in previously treated patients with FGF pathway-activated stage IV squamous cell lung cancer (SqNSCLC): LUNG-MAP sub-study SWOG S1400D. *J. Clin. Oncol.* **35**, 9055–9055 (2017).
 29. Zhao, Q. *et al.* FGFR inhibitor, AZD4547, impedes the stemness of mammary epithelial cells in the premalignant tissues of MMTV-ErbB2 transgenic mice. *Sci. Rep.* **7**, 11306 (2017).
 30. Manchado, E. *et al.* A combinatorial strategy for treating KRAS-mutant lung cancer. *Nature* **534**, 647–51 (2016).
 31. Huynh, H. *et al.* Infigratinib Mediates Vascular Normalization, Impairs Metastasis, and Improves Chemotherapy in Hepatocellular Carcinoma. *Hepatology* **69**, 943–958 (2019).
 32. Nogova, L. *et al.* Evaluation of BGJ398, a Fibroblast Growth Factor Receptor 1-3 Kinase Inhibitor, in Patients With Advanced Solid Tumors Harboring Genetic Alterations in Fibroblast Growth Factor Receptors: Results of a Global Phase I, Dose-Escalation and Dose-Expansion Stu. *J. Clin. Oncol.* **35**, 157–165 (2017).
 33. O'Hare, T. *et al.* AP24534, a pan-BCR-ABL inhibitor for chronic myeloid leukemia, potently inhibits the T315I mutant and overcomes mutation-based resistance. *Cancer Cell* **16**, 401–12 (2009).
 34. Huang, W.-S. *et al.* Discovery of 3-[2-(imidazo[1,2-b]pyridazin-3-yl)ethynyl]-4-methyl-N-{4-[(4-methylpiperazin-1-yl)methyl]-3-

- (trifluoromethyl)phenyl}benzamide (AP24534), a potent, orally active pan-inhibitor of breakpoint cluster region-abelson (BCR-ABL) kinase including th. *J. Med. Chem.* **53**, 4701–19 (2010).
35. Gozgit, J. M. *et al.* Potent activity of ponatinib (AP24534) in models of FLT3-driven acute myeloid leukemia and other hematologic malignancies. *Mol. Cancer Ther.* **10**, 1028–35 (2011).
 36. Rahimi, N. VEGFR-1 and VEGFR-2: two non-identical twins with a unique physiognomy. *Front. Biosci.* **11**, 11 (2007).
 37. Guedez, L. & Stetler-stevenson, W. G. The Textbook of Angiogenesis and Lymphangiogenesis: Methods and Applications. *Textb. Angiogenes. Lymphangiogenes. Methods Appl.* 305–309 (2012). doi:10.1007/978-94-007-4581-0
 38. Su, J. C. *et al.* Disrupting VEGF-A paracrine and autocrine loops by targeting SHP-1 suppresses triple negative breast cancer metastasis. *Sci. Rep.* **6**, 1–14 (2016).
 39. Slongo, M. L. *et al.* Functional VEGF and VEGF receptors are expressed in human medulloblastomas. *Neuro. Oncol.* **9**, 384–392 (2007).
 40. Hilberg, F. *et al.* BIBF 1120: triple angiokinase inhibitor with sustained receptor blockade and good antitumor efficacy. *Cancer Res.* **68**, 4774–82 (2008).
 41. Chen, H. *et al.* PDGF signalling controls age-dependent proliferation in pancreatic β -cells. *Nature* **478**, 349–355 (2011).
 42. Lawson, K. A. *et al.* Repurposing Sunitinib with Oncolytic Reovirus as a

- Novel Immunotherapeutic Strategy for Renal Cell Carcinoma. *Clin. Cancer Res.* **22**, 5839–5850 (2016).
43. L'Italien, L. *et al.* Mechanistic Insights of an Immunological Adverse Event Induced by an Anti-KIT Antibody Drug Conjugate and Mitigation Strategies. *Clin. Cancer Res.* **24**, 3465–3474 (2018).
 44. Xu, M., Casio, M., Range, D. E., Sosa, J. A. & Counter, C. M. Copper Chelation as Targeted Therapy in a Mouse Model of Oncogenic BRAF-Driven Papillary Thyroid Cancer. *Clin. Cancer Res.* **24**, 4271–4281 (2018).
 45. Wang, T. *et al.* BRAF Inhibition Stimulates Melanoma-Associated Macrophages to Drive Tumor Growth. *Clin. Cancer Res.* **21**, 1652–64 (2015).
 46. Chen, H. *et al.* PDGF signalling controls age-dependent proliferation in pancreatic β -cells. *Nature* **478**, 349–55 (2011).
 47. Boehme, S. A., Franz-Bacon, K., DiTirro, D. N., Ly, T. W. & Bacon, K. B. MAP3K19 Is a Novel Regulator of TGF- β Signaling That Impacts Bleomycin-Induced Lung Injury and Pulmonary Fibrosis. *PLoS One* **11**, e0154874 (2016).
 48. Dong, J., Zhang, Q., Wang, Z., Huang, G. & Li, S. Recent Advances in the Development of Indazole-based Anticancer Agents. 1490–1507 (2018). doi:10.1002/cmdc.201800253
 49. Tomassi, S. *et al.* Indazole-Based Covalent Inhibitors To Target Drug-Resistant Epidermal Growth Factor Receptor. *J. Med. Chem.* **60**, 2361–

2372 (2017).

50. Synthesis and Evaluation of Indazole Based Small Molecules for the Treatment of Breast and Colorectal Cancers.
51. Sternberg, C. N. *et al.* Pazopanib in locally advanced or metastatic renal cell carcinoma: results of a randomized phase III trial. *J. Clin. Oncol.* **28**, 1061–8 (2010).
52. Sonpavde, G., Hutson, T. E. & Sternberg, C. N. Pazopanib, a potent orally administered small-molecule multitargeted tyrosine kinase inhibitor for renal cell carcinoma. *Expert Opin. Investig. Drugs* **17**, 253–261 (2008).
53. Escudier, B. *et al.* Randomized, controlled, double-blind, cross-over trial assessing treatment preference for pazopanib versus sunitinib in patients with metastatic renal cell carcinoma: PISCES Study. *J. Clin. Oncol.* **32**, 1412–8 (2014).
54. Deng, Y. *et al.* Bioavailability, metabolism and disposition of oral pazopanib in patients with advanced cancer. *Xenobiotica* **43**, 443–453 (2013).
55. Ueda, T. *et al.* Efficacy and Safety of Axitinib Versus Sorafenib in Metastatic Renal Cell Carcinoma: Subgroup Analysis of Japanese Patients from the Global Randomized Phase 3 AXIS Trial. *Jpn. J. Clin. Oncol.* **43**, 616–628 (2013).
56. Cohen, E. E. W. *et al.* Axitinib is an active treatment for all histologic subtypes of advanced thyroid cancer: Results from a phase II study. *J. Clin. Oncol.* **26**, 4708–4713 (2008).

57. Hu-Lowe, D. D. *et al.* Nonclinical antiangiogenesis and antitumor activities of axitinib (AG-013736), an oral, potent, and selective inhibitor of vascular endothelial growth factor receptor tyrosine kinases 1, 2, 3. *Clin. Cancer Res.* **14**, 7272–83 (2008).
58. Pemovska, T. *et al.* Axitinib effectively inhibits BCR-ABL1(T315I) with a distinct binding conformation. *Nature* **519**, 102–5 (2015).
59. Harris, P. A. *et al.* Discovery of 5-[[4-[(2,3-dimethyl-2H-indazol-6-yl)methylamino]-2-pyrimidinyl]amino]-2-methyl-benzenesulfonamide (Pazopanib), a novel and potent vascular endothelial growth factor receptor inhibitor. *J. Med. Chem.* **51**, 4632–40 (2008).
60. Wilhelm, S. M. *et al.* Preclinical overview of sorafenib, a multikinase inhibitor that targets both Raf and VEGF and PDGF receptor tyrosine kinase signaling. *Mol. Cancer Ther.* **7**, 3129–3140 (2008).
61. Liu, L. P., Ho, R. L. K., Chen, G. G. & Lai, P. B. S. Sorafenib inhibits hypoxia-inducible factor-1 α synthesis: Implications for antiangiogenic activity in hepatocellular carcinoma. *Clin. Cancer Res.* **18**, 5662–5671 (2012).
62. Parsons, H. M., Chu, Q., Karlitz, J. J., Stevens, J. L. & Harlan, L. C. Adoption of Sorafenib for the Treatment of Advanced-Stage Hepatocellular Carcinoma in Oncology Practices in the United States. *Liver Cancer* **6**, 216–226 (2017).
63. Hwang, S. H. *et al.* Synthesis and biological evaluation of sorafenib- and regorafenib-like sEH inhibitors. *Bioorganic Med. Chem. Lett.* **23**, 3732–

3737 (2013).

64. Llovet, J. M. *et al.* Sorafenib in Advanced Hepatocellular Carcinoma. *N. Engl. J. Med.* **359**, 378–390 (2008).
65. Escudier, B. *et al.* Sorafenib for treatment of renal cell carcinoma: Final efficacy and safety results of the phase III treatment approaches in renal cancer global evaluation trial. *J. Clin. Oncol.* **27**, 3312–8 (2009).
66. Lencioni, R. *et al.* First interim analysis of the GIDEON (Global Investigation of therapeutic DEcisions in hepatocellular carcinoma and Of its treatment with sorafeNib) non-interventional study. *Int. J. Clin. Pract.* **66**, 675–683 (2012).
67. Goel, G. Evolution of regorafenib from bench to bedside in colorectal cancer: Is it an attractive option or merely a “me too” drug? *Cancer Manag. Res.* **10**, 425–437 (2018).
68. Wilhelm, S. M. *et al.* Regorafenib (BAY 73-4506): A new oral multikinase inhibitor of angiogenic, stromal and oncogenic receptor tyrosine kinases with potent preclinical antitumor activity. *Int. J. Cancer* **129**, 245–255 (2011).
69. Musumeci, F., Radi, M., Brullo, C. & Schenone, S. Vascular endothelial growth factor (VEGF) receptors: Drugs and new inhibitors. *J. Med. Chem.* **55**, 10797–10822 (2012).
70. Grothey, A. & Yan, Y. Molecular profiling in the treatment of colorectal cancer: focus on regorafenib. *Onco. Targets. Ther.* 2949 (2015).
doi:10.2147/ott.s79145

71. Schmieder, R. *et al.* Regorafenib (BAY 73-4506): Antitumor and antimetastatic activities in preclinical models of colorectal cancer. *Int. J. Cancer* **135**, 1487–1496 (2014).
72. Cheng, Y. D., Yang, H., Chen, G. Q. & Zhang, Z. C. Molecularly targeted drugs for metastatic colorectal cancer. *Drug Des. Devel. Ther.* **7**, 1315–1322 (2013).
73. Jiao, Q. *et al.* Advances in studies of tyrosine kinase inhibitors and their acquired resistance. *Mol. Cancer* **17**, 1–12 (2018).
74. Wagner, J., Kline, C. L., Zhou, L., Khazak, V. & El-Deiry, W. S. Anti-tumor effects of ONC201 in combination with VEGF-inhibitors significantly impacts colorectal cancer growth and survival in vivo through complementary non-overlapping mechanisms. *J. Exp. Clin. Cancer Res.* **37**, 1–12 (2018).
75. Nelson, K. M. *et al.* The Essential Medicinal Chemistry of Curcumin. (2017). doi:10.1021/acs.jmedchem.6b00975
76. Adhikari, S., Priyadarsini, K. I. & Mukherjee, T. Recent Advances in Indian Herbal Drug Research Guest Editor : Thomas Paul Asir Devasagayam Physico-Chemical Studies on the Evaluation of the Antioxidant Activity of Herbal Extracts and Active Principles of Some Indian Medicinal Plants. 174–183 (2007).
77. Basile, V. *et al.* Curcumin derivatives : molecular basis of their anti-cancer activity To cite this version : (2010). doi:10.1016/j.bcp.2009.06.105
78. Moghadamtousi, S. Z. *et al.* A Review on Antibacterial , Antiviral , and

- Antifungal Activity of Curcumin. **2014**, (2014).
79. Anand, P. *et al.* Biological activities of curcumin and its analogues (Congeners) made by man and Mother Nature. **76**, 1590–1611 (2008).
 80. Ji, H. & Shen, L. Can improving bioavailability improve the bioactivity of curcumin ? *Trends Pharmacol. Sci.* **35**, 265–266 (2014).
 81. Naksuriya, O., Okonogi, S., Schiffelers, R. M. & Hennink, W. E. Biomaterials Curcumin nanoformulations : A review of pharmaceutical properties and preclinical studies and clinical data related to cancer treatment. *Biomaterials* **35**, 3365–3383 (2014).
 82. Sa, G. & Das, T. Anti cancer effects of curcumin : cycle of life and death. **14**, 1–14 (2008).
 83. Wilken, R., Veena, M. S., Wang, M. B. & Srivatsan, E. S. Curcumin : A review of anti-cancer properties and therapeutic activity in head and neck squamous cell carcinoma. *Mol. Cancer* **10**, 12 (2011).
 84. Liu, Z. *et al.* Evaluation of a curcumin analog as an anti-cancer agent inducing ER stress-mediated apoptosis in non-small cell lung cancer cells. *BMC Cancer* **13**, 1 (2013).
 85. Vyas, A., Dandawate, P., Padhye, S., Ahmad, A. & Sarkar, F. Perspectives on new synthetic curcumin analogs and their potential anticancer properties. *Curr. Pharm. Des.* **19**, 2047–69 (2013).
 86. Shishodia, S. Review Article Molecular Mechanisms of Curcumin Action : Gene Expression. 37–55 doi:10.1002/biof.1041
 87. Perrone, D. *et al.* Biological and therapeutic activities , and anticancer

properties of curcumin (Review). 1615–1623 (2015).

doi:10.3892/etm.2015.2749

88. Ghosh, N., Chaki, R., Mandal, V. & Mandal, S. C. Cox-2 as a target for cancer chemotherapy. *Pharmacol. Reports* **62**, 233–244 (2010).
89. Leonetti, C. Efficacy of a nitric oxide-releasing nonsteroidal anti-inflammatory drug and cytotoxic drugs in human colon cancer cell lines in vitro and xenografts. *Mol. Cancer Ther.* **5**, 919–926 (2006).
90. Jamwal, R. Bioavailable curcumin formulations : a review of pharmacokinetic studies in healthy volunteers. *J. Integr. Med.* (2018).
doi:10.1016/j.joim.2018.07.001
91. Schiborr, C., Kocher, A., Behnam, D., Jandasek, J. & Toelstede, S. The oral bioavailability of curcumin from micronized powder and liquid micelles is significantly increased. 516–527 (2014).
doi:10.1002/mnfr.201300724
92. Anand, P., Kunnumakkara, A. B., Newman, R. A. & Aggarwal, B. B. reviews Bioavailability of Curcumin : Problems and Promises. **4**, 807–818 (2007).
93. Esatbeyoglu, T. *et al.* Curcumin — From Molecule to Biological Function *Angewandte*. 5308–5332 (2012). doi:10.1002/anie.201107724
94. Pongrakhananon, V. & Rojanasakul, Y. Anticancer Properties of Curcumin. (2009).
95. Zhou, D. *et al.* Synthesis and Evaluation of Curcumin-Related Compounds Containing Benzyl Piperidone for Their Effects on Human

- Cancer Cells. **61**, 1149–1155 (2013).
96. Ferrari, E. *et al.* Newly Synthesized Curcumin Derivatives : Crosstalk between Chemico-physical Properties and Biological Activity. (2011).
 97. Ahsan, M. J., Khalilullah, H., Yasmin, S., Jadav, S. S. & Govindasamy, J. Activity of Curcumin Analogues Bearing Pyrazole / Pyrimidine Ring Targeting EGFR Tyrosine Kinase. **2013**, (2013).
 98. Shim, J. S. *et al.* Hydrazinocurcumin, a novel synthetic curcumin derivative, is a potent inhibitor of endothelial cell proliferation. *Bioorg. Med. Chem.* **10**, 2987–92 (2002).
 99. Liu, K., Chen, J., Chojnacki, J. & Zhang, S. BF₃·OEt₂-promoted concise synthesis of difluoroboron-derivatized curcumins from aldehydes and 2,4-pentanedione. *Tetrahedron Lett.* **54**, 2070–2073 (2013).
 100. Jäger, R. *et al.* Comparative absorption of curcumin formulations. *Nutr. J.* **13**, 11 (2014).
 101. Schiborr, C. *et al.* The oral bioavailability of curcumin from micronized powder and liquid micelles is significantly increased in healthy humans and differs between sexes. *Mol. Nutr. Food Res.* **58**, 516–527 (2014).
 102. Gota, V. S. *et al.* Safety and Pharmacokinetics of a Solid Lipid Curcumin Particle Formulation in Osteosarcoma Patients and Healthy Volunteers. *J. Agric. Food Chem.* **58**, 2095–2099 (2010).
 103. Basavaiah, D. & Veeraraghavaiah, G. The Baylis–Hillman reaction: a novel concept for creativity in chemistry. *Chem. Soc. Rev.* **41**, 68–78 (2012).

104. Lima-Junior, C. G. & Vasconcellos, M. L. A. A. Morita-Baylis-Hillman adducts: Biological activities and potentialities to the discovery of new cheaper drugs. *Bioorganic and Medicinal Chemistry* **20**, 3954–3971 (2012).
105. da Silva, W. A. V *et al.* Synthesis and activity of novel homodimers of Morita–Baylis–Hillman adducts against *Leishmania donovani* : A twin drug approach. *Bioorg. Med. Chem. Lett.* **26**, 4523–4526 (2016).
106. Szymon, K. *et al.* Studies toward Novel Peptidomimetic Inhibitors of Thioredoxin – Thioredoxin Reductase System. (2012).
doi:10.1021/jm201359d
107. Singh, V., Pathak, R. & Batra, S. Significant yield improvement in the stereoselective synthesis of allyl cyanides from Baylis-Hillman derivatives in aqueous medium under the influence of the phase-transfer catalyst. *Catal. Commun.* **8**, 2048–2052 (2007).
108. Application, P. The two tortoitu motanul dintre hain. **1**, (2018).
109. Nelson, G. L. *et al.* Synthesis and Evaluation of Baylis-Hillman Reaction Derived Imidazole and Triazole Cinnamates as Antifungal Agents. **2018**, (2018).
110. Johnson, J. L., Jonnalagadda, S. C. & Mereddy, V. R. Synthesis and Biological Evaluation of Novel Benzoxaboroles as Potential Antimicrobial and Anticancer Agents. **50**, 814–820 (2013).
111. Ronayne, C. T. *et al.* Synthesis and biological evaluation of 2-alkoxycarbonylallyl esters as potential anticancer agents. *Bioorganic Med.*

- Chem. Lett.* **27**, (2017).
112. Inácio, Â. S. *et al.* Mitochondrial Dysfunction Is the Focus of Quaternary Ammonium Surfactant Toxicity to Mammalian Epithelial Cells. **57**, 2631–2639 (2013).
 113. Tercel, M., Wilson, W. R., Anderson, R. F. & Denny, W. A. Hypoxia-Selective Antitumor Agents . 12 . Nitrobenzyl Quaternary Salts as Bioreductive Prodrugs of the Alkylating Agent Mechlorethamine. 1084–1094 (1996). doi:10.1021/jm9507791
 114. Jennings, M. C., Minbiole, K. P. C. & Wuest, W. M. Quaternary Ammonium Compounds: An Antimicrobial Mainstay and Platform for Innovation to Address Bacterial Resistance. (2015). doi:10.1021/acsinfecdis.5b00047
 115. Datta, S. *et al.* In Vitro Evaluation of Mitochondrial Function and Estrogen Signaling in Cell Lines Exposed to the Antiseptic Cetylpyridinium Chloride. 1–7 (2016).
 116. Sinha, S. *et al.* A Lipid-Modified Estrogen Derivative that Treats Breast Cancer Independent of Estrogen Receptor Expression through Simultaneous Induction of Autophagy and Apoptosis. *Mol. Cancer Res.* **9**, 364–374 (2011).
 117. Battogtokh, G. *et al.* Mitochondria-targeting drug conjugates for cytotoxic, anti-oxidizing and sensing purposes: current strategies and future perspectives. *Acta Pharm. Sin. B* **8**, 862–880 (2018).
 118. Cantor, J. R. & Sabatini, D. M. Cancer Cell Metabolism: One Hallmark,

- Many Faces. *Cancer Discov.* **2**, 881–898 (2012).
119. Pavlova, N. N. & Thompson, C. B. The Emerging Hallmarks of Cancer Metabolism. *Cell Metab.* **23**, 27–47 (2016).
 120. Cairns, R. A., Harris, I. S. & Mak, T. W. Regulation of cancer cell metabolism. *Nat. Rev. Cancer* **11**, 85–95 (2011).
 121. Weinberg, S. E. & Chandel, N. S. Targeting mitochondria metabolism for cancer therapy. *Nat. Chem. Biol.* **11**, 9–15 (2015).
 122. Fajas, L. Re-thinking cell cycle regulators: the cross-talk with metabolism. *Front. Oncol.* **3**, 1–6 (2013).
 123. Granchi, C., Fancelli, D. & Minutolo, F. An update on therapeutic opportunities offered by cancer glycolytic metabolism. *Bioorganic Med. Chem. Lett.* **24**, 4915–4925 (2014).
 124. Kroemer, G. & Pouyssegur, J. Tumor Cell Metabolism: Cancer's Achilles' Heel. *Cancer Cell* **13**, 472–482 (2008).
 125. Lee, N. & Kim, D. Cancer Metabolism: Fueling More than Just Growth. *Mol. Cells* **39**, 847–854 (2016).
 126. Schulze, A. & Harris, A. L. How cancer metabolism is tuned for proliferation and vulnerable to disruption. *Nature* **491**, 364–373 (2012).
 127. Hsu, P. P. & Sabatini, D. M. Cancer cell metabolism: Warburg and beyond. *Cell* **134**, 703–707 (2008).
 128. Pecqueur, C., Oliver, L., Oizel, K., Lalier, L. & Vallette, F. M. Targeting Metabolism to Induce Cell Death in Cancer Cells and Cancer Stem Cells. *Int. J. Cell Biol.* **2013**, 1–13 (2013).

129. Dang, C. V. Links between metabolism and cancer. *Genes Dev.* **26**, 877–890 (2012).
130. Martinez-Outschoorn, U. E. *et al.* Stromal-epithelial metabolic coupling in cancer: Integrating autophagy and metabolism in the tumor microenvironment. *Int. J. Biochem. Cell Biol.* **43**, 1045–1051 (2011).
131. Bhattacharya, B., Mohd Omar, M. F. & Soong, R. The Warburg effect and drug resistance. *British Journal of Pharmacology* (2016).
doi:10.1111/bph.13422
132. Akins, N. S., Nielson, T. C. & Le, H. V. Inhibition of Glycolysis and Glutaminolysis: An Emerging Drug Discovery Approach to Combat Cancer. *Curr. Top. Med. Chem.* (2018).
doi:10.2174/1568026618666180523111351
133. Ganapathy-Kanniappan, S. & Geschwind, J.-F. H. *Tumor glycolysis as a target for cancer therapy: progress and prospects.* *Molecular Cancer* **12**, 152 (2013).
134. Curry, J. M. *et al.* Cancer metabolism, stemness and tumor recurrence : MCT1 and MCT4 are functional biomarkers of metabolic symbiosis in head and neck cancer. *Cell Cycle* **12**, 1371–1384 (2013).
135. Suo, Z. *et al.* Mitochondrial pyruvate carrier function is negatively linked to Warburg phenotype in vitro and malignant features in esophageal squamous cell carcinomas. *Oncotarget* (2016).
doi:10.18632/oncotarget.13717
136. Pavlides, S. *et al.* Warburg Meets Autophagy: Cancer-Associated

- Fibroblasts Accelerate Tumor Growth and Metastasis via Oxidative Stress, Mitophagy, and Aerobic Glycolysis. *Antioxid. Redox Signal.* **16**, 1264–1284 (2012).
137. Lee, M. Metabolic interplay between glycolysis and mitochondrial oxidation: The reverse Warburg effect and its therapeutic implication. *World J. Biol. Chem.* **6**, 148 (2015).
138. Liberti. The Warburg Effect: How Does it Benefit Cancer Cells? *Trends Biochem Sci* **41**, 211–218 (2017).
139. Wise, A. *et al.* A comparative analysis of inhibitors of the glycolysis pathway in breast and ovarian cancer cell line models. *Oncotarget* (2015). doi:10.18632/oncotarget.4499
140. Adijanto, J. & Philp, N. J. The SLC16A family of monocarboxylate transporters (MCTs)-physiology and function in cellular metabolism, pH homeostasis, and fluid transport. *Curr. Top. Membr.* **70**, 275–311 (2012).
141. Halestrap, A. P. The SLC16 gene family – Structure, role and regulation in health and disease. *Mol. Aspects Med.* **34**, 337–349 (2013).
142. Parnell, K. M. & McCall, J. MCT4 Inhibitors for Treating Disease, US20160362378A1. US20160362378A1 (2016).
143. Critchlow, S. E. & Tate, L. Use of a MCT1 inhibitor in the treatment of cancers expressing MCT1 over MCT4. WO 2010089580 A1 (2010).
144. Baek, G. H. *et al.* MCT4 Defines a Glycolytic Subtype of Pancreatic Cancer with Poor Prognosis and Unique Metabolic Dependencies. *Cell Rep.* **9**, 2233–2249 (2014).

145. Miranda-Gonçalves, V. *et al.* Monocarboxylate transporters (MCTs) in gliomas: Expression and exploitation as therapeutic targets. *Neuro. Oncol.* **15**, 172–188 (2013).
146. Halestrap, A. P. & Wilson, M. C. The monocarboxylate transporter family- Role and regulation. *IUBMB Life* **64**, 109–119 (2012).
147. Baltazar, F. *et al.* Monocarboxylate transporters as targets and mediators in cancer therapy response. *Histol. Histopathol.* **29**, 1511–1524 (2014).
148. Vacanti, N. M. *et al.* Regulation of substrate utilization by the mitochondrial pyruvate carrier. *Mol. Cell* **56**, 425–435 (2014).
149. Halestrap, A. & P. The mitochondrial pyruvate carrier. Kinetics and specificity for substrates and inhibitors. *Biochem. J.* **148**, 85–96 (1975).
150. Divakaruni, A. S. *et al.* Inhibition of the mitochondrial pyruvate carrier protects from excitotoxic neuronal death. *J. Cell Biol.* **216**, 1091–1105 (2017).
151. Divakaruni, A. S. *et al.* Thiazolidinediones are acute, specific inhibitors of the mitochondrial pyruvate carrier. *Proc. Natl. Acad. Sci.* **110**, 5422–5427 (2013).
152. Battogtokh, G., Cho, Y., Lee, J. Y. & Lee, H. S. Mitochondrial-Targeting Anticancer Agent Conjugates and Nanocarrier Systems for Cancer Treatment. **9**, 1–20 (2018).
153. Manning Fox, J. E., Meredith, D. & Halestrap, A. P. Characterisation of human monocarboxylate transporter 4 substantiates its role in lactic acid efflux from skeletal muscle. *J. Physiol.* **529**, 285–293 (2000).

154. Wang, Q. & Morris, M. E. The role of monocarboxylate transporter 2 and 4 in the transport of gamma-hydroxybutyric acid in mammalian cells. *Drug Metab. Dispos.* **35**, 1393–1399 (2007).
155. Sonveaux, P. *et al.* Targeting lactate-fueled respiration selectively kills hypoxic tumor cells in mice. *J. Clin. Invest.* **118**, 3930–3942 (2008).
156. Gurrapu, S. *et al.* Monocarboxylate transporter 1 inhibitors as potential anticancer agents. *ACS Med. Chem. Lett.* **6**, 558–561 (2015).
157. Gurrapu, S. *et al.* Bioorganic & Medicinal Chemistry Letters Coumarin carboxylic acids as monocarboxylate transporter 1 inhibitors : In vitro and in vivo studies as potential anticancer agents. *Bioorg. Med. Chem. Lett.* **26**, 3282–3286 (2016).
158. Curtis, N. J. *et al.* Pre-clinical pharmacology of AZD3965, a selective inhibitor of MCT1: DLBCL, NHL and Burkitt's lymphoma anti-tumor activity. *Oncotarget* **8**, 69219–69236 (2017).
159. Lamb, R. *et al.* Mitochondria as new therapeutic targets for eradicating cancer stem cells: Quantitative proteomics and functional validation via MCT1/2 inhibition. *Oncotarget* **5**, 11029–11037 (2014).
160. Noble, R. A. *et al.* Inhibition of monocarboxylate transporter 1 by AZD3965 as a novel therapeutic approach for diffuse large B-cell lymphoma and burkitt lymphoma. *Haematologica* **102**, 1247–1257 (2017).
161. Polański, R. *et al.* Activity of the monocarboxylate transporter 1 inhibitor AZD3965 in small cell lung cancer. *Clin. Cancer Res.* **20**, 926–937 (2014).

162. Bola, B. M. *et al.* Inhibition of Monocarboxylate Transporter-1 (MCT1) by AZD3965 Enhances Radiosensitivity by Reducing Lactate Transport. *Mol. Cancer Ther.* **13**, 2805–2816 (2014).
163. Gaonkar, S. L. & Vignesh, U. N. Synthesis and pharmacological properties of chalcones: a review. *Res. Chem. Intermed.* **43**, 6043–6077 (2017).
164. Zhuang, C. *et al.* Chalcone : A Privileged Structure in Medicinal Chemistry. (2017). doi:10.1021/acs.chemrev.7b00020
165. Gomes, M. N. *et al.* Chalcone Derivatives : Promising Starting Points for Drug Design. doi:10.3390/molecules22081210
166. Karthikeyan, C., Narayana, N. S. H. & Ramasamy, S. Advances in Chalcones with Anticancer Activities. 97–115 (2015).
167. Jandial, D. *et al.* Molecular Targeted Approaches to Cancer Therapy and Prevention Using Chalcones. *Curr. Cancer Drug Targets* **14**, 181–200 (2014).
168. Qian, H., Liu, D. & Lv, C. Synthesis of chalcones via Claisen-Schmidt reaction catalyzed by sulfonic acid-functional ionic liquids. *Ind. Eng. Chem. Res.* **50**, 1146–1149 (2011).
169. Wu, X.-F., Neumann, H. & Beller, M. Preparation of Chalcones by Carbonylative Heck Reaction. *Synfacts* **2010**, 1180–1180 (2010).
170. Selepe, M. A. & Van Heerden, F. R. Application of the Suzuki-Miyaura reaction in the synthesis of flavonoids. *Molecules* **18**, 4739–4765 (2013).
171. Imura, Y. K., Kiya, M. U., Asegawa, D. H., Kihisa, T. A. & Uzuki, T. S.

Xanthoangelol , a Major Chalcone Constituent of *Angelica keiskei* ,
Induces Apoptosis in Neuroblastoma and Leukemia Cells. **28**, 1404–1407
(2005).

172. Limper, C. *et al.* Compounds isolated from *Psoralea corylifolia* seeds inhibit protein kinase activity and induce apoptotic cell death in mammalian cells. *J. Pharm. Pharmacol.* **65**, 1393–1408 (2013).
173. Canela, M. *et al.* Antivascular and antitumor properties of the tubulin-binding chalcone TUB091. **8**, 14325–14342 (2017).